

Mechanism-Based Intervention in Non-Alcoholic Fatty Liver Disease:

Mapping the Muscle-Liver Axis and Exploring the Effect of L-carnitine on Liver Fat, Insulin Sensitivity and Mitochondrial Energy Kinetics

Dr P Thiagarajan (2020)

Access from the University of Nottingham repository:

<http://eprints.nottingham.ac.uk>

Copyright and reuse:

The Nottingham ePrints service makes this work by researchers of the University of Nottingham available open access under the following conditions.

This article is made available under the University of Nottingham End User licence and may be reused according to the conditions of the licence.

For more details see:

http://eprints.nottingham.ac.uk/end_user_agreement.pdf

For more information, please contact eprints@nottingham.ac.uk

Mechanism-based Intervention in Non-Alcoholic Fatty Liver Disease:

Mapping the Muscle-Liver Axis and exploring the effect of L-carnitine on liver fat, insulin sensitivity and mitochondrial energy metabolism.



Prarthana Thiagarajan MBBS, MRCP (UK)

Thesis Submitted in partial fulfilment of the requirements for the award of
Doctor of Philosophy of The University of Nottingham

Contents

Abbreviations.....	6
Acknowledgements.....	10
Declaration.....	13
Abstract.....	14
Publications and Presentations.....	17
Chapter 1.....	19
Introduction	19
1.1 Background	20
1.1.1 Epidemiology and Natural History of NAFLD	20
1.1.2 Landscape and Challenges	21
1.1.3 Drug Development.....	21
1.1.4 Endpoints in NAFLD Trials	23
1.2 Mechanisms of NAFLD pathogenesis: Insulin resistance, Oxidative Stress and Mitochondrial Dysfunction	27
1.2.1 Lipid-Induced Insulin Resistance.....	27
1.2.2 Mitochondrial Oxidative Metabolism	33
1.2.3 Modelling Hepatic Energy Kinetics	35
1.3 Dietary Interventions in NAFLD	38
1.4 L-Carnitine: Physiology, Fuel Selection and Therapeutic Potential	42
1.4.1 Background	42
1.4.2 Historical overview.....	44
1.4.3 L-Carnitine Homeostasis and Kinetics.....	46
1.4.4 Role of L-carnitine in Cellular Energy Metabolism and Fuel Selection	50
1.4.5 L-Carnitine as a candidate treatment for insulin resistance.....	52
1.4.6 Governing Metabolic Flexibility	54
1.4.7 L-Carnitine as a Candidate Treatment for NAFLD.....	57
Chapter 2.....	60
General Methods	60
2.1 Metabolic Physiology	61
2.1.1 Euglycaemic Hyperinsulinaemic Clamp	61
Heated Hand Technique	63
2.1.2 Stable Isotope Tracer Methodology	63
2.1.3 Determining Hepatic Insulin Sensitivity	64
Gas Chromatography Mass Spectrometry	67
2.1.4 Leg Glucose Uptake.....	67

2.1.5 Indirect Calorimetry	69
2.1.6 Muscle biopsies.....	71
2.1.7 Measuring Adipose Tissue Insulin Resistance.....	73
2.1.8 Dual Energy X ray Absorptiometry (DEXA).....	74
2.1.9 Blood Sample Collection	75
2.2 MR Spectroscopy	75
2.2.1 Background	75
2.2 ¹ H MRS in the Liver (3T)	78
2.2.3 ¹ H MRS in Skeletal Muscle (7T)	79
2.2.4 ³¹ P MRS with saturation transfer in the Liver (3T).....	80
2.3 Covid Statement.....	80
2.4 Clarification of Patient Pools for Studies	81
Chapter 3.....	82
Mechanisms of Insulin Resistance in NAFLD: Mapping the Muscle-Liver Axis through deep metabolic phenotyping.....	82
3.1 Introduction	83
3.2 Methods.....	84
3.2.1 Human Participants.....	84
3.2.2 Imaging and Metabolic Studies.....	88
3.2.3 Euglycaemic Hyperinsulinaemic Clamp	89
3.2.4 Substrate oxidation.....	91
3.2.5 Leg Glucose Uptake.....	92
3.2.6 Sample Analysis.....	92
3.2.7 Plasma VLDL concentrations.....	94
3.2.8 Muscle Biopsy Analyses	94
3.2.9 Confocal microscopy.....	94
3.2.10 Statistical Analysis.....	95
3.3 Results.....	96
3.3.1 Patient Demographics.....	96
3.3.2 Glucose and Lipid Kinetics.....	99
3.3.3 Liver Biochemistry.....	103
3.3.4 Substrate Oxidation and Metabolic Flexibility.....	105
3.3.5 Leg Glucose Uptake.....	107
3.3.6 Metabolic impact of fat partitioning.....	108
.....	110
3.3.7 Hepatic ATP flux.....	110

3.4 Discussion.....	113
Chapter 4.....	121
L-carnitine Supplementation in Non-alcoholic Fatty Liver Disease: A systematic review and meta-analysis.....	121
4.1 Introduction	122
4.2 Materials and Methods.....	122
4.2.1 Search Strategy	122
4.2.2 Eligibility criteria.....	124
4.2.3 Data Extraction and Quality Assessment	125
4.2.4 Statistical Analysis.....	125
4.3 Results.....	125
4.3.1 Search Results	125
4.3.2 Quality of Included Studies	129
4.3.3 Outcomes	130
4.3.3.1 ALT.....	130
4.3.3.2 AST	131
4.3.3.3 Liver fat	131
4.3.3.4 HOMA-IR and glycometabolic profile	132
4.3.4 Adverse Events.....	134
4.3.5 Inflammation and Oxidative Stress.....	134
4.4 Discussion.....	135
4.4.1 Summary of Evidence	135
4.4.2 Strengths and Limitations	135
4.4.3 Conclusion.....	137
Chapter 5:.....	138
Effect of Dietary L-carnitine supplementation on liver fat, insulin sensitivity and hepatic energy kinetics.....	138
5.1 Introduction	139
5.2 Methods.....	142
5.2.1 Ethical Approval	142
5.2.2 Recruitment	143
5.2.3 Screening visit	144
5.2.4 Randomisation	144
5.2.4 Metabolic Imaging	145
5.2.5 Statistical Analysis.....	147
5.3 Results.....	151

5.3.1 Effect of 24 weeks' L-carnitine supplementation on IHTG	152
5.3.2 Effect of L-carnitine supplementation on Glucose Metabolism	154
5.3.3 Anthropometry	157
5.3.4 Effect on Lipid Metabolism	158
5.3.5 Effect of L-carnitine on muscle lipid fractions	159
5.3.6 Effect on hepatocellular enzymes.....	160
5.3.7 Substrate Oxidation	163
Fat Oxidation.....	163
Carbohydrate Oxidation.....	164
Respiratory Quotient	166
5.3.8 Hepatic Mitochondrial energetics.....	167
5.3.9 Effect on circulating markers of inflammation	168
Leg Glucose Uptake.....	169
5.3.10 Adverse events.....	170
5.4 Discussion.....	172
5.4.1 Summary of major findings.....	172
5.4.2 Limitations.....	178
5.4.3 Controversies	179
5.5 Conclusion.....	181
Chapter 6.....	184
Applications of non-proton MR Spectroscopy in NAFLD and Quantitative Assessment of Hepatic Energy Kinetics.....	184
6.1 Introduction	185
6.1.1 Principles of MR Spectroscopy.....	186
6.1.2 Applications of MRS in Metabolic Liver Disease	187
6.1.3 ¹³ C MR Spectroscopy	190
6.1.4 Mitochondrial Oxidative Metabolism	191
6.1.5 Oxidative Stress.....	193
6.1.6 ³¹ P MRS and ATP Kinetics	194
6.1.7 Magnetisation transfer	195
6.2 Methods.....	199
6.2.1 Post Processing	200
6.3 Results.....	203
6.4 Discussion.....	204
Chapter 7: Role of Hepatokines as biomarkers in NAFLD.....	207
7.1 Introduction	208

7.1.1 Fibroblast Growth Factor 21 (FGF-21)	210
7.1.2 Leukocyte-Derived Chemotaxin 2 (LECT-2).....	212
7.1.3 Aim	213
7.2 Methods.....	213
7.2.1 Detailed procedure:	214
7.2.2 Statistical Analysis	215
7.3 Results.....	215
7.3.1 LECT2: cross sectional study	216
Stepwise Linear Regression.....	219
7.3.2 LECT2: Longitudinal Assessment.....	219
7.3.3 FGF21: Cross-sectional study	221
7.3.4 FGF21 Longitudinal Assessment	223
7.4 Discussion.....	224
Chapter 8: General Discussion	227
8.1 Aims.....	228
8.2 General Summary	229
8.3 Limitations.....	231
8.4 Mechanistic Approach to L-carnitine Treatment in NAFLD	233
8.5 Research Implications	236
Conclusion.....	239
Appendix 1	240
Appendix 2	241
Appendix 3 Measuring Endogenous Glucose Production.....	244
Appendix 4 Protocol Summary for the ECLIPSE Study.....	246
Appendix 5 Example Data Collection Sheet for Clamp Studies	247
REFERENCES.....	252

Abbreviations

°C	Degrees Celcius
6,6- ² H ₂	Dideuterated Glucose
Acetyl CoA	Acetyl Coenzyme A
ALT	Alanine Aminotransferase
AMARES	Advanced Method for Accurate, Robust, and Efficient Spectral fitting
APE	Atoms Percent Excess
AST	Aspartate Aminotransferase
ATP	Adenosine Triphosphate
AUROC	Area Under the Receiver Operating Curve
BEE	Basal Energy Expenditure
CAP	Controlled Attenuation Parameter
CHO	Carbohydrate
CPT1	Carnitine Palmitoyl Transferase 1
CrAT	Carnitine Acetyltransferase
CRP	C Reactive Protein
DAG	Diacylglycerol
DNL	De Novo Lipogenesis
EGP	Endogenous Glucose Production
ELISA	Enzyme Linked Immunosorbent Assay
EMCL	Extramyocellular Lipid
ETC	Electron Transport Chain
FATP	Forward rates of Adenosine Triphosphate Synthesis
FGF21	Fibroblast Growth Factor 21
FOX	Fat Oxidation
FXR	Farsenoid X Receptor
GCMS	Gas Chromatography Mass Spectrometry
GEM	Gas Exchange Machine
GLUT-4	Glucose Transporter 4
GDR	Glucose Disposal Rate
HDL	High Density Lipoprotein
HOMA IR	Homeostasis Model of Insulin Resistance

IGT	Impaired Glucose Tolerance
IHTG	Intrahepatic Triglyceride
IMCL	Intramyocellular Lipid
LDL	Low Density Lipoprotein
LECT2	Leukocyte cell derived Chemotaxin 2
MRE	Magnetic Resonance Elastography
MRI	Magnetic Resonance Imaging
MRS	Magnetic Resonance Spectroscopy
MUFA	Monounsaturated Fatty Acid
NAFLD	Non-alcoholic Fatty Liver Disease
NASH	Non-alcoholic Steatohepatitis
NEFA	Non-esterified Fatty Acid
OCA	Obeticholic Acid
OCTN-2	Organic Cation Transporter 2
OGTT	Oral Glucose Tolerance Test
OxPhos	Oxidative Phosphorylation
PDC	Pyruvate Dehydrogenase Complex
Pi	Inorganic Phosphate
PKC θ	Protein Kinase C Theta
PKC ϵ	Protein Kinase C Epsilon
PME	Phosphomonoesters
PDE	Phosphodiesterases
PPAR	Peroxisome Proliferator Activated Receptor
PRESS	Point Resolved Spectroscopy
REE	Resting Energy Expenditure
RER	Respiratory Exchange Ratio
ROS	Reactive Oxygen Species
RQ	Respiratory Quotient
SAE	Serious Adverse Event
SFA	Saturated Fatty Acid
STEAM	Stimulated Echo Acquisition Mode

TNF α	Tumour Necrosis Factor Alpha
UDPG	Uridine Diphosphoglucose
VCTE	Vibration-controlled Transient Elastography
VLDL	Very Low Density Lipoprotein
VO ₂ max	Maximal Rate of Oxygen Consumption

Acknowledgements

“On a huge hill, Cragged and steep, Truth stands, and hee that will Reach her, about must and about must goe; And what th’hills suddenness resists, winne so” John Donne, Satyre III

Doing a PhD is truly a labour of love. While impossible to emerge unscathed, the journey has been a great privilege, honour and educator in my life.

First and foremost, I would like to thank my supervisor, Professor Guru Aithal. His vision, passion for science and dedication to the highest quality research inspire me every day. Without his expertise, generosity, wisdom and mentorship, this work would not have existed. Of all the lessons he has taught me, perhaps the most valuable have been these two. First, that faith minus doubt equals dogma. It is through thousands of conversations that I have learned to challenge the ‘sacred cows’ of medicine (and life!) and to question received wisdom, no matter the source. Second, that science is nothing if not the relentless pursuit of truth.

I would like to thank Professor Paul Greenhaff for his limitless patience in explaining metabolic physiology to a medic, for taking the time to read my thesis drafts, and for his expertise, generosity and enthusiasm, which have added enormously to the scientific rigour of this work. I am indebted to Professor Penny Gowland and Dr Stephen Bawden, who have been exceptional mentors throughout the lifetime of this research, and wonderful guides into the world of precision imaging. Their expertise has been instrumental in the evolution of this project. I extend special thanks to Dr Stephen Bawden, who has taught me almost everything I know about metabolic imaging, engaged me in conversations from physics to philosophy to childcare and back again over long scanning hours and has managed to distil incredibly clever physics into something a very average medic can digest.

I would like to thank Dr Jane Grove for teaching me absolute scientific integrity, for introducing me to laboratory research and for teaching me ELISA and PCR techniques. I have met no better scientist. To Mel Lingaya, Yirga Falcone and Davor Kresnik, I owe you much more than Lindt chocolates for your

work in the lab with my samples. To all the nursing staff in the Biomedical Research Centre, a huge thank you for your patience and generosity in helping me with this project.

Dr Liz Simpson has been the lynchpin on which my delicate threads of knowledge converge. She has guided me with utmost patience through the euglycaemic hyperinsulinaemic clamp technique, helping me to overcome roadblocks where I didn't anticipate roadblocks. I would like to thank her for the hours spent discussing everything from feminism to fascism while teaching me how to run a complex metabolic physiology study. It is thanks to her mentorship that this project hasn't stumbled at its first, second, third or 96th hurdle.

To all the staff on the David Greenfield Human Physiology Unit, to whom I owe so much. To Jo Mallinson and Mia Keeton for all the liquid nitrogen and handling muscle biopsy specimens so professionally. To Mel, Matt and Ben for (literally) hours of compression, Aline Nixon and Dr Natalie Shur for their company, clinical skills and help on clamp days. To Dr Tariq Taylor teaching me the Bergström biopsy technique. And to Sara Brown for her hilarious anecdotes, ability to keep my patients engaged in football-related conversations mid-muscle biopsy and for acquiring literally any consumable I had reason to need during the course of these studies.

To my 'liver lobule' colleagues, Dr Jane Chalmers, Dr Edmond Atallah, Dr Mohsen Subhani, Dr Lucy Bennett, Dr Abhishek Sheth, Dr Robert Scott, Dr Naveen Palaniyappan, Dr Rebecca Harris, Dr Waleed Fateen and Dr David Gunn. Thank you for walking this journey with me, and for enriching it with your friendship and camaraderie.

I will claim back my Nespresso machine now.

Professor Neil Guha has earned the great respect of all academic liver trainees in Nottingham. I would like to thank him for taking the time to impart incredible life lessons with both humour and emotional intelligence, for taking an interest in us as people – whether it be through conversations over lunch during a busy on-call or in engaging us in rigorous debates during journal club – and for his relentless

support for our intellectual growth. His belief in our abilities, his patience and wisdom have been an inspiration to us all in navigating the labyrinths of clinical life, academic life and parenthood.

To My Family: my four parents, my in-laws, my siblings. Thank you, always, for putting up with me. Thank you for the countless hours you have dedicated in childcare, conversation and food donations to help me realise my goals. It is a truth not universally acknowledged that when a person pursues a career with devotion, it is their family who so often provide that devotion back in kind, bearing the brunt of their absence, both physical and mental. Thank you for bearing my absence, for encouraging me and for supporting me to pursue my dreams.

To all the patients who have so kindly volunteered their time to this project. Without them, this undertaking would not have been possible. I remain in awe of their determination to see the studies through, despite multiple muscle biopsies and central line insertions. It has been a genuine privilege and a highlight of my time here, getting to know each and every one of them, being gifted a glimpse into their lives, and learning that there is so much that is extraordinary in the ordinary. It has not been easy, but I am indebted to them for their contributions to this research.

To Gopal. Thank you for being my enabler in life, for seeing potential in me during times when I saw none, for reading through the hundreds of drafts of this thesis. You are the brightest, kindest and most selfless person I know. Thank you for being my best friend, the best father to our children and for weathering all manner of storms with equanimity. Thank you for teaching me to think critically and for helping me on a journey towards emotional intelligence.

And finally, to the two brightest stars in my sky. To my sons, Kailash and Kalyan. First, a sincere apology for the countless times I haven't been able to be there for you. Career and family is invariably a difficult balance, and there have been times I have fallen on the wrong side of it. I cannot wait to have more time with you in the coming months. And second, a thank you for being such incredibly enchanting, kind and considerate boys. Seeing you grow fills me with hope and pride. You inspire all that I am and all that I do, every day. I dedicate this work to you.

Declaration

Where individuals have made specific contributions to the work described herein, this has been acknowledged in relevant sections of the thesis. All other work is my own, based on studies I have undertaken in the NIHR Nottingham Biomedical Research Centre, the David Greenfield Physiology Unit/MRC-Arthritis Research UK Centre for Musculoskeletal Ageing Research Laboratory and the Sir Peter Mansfield Imaging Centre at the University of Nottingham, from May 2017 until August 2020.

Abstract

The rising prevalence of non-communicable disease reflects a global healthcare burden that is the product of overnutrition and physical inactivity. As these deleterious lifestyles persist, their metabolic consequences have reached epidemic proportions. In this context, and with its corollaries of obesity and insulin resistance, non-alcoholic fatty liver disease (NAFLD) presents a growing public health and economic challenge. With no approved pharmacological treatment currently available, NAFLD will dominate the landscape of hepatology for the foreseeable future. Its prevalence, associated complications and escalation of disease burden in coming decades together underscore a time-critical unmet need for disease-modifying therapy which is broadly applicable, safe and cost-effective.

The research presented in this thesis sought to explore mechanisms underpinning insulin resistance in a NAFLD population, and in particular to determine the role of intramyocellular lipids and muscle insulin resistance in the pathogenesis of NAFLD. Further, the role of chronic L-carnitine supplementation on liver fat, whole-body insulin sensitivity and hepatic energy metabolism in individuals with NAFLD was quantitatively evaluated in a placebo-controlled randomised trial. The data presented herein argues that chronic substrate overabundance, combined with defects in mitochondrial lipid oxidation, give rise to the '*perfect storm*' of ectopic lipid accumulation and subsequent interruption of insulin signalling pathways in target tissues. This, together with oxidative stress, creates an insulin resistant, pro-fibrogenic milieu at the level of the liver.

Leveraging a two-step euglycaemic hyperinsulinaemic clamp technique together with sophisticated precision imaging, I have demonstrated that NAFLD is associated with excess intramyocellular lipid accumulation and whole-body insulin resistance. Further, I have shown that even at an early stage in its natural history, NAFLD is associated with impaired hepatic mitochondrial energetics and defective oxidative phosphorylation. A plausible explanation linking these findings is that local muscle insulin

resistance alters the pattern of energy storage, favouring diversion of carbohydrate substrate to the liver and, through *de novo* lipogenesis, exacerbates intrahepatic lipid accumulation.

In a systematic review and meta-analysis, I have synthesised existing data detailing the effects of dietary carnitine loading on liver enzymes, insulin resistance profiles and liver fat in NAFLD. As a naturally occurring quaternary amine, L-carnitine has a well-established safety profile. In its dual role as an essential cofactor for mitochondrial fatty acid β -oxidation, and as a facilitator of muscle glycogen storage, L-carnitine stands at the nexus of glucose and lipid homeostasis. These unique properties render it an intriguing candidate therapy for NAFLD. Results from five randomised trials are presented, arguing that dietary L-carnitine supplementation may be an effective tool in the treatment of NAFLD, through lowering liver lipid, improving biomarkers of liver injury and improving metabolic phenotype.

To further explore this hypothesis, I conducted a placebo-controlled randomised trial in young, non-diabetic individuals with NAFLD comparing 24 weeks of twice daily L-carnitine therapy (plus Slimfast supplementation to provide an insulinogenic stimulus for muscle carnitine uptake) versus maltodextrin placebo (plus Slimfast) on intrahepatic triglyceride concentration (IHTG). I have shown that mean IHTG decreased in the L-carnitine group, while it increased in the placebo group (-3.5% [-5.9; -1.5] versus 6.0% [1.5; 11.0], $p = 0.002$). Further, L-carnitine treatment was associated with a decrease in intramyocellular lipid to extramyocellular lipid (IMCL: EMCL) ratio (0.92 ± 0.62 to 0.42 ± 0.30 in the L-carnitine group versus 1.53 ± 0.99 to 1.47 ± 0.36 in placebo, $p < 0.001$) and improved leg glucose uptake ($p=0.02$). Serum alanine aminotransferase (ALT) declined significantly in the L-carnitine group versus placebo ($p=0.04$). Peripheral (muscle) insulin sensitivity and adipose tissue insulin resistance were not significantly different between groups compared to baseline values ($p=0.83$ and 0.72 , respectively). Finally, we observed an improvement in forward rates of hepatic ATP synthesis with L-carnitine (+ 0.50 mM/s vs - 0.09 Mm/S in placebo group, $p=0.025$), suggesting that L-carnitine

is capable of boosting hepatic mitochondrial energy kinetics. There was no significant change in weight (kg) from baseline within or between groups ($p=0.67$).

In summary, we implicate muscle lipid deposition and insulin resistance as important contributors to NAFLD. We argue that augmenting muscle carnitine content is capable of reducing myocellular lipid and intrahepatic triglyceride. Improved liver mitochondrial energy kinetics are consistent with a reduction in liver fat following carnitine supplementation in a NAFLD population. Whether these effects are indirect, consequent to carnitine loading in muscle, or whether exogenous carnitine exerts a direct effect on hepatocyte lipid metabolism, remains to be established and will require harnessing recent advances in precision imaging to map hepatic and muscle carnitine content non-invasively.

Publications and Presentations

Publications

The following peer-reviewed publications have arisen in the course of this doctoral research:

1. Thiagarajan P, Chalmers J, Ban L, Grindlay D, Aithal GP. L-carnitine supplementation in non-alcoholic fatty liver disease: A systematic review and meta-analysis. *World J Meta-Anal* 2020; 8(1): 4-14

Thiagarajan P, Bawden SJ, Aithal GP. Metabolic Imaging in Non-Alcoholic Fatty Liver Disease: Applications of Magnetic Resonance Spectroscopy. *J Clin Med*. 2021 Feb 7;10(4):632.
2. Thiagarajan P, Aithal GP. Drug Development for Nonalcoholic Fatty Liver Disease: Landscape and Challenges. *J Clin Exp Hepatol*. 2019; 9(4):515-21.
3. Thiagarajan P, Chalmers J, Guha IN, James MW. Detecting chronic liver disease: are liver function tests the solution? *Br J Hosp Med*. 2020; 81(1):1–8.
4. Grove JJ, Thiagarajan P, Astbury S, et al. Analysis of genotyping for predicting liver injury marker, procollagen III in persons at risk of non-alcoholic fatty liver disease. *Liver Int*. 2018;38(10):1832-1838

Conference Proceedings

Oral Presentations:

“L-carnitine supplementation in NAFLD: Effects on metabolic phenotype, liver fat and mitochondrial energy kinetics” – BASL Annual Virtual Meeting, Sept 2020

“Mapping Metabolic Inflexibility in NAFLD: Comparison With Healthy Volunteers and Following L-Carnitine Intervention Using Advanced MRS ” – Selected for Oral Presentation at the International Society for Magnetic Resonance in Medicine (ISMRM) Annual Meeting, **Sydney, Australia, April 2020**
Presented virtually due to the Covid-19 Pandemic

“Mapping Metabolic Disturbances in NAFLD: Differences in substrate oxidation, intramyocellular lipid content, hepatic ATP flux and insulin sensitivity in healthy volunteers versus a non-diabetic NAFLD cohort” – Oral Presentation at the British Association for the Study of Liver Disease (BASL) Annual Meeting, **Glasgow, Scotland, September 2019**.

“Mapping metabolic inflexibility in Non-alcoholic fatty liver disease: Differences in substrate oxidation, insulin sensitivity and skeletal muscle lipid fractions in healthy volunteers versus a non-diabetic NAFLD cohort.” – Oral Presentation at the British Association for the Study of Liver Disease (BASL) Basic Science Retreat, **Alfreton, Derbyshire, June 2019**.

“Nonalcoholic fatty liver disease: the invisible epidemic” –University of Nottingham Medicine and Health Sciences Postgraduate Research Forum.

Poster presentations:

“L-carnitine supplementation in NAFLD: Effects on metabolic phenotype, liver fat and mitochondrial energy kinetics” Poster presentation at the American Association for the Study of Liver Diseases (AASLD), **Boston, Massachusetts, USA, November 2020 (Virtual Meeting)**

“Accumulation Of Intrahepatic Triglyceride Is Associated With Increased Intra-/Extra-Myocellular Lipid Ratio And Reduced Hepatic Oxidative Phosphorylation In Young, Non-Diabetic Males.” – Poster presentation at the American Association for the Study of Liver Diseases (AASLD), **Boston, Massachusetts, USA, November 2019.**

“Effect of dietary L-carnitine supplementation on Non-Alcoholic Fatty Liver Disease: a systematic review and meta-analysis” – Poster Presentation at the British Association for the Study of Liver Disease (BASL) Annual Meeting, **Glasgow, Scotland, September 2019.**

Awards

1. ‘Best of BASL’ award for oral presentation, September 2019
2. BASL Travel Award, September 2019
3. BASL Top Poster Award, September 2019
4. University of Nottingham Best IMPACT Prize, June 2018
5. Nottingham University Hospital (NUH) Charity Travel and Development Award, February 2020

Chapter 1

Introduction

1.1 Background

“The only way to keep your health is to eat what you don't want, drink what you don't like, and do what you'd rather not.”

Mark Twain (1835-1910)

1.1.1 Epidemiology and Natural History of NAFLD

Throughout history, human physiology has developed adaptive mechanisms to enable survival in environments with limited and unpredictable nutrient availability. The recent burgeoning of metabolic disease on a global scale reflects rapid societal shifts in which energy-dense foods are almost ubiquitous, while energy demands are low. The consequences of chronically positive energy balance to human physiology are manifold, with broad-ranging clinical and therapeutic implications collectively termed ‘the metabolic syndrome’. Against this background, non-alcoholic fatty liver disease (NAFLD) has rapidly emerged as a leading cause of chronic liver disease and liver transplantation in high-income economies [1]. Closely associated with obesity, atherogenic dyslipidaemia and impaired glucose tolerance, NAFLD is broadly considered to be the hepatic manifestation of the metabolic syndrome. In this context, its prevalence is expected to increase exponentially in coming decades as obesity and type 2 diabetes become increasingly common [2].

The natural history of NAFLD is characterised by progressive accumulation of lipid species within the liver parenchyma, giving rise, over time, to necroinflammation, oxidative stress and fibrogenesis. This results in a clinically heterogeneous phenotype, ranging from simple steatosis (NAFL) through to non-alcoholic steatohepatitis (NASH), fibrosis, cirrhosis and hepatocellular carcinoma (**Figure 1**). The global prevalence of NAFLD is estimated to be 25% [3], rising to 66% and 90% in type 2 diabetic and obese populations, respectively [4]. Although progression to NASH is limited to approximately 20% of individuals with NAFL [2], the high population prevalence of NAFLD heralds a looming socioeconomic burden due to the consequences of its progression, including end-stage liver disease [5]. In Europe-4

countries alone (France, Germany, Italy, UK), the annual cost associated with NAFLD is estimated to be €35 billion [6]. This cost will rise inexorably unless effective screening and intervention strategies, including disease-modifying therapies, are swiftly developed.

1.1.2 Landscape and Challenges

Emerging candidate therapies to combat NAFLD are currently limited to research settings, with no licensed pharmacological treatment available at a population level. This perhaps reflects the complexity and multifactorial aetiopathogenesis of the disease. In contrast to single aetiology conditions such as hepatitis C, NAFLD is the result of multiple cellular and molecular derangements occurring in multiple organ systems, involving a combination of genetic, dietary, metabolic and immunological triggers (**Figure 2**).

Challenges to development of effective therapy are further hindered by the heterogenous, non-linear nature of disease progression in NAFLD and the bidirectionality of its pathogenesis: NAFLD is considered to be both the driver and the consequence of its many associations. Pathways to intervention will therefore rely on an integrated approach towards deeper understanding of the molecular mediators of whole-body insulin resistance, hepatocellular lipotoxicity, inflammation and oxidative stress and their combined role in the progression of NAFLD.

1.1.3 Drug Development

Logically, drug development in NAFLD would focus on drugs which potentially exert a simultaneous influence on multiple pathophysiological processes implicated in disease progression, including insulin resistance, chronic inflammation and fibrogenesis [7]. For example, Obeticholic acid (OCA), one of the first drugs shown to demonstrate therapeutic potential in NAFLD, is an agonist of the nuclear transcription factor Farnesoid X receptor (FXR). OCA administration can therefore alter gene expression affecting multiple metabolic and cellular injury pathways, including lipid metabolism, insulin resistance and oxidative stress. However, given the diversity of triggers for a NASH phenotype,

effective long-term treatment strategies are likely to involve a combination of agents, each targeting different pathways in NAFLD pathogenesis, together with dietary and lifestyle measures. Phase 2 trials to date have focused on a wide range of therapeutic targets, including peroxisome-proliferator activated receptor (PPAR) α/δ agonists (e.g. Elafibrinor), selective inhibitors of apoptosis signal-regulating kinase 1 (ASK-1, e.g. selonsertib), glucagon-like peptide 1 (GLP-1) analogues (e.g. liraglutide, semaglutide) and C-C chemokine receptor type 2 (CCR2) inhibitors (e.g. cenecriviroc), each targeting key network mediators of inflammation and fibrogenesis with myriad downstream effects [8].

In a large retrospective cohort study involving 646 biopsy-proven patients with NAFLD, the entire group showed a trend towards higher risk for mortality than controls (HR 1.14; 95% confidence interval [CI] 0.99–1.32; $p = 0.07$) [9]. During follow-up, liver-related mortality was 7.9% in cases versus 1.4% in controls ($p < 0.001$); endocrine-related mortality including diabetes was significantly higher in NAFLD versus control groups (5.1% vs 2.7%; $p = 0.02$). NASH was also associated with a slight increase in overall mortality (HR 1.22; 95% CI 1.02–1.46; $p = 0.03$). The population prevalence of NAFLD means that the burden of morbidity and mortality, even when the minority progress to cirrhosis, still form a compelling case of need for the development of effective intervention. Nevertheless, key factors distinguishing the progressive form of NAFLD among a substantial proportion of the affected population are not yet well established.

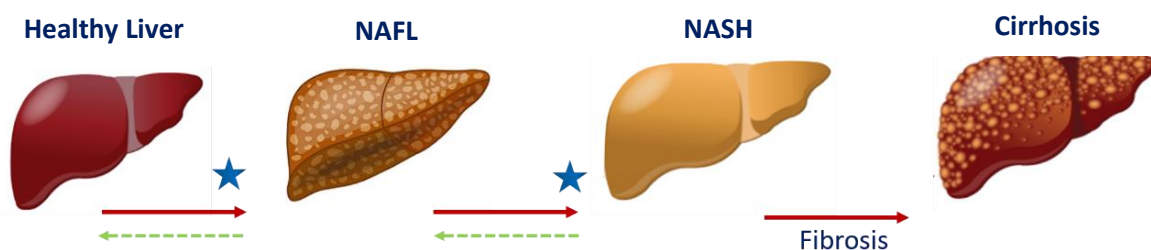


Figure 1. Natural History and Progression of Non-Alcoholic Fatty Liver Disease.

NAFL = Non-alcoholic Fatty Liver (simple steatosis), NASH = Non-Alcoholic Steatohepatitis. Red arrows denote progression. Green arrows denote potential for regression.

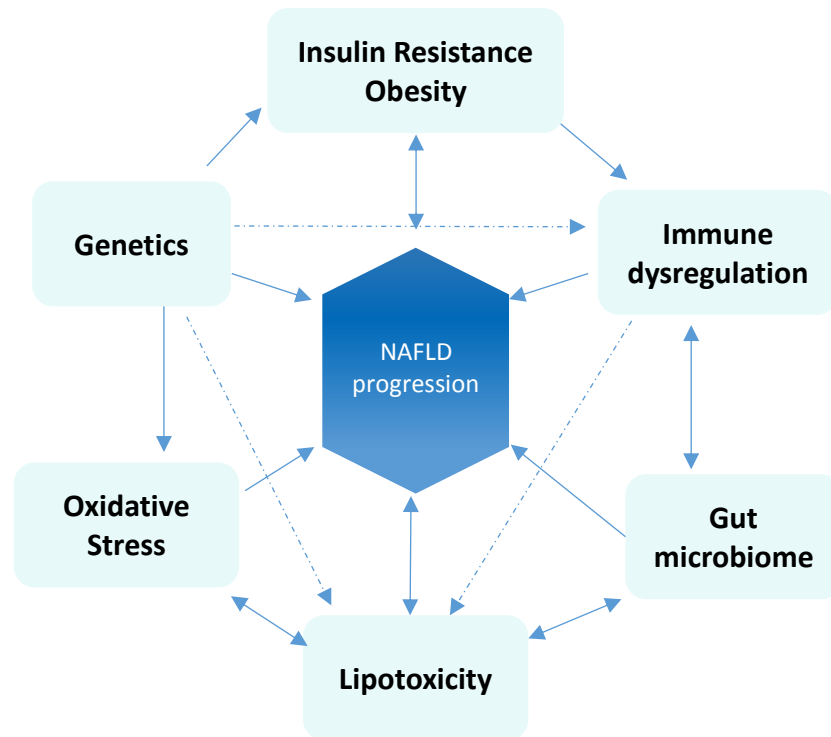


Figure 2. Multifactorial Aetiopathogenesis of NAFLD

Some putative mechanisms, notably insulin resistance, are bidirectional, with growing evidence to suggest that NAFLD is a driver, as well as a consequence, of systemic insulin resistance. From Thiagarajan P, Aithal G. *J Clin Exp Hepatol*. 2019; 9(4):515-21

1.1.4 Endpoints in NAFLD Trials

Although population prevalence of NAFLD is high, progression towards liver-related complications and extrahepatic outcomes is limited to those patients with steatohepatitis and, most importantly, hepatic fibrosis [10]. It is thus crucially important to be able to identify from the NAFLD population those individuals at higher risk of NASH and advanced fibrosis, in order to prognosticate, facilitate specialist input and prioritise high-risk patients for disease-modifying therapies. There remains a major unmet need for accurate, robust non-invasive surrogate endpoints for determining efficacy of interventions in NAFLD clinical trials. If resolved, these could accelerate therapeutic trial design, recruitment, data acquisition and availability of treatment options.

Staging NAFLD and determining efficacy of interventions in clinical trials has traditionally involved liver biopsy to grade disease severity using validated scoring tools such as the NAFLD activity score (NAS) for steatohepatitis, and the Kleiner fibrosis staging system [11]. Reliance on liver biopsy as a reference

standard has, however, limited the scope of research to date. Not only is biopsy associated with significant complications, vulnerability to sampling error and inter-observer variability, but it also lacks the ability to provide functional assessment of dynamic metabolic pathways *in vivo*. Further, its invasive nature renders it a suboptimal tool for screening and longitudinal monitoring on a population level.

Development and validation of a range of objective, quantitative biomarkers to accurately determine the presence of steatohepatitis and/or fibrosis has therefore been a research focus in recent years. Blood-based fibrosis markers either use a combination of common blood tests to generate predictive models of NAFLD progression (e.g. the NAFLD fibrosis score, FIB-4 and the BARD index), or measure direct markers of inflammatory activity (e.g. cytokeratin-18) and fibrosis (e.g. ELF, Fibrotest) [12]. Imaging-based biomarkers include magnetic resonance imaging (MRI) and spectroscopy (MRS), vibration-controlled transient elastography (TE) and MR elastography (MRE), which map hepatic anatomy, chemical composition and stiffness, respectively [13].

The advent of precision imaging has afforded a step change in the evaluation of liver architecture and metabolism *in vivo*. Together, magnetic resonance technologies provide detailed insight into hepatic structure and metabolic function across different stages of the NAFLD spectrum. Specifically, MRS has proven to be a robust and powerful tool in quantification of liver fat, glycogen stores and phosphorus metabolites, each probing different dimensions in the complex evolution of NAFLD. This is of particular relevance to the study of hepatic and whole-body insulin resistance, given the ability to simultaneously quantify glucose and lipid metabolism as well as energy homeostasis in the liver and skeletal muscle, the major insulin target tissues, using ^1H -MRS, ^{13}C MRS and ^{31}P -MRS respectively.

As higher MR field strengths (3 Tesla and 7 Tesla) become available in research settings, opportunities for evaluating substrate flux *in vivo* non-invasively are emerging. This builds a dynamic picture of liver metabolism, including processes key to the progression of NAFLD, such as disturbed mitochondrial energy kinetics and oxidative stress. Use of these modalities in combination may differentiate

between, for example, simple steatosis (NAFL) and NASH such that with time, MRI/MRS may demonstrate equivalence to liver biopsy, with added benefits of probing dynamic metabolic processes quantitatively *in vivo*. Validation of such measures against histology and mass spectrometry may ultimately enable their incorporation as important endpoints in NAFLD trials.

In conclusion, the slow nature of disease progression in NAFLD, heterogeneity of therapeutic targets and well-established limitations of serial liver biopsy to evaluate effects of intervention have significantly hampered clinical trial design and development of effective therapies. These limitations have spawned huge research interest in the development of accurate, robust and reproducible non-invasive surrogate endpoints which may ultimately supplant biopsy in trials, facilitating pursuit of effective therapies (**Table 1**) [^{8, 14}].

Clinical Endpoints	Surrogate Markers	Non-invasive surrogate endpoints
All-cause mortality	Δ CTP and MELD scores	Direct and indirect biomarkers Cardiometabolic data in NASH
Liver-related mortality	Δ HVPG	Risk prediction tools: Platelet/spleen ratio Imaging: US, TE, CT, MRI
	Progression to cirrhosis	Risk prediction tools: APRI, NFS, BARD score, FIB-4, Forns score, AST: ALT ratio Wet Biomarkers: ELF, Pro-C3, CK18 Imaging: TE, MRI, MRE
Metabolic endpoints	Δ Liver fat (*)	MRI-PDFF †, ¹ H-MRS †, USS, TE with CAP
	Δ Insulin Resistance	Euglycaemic Hyperinsulinaemic Clamp, HOMA-IR, OGTT, HbA1C, fasting glucose; indirect calorimetry (metabolic flexibility)
	Δ Inflammation (*)	Risk prediction tools: NASH resolution score, OxNASH Wet biomarkers: ALT, CK18 Imaging: multiparametric MRI, MRS
	– Oxidative Stress	– Glutathione flux (¹³ C-MRS)
	– Energy Metabolism	– ATP flux (³¹ P-MRS)
	Δ Glycometabolic profile	Lipid profile, HbA1C, OGTT, fasting glucose, change in weight/BMI
Fibrosis Endpoints	Δ fibrosis stage (*)	Risk prediction tools: NAFLD fibrosis score, FIB-4, Fibrosis improvement score, Fibrometer Imaging: TE, MRE Wet biomarkers: ELF, Pro-C3

Table 1 Relevant endpoints in NAFLD clinical trials and proposed strategies for non-invasive quantitative assessment.

*Denotes parameters for which liver biopsy is currently the reference standard

† Denotes validated non-invasive markers

CTP = Child Turcotte Pugh, MELD = Model of End-Stage Liver Disease, APRI = AST to platelet ratio index, FIB-4 = fibrosis 4, ELF = extended liver fibrosis panel, CK18 = cytokeratin-18, US = ultrasound, TE = transient elastography, MRE = MR Elastography, MRS = MR spectroscopy, HOMA-IR = homeostasis model assessment of insulin resistance, OGTT = oral glucose tolerance test, HbA1C = Haemoglobin A1C, Pro-C3 = Pro-collagen 3, HVPG = hepatic venous pressure gradient

1.2 Mechanisms of NAFLD pathogenesis: Insulin resistance, Oxidative Stress and Mitochondrial Dysfunction

"Der Mensch ist, was er ißt" (Man is what he eats) – Ludwig Feuerbach, 1862 in Das Geheimnis des Opfers Oder der Mensch ist was er ißt

1.2.1 Lipid-Induced Insulin Resistance

The concept of lipid-induced insulin resistance is key to the pathogenesis of NAFLD. In this paradigm, energy intake in excess of energy expenditure saturates subcutaneous and visceral adipose tissue lipid stores. Subsequent spillover from adipose tissue leads to excess circulating free fatty acid (FFA), which is ultimately deposited in ectopic sites, including skeletal muscle and liver (**Figure 3**).

Ectopic lipid accumulation in skeletal muscle has been strongly implicated as an early event in the development of NAFLD and whole-body insulin resistance [15]. Under insulin-sensitive conditions, skeletal muscle is responsible for 80% of insulin-mediated glucose disposal in the postprandial state [16]. It follows that defective insulin signalling at the level of muscle will ultimately lead to whole-body insulin resistance. A series of studies (discussed below) in insulin-sensitive and matched insulin-resistant phenotypes support the hypothesis that muscular lipid accumulation impairs local insulin signalling, thus attenuating insulin-mediated glucose disposal and glycogen synthesis. Resultant local insulin resistance diverts the fate of ingested carbohydrate away from muscle glycogen synthesis and towards hepatic *de novo* lipogenesis (DNL), contributing to NAFLD and atherogenic dyslipidaemia [17].

Targeting skeletal muscle fat accretion presents a logical therapeutic approach for breaking the vicious cycle of lipid-induced insulin resistance and NAFLD.

To examine the relationship between skeletal muscle insulin resistance and NAFLD at its earliest stages, Petersen and colleagues explored the response to two high carbohydrate meals of young, healthy, lean insulin-resistant subjects (n=12) compared with age, BMI, activity and fat mass-matched insulin sensitive subjects (n=12) [18]. Utilising baseline and postprandial ¹H-MRS and ¹³C-MRS, the

group studied muscle and liver triglyceride and glycogen synthesis, respectively. Through measuring incorporation of deuterated water into plasma triglycerides, the group quantitatively determined postprandial fractional hepatic DNL. Novel findings included a 60% reduction in net muscle glycogen synthesis following meals in the insulin-resistant cohort, together with a 2.5-fold net increase in hepatic triglyceride synthesis and a 2.2-fold increase in postprandial fractional hepatic DNL in these individuals. These data suggest that selective skeletal muscle insulin resistance alters the pattern of carbohydrate energy storage, favouring development of NAFLD and dyslipidaemia, and may be the earliest harbinger of the metabolic syndrome.

Flannery and colleagues reported similar findings in an elderly population, incorporating $^2\text{H}_2\text{O}$ -based DNL measurement with ^{13}C and ^1H -MRS to demonstrate that muscle insulin resistance is associated with reduced net muscle glycogen synthesis and increased hepatic DNL [19]. Further evidence to support this hypothesis comes from another study utilising ^1H and ^{13}C -MRS in insulin-resistant individuals to demonstrate that a single 45 minute bout of exercise on an elliptical trainer increased postprandial muscle glycogen synthesis following carbohydrate ingestion, resulting in a 40% reduction in hepatic DNL and a 30% reduction in hepatic triglyceride [20]. Taken together, these data implicate skeletal muscle insulin resistance as an early therapeutic target, and suggest that improving muscle insulin sensitivity may be key to the prevention of NAFLD, atherogenic dyslipidaemia and frank type 2 diabetes mellitus in young, lean, insulin-resistant individuals.

Bril and colleagues (2016) elegantly combined ^1H -MRS and euglycaemic hyperinsulinaemic clamp studies in 352 individuals to explore the relationship between progressive increases in liver fat and metabolic health of the liver, muscle and adipose tissue as quantified by tissue-specific insulin sensitivity in those organs. The group demonstrated that the MRS-based cut-off in intrahepatic triglyceride (IHTG) for defining NAFLD (5.56%) correlates closely to the onset of hepatic and whole-body insulin resistance, but that further liver fat accumulation beyond this point was not associated with progressive hepatic insulin resistance [21]. This lends further credence to the use of MRS-based

measures of IHTG as an accurate barometer of metabolic health. However, it calls into question the premise of steatosis reduction as an important endpoint in itself when in fact, organ-specific insulin sensitivity and energy homeostasis may be more relevant surrogate endpoints for predicting metabolic outcomes.

The above studies firmly characterise skeletal muscle insulin resistance as a key pathological milestone in the development of the metabolic syndrome, including NAFLD. However, the causative factors generating an insulin resistant milieu at the level of the skeletal muscle, and in particular the role of intramyocellular lipid (IMCL), deserve further probing. Within muscle tissue, lipid moieties either accumulate as droplets within myocyte cytoplasm (IMCL), or are deposited along the fibres between muscle cells as interstitial triglycerides (extramyocellular lipids [EMCLs]) (**Figure 4**). The metabolic consequences of these fractions differ - EMCL is considered metabolically inert, whereas IMCL, if supply exceeds expenditure, directly impacts upon cellular insulin signalling [22].

Recent studies evaluating the impact of obesity *per se* on muscle insulin resistance suggest that drawing a linear conclusion between peripheral insulin sensitivity and body mass index is perhaps overly simplistic. For example, Weiss *et al* (2005) studied a group of obese, insulin resistant adolescents (n=14) with age, gender and body-composition matched insulin sensitive subjects (n=14). Utilising the euglycaemic hyperinsulinaemic clamp technique to quantify whole-body insulin sensitivity, together with ¹H-MRS to assess muscle fat fractions, the group demonstrated that obese, insulin resistant subjects had greater IMCL concentrations ($2.26 \pm 0.62\%$ versus $1.64 \pm 0.68\%$ of water peak, $p = 0.017$) compared with BMI-matched insulin sensitive subjects [23]. In healthy, insulin-sensitive volunteers, Boden *et al* (2001) acutely increased plasma FFA concentration by lipid/heparin infusion, showing that this was associated with a corresponding acute increase in gastrocnemius IMCL accumulation as well as a significant increase in peripheral insulin resistance using clamp techniques [24]. These observations support the hypothesis that it is not obesity *per se*, but the location and tissue-specific distribution of lipid fractions that influences the generation of whole-body insulin resistance.

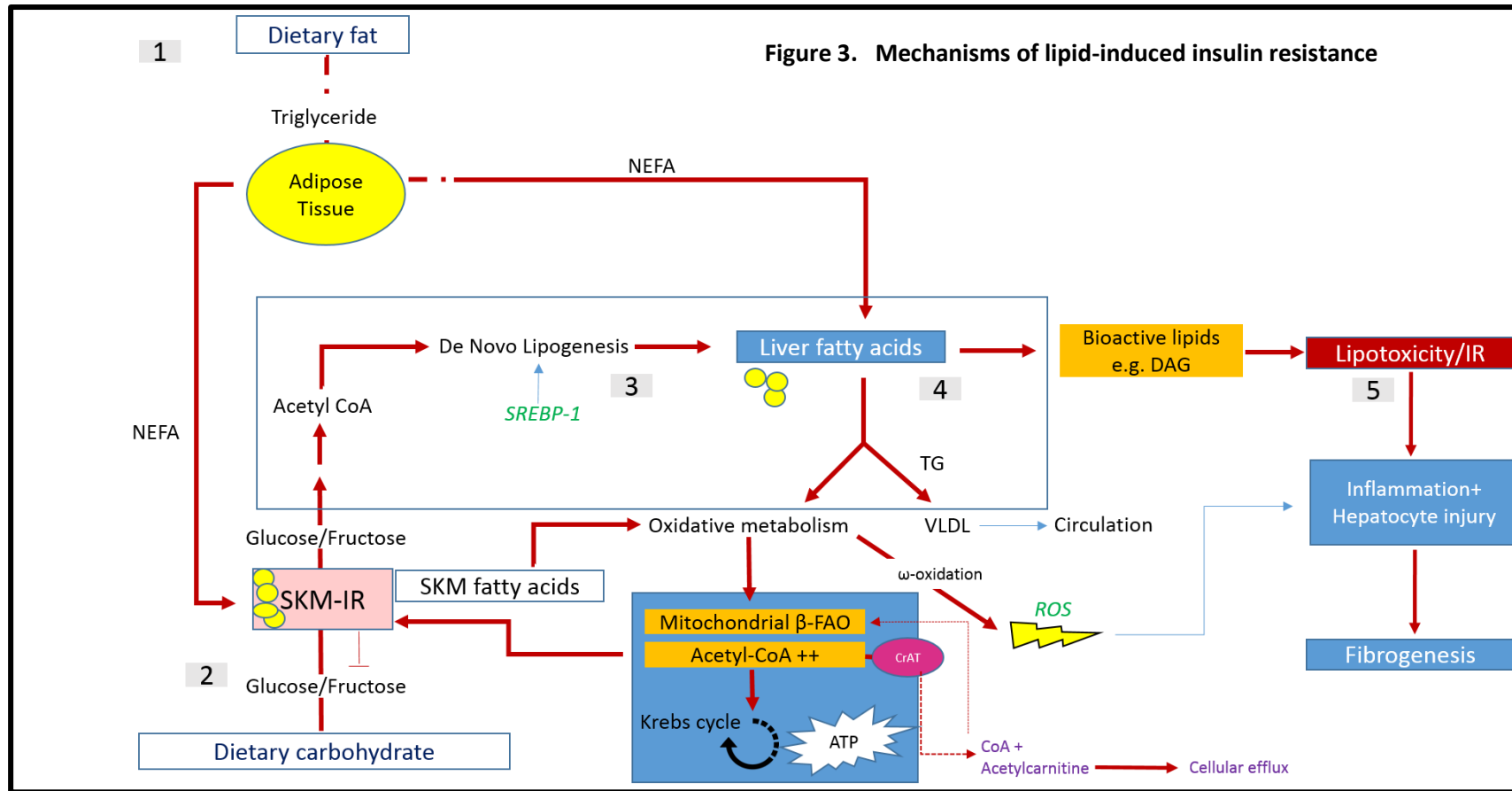


Figure 3. Mechanisms of lipid-induced insulin resistance in liver and muscle

1. An imbalance between energy intake and energy expenditure leads to ectopic lipid accumulation in skeletal muscle and liver, following saturation of adipose tissue stores. Local insulin resistance in adipose tissue also leads to unrestricted lipolysis, further exacerbating ectopic lipid deposition.
2. IMCL accumulation leads to impaired insulin signalling within myocytes and thus a reduction in glucose uptake, utilisation and glycogen synthesis by skeletal muscle. This glucose load is then diverted to the liver, where it is metabolised to free fatty acids (FFA) through de novo lipogenesis.
3. The liver thus receives dual oversupply of fatty acids, i.e. direct delivery from the portal circulation (through FFA release from visceral white adipose tissue) and also as a result of de novo lipogenesis of glucose substrate which has been diverted from insulin-resistant skeletal muscle.
4. Oversupply of liver lipid leads to accumulation of bioactive lipid precursors, such as diacylglycerol (DAG), as pathways for conversion to metabolically inert triglyceride are overwhelmed.
5. Abundant evidence now suggests that DAG accumulation is responsible for generation of local insulin resistance, both in the liver and in skeletal muscle (SKM). DAG initiates a series of downstream intracellular signalling cascades, mediated predominantly by protein kinase C epsilon (PKCε) in the liver and PKCθ in muscle, which ultimately serve to impair cellular glucose uptake and insulin signalling. Accumulation of bioactive lipid intermediates leads to lipotoxicity, hepatocellular injury, and, ultimately, inflammatory and fibrotic damage.
6. The fate of hepatic FFA rests in either oxidative metabolism or conversion to very low density lipoprotein (VLDL) and export into the systemic circulation. Mitochondrial pathways for β-oxidation of FFA are overwhelmed in the liver. This leads to cellular accumulation of long-chain fatty acyl CoA moieties, and their incomplete metabolism via alternative pathways such as ω-oxidation. This process generates inherently unstable compounds known as reactive oxygen species (ROS), which further contribute towards hepatocellular injury and inflammation.

The notion that IMCL accumulation has a potentially causal role in the development of systemic insulin resistance has gained traction in recent years; IMCL been consistently reported as a strong correlate of insulin resistance in non-diabetic individuals, including young, lean offspring of individuals with type 2 diabetes (T2DM) [25, 26].

MRS has been a valuable tool providing mechanistic insight into hepatic and whole-body insulin resistance. The original Randle hypothesis states that during insulin resistance, increased intramyocellular fatty acid β -oxidation due to circulating free fatty acid excess triggers a series of cellular negative-feedback mediated inhibitions of key enzymes resulting in decreased muscle glucose uptake [27]. In support of the Randle hypothesis, Constantin-Teodosiu et al (2012) used dichloroacetate to activate muscle pyruvate dehydrogenase complex following several days of high fat feeding, demonstrating that lipid induced-impairment of carbohydrate oxidation during exercise is reversed with dichloroacetate [28]. However, through using ^{31}P and ^{13}C MRS in humans under euglycaemic hyperinsulinaemic clamp conditions, Roden and colleagues have refuted this hypothesis, demonstrating a reduction in fatty acid oxidation together with impaired glucose transport and/or phosphorylation and a corresponding reduction in both the rate of muscle glycogen synthesis and glucose oxidation during intralipid infusion [29]. An imbalance between muscle and liver lipid supply and utilisation through β -oxidation is therefore postulated to be responsible for the generation of insulin resistance. Dysregulated integration of lipid and carbohydrate oxidation is ultimately responsible for the generation of insulin resistance, with several sites and mechanisms that could be implicated that are so far unresolved. This highlights the potential therapeutic significance of **altering mitochondrial fuel selection** in the face of increased lipid supply, as a means by which to ameliorate organ-specific insulin sensitivity and attenuate the deleterious consequences of lipid accumulation.

In summary, the body of mechanistic evidence to date provides a unifying hypothesis that ectopic lipid accumulation in specific sites such as skeletal muscle (and in particular IMCL) drives the development of local insulin resistance, thereby altering the pattern of glucose metabolism by diverting

carbohydrate substrate metabolism towards lipogenic pathways in the liver. This, in addition to the direct effect of increased caloric intake and unrestricted adipose tissue lipolysis, promotes fatty acid flux, accumulation of intrahepatic lipids and impaired insulin action. In the face of chronic energy surplus, the rate of lipid supply to insulin responsive tissues (i.e. liver and muscle) outstrips the rate of fatty acid oxidation (FAO), leading to accumulation of bioactive lipid species such as diacylglycerol (DAG). DAG has been strongly implicated in the development of insulin resistance in both muscle and liver tissue, through its ability to impair the actions of different isoforms of novel protein kinase C (θ in the muscle and ϵ in the liver) pathways, thereby impairing glucose transport via the GLUT-4 receptor at a cellular level (**Figure 3**) [30].

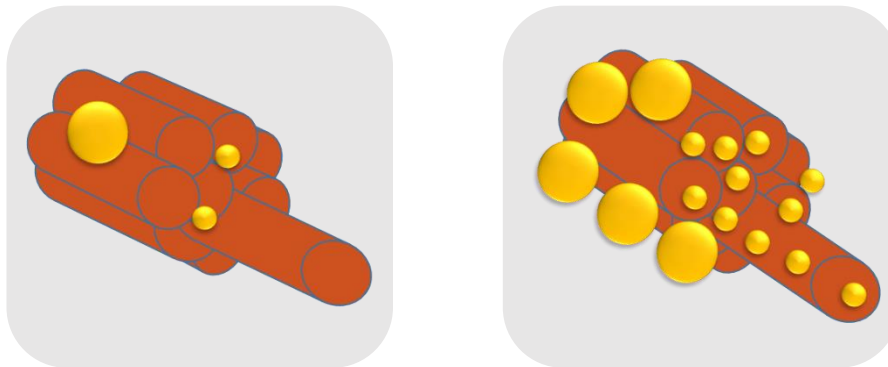


Figure 4 Skeletal Muscle Lipid Fractions (a) Schematic of a cross-section of skeletal muscle in a healthy subject, showing limited lipid deposition within and between muscle fibres. (b) Schematic of a cross section of skeletal muscle in insulin resistance, showing marked accumulation of intramyocellular and (to a lesser extent) extramyocellular lipid.

Large yellow circles = extramyocellular lipid (EMCL) i.e. intramuscular adipocytes.

Small yellow circles = intramyocellular triglyceride (IMCL).

Adapted from Laurens and Moro (2016). Intramyocellular fat storage in metabolic diseases. *Hormone molecular biology and clinical investigation*. 2016; 26(1):43-52.

1.2.2 Mitochondrial Oxidative Metabolism

Dysregulated mitochondrial performance is a pathogenic hallmark of obesity and type 2 diabetes. Incremental decay in mitochondrial biogenesis and function have been consistently demonstrated in both animal and human models of overnutrition, suggesting impaired cellular bioenergetics is a key milestone in the development and progression of a metabolically challenged phenotype [31]. The consequences of perturbed mitochondrial function are potentially far-reaching and impact on ATP production, gene expression, respiratory capacity and quality of key mitochondrial functions including oxidative metabolism.

There is evidence to suggest that the hepatic necroinflammation observed in NASH is mediated by mitochondrial metabolic dysfunction, and accumulation of toxic reactive oxygen species (ROS) which can compromise the fluency of β -oxidation [32, 33, 34]. In rodent models of obesity and T2DM, mitochondrial defects in β -oxidation have been found to precede and predispose to overt NAFLD and hepatic insulin resistance, suggesting a crucial role for mitochondria in protecting against these outcomes [35]. In skeletal muscle, reduced mitochondrial density and impaired mitochondrial function have been demonstrated in young, lean offspring of individuals with T2DM [36]. This is plausibly one of the earliest defects in the pathogenesis of whole-body insulin resistance, as impaired mitochondrial function (including attenuation in FAO) predisposes to lipid accretion, and the cascade of altered metabolic fluxes which ultimately leads to impaired insulin action.

Factors which regulate mitochondrial biogenesis and oxidative metabolism can have a beneficial effect on NASH in murine models [37]. While in humans there remains controversy over whether hepatic fatty acid β -oxidation is upregulated, diminished or unchanged in NAFLD [38, 39], what seems clear is that an imbalance exists between substrate availability and energy demand, resulting in accumulation of lipotoxic intermediary species (e.g. diacylglycerol), incomplete β -oxidation, and diversion towards oxidation via alternative pathways (**Figure 3**). Resultant inefficient utilisation of lipids as a fuel source

leads to lipotoxicity, triggering oxidative stress and pro-inflammatory events crucial to hepatocellular damage and the onset of fibrogenesis.

In a deeply phenotyped cohort of lean individuals and obese, insulin-resistant patients with and without NAFLD and NASH, Koliaki and colleagues describe a mitochondrial 'remodelling' process in which upregulated mitochondrial respiratory activity occurs in obese patients with (and without) NAFL, reflecting augmented energy metabolism via β -oxidation and the TCA cycle in response to substrate excess and higher bioenergetic demands. However, this so-called mitochondrial flexibility becomes abrogated in NASH, with a 40% reduction in mitochondrial respiratory rates compared to NAFL alone [40]. Further, NASH patients exhibit greater hepatic insulin resistance and oxidative stress, together with mitochondrial leakage and respiratory uncoupling, whereby increased respiration does not translate into efficient electron transport chain activity and ATP production therefore falls. Taken together, this data suggests that NASH is defined on a cellular level by increased oxidative stress burden, together with reduced antioxidant defences and inefficient mitochondrial bioenergetic coordination. **Capturing this failure of mitochondrial flexibility using non-invasive technology would therefore be of great clinical utility in determining the metabolic transition to NASH.** Furthermore, facilitating the ability of hepatic mitochondria to process increased lipid burden may form an avenue for therapeutic intervention.

Although MRI and mass spectrometry techniques are well established, they provide limited information regarding mitochondrial metabolism in NAFLD as they only measure static metabolite concentrations. Metabolite kinetics are by definition dynamic processes; capturing flux rates through enzymatic pathways yields deeper mechanistic insight into NAFLD pathogenesis. MRS is ideally suited to this endeavour, as molecules detectable in millimolar concentrations produce visible spectra, and repeated perturbations in metabolite kinetics following intervention can be quantitated at serial time points non-invasively [41]. Using this framework, strategies have been developed to directly determine

rates of hepatic mitochondrial oxidation as well as oxidative stress reactions non-invasively (see **Chapter 6**).

1.2.3 Modelling Hepatic Energy Kinetics

The liver plays a key role in orchestrating systemic glucose and lipid homeostasis, both by virtue of its position as the primary recipient of portal venous inflow, and as a coordinator of insulin action together with skeletal muscle and adipose tissue. Given its high metabolic activity and acute response to dietary manipulation, assessment of liver bioenergetic profile is of crucial importance in studying the metabolic syndrome and NAFLD, including the effects of dietary and pharmacological interventions. While capturing hepatic mitochondrial metabolism is possible using ^{13}C -MRS with tracer labelling techniques, the utility of localised ^{31}P MRS in quantitating hepatic ATP production has gained traction in recent years as the phosphorus isotope is present in high natural abundance, precluding the need for tracer infusion.

^{31}P -MRS enables quantification of inorganic phosphorus compounds within a specified hepatic volume of interest. These include phosphomonoesters (PME) and phosphodiester (PDE), as well as inorganic phosphate (Pi) and ATP. Together, PME and PDE provide a surrogate measure of cell membrane integrity and turnover, which can be used to assess fibrosis burden in diffuse liver diseases such as NAFLD [42]. Hepatic ATP and inorganic phosphate (Pi) levels, and more recently flux, are also detectable in the ^{31}P spectra. Their absolute quantification can provide insight into hepatic energy metabolism. This is of particular relevance in NAFLD, as progressive depletion in hepatic ATP stores is observed in individuals with the metabolic syndrome, including obesity and T2DM, reflecting impaired energy homeostasis associated with insulin resistance [43]. **Thus, non-invasive monitoring of hepatic ATP stores could serve as a quantitative imaging biomarker for NAFLD and NASH.**

Work in this unit has investigated the effects of an oral fructose challenge on hepatic ATP reserves (as measured by ^{31}P -MRS) and time to ATP depletion in healthy adult males across a spectrum of body

mass index (BMI). Fructose is well known to deplete hepatic ATP reserves through its rapid fructokinase-induced phosphorylation and lack of negative feedback regulation [44]. Through administration of a 75g oral fructose challenge followed by immediate ³¹P-MRS, Bawden *et al* (2016) demonstrated a linear negative correlation between time to minimum hepatic ATP levels and BMI, suggesting impaired hepatic energy metabolism with progressive increases in BMI (**Figure 5**) [45]. Further, rates of ATP recovery in the liver were negatively correlated with hepatic glycogen content as assessed using ¹³C MRS. Together, this data suggests that quantitative assessment of hepatic ATP reserves, and time to ATP recovery following dietary challenge, could serve as an early and sensitive indicator of insulin resistance and impaired hepatic energy homeostasis in NAFLD. ATP recovery times could serve as a dynamic ‘stress’ test for the metabolically challenged liver.

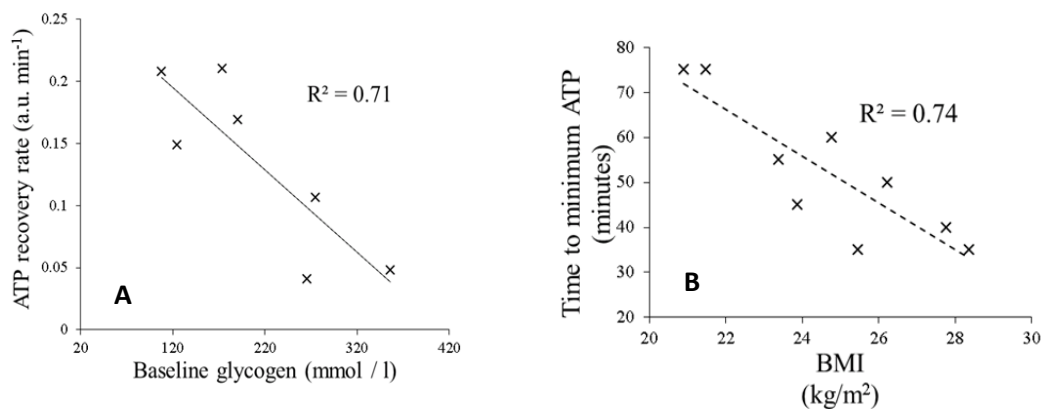


Figure 5 (A) Time to ATP recovery is inversely proportional to hepatic glycogen content (B) Increasing BMI is associated with a shorter time to hepatic ATP depletion. From Bawden, SJ *et al.* (2016). "Investigating the effects of an oral fructose challenge on hepatic ATP reserves in healthy volunteers: A ³¹P MRS study." *Clin Nutr* **35**(3): 645-649.

Szendroedi *et al* (2009) used both ¹H and ³¹P-MRS to quantify hepatic fat and energy metabolism in individuals with T2DM and two control populations, young lean controls (yCON) and age and BMI-matched controls (mCON). Combining these measurements with euglycaemic hyperinsulinaemic clamp studies, the group was able to accurately measure glucose and lipid homeostasis among diabetic individuals and control subjects. In so doing, they confirmed that hepatic γATP levels and Pi were lower in T2DM individuals compared with mCON and yCON. This finding was true even after adjustment for hepatic fat, and ATP and Pi levels were negatively correlated with hepatic insulin

sensitivity (iEGP) [46]. Taken together, this data suggests that perturbed hepatic energy metabolism may be the precursor towards overt fat development. Measuring hepatic ATP levels non-invasively could therefore provide a more sensitive imaging biomarker with which to determine those patients at high risk of steatosis and progressive liver disease.

Use of saturation transfer enables rate of hepatic ATP turnover to be measured through calculation of unidirectional forward exchange flux of the Pi-to-ATP reaction. This dynamic exchange rate constant (k) provides a surrogate, rather than direct, measure of mitochondrial oxidative metabolism. Nevertheless, high natural abundance of phosphorus metabolites *in vivo* negates the requirement for tracer labelling techniques, enhancing clinical applicability of this method in the assessment of hepatic energy metabolism. Schmid and colleagues (2011) first demonstrated that ATP production in T2DM individuals without clinical liver disease is lower than that of otherwise matched control subjects without T2DM, supporting a close association between insulin resistance and perturbed hepatic energy metabolism [47].

In a cross-sectional study assessing reproducibility of localised *in vivo* ^{31}P -MRS of the liver at 7T, Valkovic and colleagues (2014) determined differential ATP turnover between histological subtypes of NAFLD. The group demonstrated that, in comparison with healthy volunteers, individuals with NASH had significantly lower ATP production ($k=0.17 \pm 0.04$ Mm/s versus 0.31 ± 0.03 Mm/s, $p < 0.01$). Those with simple steatosis (NAFL), however, had baseline Pi to ATP exchange rates very similar to healthy controls ($k=0.30 \pm 0.05$ Mm/s) [48]. More recently, Traussnigg and colleagues (2017) employed saturation transfer ^{31}P -MRS at 7T in a prospective clinical trial to differentiate ATP flux in patients with biopsy-proven simple steatosis (NAFL) and NASH. The group confirmed that ATP synthesis rates are significantly decreased in NASH compared with NAFL (0.21 ± 0.08 Mm/s versus 0.38 ± 0.08 Mm/s, $p = 0.003$) phenotypes. Taken together, these data highlight disturbed energy metabolism in NASH compared with NAFL and support the hypothesis that hepatic mitochondrial dysfunction lies at the heart of this transition [49].

Accurate and reproducible methods for quantifying dynamic ATP turnover in the liver utilising ^{31}P -MRS with saturation transfer could enable the impact of intervention on hepatic energy kinetics to be assessed in longitudinal studies. This endpoint is difficult to capture utilising the current 'gold' standard of liver biopsy due to its inherently static nature. Incorporation of precision imaging with dynamic metabolic flux quantitation could therefore serve as a robust tool with which to assess the impact of intervention on key metabolic processes in clinical research.

1.3 Dietary Interventions in NAFLD

While novel pharmacotherapies are in experimental stages of development, each targeting different mechanisms in NAFLD pathogenesis, their eventual availability is likely, at least in the short-term, to present great cost to healthcare systems and taxpayers. Diet and lifestyle remain current standard of care, but given the prevalence of NAFLD and its deleterious consequences, there exists an urgent clinical need for immediately available adjunctive therapies to attenuate global disease burden.

Altering macronutrient composition is well known to affect liver fat accumulation, both acutely and in the long term. For example, studies investigating the effect of hypercaloric diet on liver fat have consistently concluded that hypercaloric diets enriched with either fructose or glucose acutely increase liver fat. Sevastianova *et al* (2009) evaluated the effect of a 3-week hypercaloric diet, in which participants consumed >1000 kcal/day and in which 98% of excess calories were provided as sugars. The group demonstrated a mean increase in liver fat of 27% (as measured using ^1H -MRS) after three weeks of overfeeding [50]. An increase in plasma *de novo* fatty acids suggested that much of this liver fat increase was mediated through upregulated hepatic *de novo* lipogenesis.

Hypocaloric diets involving either low carbohydrate or low fat composition have revealed mixed results; however, reducing total carbohydrate intake appears to confer a metabolic advantage with respect to liver fat reduction. Whether this occurs through attenuation of hepatic DNL (i.e. a specific effect of limiting carbohydrate intake), or through simply achieving negative energy balance, is

unclear. Browning *et al* (2011) demonstrated that low carbohydrate diet is more effective at reducing liver fat than reduced total calories without alteration of macronutrient composition [51]. However, Haufe and colleagues (2011) demonstrate that total caloric deficit reduces liver fat, regardless of whether this is achieved through restricting fat or carbohydrate intake [52].

Iso-caloric diet studies have further addressed the role of macronutrient composition on liver fat while attempting to negate the effect of weight loss. In this context, macronutrient composition does not appear to affect liver fat content and increased free sugar intake does not lead to an increase in liver fat. However, diets enriched with monounsaturated fatty acids (MUFA) appear to be more effective than high-carbohydrate low fat diets at attenuating liver fat. This could plausibly be explained by the ability of mono-unsaturated fatty acids to upregulate activity of the enzyme lipoprotein lipase in adipose tissue, thus limiting delivery of non-esterified fatty acids to the liver [53,54].

Further questions arise as to the role of proteins, and specifically *type* of protein ingestion (animal protein versus vegetable protein) in NAFLD. In rodent models, the most effective driver of NAFLD appears to be a low-protein, high fat diet (somewhat reflecting a modern 'Western' diet), whereas diets high in protein reduce probability of fatty liver development. It has been postulated that this phenomenon may be partly the effect of the 'protein leverage' paradigm, in which high protein intake is associated with satiety whereas low protein intake simply encourages further caloric consumption [55]. Furthermore, diets high in vegetable protein appear to have a metabolic benefit in NAFLD compared to diets rich in animal-derived protein [56].

Markova *et al* (2017) conducted a detailed prospective metabolic study in 37 individuals with type 2 diabetes on an isocaloric diet plan for 6 weeks, (30% protein, 40% carbohydrate, 30% fat). Eighteen patients were allocated to a diet high in animal protein and 19 were allocated to a diet high in plant protein. Euglycaemic hyperinsulinaemic clamp studies were conducted at baseline and post-intervention to determine the metabolic effects of each diet. After 6 weeks, the group concluded that both animal and plant proteins reduced intrahepatic lipid by 36-48%, with improvements in insulin

sensitivity parameters in both groups. Vegetable protein intake is considered more beneficial than animal protein intake due to reduced methionine production (methionine-rich diets have been shown to promote insulin resistance) [57].

While a specific diet-plan in NAFLD is not forthcoming, an optimal diet for preventing further fat accumulation appears to be 40-50% carbohydrate, 20% protein and 30% fat [58]. While wholesale alterations in dietary macronutrient composition are achievable, long-term compliance data is lacking. Given the multifactorial aetiopathogenesis of NAFLD, interest in nutritional supplements with anti-inflammatory, anti-fibrotic and potentially antioxidant properties has gained traction in recent years [59]. Some of these substances confer several beneficial properties on whole-body glucose and lipid metabolism, most are widely available and have a well-established safety profile. While human studies evaluating the effect of these so-called 'nutraceuticals' on liver fat itself are limited, there is abundant data to support their use in the broader context of the metabolic syndrome given their lipid-lowering, antihypertensive and anti-inflammatory effects [60]. **Table 2** lists micronutrient supplements with potential health benefits in NAFLD and the major human studies supporting their use.

As nutritional intervention forms the universal first step in treating metabolically challenged phenotypes, it is likely that early intervention with evidence-based supplementation regimens could be applied in routine clinical practice to curb NAFLD disease progression.

Nutrient	Author (journal, year)	Study population	Sample size	Duration	Diagnostic modality	Primary Outcome Measure	Result	P value
Vitamin E	Sanyal (NEJM, 2010)	Biopsy-proven NASH without diabetes	Vitamin E 84 Pioglitazone 80 Placebo 83	96 weeks	Histology (paired biopsies)	Improvement in histological features of NASH	Significant improvement in histological features of NASH in Vitamin E group Reduced hepatic steatosis No improvement in fibrosis score	0.001 0.005 0.24
Omega-3 fatty acids (Omacor)	Scorletti (Hepatology, 2014)	NAFLD diagnosis based on histology/imaging/risk factors for MetS	Omacor 51 Placebo 52	15-18 months	Magnetic Resonance Spectroscopy (intrahepatic triglyceride, %)	Change in intrahepatic triglyceride (IHTG), %	No significant reduction in IHTG with Omacor/	0.48
Vitamin D	Sakpal (JGHF, 2017)	NAFLD diagnosis based on USS (+/- elevated ALT)	Vitamin D 51 Placebo 30	6 months	Ultrasound	Improvements in serum ALT and HOMA-IR	Significant reduction in ALT in Vit D group No change in HOMA-IR	<0.001 0.162
Resveratrol	Heebøll (Scand J Gastro, 2016)	Biopsy-proven NAFLD and elevated ALT/AST	Resveratrol 14 Placebo 14	6 months	Histology (paired biopsies in 19 patients); MR spectroscopy in all	Change in plasma ALT	Resveratrol vs placebo: ALT reduction 104 to 74 IHTG reduction by 3.8% No histological improvement	0.049 0.026
Probiotics	Kobyliak (2018)	NAFLD patients with T2DM (N=58)	Placebo = 28 Probiotic = 30	8 weeks	Ultrasound	Reduction in FLI index in Probiotics vs placebo groups	Significant reduction in FLI index in probiotic group (84.33±2.23 to 78.73±2.58)	<0.001
Obeticholic Acid (OCA)	Neuschwander-Tetri (2015); FLINT trial	Biopsy-proven NASH (non-cirrhotic)	OCA = 141 Placebo = 142	72 weeks	Histology	Improvement in histological features of NASH without worsening of fibrosis	Significant improvement in histological features of NASH in OCA group	0.0002

Table 2 Summary of salient human micronutrient trials in NAFLD

1.4 L-Carnitine: Physiology, Fuel Selection and Therapeutic Potential

1.4.1 Background

L-Carnitine is a naturally occurring water-soluble quaternary amine, which acts as a crucial mediator of fatty acid metabolism *in vivo*. Carnitine serves two critical intracellular metabolic functions (**Figure 6**). First, it promotes mitochondrial lipid β -oxidation through translocation of long-chain fatty-acid moieties from the cytosolic compartment to the mitochondrial matrix. Second, carnitine favours glucose uptake in insulin-sensitive tissues by acting as a buffer for excess acetyl groups produced through oxidative metabolism [61]. This buffering action lowers the mitochondrial ratio of acetyl-Coenzyme A/Coenzyme A (CoA) through formation of acetylcarnitine, a membrane-permeable carnitine ester, and its efflux from the mitochondrial matrix [62]. Efflux of acetyl groups from cellular compartments is important for regulating mitochondrial fuel selection and improving metabolic flexibility, i.e. the ability of insulin-sensitive tissues to switch substrate from fat oxidation in the fasted state, to carbohydrate oxidation in the fed (hyperinsulinaemic) state. In addition, buffering and exporting excess acetyl groups liberates free CoA to sustain β -oxidation in the face of high substrate availability.

Tissue L-carnitine reserves are reduced in animal models of insulin resistance, including transgenic diabetic mice and high-fat diet (HFD) fed rats, together with impaired metabolic flexibility [63,64]. Dietary L-carnitine supplementation has been shown to restore mitochondrial performance, enhance insulin sensitivity and salvage metabolic flexibility in both instances. These properties have important implications for disorders underpinned by dysregulated metabolism, rendering carnitine an attractive target for therapeutic intervention in conditions associated with insulin resistance.

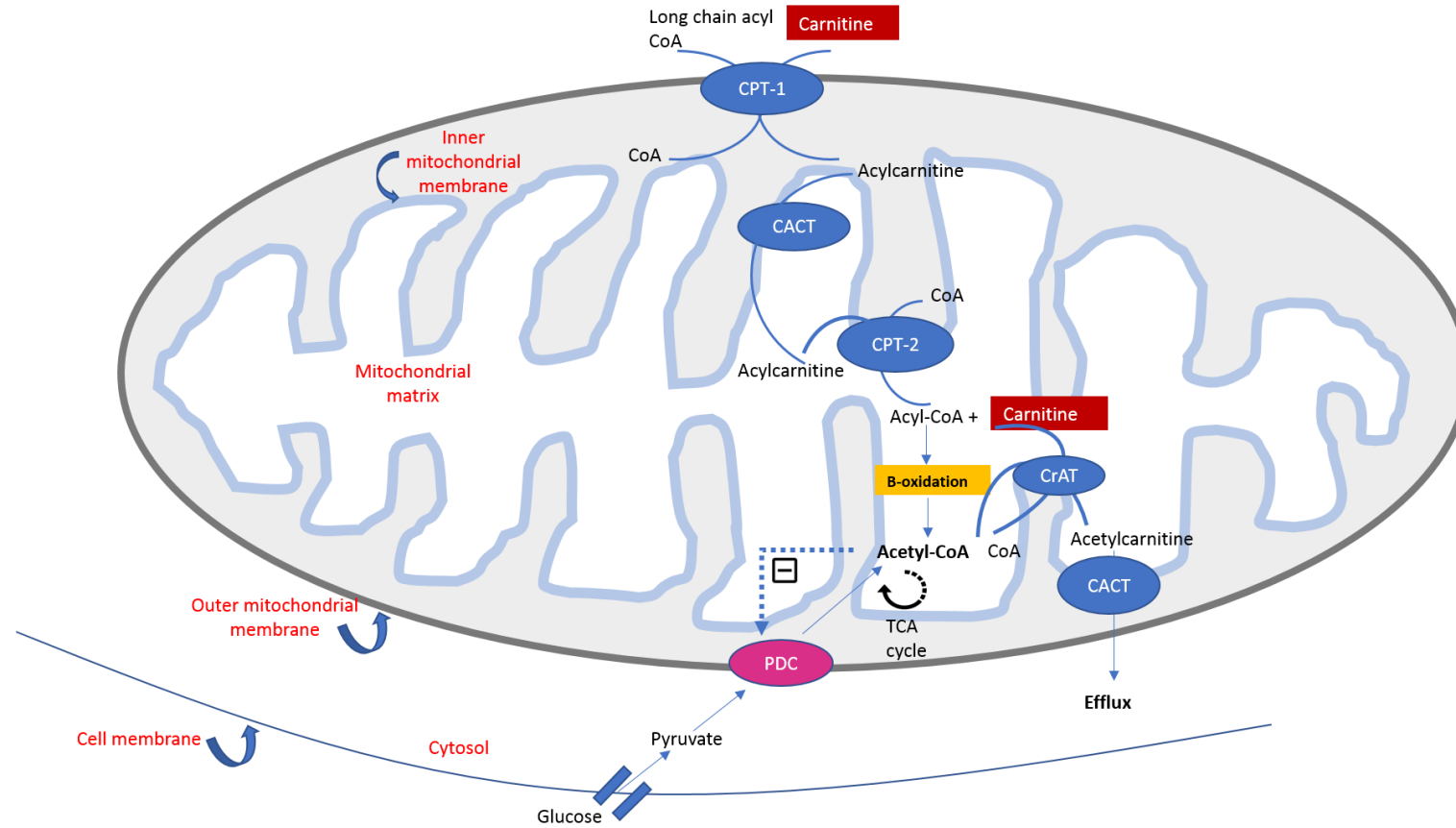


Figure 6. The Carnitine Shuttle

Carnitine acts as a crucial cofactor in the translocation of long-chain fatty acyl-CoA moieties from the cytoplasmic compartment to the mitochondrial matrix, facilitating their use as a fuel through mitochondrial β -oxidation.

1. The enzyme carnitine palmitoyltransferase-1 (CPT-1), located on the outer mitochondrial membrane, converts long-chain acyl-CoA to acylcarnitine and CoA, utilising cytosolic free carnitine.
2. Acylcarnitine is transported via the enzyme carnitine acylcarnitine translocase (CACT) across the inner mitochondrial membrane into the mitochondrial matrix.
3. Acylcarnitine and CoA are converted via the inner mitochondrial enzyme CPT-2 back into their original acyl-CoA and free carnitine moieties.
4. Long chain acyl-CoA subsequently undergoes beta-oxidation into short chain acetyl-CoA, which can enter the tricarboxylic acid cycle to yield energy in the form of ATP through oxidative phosphorylation.
5. Intramitochondrial carnitine buffers excess acetyl-CoA via the enzyme carnitine acetyltransferase (CrAT) to yield acetylcarnitine and free CoA. Acetylcarnitine is transported out of the mitochondria and ultimately, out of the cell and can be eliminated via urinary excretion.

Note: accumulation of intramitochondrial acetyl-CoA inhibits the cytosolic pyruvate dehydrogenase complex (PDC), thus limiting cellular glucose entry and glycolytic metabolism. Free carnitine can buffer excess acetyl-CoA and thus, indirectly, facilitate glucose disposal in insulin-sensitive tissues.

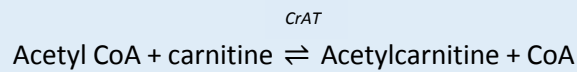
1.4.2 Historical overview

Over a century ago, the compound L-carnitine (derived from the Latin ‘carnis’, meaning ‘flesh’) was discovered in vertebrate muscle extracts by separate research groups in Germany (Kutscher, 1905) and Russia (Gulewitsch and Krimberg, 1905) [65, 66]. Elucidation of its biochemical structure and optical properties took a further 20 years; in 1927 carnitine was finally established as the quaternary amine 3-β-hydroxy-γ-trimethylaminobutyric acid, with the empirical formula $C_7H_{15}NO_3$. Its biological function, however, remained a mystery until several years later. Initial clues as to the essential physiological function of L-carnitine came from a series of experiments conducted by Fraenkel and Blewett (1947) in the mealworm *Tenebrio molitor*. The group found that mealworm larvae grown in carnitine-deficient mediums accumulated intracellular fat but died from starvation [67, 68, 69].

Fritz and colleagues (1959) subsequently isolated rat liver homogenates and confirmed that addition of L-carnitine augmented mitochondrial β-oxidation of the long chain fatty acids palmitate and stearate [70]. On this basis, the group hypothesised that carnitine facilitates translocation of long chain fatty acyl derivatives into “enzymatically active intramitochondrial sites” for oxidative metabolism. This gave rise to the hypothesis that carnitine is an essential metabolic cofactor for the translocation of long-chain fatty acyl CoA moieties from cytosolic to mitochondrial cellular compartments, a mechanism subsequently validated in different mammalian tissues [71].

A second role for carnitine in the modulation of carbohydrate metabolism during exercise was discovered in pioneering work by Childress and colleagues (1967), who studied fuel selection in the blowfly flight muscle *in vitro*. Despite not oxidising lipids during flight, the blowfly flight muscle was found to be rich in carnitine and the enzyme carnitine acetyltransferase (CrAT) [72]. On initiation of flight, glycolytic flux within the flight muscle increased, leading to a corresponding increase in intracellular pyruvate and (via the pyruvate dehydrogenase complex, PDC) Acetyl CoA formation, at a rate exceeding its utilisation by the tricarboxylic acid (TCA) cycle. Simultaneously, formation of acetylcarnitine was increased 4-fold, leading the group to hypothesise that, by acting as a buffer for

excess Acetyl CoA, free carnitine lowers the intramitochondrial Acetyl CoA/CoA ratio, ensuring a viable pool of free CoA to facilitate an oxidative rather than anaerobic fate for cytosolic pyruvate.



During high intensity exercise, the intracellular ratio of Acetyl CoA/free CoA increases as a result of increased glycolytic flux [73]. Through end-product inhibition, this increased ratio blunts PDC activation and becomes limiting to pyruvate flux (**Figure 6**). By acting as an acceptor of acetyl groups, L-carnitine lowers the intramitochondrial Acetyl CoA/CoA ratio, thereby removing allosteric inhibition of PDC and facilitating glucose uptake. The metabolic advantages of this buffering system are twofold: first, limiting cellular lactate production and second, facilitating continued production of ATP via the TCA cycle (rather than through glycolysis alone) [74]. Through modulating the intramitochondrial Acetyl CoA/CoA ratio, L-carnitine therefore facilitates non-oxidative glucose disposal in skeletal muscle and plausibly attenuates fatigue development through limiting lactate production. This model has been successfully borne out in human skeletal muscle *in vivo* [75].

Taken together, these findings underscore key metabolic properties of L-carnitine at the nexus of carbohydrate and lipid metabolism, as a pivotal mediator of intramitochondrial bioenergetics [76]. Research in recent decades has focused on carnitine-mediated integration of muscle fuel metabolism in the context of both exercise and conditions typified by mitochondrial inflexibility. Through its ability to regulate mitochondrial substrate selection and trafficking, and in particular its function as an acyl group buffer, carnitine performs a central role in limiting mitochondrial carbon stress and restoring metabolic flexibility.

1.4.3 L-Carnitine Homeostasis and Kinetics

L-carnitine homeostasis *in vivo* is maintained through a combination of dietary intake, endogenous biosynthesis from the amino acids lysine and methionine, and efficient renal reabsorption (**Figure 7**). Predominant sources of dietary carnitine include red meat, asparagus, dairy products and fish. Dietary intake accounts for the majority of the body carnitine pool, ranging from 1-15 $\mu\text{mol/kg/day}$ depending on carnitine content in the foods ingested [77]. Endogenous biosynthesis (predominantly in the liver and kidneys), in contrast, accounts for approximately 1-2 $\mu\text{mol/kg/day}$ [78]. Bioavailability of dietary carnitine appears to depend on the renally filtered load, with renal reabsorption displaying *saturation kinetics* [77]. Thus, in the face of increased circulating carnitine concentrations (whether through dietary supplementation or acute intravenous infusion) reduced efficiency of renal reabsorption and augmented urinary clearance is observed. This adaptive response maintains circulating carnitine concentrations within a narrow homeostatic range despite variability in dietary intake, to prevent frank carnitine deficiency.

Given this 'threshold' effect, the question arises as to whether augmenting the body carnitine pool is possible with dietary supplementation. The oral bioavailability of L-carnitine has been demonstrated in several studies to be in the order of 10-20%, with plasma concentrations returning to baseline 24 hours after a single dose [79,80]. However, multiple dose administration of oral L-carnitine (2 g per day in three divided doses) was shown to elevate steady state plasma carnitine concentrations in healthy adult males compared to an unsupplemented cohort. Further work in exercising cohorts has demonstrated modest elevations in skeletal muscle carnitine content following chronic dietary supplementation (1 gram per day for 120 days) [81]. Thus, chronic multiple-dose dietary supplementation is capable of augmenting tissue and circulating L-carnitine concentrations despite the saturability of renal reabsorption [77].

However, until recently, attempts to measurably augment tissue carnitine concentrations by dietary or intravenous means have produced equivocal results. It is worth noting that carnitine transport into

muscle occurs against a sharp concentration gradient and is therefore dependent upon active transport via a sodium-dependent organic cation-2 transporter (OCTN2), which may be activated in the insulin-stimulated state. Leveraging this hypothesis, Stephens *et al* (2006) administered a supraphysiological insulin infusion during hypercarnitinaemia, demonstrating acutely increased skeletal muscle carnitine content in healthy males (n=8), which was accompanied by an increase in muscle OCTN2 messenger RNA (mRNA) expression [82]. Further work in the same unit used an insulinogenic stimulus in the form of carbohydrate supplementation in conjunction with chronic dietary carnitine supplementation, to demonstrate that whole-body carnitine retention in healthy subjects can indeed be augmented by dietary means alone, *and that this process is dependent on hyperinsulinaemia* [83].

In mammalian tissue, L-carnitine exists in equilibrium in its free and esterified forms, the most abundant of which is acetylcarnitine. While carnitine is ubiquitous, it is highly concentrated in tissues with high energy requirements and thus high rates of ATP turnover [74]. This is consistent with experiments demonstrating that more than 95% of the body's carnitine pool is sequestered in skeletal muscle [84,85] (**Table 3**). Therefore, plasma carnitine levels are not necessarily representative of the body's carnitine status.

Landmark work by Rebouche *et al* (1991) using radiolabelled tracer methodology enabled derivation of a mathematical three compartment open model of carnitine kinetics in humans (**Figure 8**). The group administered intravenous radiolabelled [Methyl-³H] carnitine tracer in six healthy human volunteers to determine the metabolic fate of dietary carnitine, defining three discrete body carnitine pools: (1) extracellular fluid (including plasma), (2) small, rapidly equilibrating tissues (most likely to represent liver and kidneys) and (3), large, slow turnover tissues (skeletal muscle) demonstrating that urinary excretion is increased in parallel with dietary carnitine content and oral bioavailability is higher (66-86% versus 54-72%) in low-versus-high carnitine diets [78]. Incorporation of carnitine into skeletal

muscle is clearly a slow process (uptake in the order of several weeks); therefore to obtain any appreciable, sustained increase in muscle carnitine content would require chronic supplementation.

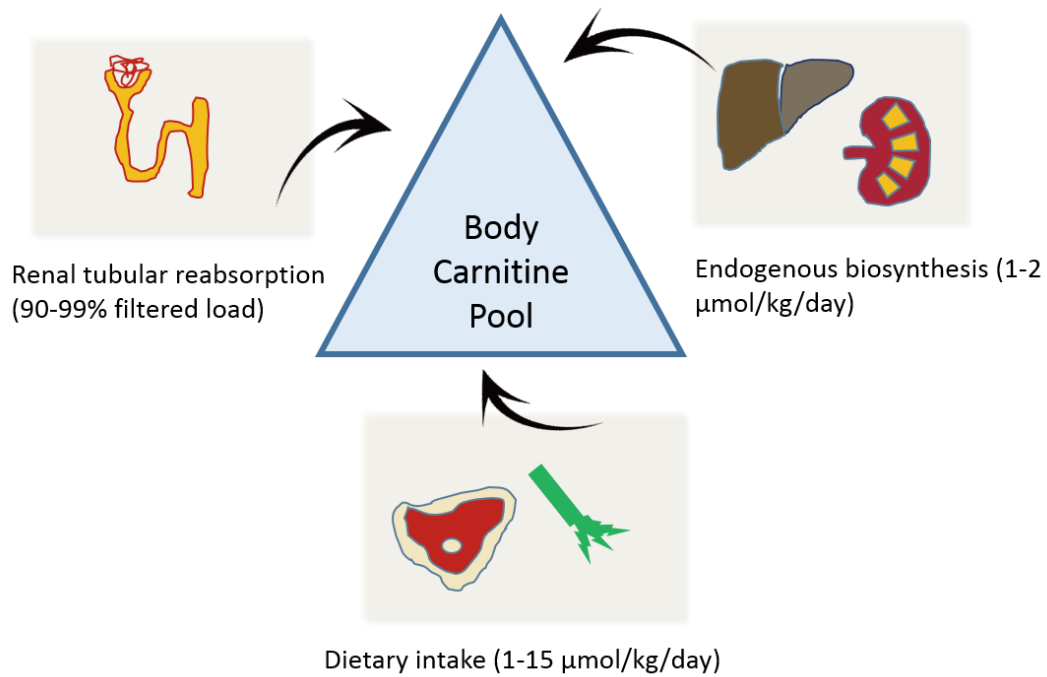


Figure 7. Whole body L-carnitine homeostasis is reliant on dietary intake, endogenous synthesis and renal tubular excretion and reabsorption.

Compartment	Concentration (μmol/kg) [64]	Estimated content (mmol)	Estimated content (% total carnitine pool).
Extracellular fluid (including plasma)	40-50	0.5	-0.4
Liver	500-1000	1.3	-1
Kidneys	330-600	0.2	-0.2
Skeletal muscle	4000	126.4	98
Total		128.4	

Table 3. Distribution of L-carnitine among different tissue compartments.

Adapted from Evans et al, 2003.

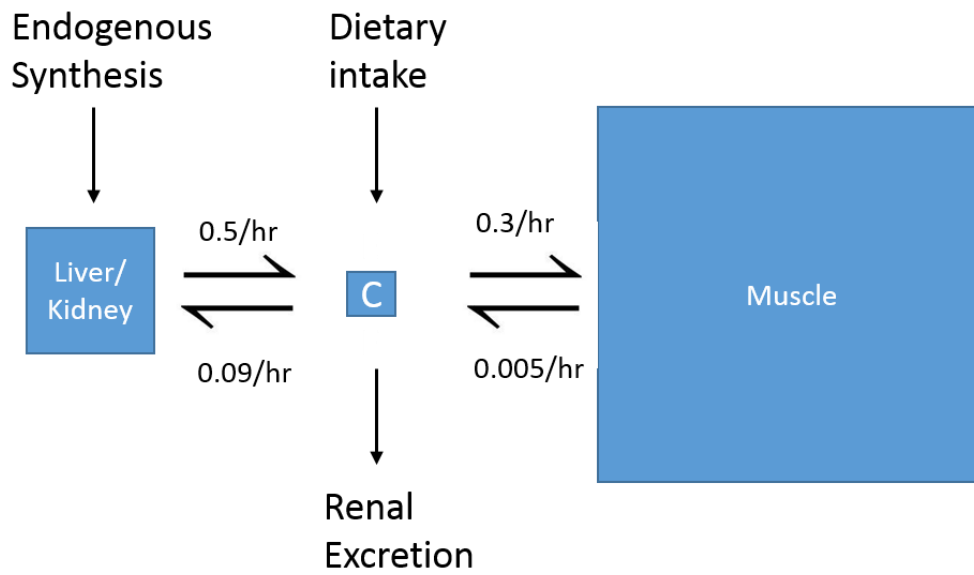


Figure 8. L-carnitine kinetics. Three compartment open model for Carnitine kinetics in humans. Based on radiotracer experiments conducted by Rebouche *et al* (1984). The rate constants represent the fractional content of each compartment moving into the receiving compartment per unit time. For example, the fraction of muscle content moving into the central pool per hour is 0.005 (0.5%).

C= central compartment i.e. extracellular fluid

1.4.4 Role of L-carnitine in Cellular Energy Metabolism and Fuel Selection

Sophisticated physiological studies in healthy volunteers have described carnitine-induced alterations in cellular energy kinetics, substrate metabolism and fuel selection. Wall *et al* (2011) conducted a placebo-controlled randomised trial in healthy male athletes (n=14) to establish the effects on skeletal muscle energy metabolism and fuel selection of 24 weeks' chronic carnitine loading [75]. Work output, muscle glycogen stores, total muscle carnitine content and PDC activation were quantified at baseline and post-intervention. The group confirmed that dietary carnitine loading (2 grams BD) for a 24-week period, together with insulinogenic stimulus in the form of carbohydrate supplementation, is capable of augmenting muscle free carnitine concentration. Further, this was associated with muscle glycogen sparing during low intensity exercise (consistent with increased muscle lipid oxidation as a primary fuel source) and an increase in glycolytic flux during high intensity submaximal exercise (80% $\dot{V}O_2$ max), limiting anaerobic respiration.

Thus, carnitine has a dual role in muscle fuel metabolism through (a) mediating translocation of long-chain fatty acids into the mitochondrial matrix for β -oxidation and (b) acting as an acetyl group buffer in conditions of high intensity exercise, replenishing the cytosolic free CoA pool and thus optimising the Acetyl CoA/CoA ratio to attenuate Acetyl CoA-mediated inhibition of PDC flux (**Figure 9**). Its particular glycogen-sparing role at 50% $\dot{V}O_2$ max suggests that L-carnitine supplementation in conjunction with low intensity exercise might form an attractive therapeutic avenue for insulin resistant patients with the metabolic syndrome.

Porter and colleagues (2017) employed a murine model to establish the metabolic effects of mildronate, an inhibitor of endogenous carnitine biosynthesis. Mildronate supplementation depleted muscle carnitine content, which was associated with altered substrate metabolism, including a reduction in whole-body fat oxidation, increased carbohydrate oxidation and a reduction in glycogen content in both liver and muscle [86]. This work consolidates a primary role for L-carnitine as a mediator of fuel selection *in vivo* and a facilitator of glucose disposal in insulin responsive tissues

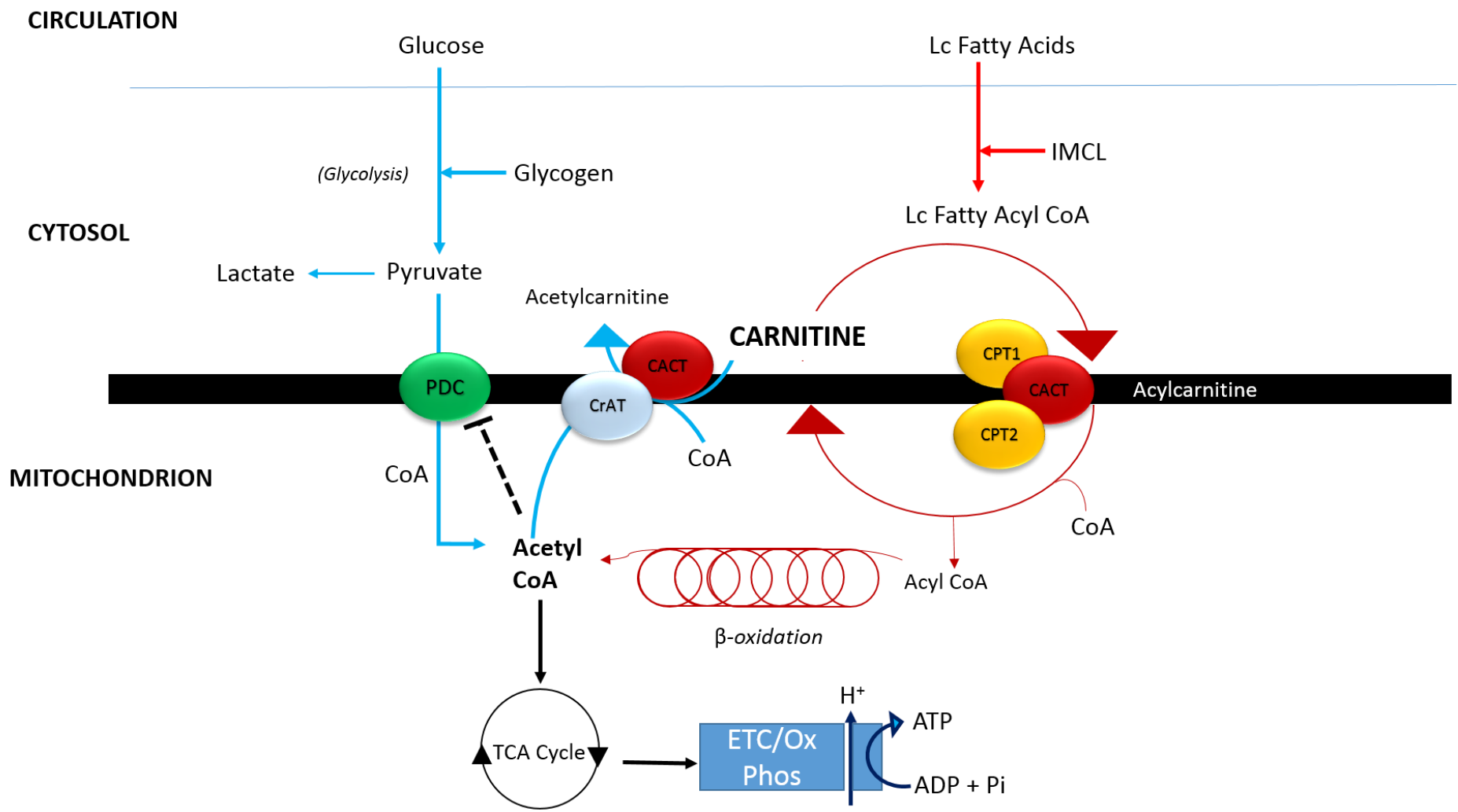


Figure 9. Mechanistic Model of Carnitine Action

Adapted from Stephens et al (2007). The duality of L-carnitine's metabolic role at the nexus of Carbohydrate and Lipid metabolism is shown. L-carnitine facilitates translocation of long-chain fatty acyl CoA moieties from cytosolic compartment to mitochondrial matrix, enabling beta-oxidation to Acetyl CoA (red arrows). L-carnitine also buffers excess acetyl-CoA during conditions of high glycolytic flux e.g. intense exercise (blue arrows). CoA = coenzyme A, Lc = long chain, ETC = electron transport chain, OxPhos = oxidative phosphorylation, PDC = pyruvate dehydrogenase complex, CACT = carnitine acylcarnitine transferase, CrAT = carnitine acetyltransferase, CPT1 = carnitine palmitoyltransferase 1, CPT2 carnitine palmitoyltransferase 2, IMCL = intramyocellular lipid

1.4.5 L-Carnitine as a candidate treatment for insulin resistance

The role of carnitine as a key regulator of intracellular bioenergetics has gained traction in the search for broadly applicable treatments for metabolic disorders, including obesity and T2DM. The ability of carnitine to regulate muscle mitochondrial fuel selection, through promoting both lipid oxidation and non-oxidative glucose disposal, renders it an attractive target for therapeutic intervention in the context of insulin resistance.

At its core, NAFLD is a disorder of mitochondrial fuel selection. Cumulative evidence in both animal and human models suggests that intrahepatic and skeletal muscle fatty acid transport and oxidation is impaired in NAFLD and insulin resistance, such that excessive lipid accretion is not matched by efficient utilisation [87,88]. Insulin resistant tissue is thus **metabolically inflexible**, unable to augment lipid oxidation in the face of increased supply. Alleviating the dysregulation of mitochondrial fuel selection in skeletal muscle and/or liver tissue may therefore attenuate both fat and whole-body insulin resistance.

Plasma and tissue carnitine reserves are compromised in states of sustained metabolic stress, including insulin resistance in both animals and humans [89]. In high-fat-diet fed rodents (a model for insulin resistance), this relative carnitine deficiency was associated with skeletal muscle mitochondrial dysfunction and impaired fatty acid β -oxidation. Eight weeks of carnitine supplementation reversed this effect and improved whole-body glucose tolerance [63]. In human studies, carnitine supplementation has been shown to improve the metabolic phenotype of both healthy volunteers and insulin resistant subjects [90,91]. Work in the University of Nottingham's Human Physiology Unit has demonstrated that dietary carnitine supplementation in healthy volunteers can increase tissue free carnitine content, whole-body fat oxidation and glycogen stores in muscle, as well as upregulating gene networks involved in mitochondrial fuel metabolism under hyperinsulinaemic conditions [75,92,93]. Mingrone et al (1999) also demonstrated in diabetic patients that L-carnitine infusion increased whole-body glucose disposal and glucose oxidation rates [91].

In a landmark study, Muoio (2012) confirmed that dietary carnitine supplementation improved whole-body glucose homeostasis in insulin-resistant humans and rescued muscle metabolic flexibility, promoting glucose uptake and glycolytic flux [94]. In a systematic review of five randomised controlled trials, dietary L-carnitine was superior to placebo in terms of lowering insulin resistance as assessed indirectly via HOMA-IR ($p < 0.0001$) [95].

Most recently, Savic and colleagues (2019) established type 2 diabetes and NAFLD in a Wistar rat population using streptozocin, followed by intravenous L-carnitine supplementation versus saline buffer for 3 weeks. Employing dynamic precision imaging strategies (^{13}C -labelled pyruvate with ^{13}C -MRS) with liver histology and metabolomics, the group demonstrated reduced serum triglyceride levels in L-carnitine-treated rats, as well as increased liver choline content and decreased hepatic betaine [96]. Diabetic rats treated with L-carnitine demonstrated reduced hepatic glutamate content (indicative of attenuation in oxidative stress). Finally, carnitine treatment was associated with an improvement in cardiac end-diastolic function as quantified by MRI measurements of end-diastolic lumen. Hyperpolarised MRS demonstrated increased flux through the cardiac PDC pathway in diabetic rats treated with carnitine, while PDC flux was reduced in control populations.

Taken together, this data suggests that L-carnitine mediates its beneficial effects in liver through modulating hepatic choline levels (which are known to be attenuated in NAFLD [97]), and that L-carnitine exerts directly beneficial effects on the myocardium. While demonstrated in an animal mode (and therefore potentially not directly translatable to human physiology), this is of particular relevance in NAFLD populations, as epidemiological data has consistently shown that the primary cause of death in NAFLD is cardiovascular disease [98]. Through its ability to positively modulate fuel selection, pathway kinetics and oxidative stress (through buffering incompletely metabolised acyl groups, and facilitating their excretion as carnitine esters), L-carnitine may present a strong candidate adjunctive treatment in insulin-resistant populations with potentially far-reaching metabolic benefits.

1.4.6 Governing Metabolic Flexibility

The term ‘metabolic flexibility’ refers to the ability of an organism to switch catabolic substrate according to the nutritional context. In healthy humans, a carbohydrate-rich meal will initiate a surge in circulating insulin concentrations, facilitating glucose uptake into responsive tissues, primarily skeletal muscle and liver. Glucose is the predominant oxidative fuel in this fed (hyperinsulinaemic) state, while fat oxidation is reciprocally suppressed. As time progresses towards the postprandial, post-absorptive and ultimately fasting state, there is a gradual switch in catabolic substrate from glucose to fatty acids (**Figure 10**). During insulin resistance, this ability to switch ‘metabolic currency’ in response to nutritional supply is lost [99].

It is noteworthy that human physiology evolved as an adaptive response to an environment in which calorie availability was scarce and unpredictable. Substrate switching evolved to maximise efficient storage and utilisation of macronutrients as metabolic “currency”, enabling long periods of starvation with short bursts of excess (i.e. a ‘feast and famine’ model of nutrition). The chronically positive energy balance associated with modern living in industrialised economies drastically disrupts this elegant evolutionary biology, as energy supply consistently outweighs demand [100]. This results in impaired or incomplete fatty acid oxidation, the production of partially metabolised acyl groups, oxidative stress and ultimately impaired mitochondrial respiratory capacity.

Insulin resistance is associated with impaired metabolic flexibility, manifested in the liver as failure to suppress gluconeogenesis and failure to stimulate hepatic glycogen synthesis (i.e. net hepatic glucose production in the fed state). This contributes to the fasting and postprandial hyperglycaemia which constitute the hallmark feature of T2DM [101]. During insulin resistance, inappropriate lipolysis from white adipose tissue (WAT) increases free fatty acid flux to the liver, promoting accumulation of acetyl-CoA, a key regulator of mitochondrial substrate traffic. Allosteric activation of hepatic pyruvate carboxylase activity by acetyl-CoA favours glucose production through the conversion of pyruvate to glucose [102]. A simultaneous mismatch between fatty acid supply and enzymatic capacity, β -oxidation

and TCA cycle flux results in accumulation of toxic intermediary species, including diacylglycerol (DAG) (mediating impaired insulin action via PKC ϵ), acylcarnitine and acyl-CoA moieties, which promote oxidative stress and lipotoxicity [103]. Intracellular acetyl-CoA accumulation favours synthesis of malonyl-CoA, a substrate for *de novo* lipogenesis and a potent inhibitor of carnitine palmitoyl transferase 1 (CPT1). This duality of malonyl-CoA action (i.e. both increasing fatty acid synthesis and inhibiting oxidation) promotes metabolic inflexibility [104].

Through its ability to buffer mitochondrial acetyl CoA and promote fatty acid catabolism in the context of oversupply, carnitine can salvage metabolic flexibility in insulin-resistant tissues [95]. The generation of acetylcarnitine via CrAT lowers the intracellular acetyl CoA/CoA ratio and limits substrate for malonyl-CoA formation. This in turn relieves malonyl-CoA mediated inhibition of fatty acid oxidation and also removes substrate for *de novo* lipogenesis. Via the enzyme carnitine acetyltransferase, carnitine modulates the intracellular ratio of acetyl-CoA/CoA, thereby plausibly limiting inappropriate hepatic glucose production. In amplifying CPT-1 mediated transport of fatty acids to the mitochondrial matrix for β -oxidation, carnitine can promote fatty acid catabolism in the context of lipid oversupply.

Recent work by Bruls *et al* (2019) elegantly combined euglycaemic hyperinsulinaemic clamp studies with muscle biopsies and a novel long-echo time ^1H -MRS protocol for evaluating skeletal muscle acetylcarnitine species, in subjects with impaired glucose tolerance (IGT, n=11) and controls (n=12) [105]. The group randomised IGT individuals to receive L-carnitine 2g daily or placebo for 36 days in a crossover design. Metabolic flexibility as measured through indirect calorimetry was blunted in IGT versus controls, as expected. However, upon carnitine supplementation, metabolic flexibility was rescued in IGT subjects during a high energy meal test. The lower whole-body Respiratory Exchange Ratio (RER) in the fasted state upon carnitine supplementation suggests more complete oxidation of lipid substrates. Further, skeletal muscle acetylcarnitine concentrations at rest and over the day were enhanced in L-carnitine supplementation, with a reduction in long-chain acylcarnitine species, pointing towards more complete fat oxidation with carnitine.

Taken together, data thus far suggests that the ability to form acetylcarnitine is crucial to the maintenance of a metabolically flexible phenotype. Manipulating cellular acetyl CoA and free CoA pools during conditions of mitochondrial substrate excess can restore the balance of fuel selection towards appropriate use in the nutritional context. Lowering the acetyl CoA/CoA ratio removes allosteric inhibition of the pyruvate dehydrogenase complex, resulting in augmented PDC activity and glucose uptake. Further, decreased cellular acetyl CoA removes the stimulus for malonyl-CoA production, thus releasing inhibition of CPT-1 activity and permitting augmented lipid oxidation. Evidence in preclinical models, including CrAT $-/-$ knockout mice, in whom muscle accumulation of long-chain acylcarnitines occurs together with attenuated metabolic flexibility [94], and in human myotubes in which gain of function CrAT mutations were associated with higher rates of acetylcarnitine formation and increased metabolic flexibility, lend further credence to the hypothesis that acetylcarnitine formation is an important mediator of metabolic flexibility *in vivo*. This recent work by Bruls and colleagues supports an argument for exogenous carnitine supplementation to manipulate intramitochondrial acetylcarnitine pools and thus salvage metabolic flexibility in insulin resistant humans.

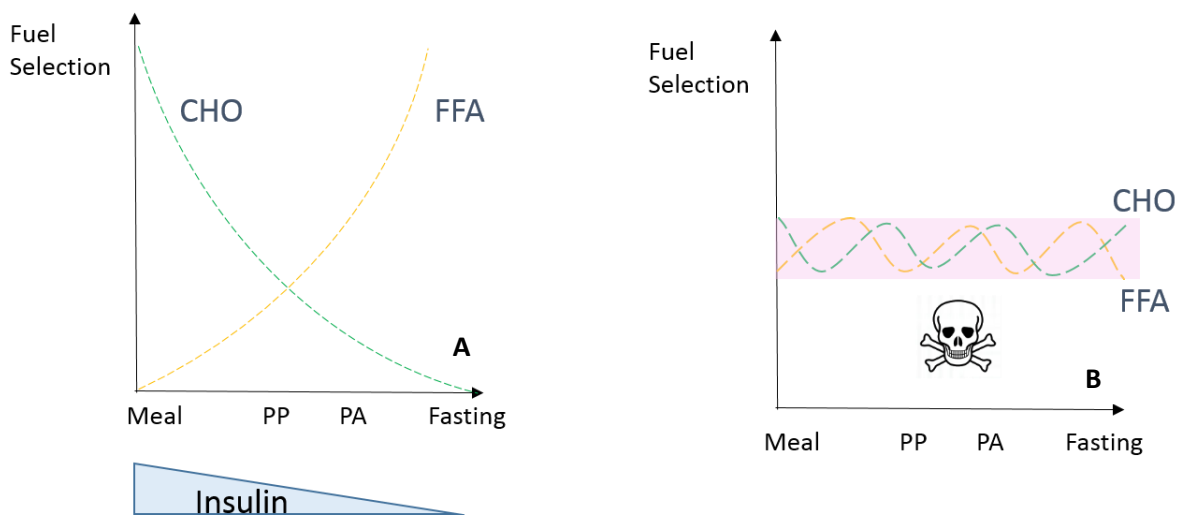


Figure 10. Fuel selection according to nutritional context in (A) insulin sensitive and (B) insulin resistant phenotypes. Under insulin sensitive conditions, a meal will trigger a spike in circulating insulin concentrations, favouring glucose (CHO) as the primary fuel source for cellular energy production, while free fatty acid (FFA) oxidation is reciprocally suppressed. As time progresses towards the fasting state, circulating insulin concentrations fall, and fatty acid oxidation is increased. This ability to switch substrate according to nutritional load is lost in insulin resistance, such that mitochondria consistently oxidise a combination of fuels, increasing mitochondrial stress.

1.4.7 L-Carnitine as a Candidate Treatment for NAFLD

The effect of carnitine supplementation in the context of NAFLD has been the focus of recent interest. A summary of published clinical trials evaluating the effect of L-carnitine on liver fat and/or parameters of metabolic health is summarised in **Chapter 4**.

Whether carnitine exerts any direct effect on liver energy metabolism is unclear. Perhaps the most extensive study of carnitine metabolism in the human liver comes from Krahenbühl *et al* (1997). In this study, patients with non-cirrhotic chronic liver disease (n=22) and with differing aetiologies of cirrhosis (n=57) were studied, with the group reporting that patients with cirrhosis (in particular cirrhosis secondary to alcohol) had an increase in the total plasma long chain acylcarnitine pool [106]. Long chain acylcarnitines are associated with insulin resistance and metabolic inertia [107]. This increase closely paralleled an increase in total plasma carnitine content, which the authors postulate may be due to increased carnitine biosynthesis as a result of increased muscle turnover and protein breakdown in sarcopaenic cirrhotic patients. However, a major drawback of this study is that tissue carnitine concentrations were not quantitatively assessed. As described previously, carnitine kinetics *in vivo* are complex and dynamic, with plasma pools unable to adequately approximate tissue carnitine load.

Rudman *et al* (1977), by contrast, evaluated hepatic carnitine concentrations in cirrhotic patients post-mortem, finding that liver carnitine concentrations were less than one half of those from the livers of non-cirrhotic patients (2.9 ± 0.2 versus 1.0 ± 0.1 , $p < 0.05$) [108]. The group hypothesised that this tissue carnitine deficiency could be driven by a reduction in dietary carnitine as well as a failure of hepatic carnitine synthesis from the amino acids lysine and methionine, consistent with the synthetic failure seen in advanced chronic liver disease. Liver and muscle carnitine content appear to be consistently reduced in experimental animal models of obesity and insulin resistance [109]. However, a more recent study of liver carnitine content in obese women with NAFLD suggests that hepatic carnitine stores may in fact be increased in this population [110]. Thus, whether liver carnitine stores are increased,

unchanged or decreased in the context of liver disease and insulin resistance remains unclear, and will require mechanistic research to elucidate.

Nevertheless, there is mounting evidence to suggest a beneficial effect of dietary carnitine supplementation on liver fat, liver biochemistry and indirect markers of insulin resistance in the context of NAFLD (See **Chapter 4**). From a mechanistic viewpoint, the ability of carnitine to decrease hepatic fat content may be postulated to occur through one (or more) of the following routes:

(a) An increase in skeletal muscle lipid β -oxidation with chronic carnitine elevation, leading to elevated muscle lipid flux capacity, liberating muscle tissue to act as a 'sink' for excess lipid storage and thus sparing the liver itself.

(b) A carnitine-mediated increase in muscle glucose uptake limits diversion of carbohydrate substrate to the liver, thus mitigating the effect of *de novo* lipogenesis on hepatic fat stores.

(c) A direct effect of L-carnitine on liver fuel metabolism through promoting hepatic mitochondrial β -oxidation, and sensitising liver tissue to insulin-mediated suppression of gluconeogenesis.

Through any (or all) of these mechanisms, we hypothesised that carnitine **decreases hepatic fat and improves liver and whole-body insulin sensitivity**, thus ameliorating the metabolic phenotype of NAFLD.

The studies presented in this thesis sought to build upon the concepts discussed herein, and have focused specifically upon on the following aims:

- 1) To deeply phenotype a cohort of young, non-diabetic subjects with NAFLD and to map degree of metabolic disturbance to muscle fat fractions, substrate oxidation and hepatic energy kinetics compared to healthy control subjects. In **Chapter 3**, I explore the pathophysiology of NAFLD using metabolic and precision imaging techniques, demonstrating an association between skeletal muscle lipid accumulation and the development of a metabolically challenged phenotype.

- 2) To synthesise existing evidence base for the effect of L-carnitine on metabolic health in NAFLD through systematic review and meta-analysis. In **Chapter 4**, I construct a narrative and quantitative synthesis of existing evidence for a role of dietary L-carnitine supplementation in NAFLD.
- 3) To evaluate the impact of chronic dietary L-carnitine loading on metabolic phenotype in NAFLD, including liver fat, hepatic and whole-body insulin resistance, fuel selection and hepatic bioenergetics, and to build mechanistic insights into L-carnitine action in liver and muscle. In **Chapter 5**, male NAFLD patients from the cross-sectional study (Chapter 3) were randomised in a 1:1 ratio to receive dietary L-carnitine versus placebo supplementation for 24 weeks. I discuss the design, implementation and results of a placebo-controlled, double-blind randomised trial evaluating the impact of L-carnitine supplementation on liver fat, insulin sensitivity and hepatic bioenergetics in NAFLD.
- 4) To develop clinically applicable techniques for the determination of hepatic ATP flux through exploiting ^{31}P MRS with novel saturation transfer techniques. In **Chapter 6**, I discuss the principles of non-proton MRS and saturation transfer experiments performed to quantify hepatic ATP flux and thus determine (a) hepatic energy kinetics in NAFLD subjects compared with healthy volunteers and (b) the impact of L-carnitine supplementation on hepatic energy kinetics.
- 5) To evaluate the role of circulating biomarkers including FGF21 and LECT2 in predicting metabolic phenotype and to determine responsiveness to long term dietary intervention in NAFLD. In **Chapter 7**, I probe serum concentrations of two well-characterised Hepatokines with a view to exploring their putative potential as serum biomarkers in NAFLD and the metabolic syndrome.

Chapter 2

General Methods

2.1 Metabolic Physiology

“Plan for what it is difficult while it is easy, do what is great while it is small.” Sun Tzu, The Art of War

2.1.1 Euglycaemic Hyperinsulinaemic Clamp

The euglycaemic clamp technique was first applied in humans by De Fronzo, Tobin and colleagues (1979) [111]. To date, this technique is the most sophisticated and reproducible method for quantifying glucose disposal *in vivo*. The clamp technique is considered to be the gold standard method for measuring insulin sensitivity, with an intraindividual coefficient of variation of 10% under steady state conditions [112, 113]. The clamp relies on maintaining (i.e. ‘clamping’) plasma glucose at a fixed, pre-defined target level (in this case euglycaemia, 4.50 mmol/l) during hyperinsulinaemia. The subject receives a primed, continuous fixed-rate insulin infusion to maintain plasma insulin levels in the supraphysiological range, together with a 20% dextrose infusion, titrated to achieve euglycaemia. Plasma glucose is assessed by the operator at 5-minute intervals and the rate of exogenous glucose infusion is altered in response, with the aim of returning plasma glucose to 4.50 mmol/l. In this manner, the feedback loop between insulin secretion and glucose disposal is ‘opened’ and placed under control of the operator.

Under steady state conditions, the rate of exogenous glucose infusion (GIR) needed to maintain euglycaemia is well matched with the rate of glucose uptake by skeletal muscle. This provides an index of metabolisable (M) glucose i.e. glucose disposal rate, a measure of insulin sensitivity at the level of the muscle. This model makes a number of assumptions, namely that there is no net change in glucose concentrations under steady state conditions and that hepatic glucose production is completely suppressed during hyperinsulinaemia [114]. The technique can be combined with stable isotope tracer infusions (e.g. dideuterated glucose) to map insulin sensitivity at the level of the liver. Hepatic insulin sensitivity is then calculated as the percentage (%) suppression of endogenous glucose production

(EGP), as measured by glucose isotope enrichment. The clamp technique can also be combined with other sophisticated metabolic experiments to provide information regarding whole-body substrate oxidation, leg glucose uptake and muscle metabolism under hyperinsulinaemic conditions.

All participants recruited to this study underwent a dual-step euglycaemic hyperinsulinaemic clamp protocol to assess both hepatic and peripheral insulin sensitivity, in combination with vastus lateralis muscle biopsies, indirect calorimetry and leg glucose uptake assessments (**Figure 1**). A primed, continuous infusion of dideuterated [6,6 $^2\text{H}_2$] glucose (0.04 mg/kg/hr) was commenced 120 minutes prior to initiation of the low-dose clamp, and was continued for the duration of the study to enable quantification of endogenous (hepatic) glucose production under steady state conditions using the isotope dilution method.

An example of the clamp data collection form is included in [Appendix 5](#). An example of the clamp study day schematic is shown in **Figure 3, Chapter 3**.



Figure 1 NAFLD Patient undergoing euglycaemic hyperinsulinaemic clamp study with indirect calorimetry.

Heated Hand Technique

In order to accurately assess glucose kinetics *in vivo*, arterial blood glucose monitoring is considered more reliable than venous measurements, as venous values will be significantly influenced by regional tissue metabolism and temperature [115]. Nevertheless, arterial cannulation carries a small but significant complication risk, including dissection, thrombosis and limb ischaemia. To circumvent this problem, the heated hand technique was developed in order to enable measurement of ‘arterialised’ glucose, benefiting from shorter capillary transit time and lower irreversible glucose loss [116]. During clamp conditions, the participant’s left hand was placed inside a warming device, heated to an air temperature of 55°C in order to ‘arterialise’ the venous drainage of the hand. This has been shown to closely approximate the true arterial blood glucose value [117] and has been validated in external cohorts [118]. However, it remains imperfect, with some studies demonstrating significant discordance between glucose concentrations measured in arterial versus arterialised samples [119].

2.1.2 Stable Isotope Tracer Methodology

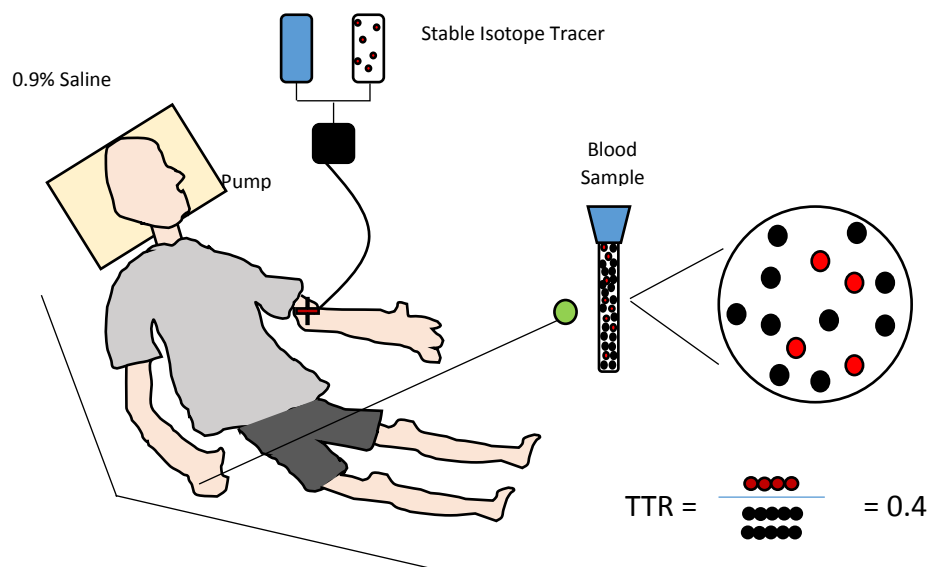


Figure 2 Schematic of Stable Isotope Infusion in Human Metabolic Research. The tracer is introduced intravenously into the systemic circulation. Under steady state conditions, blood is sampled from the contralateral arm. Isotopic enrichment is calculated as the tracer to tracee ratio (TTR) using gas or liquid chromatography mass spectrometry. Adapted from Kim et al. *Experimental & Molecular Medicine* (2016)

Tracer dilution methodology was employed to assess glucose kinetics during the clamp studies. Isotope tracers are ideally suited to the endeavour of studying substrate flux *in vivo*, given that human physiology exists in dynamic homeostasis (i.e. a constant rate of turnover) [¹²⁰]. At its simplest level, a tracer is a 'labelled' form of a substrate which can be tracked, and undergoes the same metabolic fate as its unlabelled counterpart (the 'tracee'). In metabolic research, tracers are structurally and functionally identical to the tracee, except for possessing slightly different atomic mass due to differences in the numbers of neutrons in their nuclei.

Metabolism of the more naturally abundant tracee can be tracked with precision by following the metabolic fate of the tracer. Tracers may be either stable (i.e. naturally occurring and do not decay over time) or radioactive (i.e. emit radiation as a by-product of spontaneous decay). Radioactive tracers have a limited role in human metabolic research due to the inevitable radiation exposure associated with their use. Overwhelmingly, therefore, stable isotope tracers are favoured for research purposes. Most stable isotope tracers are heavier than the most abundant form of naturally occurring substrate, enabling calculation of isotopic enrichment through ascertaining the tracer: tracee ratio (TTR) in blood samples under steady state conditions, using gas chromatography mass spectrometry (GC/MS), see **Figure 2**.

2.1.3 Determining Hepatic Insulin Sensitivity

Applying these principles to glucose kinetics, the tracer dilution technique can be used to measure endogenous glucose production (EGP) by the liver, in which unlabelled glucose (produced by the liver) progressively dilutes the concentration of infused dideuterated [6,6- ²H₂] glucose tracer. In the postprandial state, glucose metabolism can be modelled using Steele's single compartment equation [¹²¹]. Simplified, this is analogous to a bathtub in which water enters through a single tap (EGP) and leaves via a single drain (glucose disappearance, Rd). When EGP > Rd, water level in the bathtub rises, and when Rd > EGP, water level falls. During fasting or during steady state in the clamp study, where peripheral glucose concentration is kept constant, EGP = Rd. Subsequent addition of a dye (i.e. tracer)

that can be uniformly distributed amongst the water in the bathtub, would enable calculation of EGP if one assumes that the rate of tracer infusion is constant and that water loss via the drain does not alter concentration of tracer in the bathtub [122].

By contrast, water entering via the tap is ‘unlabelled’ and will, over time, dilute the concentration of dye (i.e. tracer) in the bathtub. During steady state, with a constant rate of tracer infusion, one assumes that tracer and tracee are cleared at the same rate and thus, that the rate of infusion reflects the concentration of tracer in the system. Tracer dilution may be measured as described above, enabling derivation of EGP.

$$\text{Enrichment} = \frac{\text{tracer}}{\text{tracer} + \text{tracee}}$$

Isotopic enrichment needs to be corrected to account for background enrichment i.e. presence of naturally occurring stable isotopes. For this reason, isotopic enrichment is expressed as atoms percent excess (APE).

$$\text{APE} = \frac{\text{tracer}}{\text{tracer} + \text{tracee}} \times 100$$

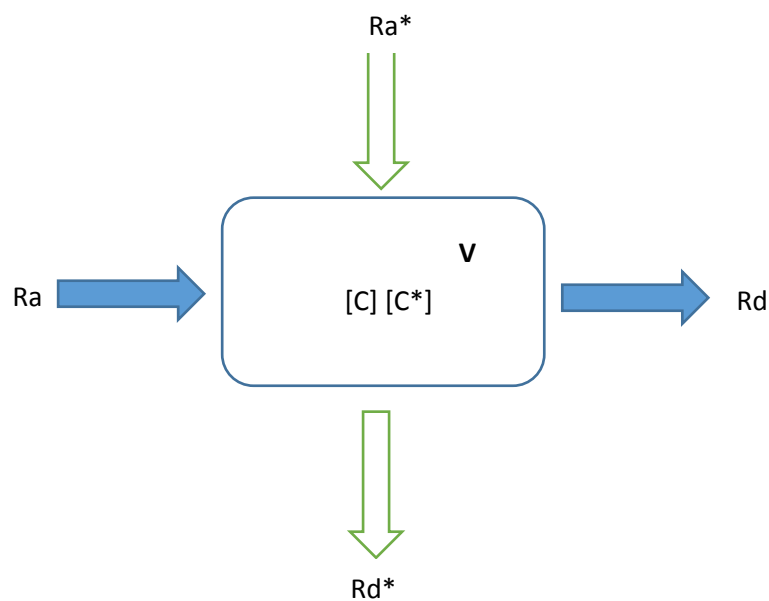


Figure 3 Single compartment Model (based on model from Steele, 1959). Figure adapted from Choukem & Gautier, 2008. R_a : hepatic glucose production rate; R_a^* : tracer infusion rate; C : plasma glucose concentration; C^* : plasma tracer concentration; R_d : rate of glucose disappearance; R_d^* : rate of tracer disappearance; V : volume of compartment.

In non-steady state conditions, calculation of glucose kinetics must account for a variety of exogenous perturbations. In the context of the labelled euglycaemic hyperinsulinaemic clamp, hepatic glucose production (EGP) will rapidly decrease as a response to supraphysiological insulin infusion, reducing the amount of 'cold' glucose available to dilute the tracer pool. The Steele equation can be used to estimate glucose fluxes under non-steady state conditions. The Steele equation assumes that tracer and tracee are distributed within a single pool (**Figure 3**) with constant volume (V). Under physiological steady-state conditions, the rate of glucose appearance (Ra) into the blood compartment is equal to its rate of disappearance (Rd), i.e. Ra = Rd. Plasma tracer/tracee ratio (C*/C) is equal to ratio of tracer infusion/glucose Ra (Ra*/Ra) [123]. Therefore, tracer enrichment (ε) is equal to the ratio of tracer infusion rate/glucose rate of appearance (Ra*/Ra). Therefore, as EGP corresponds to Ra under steady-state conditions:

$$\epsilon = \frac{Ra^*}{Ra} \longrightarrow EGP = \frac{Ra^*}{\epsilon}$$

EGP provides an index of hepatic insulin resistance, but must be corrected for plasma insulin concentration to provide a meaningful value for the liver's response to the suppressive action of insulin on glucose production. Hepatic insulin resistance indices are therefore calculated as the product of EGP and the plasma insulin concentration at the relevant time being assessed (e.g. fasting plasma insulin in the basal state, or insulin concentration during the plateau phase of the low-dose euglycaemic hyperinsulinaemic clamp) [123]. The equation used for calculating hepatic insulin sensitivity index (HISI) and % suppression of EGP as given below:

$$\%EGP_{\text{supp}} = (EGP \text{ at low-dose insulin infusion} - \text{basal EGP}) / \text{basal EGP} \times 100$$

While the Steele equation remains most widely used for calculating hepatic glucose production *in vivo*, there are inherent and important limitations. Firstly, it works on the assumption that the liver is the only glucose-producing organ in the fasted state. It is well established, however, that the kidneys are

important contributors to the plasma glucose pool via gluconeogenesis [124]. Secondly, the single compartment model is flawed – *in vivo*, glucose does not enter a uniform pool and *a priori* assumptions of the Steele model (i.e that the sampled pool is entirely separate from the infusion pool) are not viable. Finally, under clamp conditions, Steele’s single compartment model has been shown to underestimate glucose turnover, sometimes giving rise to paradoxically negative values for EGP [125]. This may be due to labelling impurities or the mathematical model itself. For the purposes of this research, negative values for EGP were assumed to be equal to zero, i.e. complete suppression of EGP by supraphysiological insulin infusion.

Gas Chromatography Mass Spectrometry

Glucose isotopic enrichment, expressed as atoms percent excess (APE), was quantified using GC/MS as the oxime/trimethylsilyl derivative (Agilent Technologies, UK) by Professor Kenneth Smith and Dr Hannah Crossland at the Derby Medical School, University of Nottingham. Selected monitoring of ions at m/z values of 319 and 321 isotope ratios was utilised to determine the concentration of atoms. EGP in the basal and low-dose insulin-stimulated state were then calculated as described in [Appendix 3](#) to determine hepatic insulin sensitivity using the percentage suppression of EGP (% EGP_{supp}) during low dose insulin infusion.

2.1.4 Leg Glucose Uptake

A wealth of evidence to date localises the primary defect in whole-body insulin resistance to impaired insulin action at the level of skeletal muscle. Reduced insulin-stimulated uptake within muscle tissue has been further characterised as a reduction in glucose transport activity [126]. To probe differences in leg glucose kinetics in the studies included (both between NAFLD and healthy volunteers, and longitudinally within the NAFLD cohort) leg blood flow was calculated using a Doppler ultrasound technique together with femoral vein cannulation. Leg glucose uptake could then be measured using the Fick Principle, as described previously [127].

$$\text{Leg Glucose Uptake} = A_G - V_G \times \text{leg blood flow}$$

Arterial glucose was approximated by measuring ‘arterialised’ venous glucose from the dorsum of the left hand, which was placed in a warming device as shown in **Figure 4**. The data recording sheet used during clamp protocol for leg glucose uptake is shown in [Appendix 5](#). Doppler ultrasound (Interspec Inc., Ambler, PA, USA) was employed to measure femoral arterial blood flow (cross sectional area × blood velocity) at baseline (fasting) and during hyperinsulinaemia under steady state conditions at each stage of the clamp. This technique has been validated against the thermodilution method for femoral vein blood flow, demonstrating excellent concordance [128]. Briefly, images of the common femoral artery (approximately 2 cm below the bifurcation) were obtained and frozen in cross-section for determination of vessel diameter. This was measured in triplicate during systole and diastole and the mean arterial value was calculated, as per mean arterial pressure $[(2 \times \text{diastolic}) + \text{systolic}]/3$. Subsequently, pulsed Doppler measurements were obtained and the mean velocity trace was determined from a sample volume across the vessel as previously described [129].

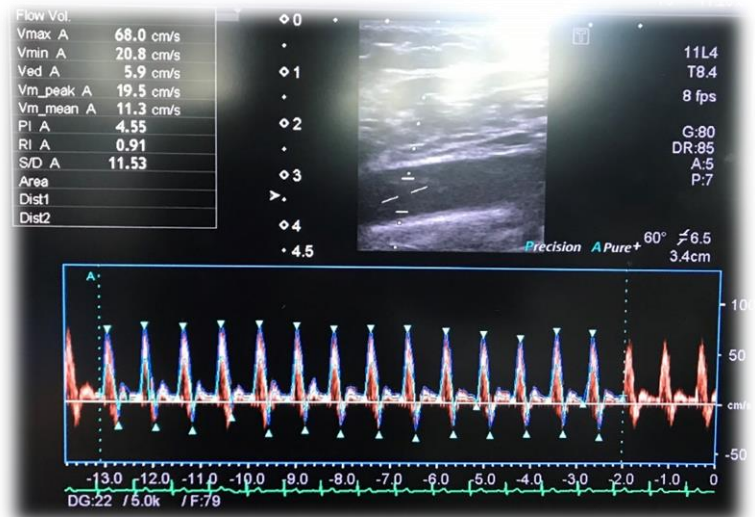


Figure 4. Measuring Leg Glucose Uptake. Femoral vein cannulation and simultaneous blood draws from ‘arterialised’ and femoral venous catheters was undertaken to determine arteriovenous difference.

2.1.5 Indirect Calorimetry

The final common pathway for extracting chemical energy from food substrates is oxidation, whereby carbon-based fuels undergo a series of enzymatic reactions in the presence of oxygen (O₂) to liberate carbon dioxide (CO₂) and water (H₂O). Oxidation releases heat as a by-product of combustion, which serves to maintain body temperature. The chemical energy yielded from oxidation is trapped in high energy compounds, the most abundant and physiologically relevant of which is adenosine triphosphate (ATP) [130].



The ability to measure whole-body substrate oxidation and energy production *in vivo* yields important insights into nutrient metabolism, including the pathogenesis of metabolic inflexibility and insulin resistance. Indirect calorimetry provides a method for quantifying gas exchange i.e. whole-body oxygen consumption and CO₂ production in real time, thereby enabling the calculation of total energy production. This method works on the assumption that all O₂ is used to oxidise carbon-based fuels and that all the CO₂ released from this process is recovered [131]. Accepting such assumptions, it is possible to calculate the total amount of energy produced by the organism. The apparatus used for indirect calorimetry is shown in **Figure 1**. Briefly, a ventilated canopy or hood system with constant airflow is placed over the subject's head for a period of approximately 15 minutes. During this time, continuous sampling of expired gases takes place via O₂ and CO₂ analysers, with results adjusted for inspired air concentration (measured at the start and end of the measurement period) and displayed on dedicated software in real time (GEM Nutrition, Windows 93). The measurements thus derived are normalised to metabolically active (i.e. lean) body mass, as estimated by body surface area.

Thus, whole-body O₂ consumption and CO₂ production can provide an index of metabolic flexibility when assessed in the fasted and insulin-stimulated state, as rates of whole-body fat and carbohydrate oxidation can be quantified together with resting energy expenditure (REE). It is worth noting that

while indirect calorimetry measures energy production and not expenditure *per se*, under steady state conditions net energy production is assumed to be equal to REE.

In all experiments described in this thesis, indirect calorimetry was measured using the Gas Exchange Monitor (GEM Nutrition Ltd, Cheshire, UK) at 3 stages throughout each clamp procedure, during steady state conditions.

- 1) At baseline in the post-absorptive state (basal energy expenditure, BEE)
- 2) Under low-dose insulin stimulated conditions
- 3) Under high-dose insulin stimulated conditions.

The respiratory exchange ratio (RER), defined as the ratio of carbon dioxide production to oxygen consumption (VCO_2/VO_2), reflects metabolic flexibility through approximating substrate use at the cellular level. When fat is the primary metabolised fuel, the RER is 0.70, when protein is metabolised it is 0.80 and when carbohydrate is metabolised it is 1.0 [¹³²].

A calibration routine is required to optimise accuracy of the analysers and consistency of results. In the experiments conducted herein, we used a two-point calibration system with (1) Zero Gas (Oxygen free nitrogen) and (2) Span Gas (0.8% CO₂, 20% O₂, balanced Nitrogen). Calibration was performed before each of the three substrate oxidation time points in each clamp study. Quality Control was assessed monthly during the data collection period, using alcohol burning.

Reliability of data acquisition necessitates a collaborative participant and can be affected by multiple factors, including hyperventilation, hypoventilation talking or restlessness. To calculate whole-body rates of substrate oxidation, we worked under the assumption that protein oxidation did not vary throughout the clamp experiment. Thus, the non-protein equations of Péronnet and Massicotte (1991) have been used for the purposes of our experiments [¹³³].

$$\text{Carbohydrate oxidation: } 4.585 * VCO_2 - 3.226 * VO_2$$

$$\text{Fat oxidation: } 1.695 * VO_2 - 1.701 * VCO_2$$

2.1.6 Muscle biopsies

A variety of percutaneous methods exist to extract *vastus lateralis* skeletal muscle tissue from human volunteers under research conditions. Of these, the technique described by Bergström in 1975 was chosen in view of its simplicity, reproducibility and safety [134]. The modified Bergström technique, proposed by Evans et al (1982), applies suction to the cutting needle trocar, enhancing yield by up to 5-fold [135]. The modified Bergstrom technique was applied in all patients undergoing clamp studies during the course of this research.

The technique has been described in detail elsewhere [135]. Briefly, a blunt Bergström needle is introduced into the vastus lateralis muscle with a suction port attached. The Bergström needle contains an outer cannula with a 'window' and an inner trocar with a cutting blade [136].

The biopsy site was located clinically anterior to the *fascia lata* (illiotibial band), approximately 15 cm above and 3-4 cm lateral to the patellar insertion of the vastus lateralis muscle. Aseptic technique was used throughout the procedure. Local anaesthetic (lignocaine 1% w/v) was infiltrated subcutaneously and subsequently advanced vertically into the incision site to infiltrate superficial to the fascia. A straight 1cm incision was made into the skin and subcutaneous tissue once local anaesthesia was established. The scalpel used to make this incision was then advanced through the fascia and into the vastus lateralis muscle. Direct compression was applied immediately to minimise blood loss and haematoma formation. Technician support was required to attach extension tubing and a 3-way stopcock to a disposable 60 ml syringe. One end of the plastic extension tubing was attached to the inner trocar and 5 mm biopsy needle, while the other end was attached to the syringe. The needle was assembled by the operator (me), with checking of alignment, sliding action and suction. The needle was then advanced into the vastus lateralis muscle via the skin incision, through the fascia and into the muscle tissue itself. Suction was applied to the trocar and the outer trocar was pulled back and forth rapidly, with 90 degree rotation, drawing muscle tissue through a 'clipping' action into the

'window' of the outer cannula. Utilising this technique, typical yield for muscle biopsy specimens is approximately 150 mg [136]. A maximum of two attempts at muscle biopsy were made on each occasion as per research ethics committee (REC) stipulations. After the biopsy, a clear Tegaderm dressing was applied to the incision site with an adhesive compression bandage (Coban™, 3M, Berkshire, UK) applied tightly for several hours over it, to minimise bleeding (see **Figure 5**). Subjects removed Coban™ dressing on the evening following the clamp studies, and were able to resume activities of daily living immediately. They were advised to avoid heavy exercise for 48-72 hours post-procedure.

Once retrieved, muscle specimens were immediately snap frozen in liquid nitrogen and any extra muscle tissue obtained was mounted "fresh" for analysis of IMCL content and muscle fibre type. IMCL was quantified on biopsy specimens using the fluorescent dye Bodipy-493/503 (D3922, ThermoFisher) as previously described [137]. Briefly, frozen vastus lateralis samples were embedded in OCT mounting medium (361603E, VWR Chemical) before being secured to the object holder of a Leica CM3050 S Research Cryostat. Cryostat chamber temperature was maintained at -20 °C while the temperature of the object holder was maintained at -18 °C. Transverse sections of 15 µm thickness were trimmed and collected from each frozen muscle biopsy block. These sections were mounted on SuperFrost Plus adhesion microscope slides (631-0108P, VWR Chemical).

Two muscle biopsies were taken on each clamp visit; one at baseline prior to the initiation of the clamp from the right leg, and one immediately following cessation of the second step of the clamp from the left leg. In the course of this work, approximately 110 muscle biopsies were performed. Of these, one patient experienced a moderately severe adverse event (vasovagal syncope) which completely resolved with basic supportive measures. A further three patients reported mild haematomas/bruising, and one patient had temporary loss of sensation over the skin of the biopsy site. All mild adverse events resolved spontaneously.



Figure 5 (A) Snap frozen muscle biopsy specimen (B) Equipment used for mounting of fresh muscle tissue for IMCL and fibre type analysis (C) Preparation of equipment for muscle biopsy procedure and (D) Application of Tegaderm and Coban® dressing following muscle biopsy.

2.1.7 Measuring Adipose Tissue Insulin Resistance

Adipo-IR was calculated as a surrogate measure of adipose tissue insulin resistance in this research. Adipose tissue has been well-established as a key player in the development of the metabolic syndrome, with unrestricted lipolysis in the insulin resistant state facilitating increased circulating free fatty acids and therefore ectopic lipid deposition. Adipo-IR index has been validated extensively and correlates well with the gold standard multi-step pancreatic clamp, which involves infusion of [U-¹³C] palmitate tracer and calculates the insulin concentration required to suppress lipolysis (i.e. palmitate flux) by 50% (IC₅₀). Adipo IR has been shown to be a robust and reproducible surrogate marker for IC₅₀ (coefficient of variation <10%) and insulin-mediated suppression of glycerol using stable isotope

labelled glycerol tracers [¹³⁸,¹³⁹]. Changes in Adipo-IR have also shown strong correlations with histological changes in liver fat following intervention in NAFLD clinical trials, probably reflecting altered patterns of lipid storage i.e. a reduction in ectopic lipid deposition [¹⁴⁰, ¹⁴¹].

2.1.8 Dual Energy X ray Absorptiometry (DEXA)

Dual Energy X Ray Absorptiometry (DEXA, Lunar Prodigy, GE Healthcare) was used to assess body composition in both the cross-sectional and longitudinal studies. DEXA is a widely used tool in metabolic research (as well as clinical practice) and enables differentiation of adipose tissue, bone, soft tissue and lean tissue mass. DEXA is a convenient, non-invasive method for quantifying body composition and entails minimal (0.8 μ Sv) radiation exposure. In these studies, all DEXA scans were performed by a single operator on the same machine to reduce inter-observer and non-biological variability.

The basic principle of DEXA acquisition is based on differences in the attenuation of beams which occur at these high and low x-ray levels. The attenuation of each energy part is measured by a detector and the ratio of the low energy to high energy attenuation, termed the R value, can be calculated. Using these R values, the DEXA software can calculate the mass fraction of two tissue components, using the mass attenuation coefficients for each tissue type. Although the human body is composed of many tissues, it can be considered in terms of dual compartments, each of which has a unique mass attenuation coefficient e.g. bone vs. non-bone (fat, lean), fat vs. fat-free mass (bone, lean) and where there is no bone present, fat vs. lean. The DEXA software can analyse each pairing and then combine the results to create an estimate for bone, fat and lean mass. Accuracy of the DEXA is monitored by executing a daily Quality Assurance scan using a phantom block of known attenuation coefficient value (CV of these measurements <2%).

2.1.9 Blood Sample Collection

Whole blood was collected at serial time points during the euglycaemic hyperinsulinaemic clamp (see **Figure 3, Chapter 3**), as well as during participant screening and at the end-of-study visit. Once collected, whole blood was centrifuged at 4°C at a speed of 2000 revolutions per minute to separate serum and plasma components. These components were subsequently stored at minus 80°C for batch analysis of plasma insulin, triglyceride, CRP and free fatty acids (FFA) following completion of both the cross-sectional study and the randomised controlled trial. Total blood volume collected per visit per volunteer was approximately 250 mls.

2.2 MR Spectroscopy

2.2.1 Background

While MRI allows detailed insight into tissue structure and spatial localisation, MR Spectroscopy provides functional information about tissue metabolite concentrations in health and disease. Chemical properties of MR visible nuclei in tissue pools of interest can be quantitatively determined, allowing both static and dynamic metabolite concentrations to be calculated in real time. Originally developed for neuroradiology research, the role of MR spectroscopy has vastly expanded in recent years, to include interrogation of liver and muscle metabolism. Proton (^1H) MRS is widely accepted as the gold-standard technique for non-invasive quantification of liver fat [¹⁴²,¹⁴³].

MRS focuses on excitation of a localised cubic volume of tissue (“voxel”) to calculate a chemical shift spectrum, with peaks corresponding to specific nuclei (e.g. hydrogen ions) within molecules of interest, for example water and fat when employing ^1H MRS [144]. A radiofrequency pulse is applied to the voxel and the corresponding received signal is Fourier transformed to provide a read-out (spectrum) of metabolite frequency. Differential frequencies (i.e. different positions along the x axis) correspond to different tissue metabolites. For example, in the proton (^1H) MR spectrum the predominant signal is from water (4.7 ppm), whereas protons from fatty acids in triglyceride align at different frequencies (CH_2 peak at 1.3 ppm), enabling separation of different metabolites of interest (**Figure 6**). The signal amplitude (position on the y axis) and breadth of the peak enable quantitation of metabolite concentrations through ‘area under the curve’ analyses. Metabolite frequency is usually expressed relative to the most abundant metabolite within the region of interest e.g. in the liver, water is the dominant signal, so fat frequency is expressed relative to water frequency.

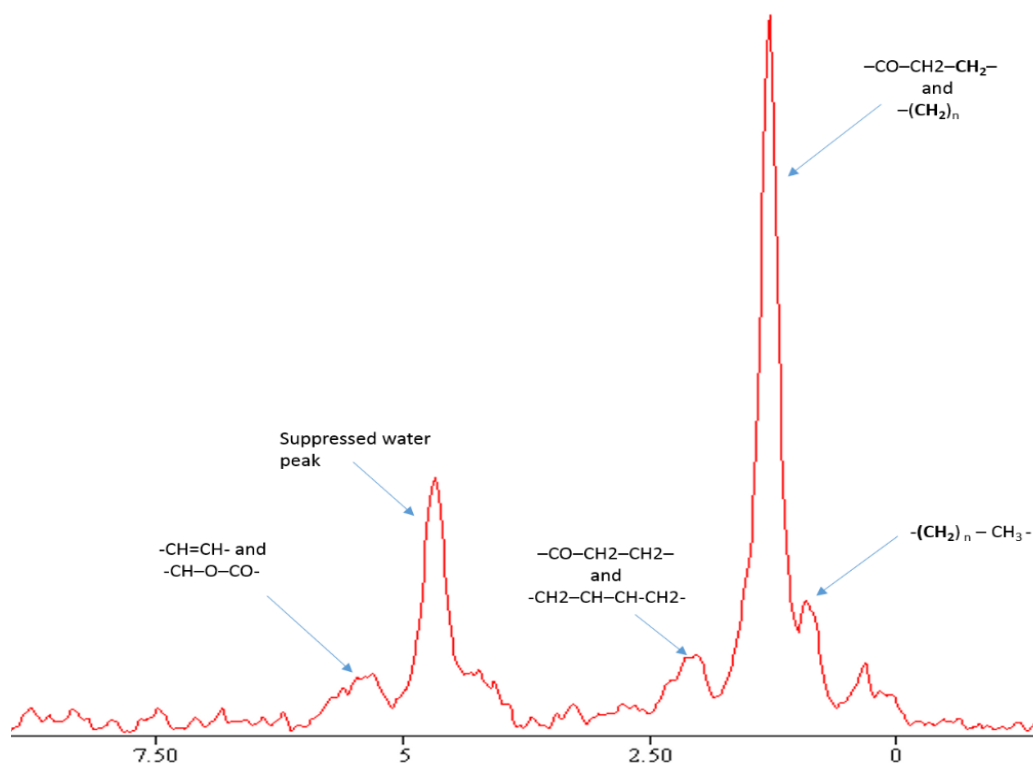


Figure 6. Typical STEAM-localised ^1H MR Spectra with water suppression from an individual with NAFLD, obtained during this research study (TE = 20 ms). The spectrum demonstrates the complexity of triglyceride in the liver, with multiple lipid peaks. Spectral resolution at 3T is excellent, allowing for accurate fitting and quantification of IHTG. The fat fraction is derived from dividing the fat content by the combination of fat and water content.

In vivo localisation techniques aim to optimise spectral resolution through maintaining high signal to noise ratio. The main sequences used to measure liver fat with ^1H MRS are Point Resolved Spectroscopy (PRESS) and Stimulated Echo Acquisition Mode (STEAM). STEAM involves administering three slice-selective simultaneous pulses at 90° from each other along three orthogonal gradients (x, y and z axes) to generate a voxel [145]. Only protons lying at the intersection of all three pulses are included in the stimulated echo. This allows selection of a well-defined cuboid voxel, with minimal contamination from extraneous sources (e.g. blood vessels or soft tissue), but sacrifices signal intensity. In contrast, with PRESS, slice-selective pulses are applied at 90° , 180° and 180° along three orthogonal gradients and a spin echo is derived from protons at the intersection of these axes (rather than a stimulated echo with STEAM sequence). With PRESS, the signal intensity, and therefore signal to noise ratio, is significantly higher. However, as echo time takes longer with PRESS, this impacts upon ability to resolve metabolites with short T2 relaxation times. This becomes more relevant at higher magnetic field strengths, as T2 decay is inversely related to magnetic field strength [146].

To obtain high quality MRS data, field inhomogeneities need to be corrected. Uniformity of water suppression and clarity of fat peaks relies on the presence of a homogenous magnetic field. However, air or soft tissue artefact can obscure spectral resolution of these resonances. For this reason, a process known as shimming is applied to correct field inhomogeneity. Shimming uses small, calibrated electrical circuits within the coils with the aim of fine-tuning the signal over a sampled volume of tissue, optimising peak sharpness and spectral resolution. Much of the volume shim is achieved through automatic pre-scanning (approx. 15 seconds) with further refinements possible through manual shimming.

Single voxel spectroscopy (SVS) is overwhelmingly preferred over multi-voxel procedures in body MRS, due to better spatial localisation, homogeneity of shimming procedures, higher quality of water suppression and shorter acquisition time. However, it is worth noting that SVS obtains data over a

relatively small volume of tissue. In diffuse liver disease, this limitation is not particularly relevant; however, in more focally distributed pathology (e.g. malignancies) it may be suboptimal.

In the experiments described herein, single voxel ^1H MRS was employed at 3 Tesla (3T) using STEAM localisation for quantification of intrahepatic triglyceride (IHTG) and at 7 Tesla (7T) for mapping of intra and extramyocellular lipid fractions in the vastus lateralis muscle.

2.2 ^1H MRS in the Liver (3T)

IHTG was measured from a 20 x 20 x 20 mm region of interest (ROI) in lower right hepatic lobe using TE varying STEAM localised ^1H MRS (Philips 3T Achieva with XL 16 channel torso coil, T2 corrected fat fraction measure using jMRUI fitting). Scout images were acquired *a priori*, to permit adequate voxel placement in the liver parenchyma, away from adjacent blood vessels, biliary structures or soft tissue. Non water suppressed spectra (**Figure 7**) were acquired during a single breath hold (TR=4000 ms, TE=20, 40, 80, 160ms) and repeated with water suppression (4 averages per spectra). Data was post-processed using jMRUI software (manually phase corrected, frequency aligned, line broadened) and fitted using the Advanced Method for Accurate, Robust and Efficient Spectral fitting (AMARES) algorithm with prior knowledge for peak fitting [147]. Amplitudes were fitted to a monoexponential decay for water and fat T2, and the fat fraction was calculated from T2 corrected fat/water ratios.

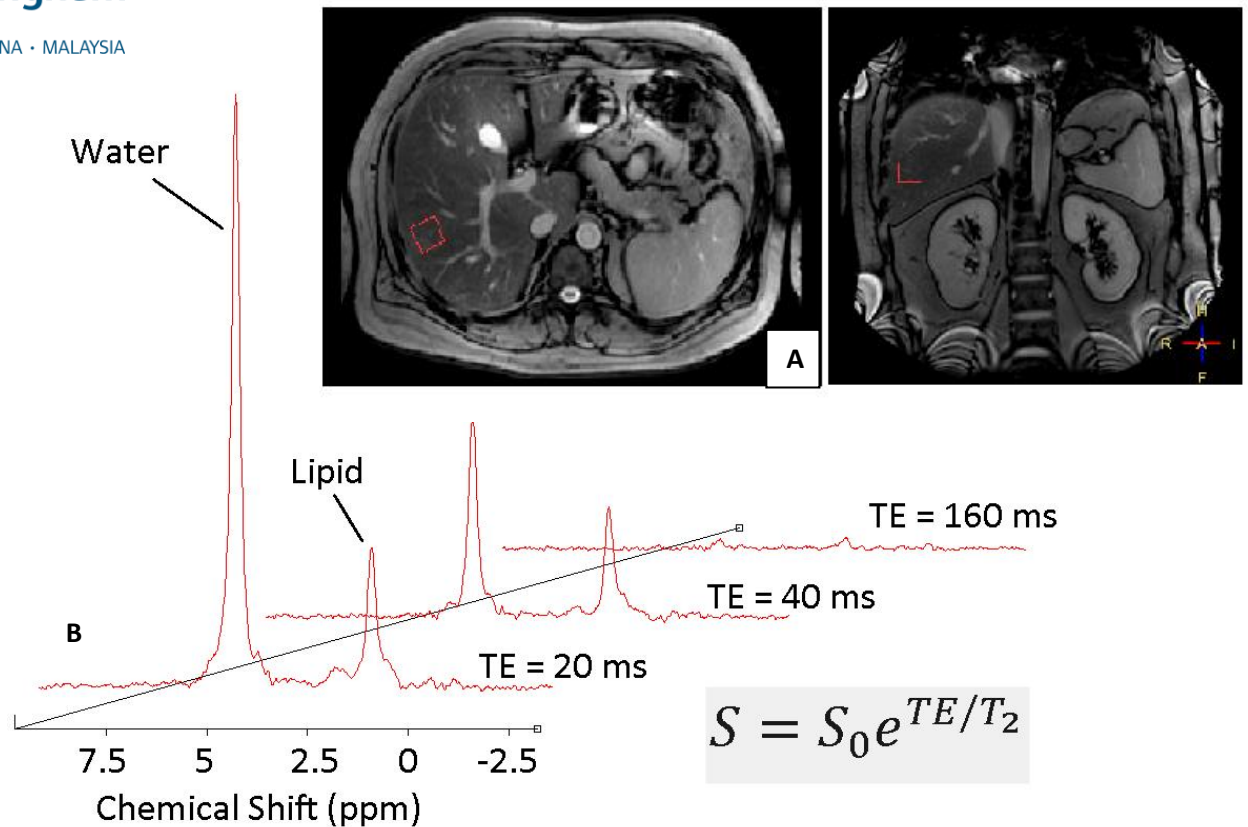


Figure 7 (A) *In vivo* voxel localisation within the right lobe of the liver, ensuring distance from major blood vessels and subcutaneous tissue to optimise spectral quality and minimise artefact. (B) Typical spectra from NAFLD patient (non-water suppressed). Note that spectra are taken at four different echo times and averaged.

2.2.3 ¹H MRS in Skeletal Muscle (7T)

High magnetic field strengths (7T) were used for *in vivo* quantification of muscle lipid fractions in the *vastus lateralis* muscle. A dedicated radiofrequency coil (MRCoils quadrature surface coil) was placed over the thigh, with scout images obtained to permit voxel placement. STEAM-localised ¹H MRS sequences were acquired from a 10 x 30 x 50 mm voxel were obtained (Philips 7T Achieva scanner, TR=4000ms, 16 averages at TE=20ms and 8 averages at TE=40, 80 and 160ms). Spectral peaks were line broadened and phase corrected using an in-house Matlab script, and a peak-dispersion fitting algorithm was developed to fit EMCL and IMCL peaks accounting for muscle fibre orientation. Multi-echo amplitudes were used to determine water and fat T₂, lipid fraction and IMCL/EMCL ratios.

2.2.4 ^{31}P MRS with saturation transfer in the Liver (3T)

Slice localized ^{31}P MRS spectra were acquired from the liver using a Philip ^{31}P single loop surface coil. Apparent T1 ($T_{1\text{app}}$) was measured using progressive saturation ^{31}P MRS (5 spectra fitted using jMRUI) as described previously [148]. The ATP rate constant (k) was then calculated from two ^{31}P MRS spectra, one fully saturating γ -ATP (-2.5ppm) and the second mirrored about the inorganic phosphate (Pi) peak (14 ppm). Total scan time for each participant was approximately 1 hour and 15 minutes. The ^{31}P MRS experiments are described in detail in [Chapter 6](#).

2.3 Covid Statement

All muscle analysis has been delayed due to Covid-19 restrictions, in place since March 2020. This has mandated the cessation of all radioisotope work in the Medical School at the University of Nottingham, which has precluded data analysis being included in this thesis.

2.4 Clarification of Patient Pools for Studies

Healthy volunteers and NAFLD patients were recruited for inclusion in the baseline cross-sectional study, discussed in **Chapter 3**. The same NAFLD patients from this cross-sectional study were subsequently enrolled into a double-blind, placebo-controlled trial which is discussed further in Chapter 5. In Chapters 6 and 7, specific analyses (ATP flux and Hepatokines, respectively) from both the cross-sectional study and the RCT are described in detail. Patient pools are displayed as a schematic in **Figure 8**.

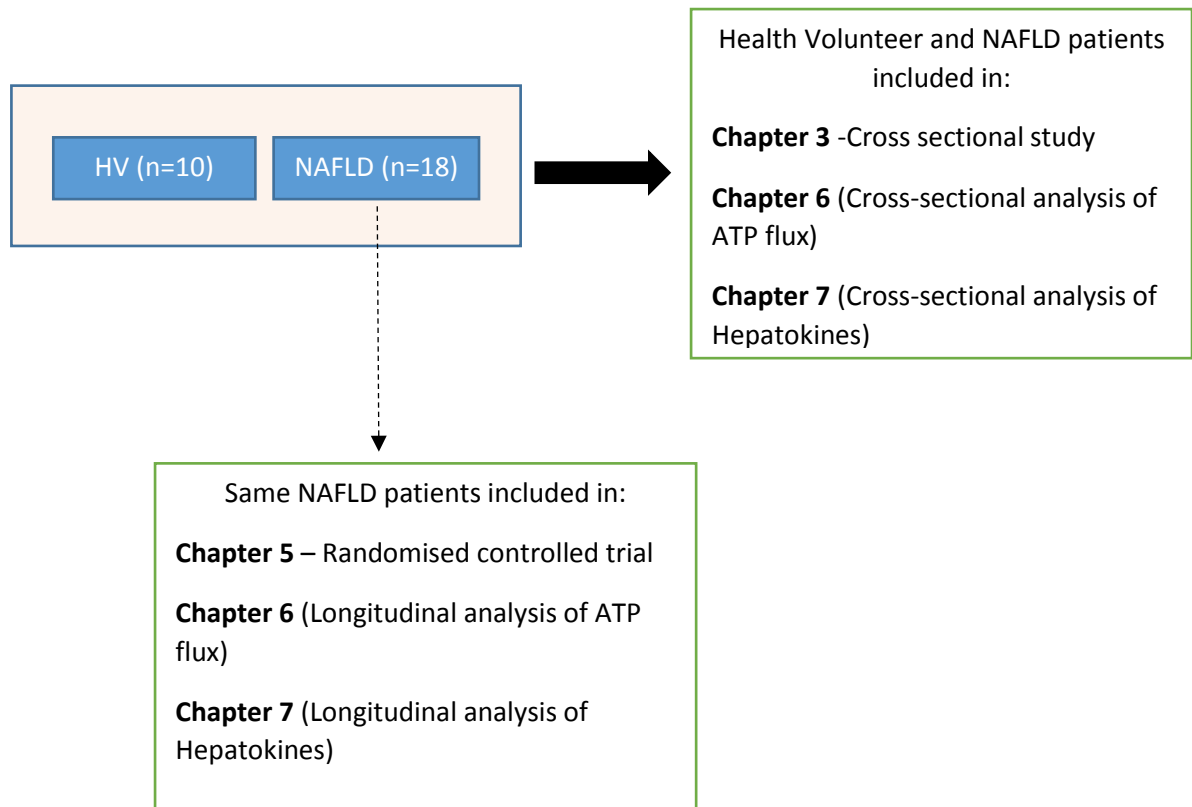


Figure 8. Patient pools used in the body of this research, and the chapters pertaining to them

Chapter 3

Mechanisms of Insulin Resistance in NAFLD: Mapping the Muscle-Liver Axis through deep metabolic phenotyping.

3.1 Introduction

Insulin resistance is the pathogenic hallmark of NAFLD and the unifying feature linking individual components of the metabolic syndrome. The mechanisms underpinning development of selective hepatic, and ultimately whole-body, insulin resistance, are nuanced and far from well established. In particular, the apparent bidirectional relationship between insulin resistance and ectopic lipid deposition further complicates the elucidation of mechanistic pathways, as a simple linear “cause and effect” model cannot be assumed.

Dynamic imaging and sophisticated metabolic studies *in vivo* have confirmed a role for skeletal muscle insulin resistance in the pathogenesis and propagation of NAFLD. In young, lean offspring of individuals with type 2 diabetes, skeletal muscle lipid was found to be elevated together with increased whole-body insulin resistance compared with age matched subjects [149]. Key experiments by Petersen *et al* (2007) further noted skeletal muscle insulin resistance promotes the development of systemic dyslipidaemia and diverts the fate of ingested carbohydrate away from muscle glycogen synthesis, towards intrahepatic storage through upregulating hepatic *de novo* lipogenesis [18].

Generalised adiposity *per se* does not fully explain inter-individual variations in insulin sensitivity. Rather, robust metabolic experiments conducted over the last decade have highlighted the primacy of fat *location* in predicting presence and degree of metabolic dysregulation. Lara-Castro *et al* (2008) metabolically characterised both diabetic and obese non-diabetic subjects (n=12), demonstrating that intramyocellular lipid (IMCL) was most strongly associated with systemic insulin resistance ($r = -0.69$, $P < 0.01$), but did not parallel indices of generalised adiposity (body mass index, total body fat or body fat percentage) [150]. Particular sub-locations of lipid within muscle tissue have been linked to a metabolically challenged phenotype [151]. Krssak *et al* (1999) demonstrated a strong positive correlation between muscle lipid located within myocytes (IMCL) and whole-body insulin resistance [152]. Accumulation of intramyocellular lipid is likely due to a combination of increased supply and

defective fatty acid oxidation within the myocyte. Once present, bioactive lipid droplets within myocytes directly interfere with insulin signalling through the novel protein kinase c (PKC θ) isoform, ultimately serving to blunt insulin-stimulated glucose transport [153].

The relationship between skeletal muscle IR and overt phenotypic features of the metabolic syndrome is well-established. However, the relationship between ectopic lipid deposition and insulin resistance in NAFLD populations is not clear. In this study, we aimed to investigate associations between liver fat, muscle fat fractions and insulin sensitivity profiles in NAFLD patients versus age matched healthy volunteers. We also aimed to probe hepatic mitochondrial metabolism non-invasively to establish whether mitochondrial dysfunction is a feature of NAFLD early in its natural history.

3.2 Methods

3.2.1 Human Participants

Ten healthy male volunteers (mean age 33.8 ± 9.3 years) and 18 age-matched male NAFLD patients (mean age 36.3 ± 9.1 years) were recruited to this study. The study was sponsored by the University of Nottingham and approved by the Nottingham 2 Research Ethics Committee, Health Research Authority and local NHS Research and Innovation (R&I) departments ([Appendix 2](#)). All research was conducted in accordance with the Declaration of Helsinki and all participants gave written, informed consent prior to enrolment. The recruitment process for healthy volunteers is summarised in **Figure 1**. The recruitment process for NAFLD patients is discussed in detail in **Chapter 5**.

Recruitment took place between April 2018 and October 2019. The recruitment strategy for healthy volunteers consisted of University sited advertisement flyers, advertisement through the Call for Participants website (<https://www.callforparticipants.com/study/poster/J572X>) and newspaper advertisements. Patients with suspected NAFLD were primarily recruited through a locally

commissioned NHS stratification pathway for liver disease (the Scarred Liver Project) which entailed use of Fibroscan® with controlled attenuation parameter to assess fibrosis burden and evaluate for presence of intrahepatic lipid. Following ethics approval, this database was searched and individuals with a liver stiffness measurement <8 kilopascals and CAP > 288 dB/m were contacted about the study. The CAP cut off of 288 dB/m was based upon a published cross-sectional study evaluating optimal CAP thresholds for the diagnosis of NAFLD (MRI-Proton Density Fat Fraction $\geq 5\%$), with an area under the receiver operating curve (AUROC) of 0.80 for at the cut-point of 288 dB/m [154]. Those expressing an interest were sent a copy of the patient information sheet and were invited to attend the Nottingham Digestive Diseases Centre for a screening visit.

All participants underwent an initial medical screening visit, including a history and physical examination, 12-lead electrocardiogram (ECG), routine safety bloods, bloods to exclude concomitant liver disease (e.g. haemochromatosis, alpha 1 antitrypsin deficiency, autoimmune liver disease, chronic viral hepatitis B or C), anthropometric measures (weight, height, waist circumference, hip circumference) and evaluation of fasting blood glucose concentrations.

Inclusion criteria included: age ≥ 18 years and <50 years, male gender, BMI ≤ 40 kg/m², ability to consent to MRI scanning protocols. Exclusion criteria included: type 2 diabetes, significant alcohol consumption (≥ 21 units per week), an alternative cause of liver disease based on history and screening blood tests, active smoking history, cardiovascular disease, chronic respiratory disease, medications including steroids, calcium channel blockers, lipid-lowering drugs, methotrexate, antihistamines, biologics or intercurrent antibiotic therapy at the time of first study visit. Other exclusions included any surgery within the previous 6 months, history of any surgery affecting the gastrointestinal tract or liver, hypothyroidism or other autoimmune disease, adherence to any special diets (e.g. ketogenic diet, intermittent fasting), vegetarianism or veganism, claustrophobia or any other contraindication to MRI scanning (such as metallic implants incompatible with the scanner).

Flow through the study is outlined in **Figure 2**. Following the screening visit and prior to metabolic and imaging experiments, subjects completed a 4-day diet diary for baseline assessment of energy intake and dietary macronutrient composition. During a 10-day washout period prior to baseline study visits, subjects were instructed to follow an *ad libitum* diet and to avoid alcohol intake. They were subsequently invited to the Sir Peter Mansfield Imaging Centre for a baseline MRI scan. Non-alcoholic fatty liver disease (NAFLD) was confirmed if baseline intrahepatic triglyceride $\geq 5.56\%$ on $^1\text{H-MRS}$.

Figure 1. Recruitment process for Healthy Volunteers

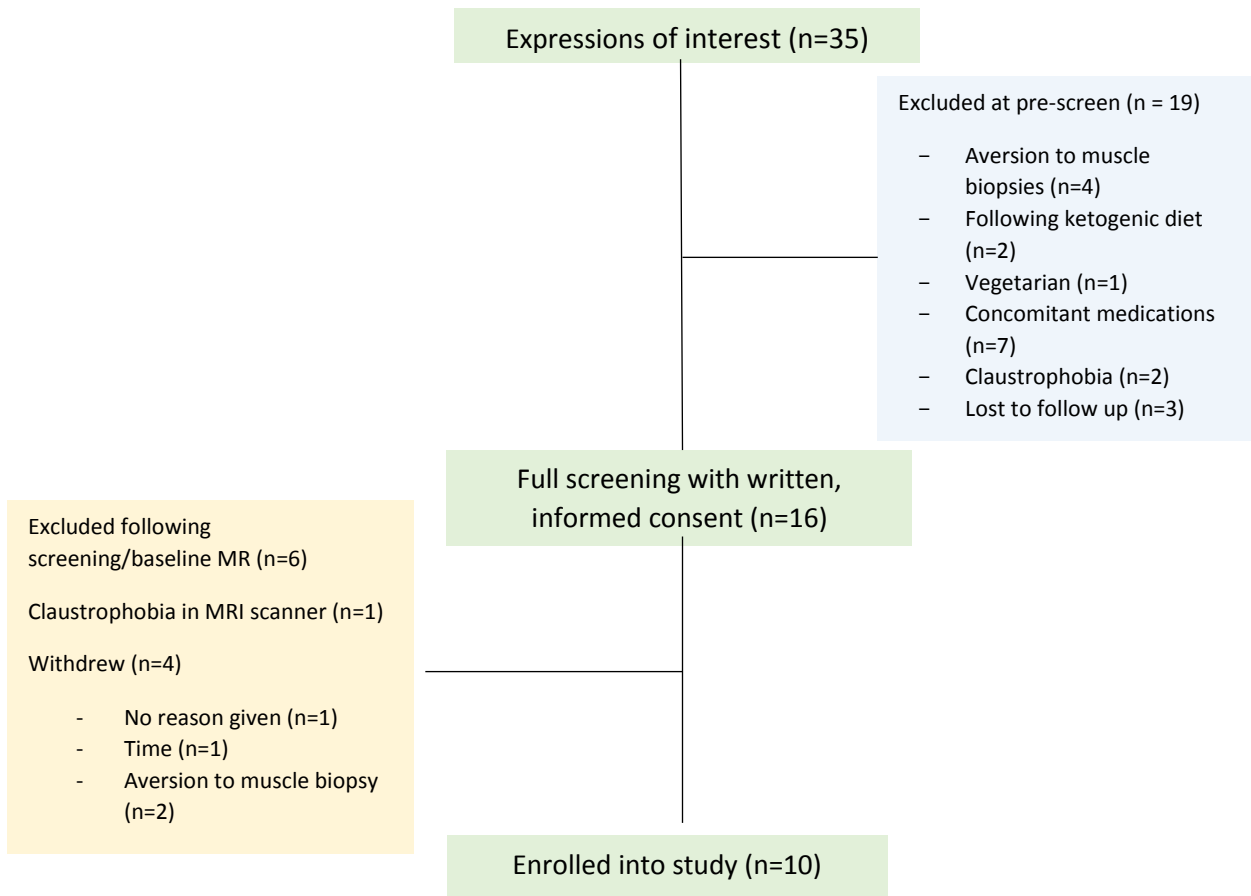
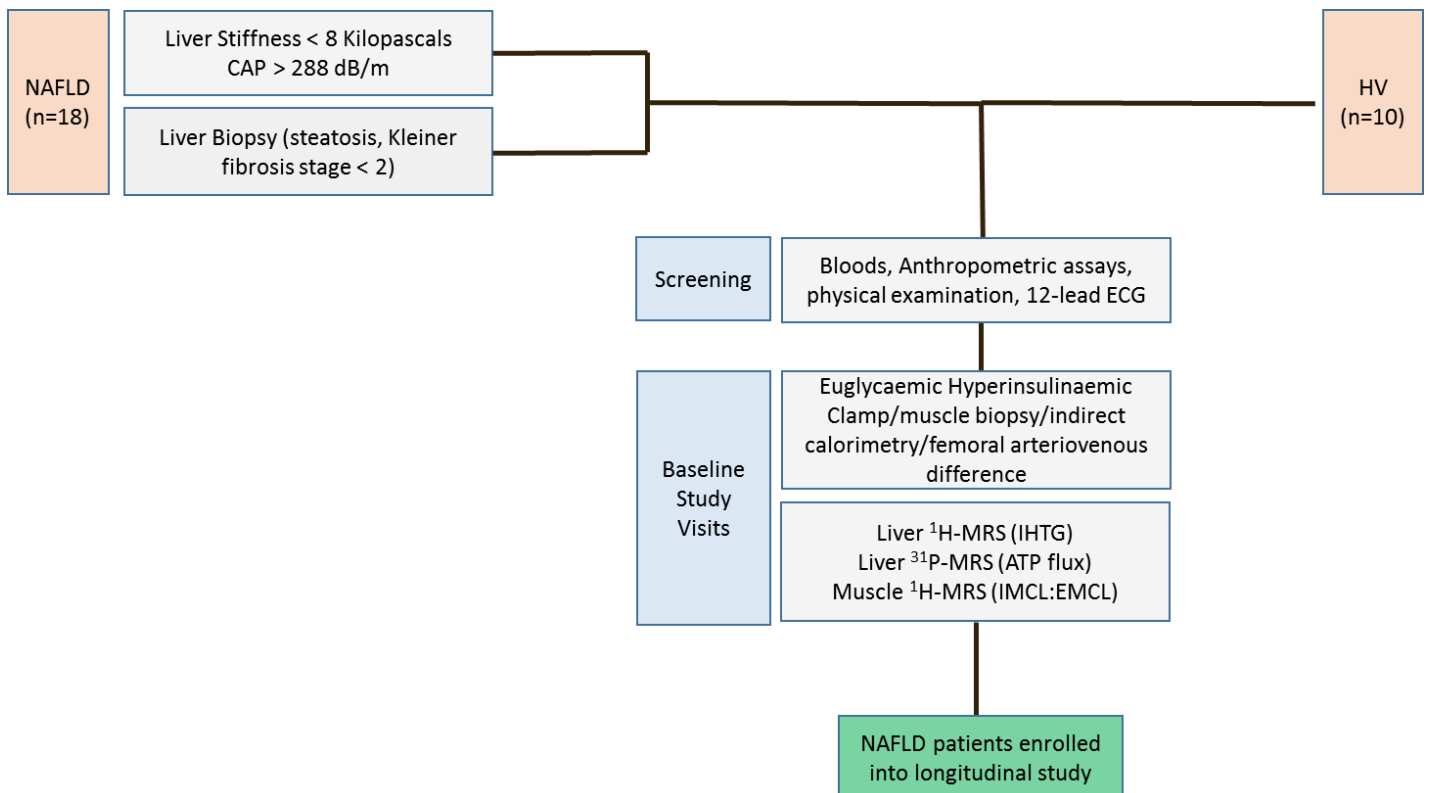


Figure 2. Flow through the research study



3.2.2 Imaging and Metabolic Studies

All imaging and metabolic assessments were carried out in the postabsorptive state, after an overnight fast. Following a 10-day cooling-off period from initial screening, subjects were invited to the Sir Peter Mansfield Imaging Centre (SPMIC), University of Nottingham for baseline MR spectroscopy scans. Three separate scanning sessions took place in a single morning, with a total scanning time of approximately 2 hours. Spectra were analysed by the author. Scanning was performed by Dr Stephen Bawden, Senior Research Fellow in the School of Physics, University of Nottingham.

3.2.2.1 ^1H MRS in the Liver

Liver MR measurements were all conducted on a Phillips Achieva 3T scanning system with a Philips XL 16 channel torso coil. Scout images were initially obtained for voxel placement away from major blood vessels or subcutaneous tissue. Subsequently, STEAM-localised ^1H MR Spectra were acquired from a 20 x 20 x 20 mm voxel sited in the right lower lobe of the liver. Spectra were obtained using a respiratory triggered, STEAM sequence during a single breath hold (relaxation time (TR) = 4000 milliseconds, echo time (TE) = 20, 40, 80, 160 milliseconds) and were repeated with water suppression, using 4 averages per spectral acquisition. Two spectra were collected without water suppression for correction to absolute lipid fat fractions as described previously. Data was post-processed using jMRUI software, including manual phase correction, frequency alignment and line broadening. Spectra were fitted using AMARES peak fitting with prior knowledge. Multi-echo amplitudes were used to determine water and fat T2, and IHTG was calculated based on proton density fat fractions.

3.2.2.2 ^1H MRS in the muscle

STEAM localized ^1H MRS were acquired from a 10 x 30 x 50 mm voxel in the vastus lateralis muscle with an MRCoils quadrature surface coil on a Philips 7T Achieva scanner. Non-water suppressed and water suppressed spectra were acquired at 4 different echo times (TR=4000ms, 16 averages at

TE=20ms and 8 averages at TE=40, 80 and 160ms). Spectra were line broadened and phase corrected using an in-house Matlab script, and a peak-dispersion fitting algorithm was developed to fit EMCL and IMCL peaks accounting for muscle fibre orientation. Multi-echo amplitudes were used to determine water and fat T2, lipid fraction and IMCL: EMCL ratios.

3.2.2.3 ³¹P MRS in the Liver

Slice localized ³¹P MR spectra were acquired from the liver using a Philips ³¹P single loop surface coil. Apparent T1 (T_{1app}) was measured using progressive saturation transfer ³¹P MRS (spectra fitted using jMRUI), whereby block pulses were applied to selectively irradiate the γATP resonance in the phosphorus spectrum. Total scan time for each participant was ~1 hour 15 minutes. Application of selective irradiation perturbs magnetisation of the ATP molecule from the equilibrium state (M₀) to steady state (M_z). The fractional change between these two states can then be mirrored around the inorganic phosphate (Pi) peak to measure the effect on its exchange partner. A first order rate constant (k) was then calculated from two ³¹P MRS spectra, one fully saturating γ-ATP (-2.5ppm) and the second mirrored about the inorganic phosphate (Pi) peak (14ppm). Forward rates of exchange through the ATP synthesis/hydrolysis cycle flux was then calculated as follows:

$$k = (1 - M_z/M_0) * \left[\frac{M_{0ATP}}{M_{0ATP} - M_{zATP}} \right] / T_{1app}$$

Where M₀ and M_z are the magnetisation of the exchange partner (Pi) in the steady and equilibrium states, respectively. M_{0ATP} is the ATP magnetisation in the control experiment, whereas M_{zATP} is the residual magnetisation of the saturated ATP in the T_{1app} is the apparent T1 relaxation time, calculated through a progressive saturation sequence.

3.2.3 Euglycaemic Hyperinsulinaemic Clamp

All participants underwent a dual-step euglycaemic hyperinsulinaemic clamp protocol within 10 days of their baseline MRI scan. This lasted for 6 hours in total, consisting of three main stages, in

combination with vastus lateralis muscle biopsies, indirect calorimetry and leg glucose uptake assessments (**Figure 3**).

Participants arrived in the David Greenfield Human Physiology Unit at 08:00 after an overnight fast. A dual energy X-ray absorptiometry (DEXA) scan (Lunar Systems, GE, USA) was performed to evaluate body composition. Parameters assessed included body fat mass, fat free mass, leg, arm and trunk composition. Subjects subsequently settled at a 45-degree angle (semi-supine) on a bed and underwent a muscle biopsy from the vastus lateralis muscle of the right leg. Muscle biopsy was performed by the author utilising the Bergström technique as described in **Chapter 2**. A maximum of two passes was performed per subject with a view to optimising tissue extraction.

Muscle tissue was snap frozen in liquid isopentane and subsequently liquid nitrogen to -160°C as described previously. Any further muscle tissue was mounted at room temperature for quantification of intramyocellular lipid fractions. Following muscle biopsy, subjects rested semi-supine while cannulae were inserted antegrade into the both antecubital fossae and retrograde into the dorsum of the left hand. The left hand was subsequently placed inside a warming box at 55°C to arterialise the venous drainage of the hand for blood glucose sampling. A central venous catheter was inserted into the participant's right femoral vein under ultrasound guidance, using aseptic technique, to enable quantification of leg glucose uptake (see below).

At approximately 09:00, 120 minutes prior to commencement of the hyperinsulinaemic clamp, a primed, continuous infusion of dideuterated $[6, 6\text{-}^2\text{H}_2]$ glucose was commenced and was continued for the duration of the dual-step clamp to allow for subsequent calculation of hepatic insulin sensitivity through quantification of glucose isotope enrichment. At 11:00, a primed infusion of human insulin was started at $15 \text{ mU/m}^2/\text{min}$ to suppress hepatic endogenous glucose production, and was continued for 120 minutes ("low dose" clamp, stage 1). After 120 minutes, (at approximately 13:00) the insulin infusion rate was increased to $60 \text{ mU/m}^2/\text{min}$ and was continued for a further 120 minutes ("high-

dose” clamp, stage 2). Throughout the insulin infusion, 20% dextrose (spiked with 1% dideuterated glucose to maintain plasma isotope enrichment) was infused at a variable rate to titrate blood glucose towards a euglycaemic target (4.50 mmol/l). Arterialised blood glucose was sampled at 5-minute intervals from the dorsum of the (heated) left hand and analysed in real time (Yellow Springs, USA).

Hepatic insulin sensitivity was determined using percentage suppression of Endogenous Glucose Production (EGP), calculated from stable isotope tracer data as the relative difference from baseline in glucose rate of appearance (Ra) during low dose insulin infusion, detailed in [Appendix 3](#). Skeletal muscle (i.e. whole-body) insulin sensitivity was calculated by evaluating the ability of insulin to stimulate glucose disposal (Rd), quantified as the relative increase above baseline in whole-body glucose Rd during high-dose insulin infusion in the second stage of the clamp.

3.2.4 Substrate oxidation

Indirect calorimetry was performed at baseline and for 15 minutes during steady state phases of each clamp step. Resting Energy Expenditure (REE) was calculated using Gas Exchange Measurement (GEM) systems as described in **Chapter 2**. Measurement of expired gases allowed for calculation of respiratory quotient, whole-body fat and carbohydrate oxidation under basal and progressively hyperinsulinaemic conditions.

At the end of the high-dose clamp, participants underwent a further muscle biopsy in the left vastus lateralis muscle. Insulin infusion was subsequently stopped and participants were fed with a high carbohydrate meal. Blood glucose was monitored for a further 60 minutes to ensure adequate endogenous control. Central and peripheral venous catheters were removed, and participants finished the study at approximately 17:00.

3.2.5 Leg Glucose Uptake

Net leg glucose uptake (LGU) was quantified using Fick's principle from the arteriovenous difference method. Femoral venous and 'arterialised' glucose samples (from the heated hand vein) were drawn simultaneously at seven time points during the clamp study (at baseline $t = 0$ and then at $t = 90, 105$ and 120 min during each stage of the clamp, corresponding to steady state conditions). Blood flow was calculated from the blood velocity and diameter of the femoral artery, determined at the level of the inguinal groove at each time point using B-Mode imaging and Doppler Ultrasound (5-7.5 MHz linear array probe, Toshiba Aplio, Japan). Leg glucose uptake was subsequently determined as the product of leg blood flow and the arterial minus femoral venous glucose concentration. Leg glucose extraction data are expressed relative to leg mass, as determined by DEXA scan.

$$\text{Leg Glucose Uptake} = A_G - V_G \times \text{leg blood flow}$$

3.2.6 Sample Analysis

Fresh whole blood was collected at 15-minute intervals during steady state conditions in both the low and high dose phases of the clamp. The blood was spun at 3000G, separated into its plasma and serum components and aliquoted into Eppendorf tubes. Samples were frozen at -80°C to enable subsequent batch analysis of plasma non-esterified fatty acids (NEFA), CRP, triglycerides, insulin and glucose isotope enrichment at serial time points over the clamp study. Rates of endogenous glucose production (EGP) were calculated based on stable isotope enrichment from gas chromatography mass spectrometry (GC-MS), as described in **Chapter 2**.

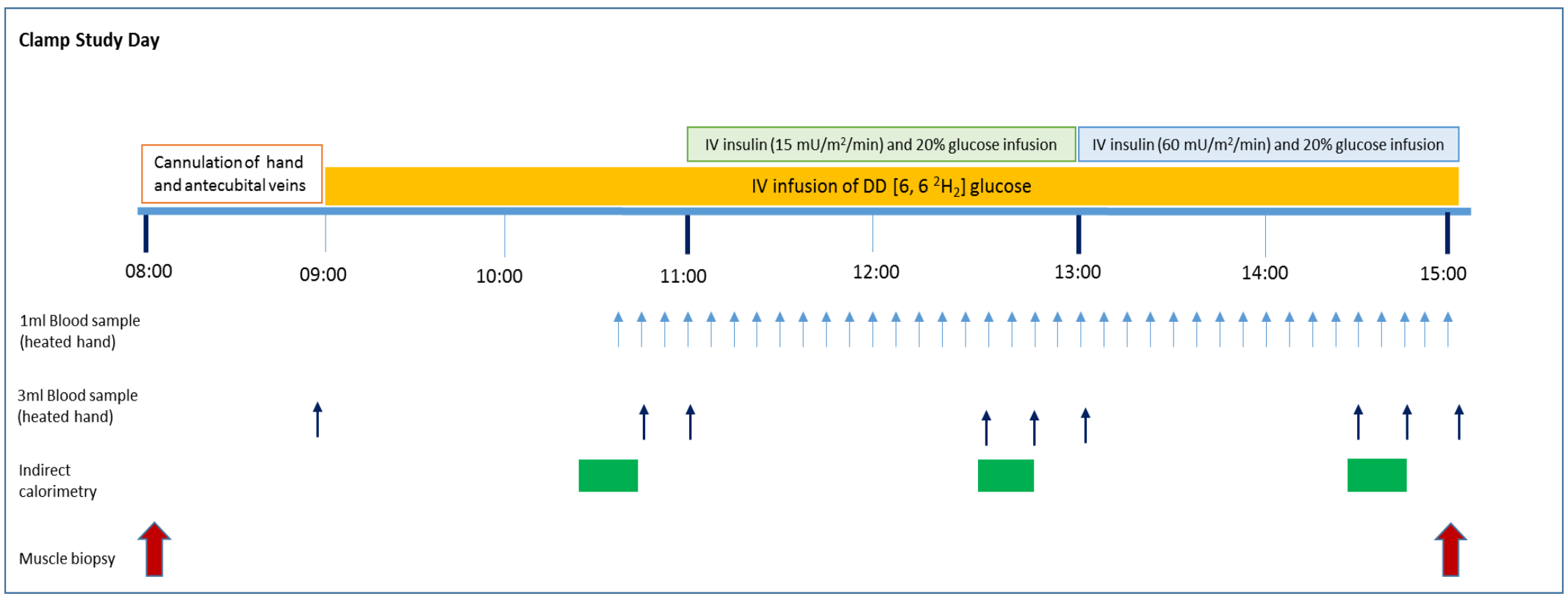


Figure 3 Schematic for the two-step euglycaemic hyperinsulinaemic clamp protocol

Subjects arrived at 08:00 following an overnight fast. After initial DEXA scan for body composition, a muscle biopsy was performed in the right vastus lateralis. Following this, both antecubital fossae were cannulated and a cannula was placed retrograde into the dorsum of the left hand. A primed continuous infusion of dideuterated glucose was started at approximately 09:00, following muscle biopsy and cannulation. This was continued throughout the clamp to obtain glucose isotope enrichment for subsequent calculation of hepatic insulin sensitivity. The low-dose (1st step) insulin infusion was commenced at 11:00 and the high dose (2nd step) infusion began at 13:00. Steady state was assumed in the final 30 minutes of each stage of the clamp. Blood was drawn at 15-minute intervals during steady state conditions measurement of arteriovenous difference (leg glucose uptake), non-esterified fatty acids, triglycerides, CRP and insulin. Indirect calorimetry was performed at baseline and during steady state in both stages of the clamp to assess resting energy expenditure and whole body substrate oxidation. 0.5 mls of blood was drawn at 5-minute intervals from the retrograde cannula in the warming device for assessment of ‘arterialised’ glucose concentration. Exogenous dextrose infusion was titrated according to these measurements to achieve a euglycaemic target value of 4.50 mmol/l.

3.2.7 Plasma VLDL concentrations

Whole blood was separated into plasma components and refrigerated at 4°C until the following day. Plasma samples were then delivered to the University of Nottingham Sutton Bonnington campus, where very low-density lipoprotein (VLDL) subfractions were isolated from plasma through density gradient ultracentrifugation. [These experiments have been delayed due to Covid restrictions. Results are not presented in this thesis].

3.2.8 Muscle Biopsy Analyses

Muscle biopsy samples were snap-frozen and crushed in liquid nitrogen and stored at – 80 °C for subsequent analysis. Tissue homogenates were transferred to an Eppendorf tube, freeze dried for 24 hours and then powdered in a mortar. Specimens were dissected free of connective tissue and blood clots using a scalpel and forceps. Powdered tissue samples were aliquoted into Eppendorf tubes for perchloric acid extraction to determine tissue concentrations of free carnitine, long chain acylcarnitines and acetylcarnitine (with total carnitine content representing the sum of these subfractions) using the radioisotopic method described by Cederblad (1990) [155].. Remaining muscle tissue was preserved for glycogen, ATP and phosphocreatine extraction and determination. [These experiments have been delayed due to Covid restrictions. Results are not presented in this thesis].

3.2.9 Confocal microscopy

Fresh samples from the muscle biopsy were mounted, fixed in 1% osmium tetroxide, dehydrated in ethanol and prepared in resin. Fine transverse slices (15 µm thickness) were prepared using an ultramicrotome and the sections were analysed using confocal microscopy. Micrographs from at least 4 sections of muscle were chosen at random and analysed by the operator, who was blinded to subject characteristics. A Zeiss LSM700, Axio Imager 2 confocal microscope (Zeiss International, Germany) operating ZEN (Black Edition) software from ZEISS International was used to image stained sections at 20x magnification. Scanned fibre type images were analysed with ZEN Blue software while IMCL

images were opened in FIJI to outline individual fibres in regions of interest (ROIs). % IMCL was calculated total lipid area within each sample $[(\text{Total lipid Area}) / (\text{Total Tissue Area})]$ within each ROI (**Figure 4**). These assessments were carried out by Prince Chivaka, doctoral research fellow, School of Life Sciences. [These experiments have been delayed due to Covid restrictions. Results are not presented in this thesis].

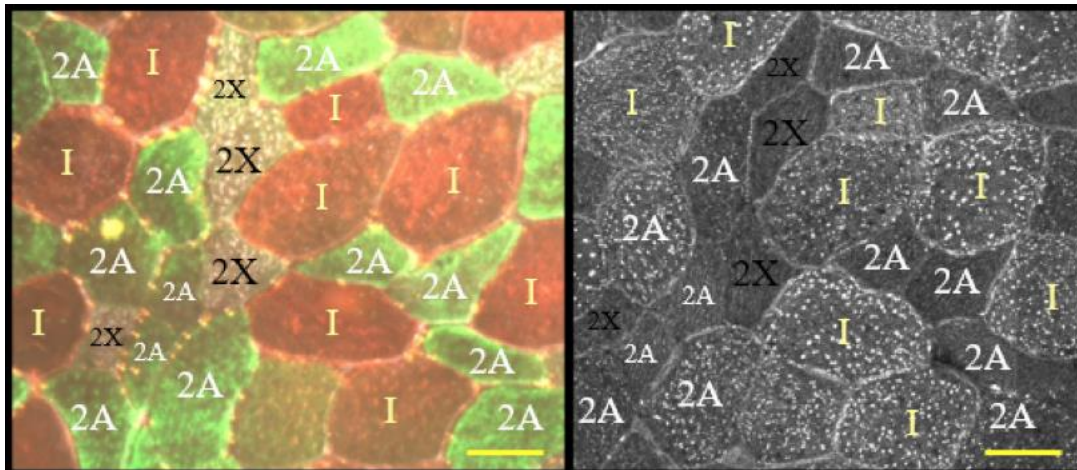


Figure 4 Immunohistochemical staining of muscle fibre type is shown in the left panel while fluorescent staining of lipid droplets with Bodipy-493/503 is shown in the right panel. Yellow bar reflects 50 μM .

3.2.10 Statistical Analysis

All analyses were conducted using SPSS software version 24.0 (IBM, Armonk, NY, USA) and *R* software. Data were tested for normality using the Kolmogorov-Smirnoff and Shapiro Wilks tests, with criteria for normality met if $p > 0.05$. Differences in baseline characteristics between healthy volunteers and NAFLD participants were compared using the student's independent *t* test for normally distributed continuous data. Normally distributed baseline data is provided as mean (SD). Non-normally distributed data are presented as median \pm interquartile range.

Comparisons between non-parametric data were made using the Independent Samples' Mann-Whitney U Test. Pearson's and Spearman's bivariate correlation coefficients were used to describe relationships between continuous variables as appropriate. Two-way mixed analysis of variance

(ANOVA) was used to determine interactions between groups for continuous variables over time. The paired student's *t* test was used to compare data within participant groups over two time periods and the one-way ANOVA was used to compare groups across 3 time periods.

3.3 Results

3.3.1 Patient Demographics

A total of 10 healthy volunteers and 18 NAFLD subjects were studied. Baseline anthropometric, demographic and metabolic characteristics of these groups are shown in **Table 1**. As expected, anthropometric measures corresponding to cardiometabolic risk were significantly higher in the NAFLD versus control participants (BMI, waist circumference, waist: hip ratio, body fat %). Groups were well matched in age ($p=0.48$) and fasting plasma glucose concentration was not significantly different between groups ($p=0.06$). Fasting plasma insulin, HOMA-IR and Adipo-IR concentrations were all significantly higher in the NAFLD versus control participants ($p<0.001$, <0.001 and 0.003 , respectively), suggesting clinically significant whole-body insulin resistance (**Figure 5**). A negative correlation between Adipo-IR and whole-body insulin sensitivity was shown (**Figure 6A**), as well as between IHTG and %FFA suppression during low-dose hyperinsulinaemia (a marker of adipose tissue insulin sensitivity) (**Figure 6B**). Circulating lipid fractions tended to be higher in the NAFLD group, who had significantly higher triglyceride ($p<0.001$) and lower HDL ($p=0.03$) concentrations. Although LDL concentration was higher in the NAFLD participants, this did not reach statistical significance ($p=0.08$). Mean plasma insulin concentration in NAFLD participants was significantly higher than in subjects with normal IHTG content ($p<0.001$).

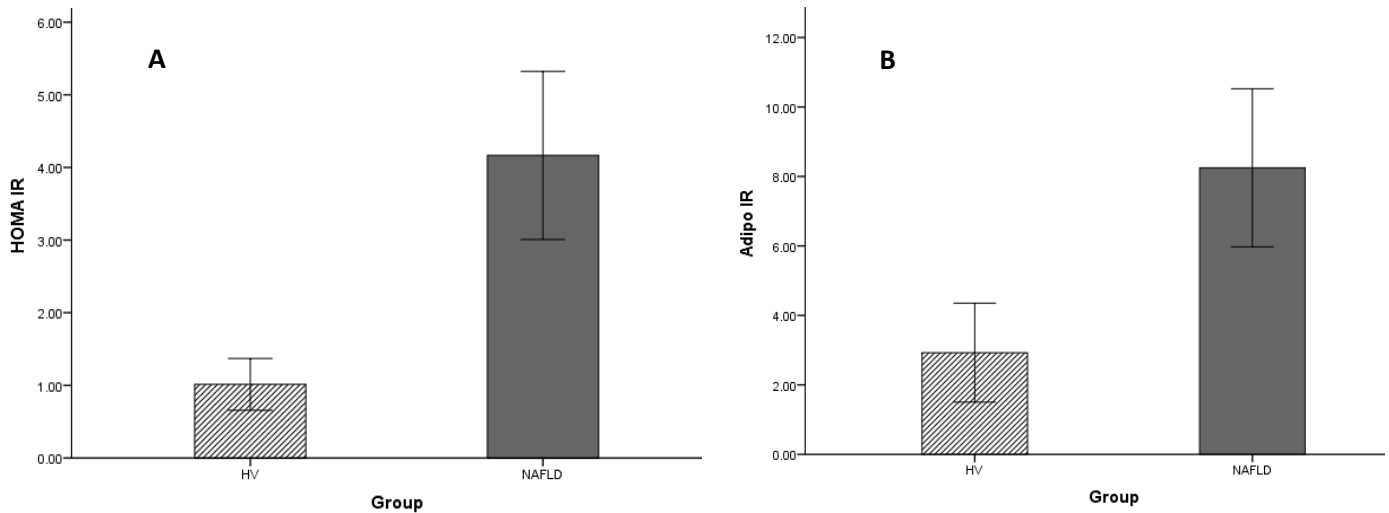


Figure 5 (A) Mean HOMA-IR in healthy volunteers versus NAFLD participants (1.01 ± 0.56 vs 4.16 ± 2.52 , 95% CI -4.40 — 1.89 , $P < 0.0001$) and (B) Mean Adipo-IR in healthy volunteers and NAFLD participants (2.93 ± 2.25 vs 8.25 ± 4.95 , 95% CI, $P = 0.003$)

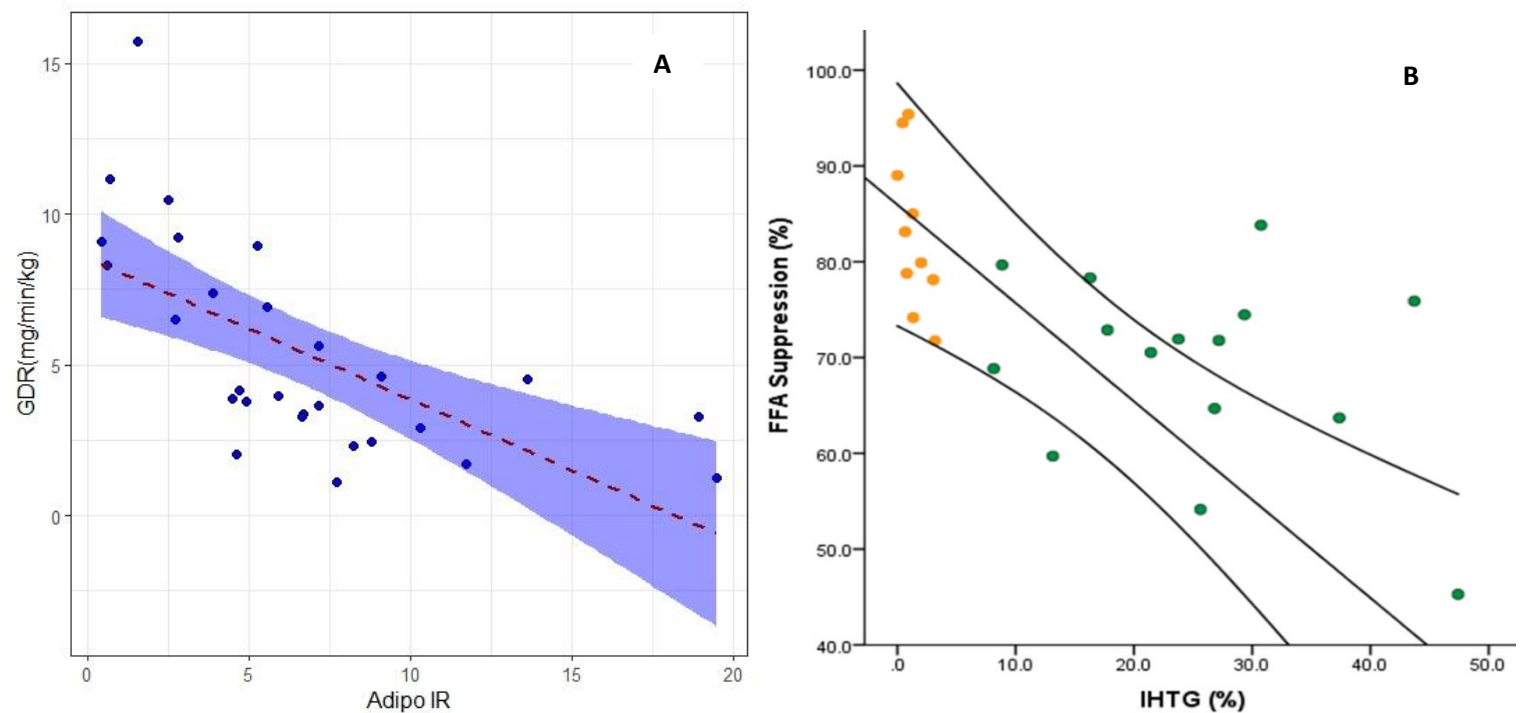


Figure 6 Relationship between indices of adipose tissue insulin resistance, whole body insulin sensitivity and liver fat. (A) Adipose tissue insulin resistance correlated negatively with whole-body insulin sensitivity ($r = -0.64$, $p < 0.001$). (B) Percentage suppression of plasma free fatty acids during low dose hyperinsulinaemia (low-dose clamp) is another method of quantifying adipose tissue insulin sensitivity, and correlated negatively with intrahepatic triglyceride ($r = -0.612$, $p = 0.001$). Healthy volunteers are shown in yellow circles, patients with NAFLD are shown in green circles.

	Reference Range	Healthy volunteers (n=10)	NAFLD subjects (n=18)	P value
<i>Anthropometrics:</i>				
Age (years)		33.8 ± 9.3	36.3 ± 9.1	0.48
Height (m)		1.74 ± 0.06	1.79 ± 0.06	0.06
Body Weight (kg)		77.8 ± 11.0	104.7 ± 16.7	<0.001
BMI (kg/m ²)		25.5 ± 2.2	32.2 ± 4.4	<0.001
Waist circumference (cm)		91.1 ± 9.6	107.5 ± 9.0	0.001
Hip circumference (cm)		98.2 ± 8.9	111.5 ± 9.1	0.002
Waist:Hip Ratio		0.93 ± 0.044	0.96 ± 0.037	0.03
Body fat (%)		28.4 ± 8.16	36.1 ± 5.56	0.007
<i>Liver Biomarkers:</i>				
ALT (IU/L)	0-45	25.6 ± 12.7	65.9 ± 30.8	<0.001
AST (IU/L)	0-35	31.0 ± 14.9	45.5 ± 30.2	0.09
<i>Metabolic biomarkers:</i>				
Fasting plasma glucose (mmol/l)	6-25	4.53 ± 0.52	4.95 ± 0.65	0.06
Fasting insulin (mIU/L)		4.91 ± 2.5	16.6 ± 7.2	<0.001
HOMA-IR		1.01 ± 0.56	4.16 ± 2.52	<0.001
NEFA (mmol/l)		0.51 ± 0.21	0.46 ± 0.15	0.453
ADIPO-IR	≤ 5.0	2.93 ± 2.25	8.25 ± 4.96	0.003
Total Cholesterol (mmol/l)	0.4-1.8	4.41 ± 0.95	4.94 ± 0.91	0.148
Triglycerides (mmol/l)	≤ 1.0	0.90 ± 0.28	1.75 ± 0.80	<0.001
HDL cholesterol (mmol/l)	≤ 3.0	1.52 ± 0.65	1.15 ± 0.19	0.03
LDL cholesterol (mmol/l)	15 -53	2.44 ± 0.82	3.02 ± 0.82	0.08
Plasma Free Carnitine		35.9 ± 5.1	37.5 ± 7.8	0.59
Glucose disposal rate (mg/kg/min)		8.99 ± 3.20	3.43 ± 1.58	<0.001
%EGP Suppression		40.1 ± 30.0	15.9 ± 15.6	0.009
<i>Liver/Muscle Fat</i>				
IMCL:EMCL Ratio		0.20 ± 0.18	1.16 ± 0.81	<0.001
IHTG (%)	<5.56	1.44 ± 1.1	25.46 ± 12.1	<0.001

Table 1 Baseline clinical characteristics and laboratory parameters: comparison between NAFLD participants and healthy control volunteers. Data expressed as mean (± SD) if normally distributed and median (± IQR) if non-normally distributed.

3.3.2 Glucose and Lipid Kinetics

Intrahepatic triglyceride content was positively correlated with the adipose tissue insulin resistance index ($r = 0.498$, $p = 0.006$) and negatively correlated with peripheral insulin sensitivity ($r = -0.738$, $p < 0.0001$). During hyperinsulinaemia (high dose insulin infusion, stage 2), NAFLD was associated with lower whole-body glucose disposal compared to control volunteers (3.43 ± 1.58 versus 8.99 ± 3.20 mg/kg/min, $p < 0.001$), consistent with peripheral insulin resistance in this young, non-diabetic cohort (**Figure 7**). Selective hepatic insulin resistance was demonstrated in the NAFLD group, with significantly attenuated suppression of EGP during low dose hyperinsulinaemia compared to controls ($15.9 \pm 15.6\%$ versus $40.1 \pm 30\%$, $p = 0.009$), **Table 3**. The relative suppression of endogenous glucose production (EGP) during the low-dose insulin infusion was negatively correlated to IHTG content ($r = -0.407$, $p = 0.032$) (**Figure 8B**). Percentage suppression of circulating non-esterified (free) fatty acids during the low-dose insulin infusion correlated negatively with IHTG ($r = -0.612$, $p = 0.001$), again signalling progressively impaired suppression of lipolysis with increasing liver fat content.

Serial plasma insulin concentrations during the hyperinsulinemic-euglycemic clamp procedure were higher in the NAFLD cohort than in healthy volunteers during the low dose (49.5 ± 24.6 versus 27.7 ± 5.5 mIU/L, respectively, $p = 0.01$) and high dose (125.4 ± 28.6 versus 105.1 ± 18.0 respectively, $p = 0.05$) insulin infusions, **Figure 9**. While basal plasma NEFA concentrations were not significantly different between NAFLD and control groups (0.46 ± 0.15 versus 0.51 ± 0.21 mmol/l, respectively, $p = 0.453$), serial plasma NEFA concentrations remained elevated in the NAFLD cohort during both stage 1 (0.18 ± 0.13 versus 0.09 ± 0.06 mmol/l, $p = 0.05$) and stage 2 (0.06 ± 0.016 versus 0.01 ± 0.003 mmol/l, $p = 0.014$) of the clamp, indicating impaired insulin-mediated suppression of lipolysis despite higher steady-state insulin levels in the NAFLD cohort (**Figure 10**). The adipose tissue insulin resistance index (Adipo IR) correlated negatively with Glucose Rd (**Figure 6**).

A multivariate linear regression model was built to evaluate independent factors predictive of hepatic and whole-body insulin resistance. Stepwise linear regression confirmed that IHTG was the strongest predictor of whole-body insulin resistance ($F(1, 21) = 21.9, r^2 = 0.591, p < 0.0001$), accounting for 59% of the variability (**Table 2A**). This effect was independent of BMI, IMCL: EMCL ratio, Waist: Hip ratio, plasma NEFA and fasting serum insulin. Circulating triglyceride concentration was also an independent predictor of whole-body insulin resistance and added to the model in a statistically significant manner ($F(2, 19) = 21.9, r^2 = 0.697, p = 0.018$), accounting for a further 10% in variability. Stepwise linear regression demonstrated that muscle lipid fraction (IMCL: EMCL ratio) was the strongest predictor of hepatic insulin resistance ($F(1, 20) = 7.9, r^2 = 0.285, p = 0.001$), **Table 2B**.

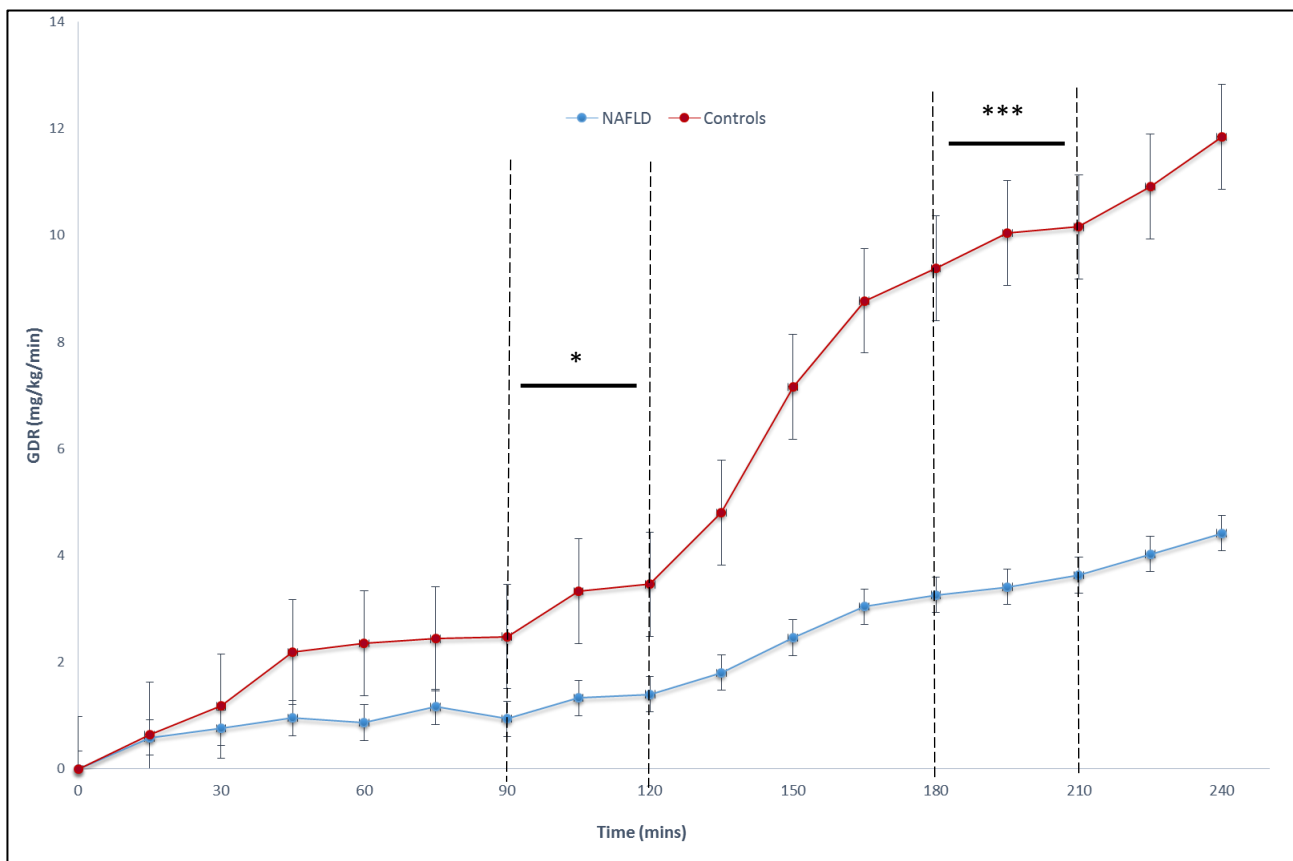


Figure 7 Glucose disposal rate ('M') over the course of the two-step euglycaemic hyperinsulinaemic clamp. From T_0 - T_{120} , a low dose insulin infusion ($15 \text{ mU/m}^2/\text{min}$) was administered for assessment of hepatic insulin sensitivity. From T_{120} - T_{240} , a high dose insulin infusion was administered to assess peripheral (i.e. whole body) insulin sensitivity. Values represented as mean \pm SEM * $P < 0.05$ *** $P < 0.001$

Coefficients ^a										
Model		Unstandardized Coefficients		Standardized Coefficients	t	Sig.	95.0% Confidence Interval for B		Collinearity Statistics	
		B	Std. Error	Beta			Lower Bound	Upper Bound	Tolerance	VIF
1	(Constant)	8.573	.825		10.395	.000	6.853	10.294		
	IHTG	-.180	.033	-.769	-5.378	.000	-.250	-.110	1.000	1.000
2	(Constant)	10.533	1.052		10.016	.000	8.332	12.734		
	IHTG	-.167	.030	-.715	-5.589	.000	-.230	-.105	.973	1.027
	TrigConc	-1.447	.560	-.330	-2.583	.018	-2.620	-.274	.973	1.027

a. Dependent Variable: GDR

Table 2A Multiple Linear Regression Results for Predictors of whole-body insulin

Coefficients ^a								
Model		Unstandardized Coefficients		Standardized Coefficients	t	Sig.	Collinearity Statistics	
		B	Std. Error	Beta			Tolerance	VIF
1	(Constant)	38.647	6.702		5.766	.000		
	IERatio	-15.965	5.648	-.534	-2.827	.010	1.000	1.000

a. Dependent Variable: EGPsupp

Table 2B Multiple Linear Regression Results for Predictors of hepatic insulin resistance

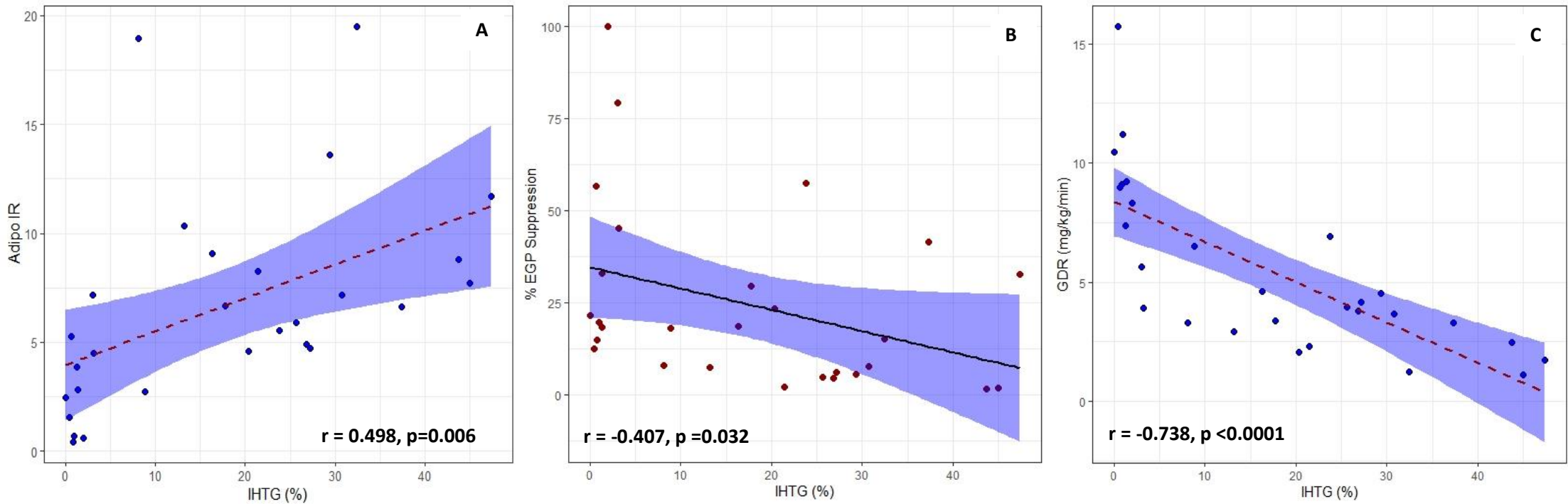


Figure 8 Relationships between (A) Adipose Tissue Insulin Resistance indices and IHTG content (B) Insulin-mediated suppression of Endogenous Glucose Production during stage 1 of the euglycemic-hyperinsulinemic clamp procedure and IHTG content and (C) insulin-mediated stimulation of glucose uptake (glucose disposal rate) during stage 2 of the euglycemic-hyperinsulinemic clamp procedure and IHTG content.

	Indicator	Subjects	Low dose	High dose
Glucose Rd (mg/kg/min)	Skeletal muscle insulin sensitivity	HV	2.63 ± 1.6	8.99 ± 3.2
		NAFLD	1.22 ± 0.63	3.43 ± 1.6
% EGP Suppression	Hepatic insulin sensitivity	HV	40.13 ± 30	N/A
		NAFLD	15.9 ± 15.6	N/A
Adipo IR (NEFA x plasma insulin)	Adipose Tissue Insulin Resistance	HV	2.25 ± 2.62	1.35 ± 1.82
		NAFLD	5.41 ± 6.22	4.26 ± 3.98

Table 3 Substrate kinetics during stage 1 (low dose insulin infusion) and stage 2 (high dose insulin infusion) of the euglycaemic hyperinsulinaemic clamp in NAFLD patients and controls. Results expressed as mean (SD) for normally distributed data. Serial Adipo IR was not normally distributed, hence results are presented as median (IQR).

3.3.3 Liver Biochemistry

Plasma transaminase concentrations (alanine and aspartate aminotransferase) were higher in NAFLD than in subjects with a normal IHTG content. This reached significance for ALT differences (65.6 ± 30.8 versus 25.6 ± 12.7 U/L, $p < 0.001$) but not AST ($p = 0.09$). Serum ALT concentration correlated positively with Intrahepatic triglyceride (Spearman's rho $r = 0.726$, $p < 0.0001$) and inversely with skeletal muscle insulin sensitivity ($r = -0.630$, $p < 0.0001$) and hepatic insulin sensitivity ($r = -0.318$, $p = 0.09$) and positively correlated with adipose tissue insulin resistance ($r = 0.593$, $p = 0.001$).

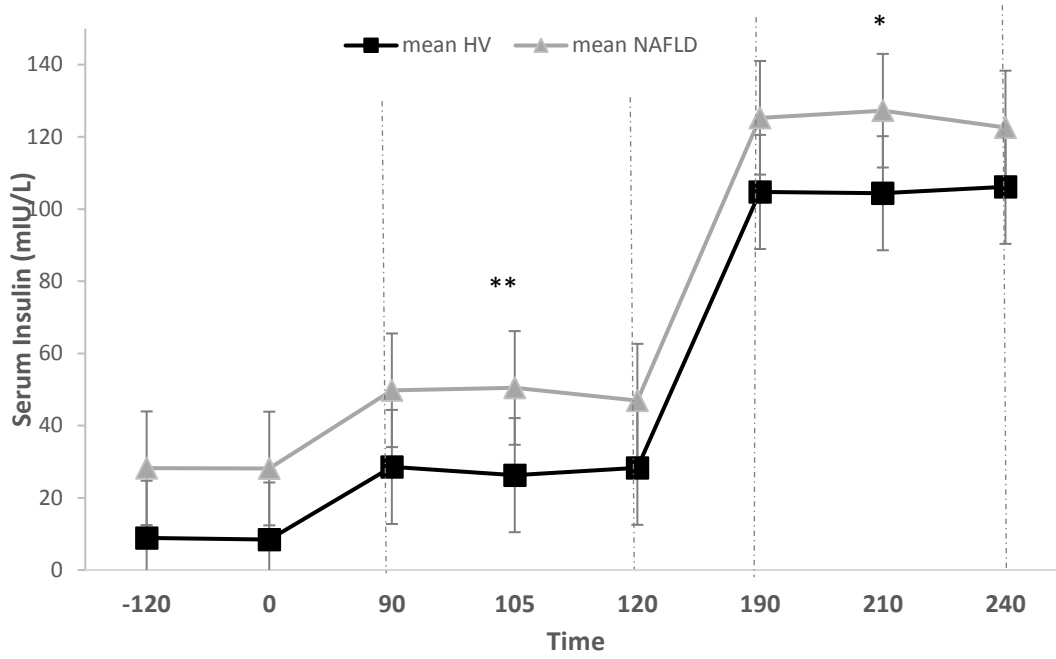


Figure 9 Serum insulin concentration over time through the course of the two-step euglycaemic hyperinsulinaemic clamp. Values represented as mean \pm SEM * $P < 0.05$

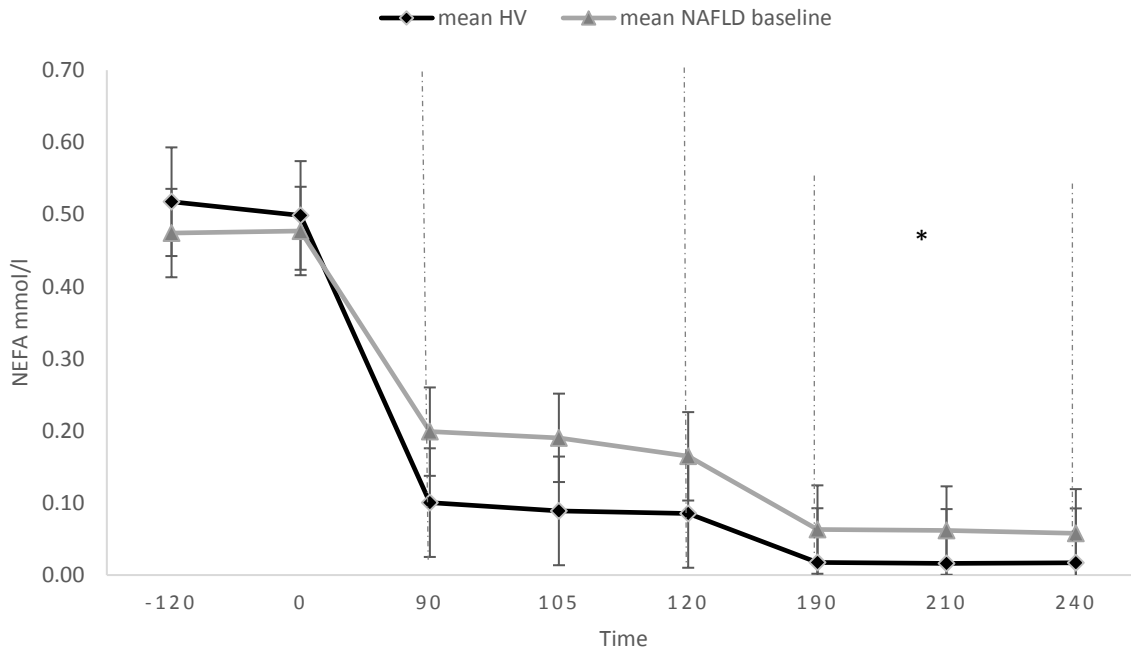


Figure 10 Serum NEFA concentrations over time through the course of the two-step euglycaemic hyperinsulinaemic clamp. Values represented as mean \pm SEM * $P < 0.05$

3.3.4 Substrate Oxidation and Metabolic Flexibility

Indirect calorimetry confirmed the presence of metabolic inflexibility in the NAFLD cohort, with blunted substrate switching from lipid to carbohydrate in the face of hyperinsulinaemia (**Table 4**). The rate of carbohydrate oxidation during Stage 2 (high-dose insulin infusion) of the clamp was significantly attenuated in NAFLD versus control participants (2.04 ± 0.85 versus 3.33 ± 0.89 mg/kg/min, $p = 0.001$) but did not differ significantly at baseline (1.06 ± 0.37 versus 1.36 ± 0.67 mg/kg/min, $p = 0.174$) or during the low-dose infusion in stage 1 (1.17 ± 0.62 versus 1.62 ± 0.73 mg/kg/min, $p = 0.102$). See **Figure 11A**.

The rate of lipid oxidation adjusted for weight was similar in the basal (postabsorptive) state between NAFLD and control groups (1.04 ± 0.29 versus 1.20 ± 0.23 mg/kg/min, $p = 0.136$). No significant change in fat oxidation rates between groups was observed during Stage 1 (1.21 ± 0.78 versus 1.07 ± 0.37 mg/kg/min, $p = 0.596$) or Stage 2 of the clamp (0.71 ± 0.33 versus 0.51 ± 0.23 mg/kg/min, $p = 0.09$), **Figure 11B**. Control subjects suppressed their lipid oxidation rates by $57.5\% \pm 9.2\%$ of baseline,

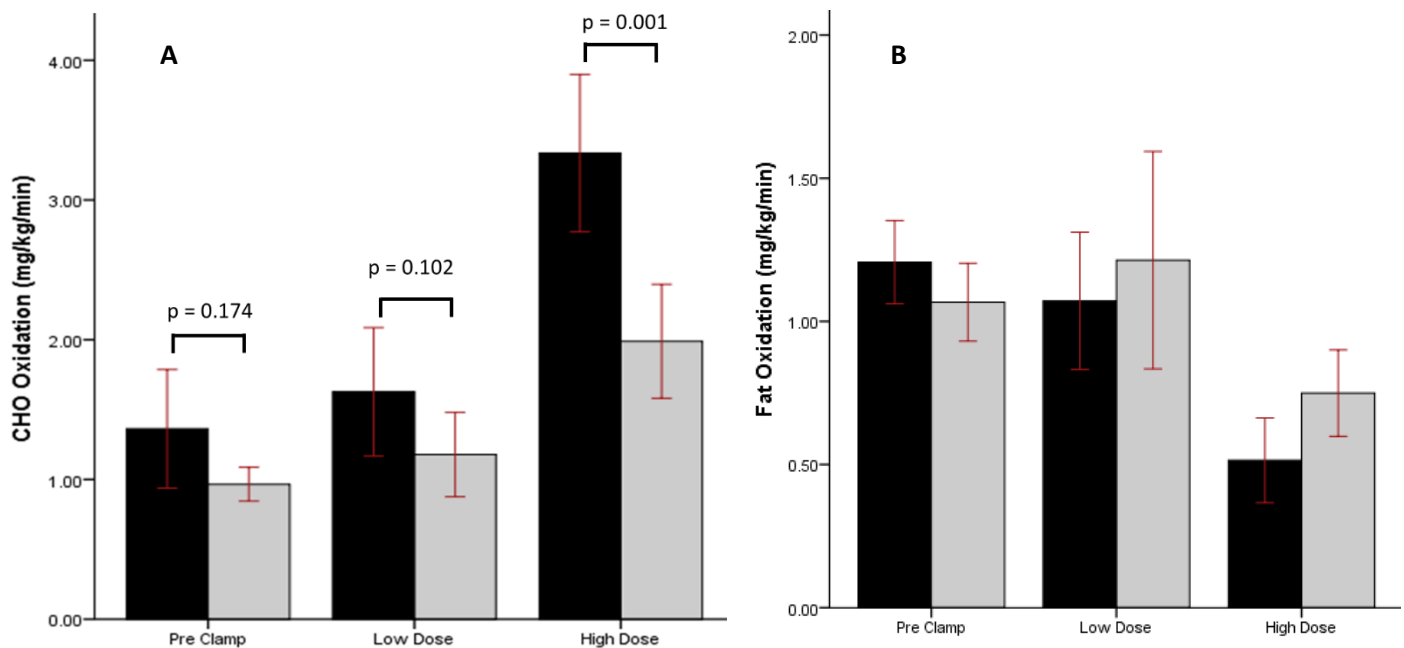


Figure 11 (A) Carbohydrate and (B) Lipid Oxidation during the euglycaemic hyperinsulinaemic clamp in healthy volunteer (black bars) versus NAFLD (grey bars) cohorts. Data expressed as mean \pm SEM.

compared with a smaller suppression of $31.7 \pm 9.1\%$ of baseline in the NAFLD group ($p = 0.004$ for control versus NAFLD).

		NAFLD (n =18)	Control (n=10)	P value
Respiratory Quotient	Basal	0.79 ± 0.05	0.79 ± 0.04	0.979
	Stage 1	0.79 ± 0.04	0.82 ± 0.05	0.227
	Stage 2	0.85 ± 0.06	0.91 ± 0.05	0.006
CHO Oxidation (mg/kg/min)	Basal	1.06 ± 0.37	1.36 ± 0.67	0.174
	Stage 1	1.17 ± 0.62	1.62 ± 0.73	0.102
	Stage 2	2.04 ± 0.85	3.33 ± 0.89	0.001
Fat Oxidation (mg/kg/min)	Basal	1.04 ± 0.29	1.20 ± 0.23	0.136
	Stage 1	1.21 ± 0.78	1.07 ± 0.37	0.596
	Stage 2	0.71 ± 0.33	0.51 ± 0.23	0.09
Energy Expenditure (kcal/kg/day)	Basal	18.5 ± 2.16	21.3 ± 3.11	0.008
	Stage 1	17.9 ± 1.76	21.0 ± 2.29	0.001
	Stage 2	18.6 ± 1.87	22.5 ± 2.94	$P < 0.0001$

Table 4. Respiratory Quotient, substrate oxidation and energy expenditure at baseline and during both stages of the euglycaemic hyperinsulinaemic clamp

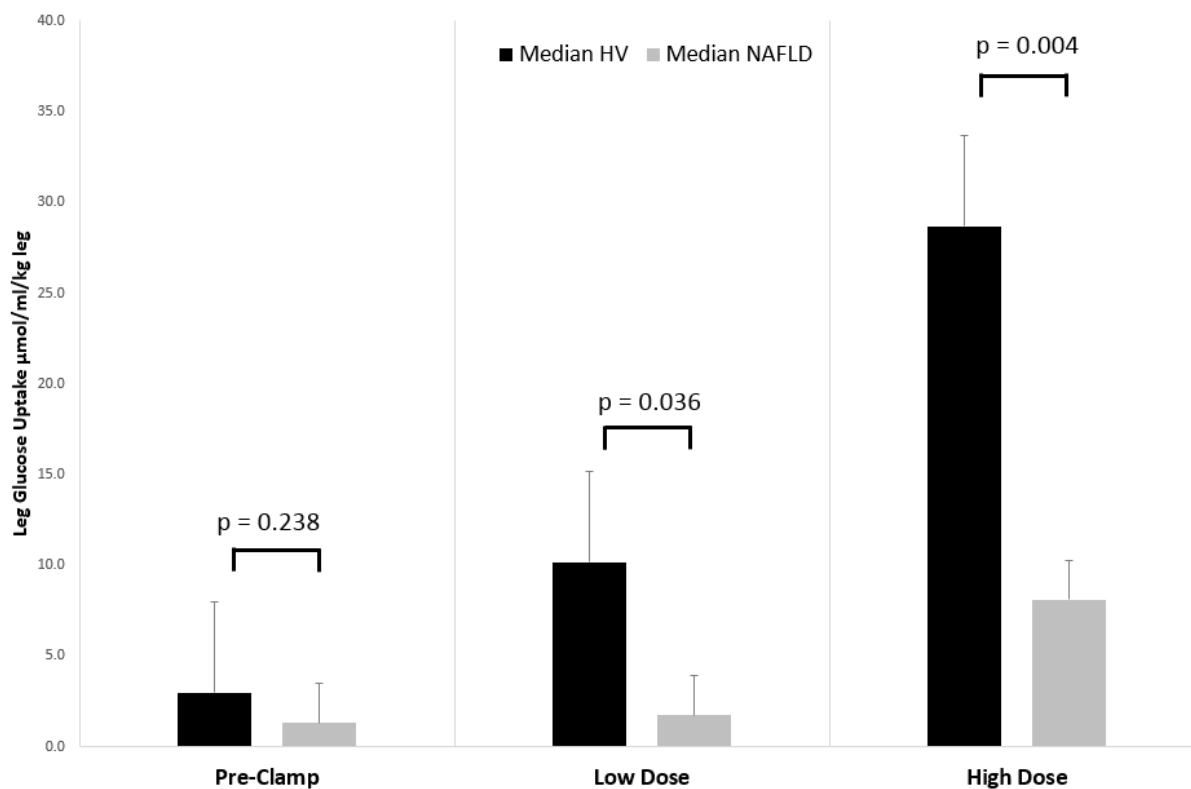


Figure 12 Leg Glucose Uptake in control versus NAFLD groups, corrected for lean leg mass (kg). Data expressed as median \pm IQR. Note: comparisons made using the Independent samples Mann Whitney U Test as leg glucose uptake data were not normally distributed in the NAFLD group.

3.3.5 Leg Glucose Uptake

Net leg glucose uptake adjusted for lean leg mass was not significantly lower in NAFLD compared to control groups in the basal (postabsorptive) state (1.31 ± 1.60 versus 2.98 ± 6.24 $\mu\text{mol/ml/kg}$ leg mass, $p = 0.238$). However, insulin-mediated leg glucose uptake was significantly higher in control versus NAFLD subjects during low-dose (1.74 ± 3.07 versus 10.16 ± 16.3 $\mu\text{mol/ml/kg}$, $p = 0.036$) and high-dose (8.09 ± 15.0 versus 28.67 ± 42.4 $\mu\text{mol/ml/kg}$, $p = 0.004$) hyperinsulinaemia (**Figure 12**). Insulin infusion increased leg blood flow significantly in the control group (40.2 ± 17.4 to 61.0 ± 23.3 ml/min/kg from basal to stage 2 of the clamp, $p = 0.002$) and NAFLD group (20.7 ± 12.7 to 26.1 ± 11.6 $p = 0.01$), but the magnitude of this change was far greater in the control group (52.5% versus 26.2%). A significant difference between groups was demonstrated when comparing basal leg blood flow to leg blood flow during the high dose clamp (one-way ANOVA, $p = 0.003$, **Figure 13**). For the control group, leg blood flow (LBF) did not increase significantly between basal and low-dose insulin infusion time points ($M = 1.58$, $SE = 3.61$, $p = 1.00$), but was significantly increased during the high dose insulin infusion compared to baseline ($M = 20.9$, $SE = 5.08$, $p = 0.02$) and at high-dose compared to low-dose ($M = 0.33$, $SE = 0.03$ mmol/L , $p < .0005$).

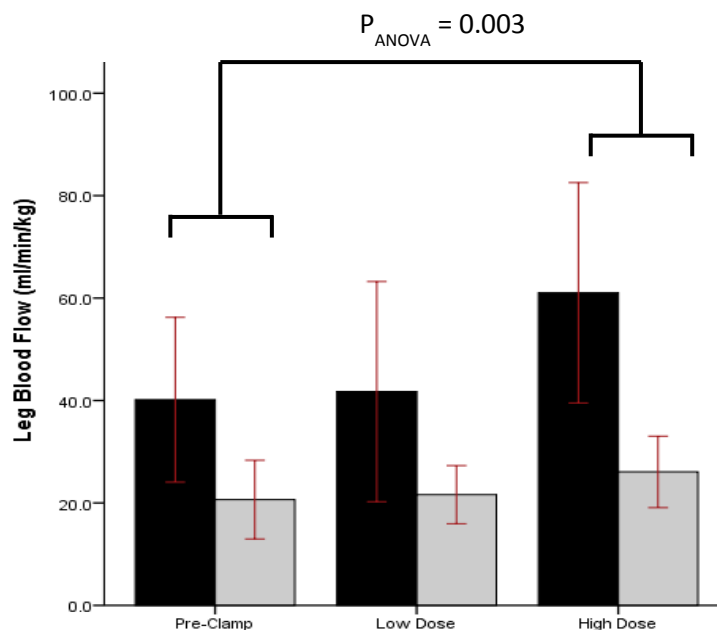


Figure 13 Leg Blood flow under basal conditions and during progressive hyperinsulinaemia, in NAFLD (grey bars) and healthy volunteers (black bars).

3.3.6 Metabolic impact of fat partitioning

IMCL: EMCL ratio correlated inversely with whole-body glucose disposal ($r = -0.601$, $p=0.002$, **Figure 14A**) and correlated positively with indices of adipose tissue insulin resistance ($r= 0.531$, $p =0.008$, **Figure 14B**). There was a significant negative correlation between IMCL: EMCL ratio and hepatic insulin sensitivity ($r = -0.69$, $p <0.001$, **Figure 15**). Intrahepatic triglyceride was positively associated with muscle IMCL: EMCL ratio ($r = 0.567$, $p = 0.004$), **Figure 16**. The ratio of intra-to-extramyo cellular lipid (IMCL: EMCL ratio) was significantly higher in the NAFLD versus control group (1.16 ± 0.80 versus 0.20 ± 0.18 , $p<0.0001$, **Figure 17**). Muscle lipid fractions were the strongest independent predictor of hepatic insulin resistance in a multivariate regression model ($p = 0.001$, **Table 2B**).

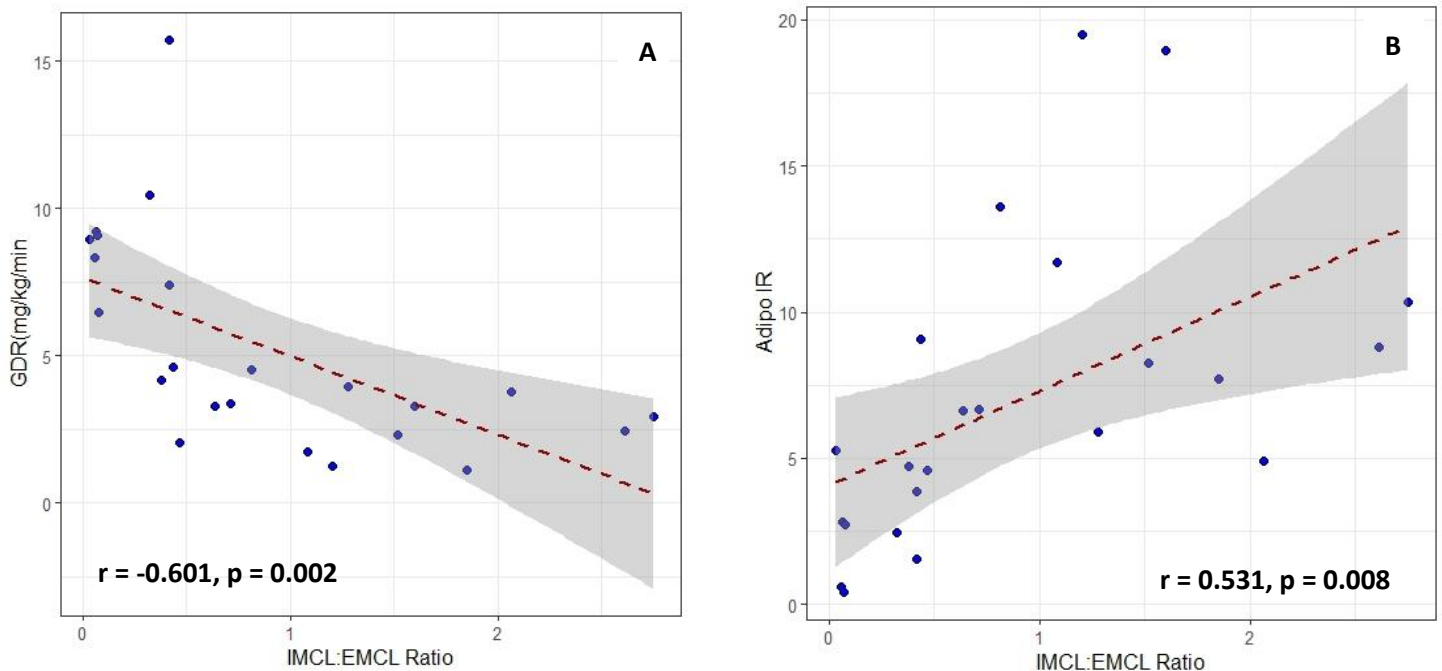


Figure 14 Panel (A) Relationship between IMCL: EMCL ratio and Glucose Rd (B) Relationship between IMCL: EMCL ratio and adipose tissue insulin resistance in healthy volunteers ($n=10$) and NAFLD patients ($n = 18$).

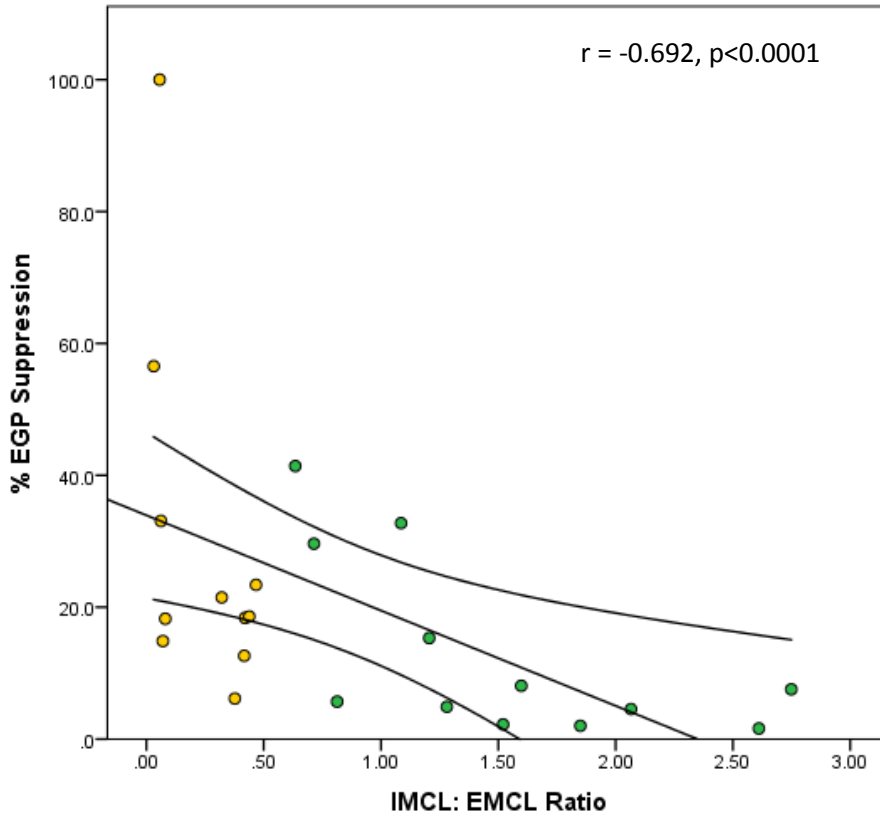


Figure 15 Relationship between Muscle lipid fractions and hepatic insulin sensitivity ($r = -0.692, p < 0.0001$). NAFLD participants are shown in green circles, healthy volunteers are shown in yellow circles.

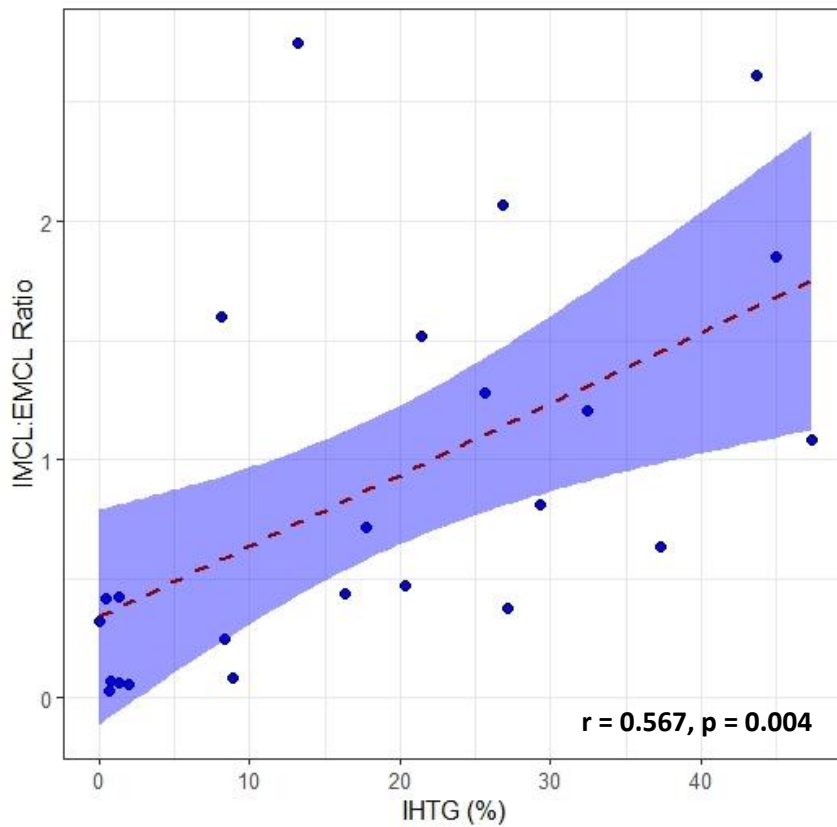


Figure 16 Relationship between IMCL: EMCL ratio and intrahepatic triglyceride

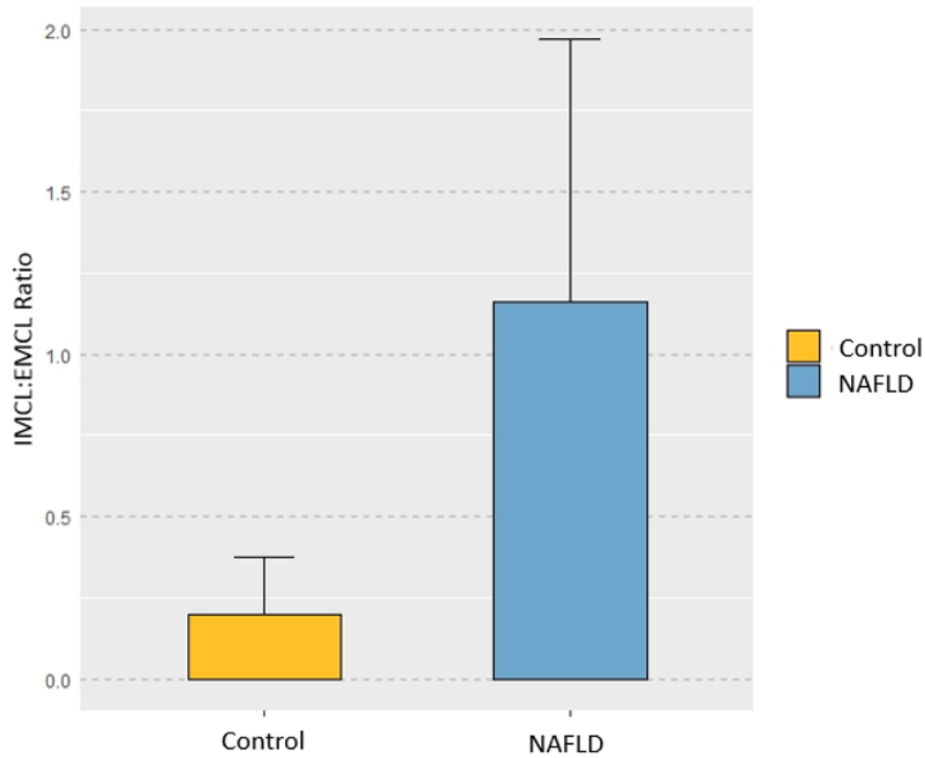


Figure 17 Mean IMCL: EMCL Ratio in healthy volunteers versus NAFLD patients

3.3.7 Hepatic ATP flux

ATP flux data was normally distributed in the healthy volunteer but not the NAFLD group. Therefore, an independent samples Mann Whitney U Test was undertaken to explore differences in Forward rates of ATP synthesis between groups. Median forward exchange flux through the ATP synthesis/hydrolysis cycle was significantly lower in NAFLD compared to healthy volunteers (F_{ATP} (mM/s) = 0.98 ± 0.99 vs 0.25 ± 0.34 , $p < 0.001$, **Figure 18**), indicative of impaired hepatic mitochondrial fat oxidation in NAFLD.

Hepatic ATP flux correlated positively with hepatic insulin sensitivity ($r = 0.476$, $p = 0.014$, **Figure 19**) and negatively with IHTG ($r = -0.448$, $p = 0.019$, **Figure 20**) confirming close associations between hepatic fat, hepatic insulin resistance and perturbed energy metabolism in the liver.

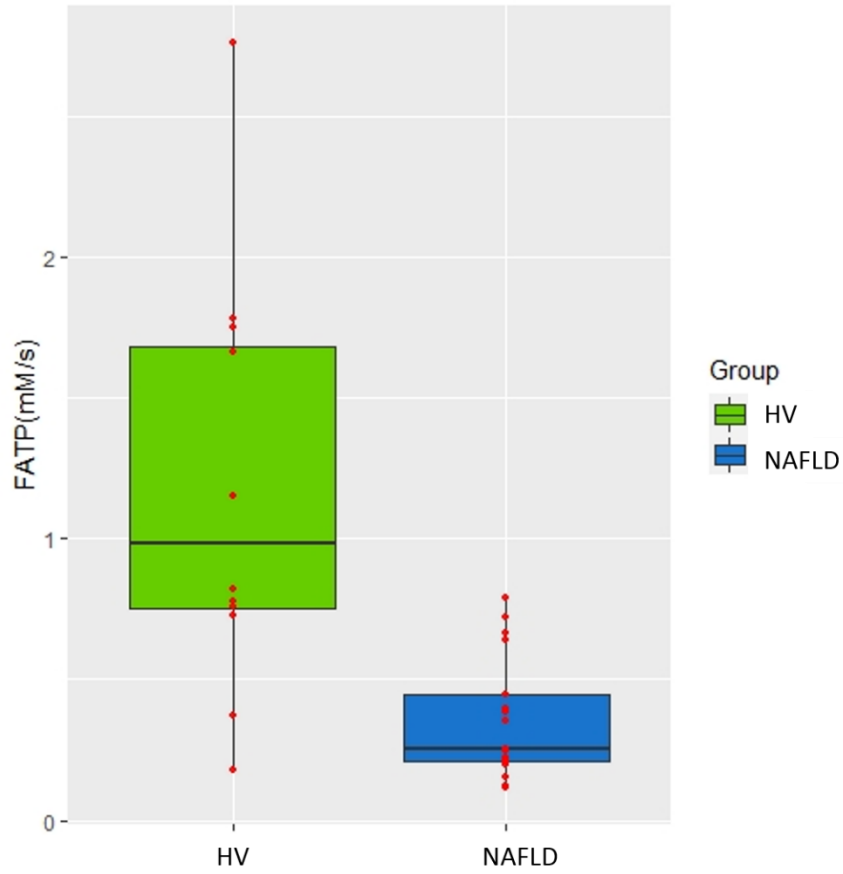


Figure 18 Forward rates of hepatic ATP synthesis in NAFLD versus healthy volunteers

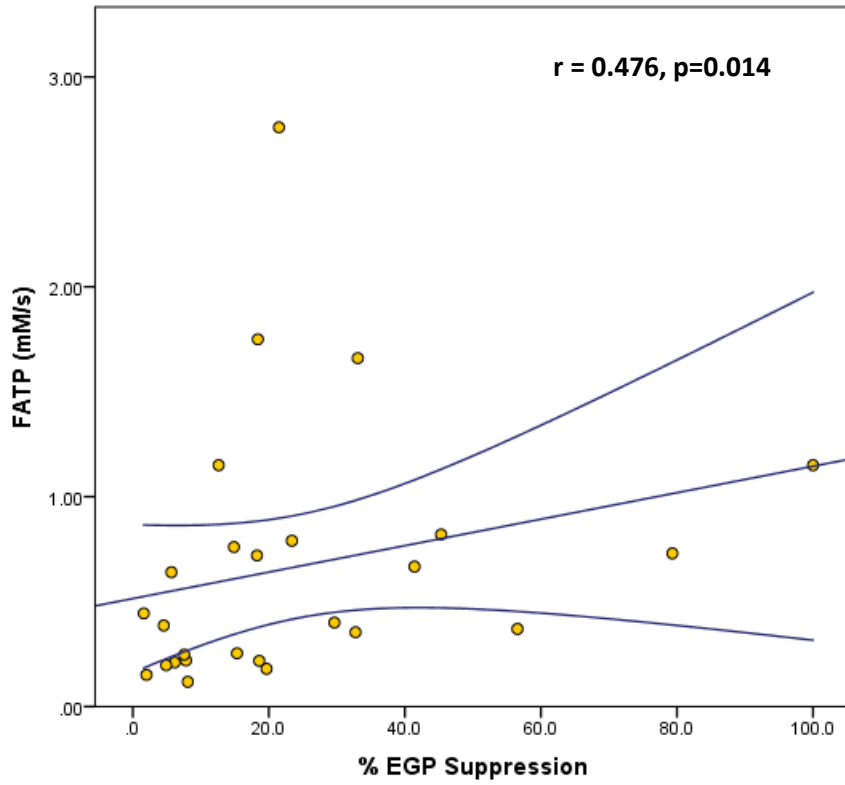


Figure 19 Relationship between liver energy metabolism (measured as forward rate of ATP synthesis) and hepatic insulin sensitivity

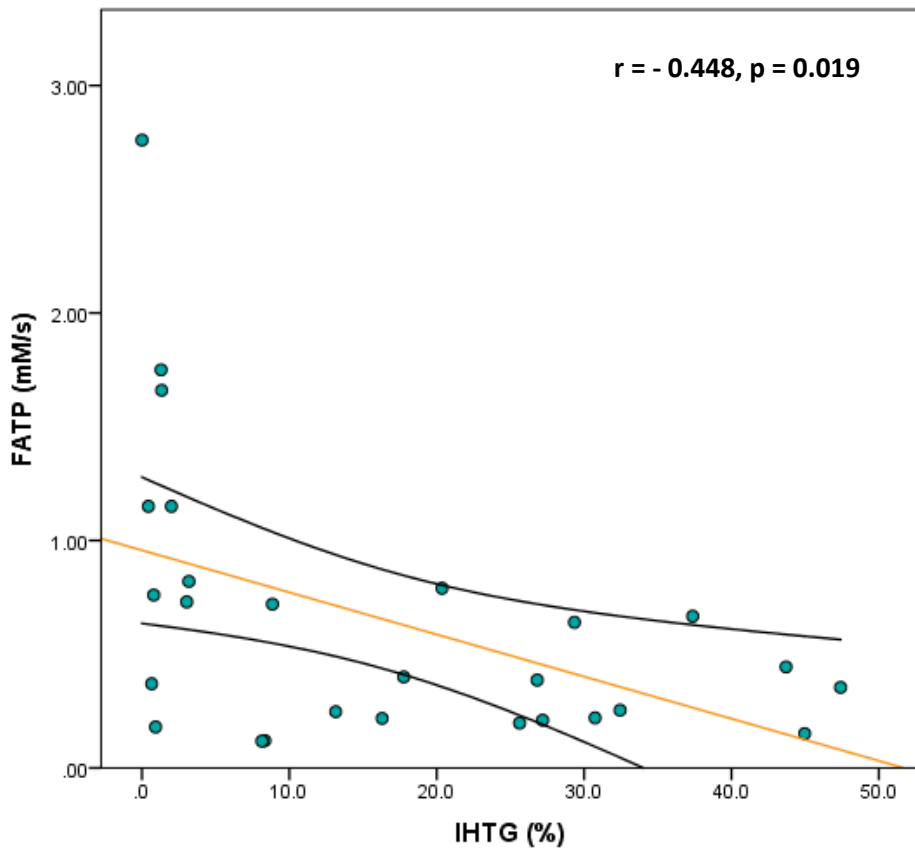


Figure 20 Relationship between liver energy metabolism (measured as forward rate of ATP synthesis) and liver fat.

3.4 Discussion

In this cross-sectional study, we deeply phenotyped a cohort of young, non-diabetic men with NAFLD early in its natural history. We have demonstrated that NAFLD, in the absence of advanced fibrosis, is associated with intramyocellular lipid accumulation, blunted metabolic flexibility, tissue-specific and whole-body insulin resistance, and reduced oxidative phosphorylation in the liver. We have thus identified a discrete metabolic phenotype in NAFLD patients with ostensibly normal glucose tolerance. These results support the paradigm of lipotoxicity as a key pathological milestone in the development of systemic insulin resistance. In the correlation analyses, there were outliers as indicated in graphs in the Results section. These were analysed to assess for any obvious physiological or behavioural differences which may account for their outlying results but no specific trends were found. All participants were asked to avoid strenuous exercise and alcohol consumption for 48 hours prior to study days, and to undertake an overnight fast prior to arrival on study days. While it is not possible to quantify adherence to this advice, outlier trends were not attributable to the same individuals in each case, suggesting that the distribution simply reflects variation in normal physiology, rather than deviation from dietary or lifestyle advice from a single participant or group of participants. Thus, these data points were included in the analysis to give a more complete picture of phenotypic differences.

These findings are important and carry several clinically meaningful implications. First, insulin resistance is inextricably intertwined with ectopic lipid deposition. We have confirmed strong correlations between hepatic and whole body insulin resistance, lipid accumulation in the liver, lipid accumulation in skeletal muscle and dysregulated adipose tissue metabolism. We confirm that IHTG accumulation is strongly associated with insulin resistance across the liver-muscle-adipose tissue axis, and with intramyocellular lipid depots. Indeed, IHTG proved to be the strongest predictor of systemic insulin resistance in this cohort. While causality and directionality cannot be determined from this study alone, our data in conjunction with previous studies points to IMCL accumulation as an early feature of insulin resistance [¹⁵⁶, ¹⁸]. Indeed, IMCL: EMCL ratio was a strong predictor of hepatic insulin

resistance. While body mass index and body fat percentage were different between our control and NAFLD cohorts, the effects of IHTG and muscle lipid fractions on insulin resistance profiles were independent of BMI. Dissecting the contribution of specific fat fractions to a metabolically challenged phenotype opens considerable scope for therapeutic intervention.

Second, we argue that NAFLD is characterised by disturbed hepatic energy metabolism, through reduced hepatic ATP turnover. This supports a growing body of pre-clinical and clinical data pointing towards mitochondrial structural and functional disturbances in non-adipose tissue underpinning the development of an insulin resistant phenotype. Morino and colleagues (2005) compared mitochondrial density and performance in the skeletal muscle of lean, insulin-resistant (IR) offspring of individuals with T2DM to that of healthy control volunteers. The group reported a 60% increase in IMCL content in the IR group, together with a 70% reduction in net glucose disposal during a euglycaemic hyperinsulinaemic clamp. These findings were tightly associated with lipid-induced activation of a serine kinase cascade leading to increase in insulin-receptor substrate 1 (IRS-1) phosphorylation and a 60% reduction in insulin-mediated *Akt* expression. The group further reported a 38% reduction in vastus lateralis muscle mitochondrial density in the IR group versus controls. Further findings included downregulation of key transcriptional factors and cofactors regulating mitochondrial biogenesis and function, which were associated with a 30% reduction in muscle mitochondrial oxidative phosphorylation. Together, this work suggests that (a) multifaceted reductions in mitochondrial function favour cellular lipid accumulation in muscle tissue (b) lipid accretion is a key culprit in the development and propagation of tissue insulin resistance, with bioactive lipid species directly interfering with cellular insulin signalling machinery, leading to reduced insulin-mediated glucose transport and (c) dysregulated muscle mitochondrial function and impaired fatty acid handling may be some of the earliest pathological harbingers of type 2 diabetes [157].

Several previous studies have implicated mitochondrial oxidative metabolism in the transition between simple steatosis (NAFL) and NASH. Koliaki et al (2015) confirmed a 30% reduction in hepatic

mitochondrial respiratory capacity in subjects with NASH compared to healthy controls [40]. Traussnigg et al (2017) compared hepatic ATP flux in individuals with biopsy-proven simple steatosis (NAFL) and with established NASH, with findings suggesting that reduced hepatic mitochondrial ATP flux may signal a metabolic ‘threshold’ in the natural history of NAFLD, opening scope for a non-invasive method with which to detect the transition from ‘simple’ steatosis to NASH [49].

Although NAFLD has been firmly linked to systemic insulin resistance, the tissue-specific contributions to whole body insulin action remain poorly uncharacterised, especially in a non-diabetic cohort without advanced fibrosis. Bril and colleagues (2017) conducted a prospective study in 352 individuals with NAFLD, pinning down adipose tissue as a culprit marker with a linear relationship to intrahepatic triglyceride [21]. Interestingly, their group also demonstrated that selective hepatic insulin resistance was present at relatively low levels of liver fat (IHTG $\geq 1.5\%$) and that a clear threshold exists beyond which both liver and muscle (whole-body) insulin resistance are fully established. Thus, even a small amount of liver fat is associated with hepatic insulin resistance [158].

Through using sophisticated metabolic and precision imaging techniques, we demonstrate that intrahepatic triglyceride is a strong predictor of impaired insulin action at the level of the muscle, liver and adipose tissue. Through a stepwise linear regression model, we determined that IHTG is a stronger predictor than BMI, plasma insulin or lipid profile for whole-body insulin resistance. This is potentially relevant because NAFLD in its early stages tends to be asymptomatic, and even if it is detected incidentally (e.g. on abdominal ultrasound), no specific intervention strategies are offered in clinical practice to reduce individual cardiometabolic risk.

Several strategies have been proposed to optimise detection of chronic liver disease in community settings [159, 160]. These strategies tend to focus on the non-invasive detection of advanced fibrosis or compensated cirrhosis and aim to stratify individuals based on risk of liver decompensation or mortality. The vast majority of these techniques, including imaging and wet biomarkers (or a combination of both) have been extensively validated in NAFLD cohorts [161]. While such individuals

– who are vulnerable to liver-related morbidity and mortality - are clearly important to identify, our central argument proposes that metabolic risk is present at a much earlier stage in the natural history of NAFLD. In the largest retrospective cohort study of patients with biopsy-proven NAFLD to date (n=646, mean follow up 20 years), Hagström and colleagues report that of the 214 patients who died, 36.9% of deaths were attributable to cardiovascular causes. In contrast, liver disease accounted for 7.9% of deaths [9].

Our findings suggest that liver fat accumulation *per se* defines a category of overweight individuals who are at heightened future risk of developing adverse metabolic outcomes associated with insulin resistance. We therefore propose that identification of individuals with elevated liver fat (not simply fibrosis) in the community setting may be of value. In the longer term, development and validation of specific disease-modifying interventions (e.g. bespoke exercise regimes, dietary, nutritional and pharmacological treatments) may be possible, with a view to reducing long term cardiometabolic risk in this population.

Current EASL guidelines stipulate that *“steatosis...predicts future diabetes mellitus, cardiovascular events and arterial hypertension.”* Their statement goes on to say *“In clinical practice, quantification of fat content is not of interest, except as a surrogate of treatment efficacy, and is therefore not generally recommended [162].”* We argue that since even a relatively modest amount of liver fat can significantly impact upon metabolite kinetics and insulin sensitivity, there may be value in identifying (and if possible quantifying) liver fat accurately. While MRI-PDFF and ¹H-MRS represent the gold-standard noninvasive techniques for quantification of liver fat, neither is applicable as a point of care tool in community based settings. However, Fibroscan[®] with controlled attenuation parameter would be ideally suited to the endeavour of quantifying both steatosis and fibrosis. Caussy *et al* (2018) determined an optimal CAP cut-off value of 288 dB/m, which had diagnostic accuracy of 80% in predicting IHTG > 5% on MRI-PDFF [154].

Natural history studies in NAFLD have been famously unforthcoming, limited in scope due to insufficient sample size or duration of follow-up. A robust recent analysis by Allen and colleagues retrospectively evaluated 4500 individuals with NAFLD (diagnosed by coding algorithms and subsequently individual chart review) to determine the impact of NAFLD on incident metabolic comorbidities (including type 2 diabetes, hypertension and dyslipidaemia). Using a 1:4 control group ratio, the group demonstrated over a median follow up period of 7 years that NAFLD is an independent risk factor for cardiometabolic outcomes. Using multistate modelling, they demonstrated that the individual contribution of NAFLD towards these outcomes decreases as metabolic burden increases. Individuals with NAFLD – even in the absence of metabolic comorbidities – had a life expectancy which was on average 4 years lower than that of their counterparts. In their conclusion, the group state that therapeutic intervention *“may have a higher impact on hard outcomes such as mortality or cardiovascular disease if introduced before the onset of a high dysmetabolic burden”* [163]. This underscores a critical unmet need for identification of individuals at high metabolic risk prior to the onset of established comorbidity such as type 2 diabetes etc. We propose that identification of individuals with elevated liver fat in community based settings should prompt more detailed assessment of metabolic risk and possibly novel interventional strategies to alleviate this risk and optimise metabolic profile in the longer term.

There is ample scope for development and validation of risk stratification algorithms and bespoke pathways, tailored towards individual risk to mitigate adverse cardiometabolic outcomes. Empirical interventions in individuals with steatosis alone have, to our knowledge, not been undertaken. Robust prospective studies evaluating lifestyle interventions, lipid-lowering therapy and possibly empiric use of insulin sensitising therapy (as is the case in, for example, polycystic ovary syndrome) with external validation could be developed to address and mitigate risk profiles in these groups. One option would be the inclusion of controlled attenuation parameter in community pathway screening employing Fibroscan[®], and a subsequent intervention strategy based on validated cut-off scores.

It is nevertheless noteworthy that the weight of evidence to date argues against clinically meaningful implications of 'simple' steatosis. Ekstedt et al (2006) studied biopsy-proven NAFLD patients (n=129) prospectively over a median follow-up period of 13.7 years. The group found that steatosis alone (in the absence of necroinflammation and fibrosis) does not confer increased risk of all-cause mortality compared to a reference population without elevated liver fat [164]. Similarly, Dam-Larsen and colleagues (2004) demonstrated in a cohort with simple fatty liver (n=109) that mortality was not significantly different from the Danish general population over a 16.7 year follow up period [165]. It is important to note that cardiovascular outcomes were not specifically assessed in this study, and that in terms of incident cardiovascular risk, follow-up periods in both studies may have been insufficient. It is also noteworthy that cardiovascular mortality in Ekstedt's non-NASH cohort was 8.6%, which was still higher than that in the reference population (7.5%). No published literature exists to our knowledge evaluating the impact of pure steatosis alone on cardiovascular morbidity and mortality.

That NAFLD is an independent risk factor for cardiovascular morbidity and mortality is well established [166]. A recent systematic review and meta-analysis including 34 studies demonstrated that NAFLD was associated with higher incident coronary artery disease compared to individuals with normal liver fat [167]. While other metabolic conditions constitute important covariates (e.g. T2DM), the strong association between NAFLD and incident cardiovascular disease persisted after controlling for those variables in a logistic regression model. From a pathophysiological viewpoint, the independent contribution of NAFLD to cardiovascular risk is difficult to dissect from those of other metabolic comorbidities, since these are highly prevalent in the NAFLD population. However, cardiovascular disease remains consistently a leading cause of death in NAFLD and efforts to modify risk in this population are not without merit.

Our second major finding was that NAFLD impacts upon ATP turnover (i.e. oxidative phosphorylation) at the level of the liver. This supports a paradigm of impaired mitochondrial biogenesis or function (or both) lying at the heart of the transition towards lipotoxicity and mishandling of increased lipid flux.

Mitochondria overwhelmed with substrate 'struggle' to coordinate effective lipid metabolism such that fat accumulation becomes inevitable due to the imbalance between supply and net utilisation. While whole-body rates of lipid oxidation were not significantly different in NAFLD versus control groups in this study, sites of ectopic lipid deposition are likely to experience local lipotoxic effects resulting in upregulated expression of pro-inflammatory mediators, a dysregulated intracellular redox state and altered acetyl-CoA/CoA ratio, all of which conspire to damage mitochondrial performance. This is reflected in the metabolic inflexibility demonstrated in our NAFLD cohort, with evidence of impaired substrate switching from fat to carbohydrate oxidation in response to hyperinsulinaemic conditions.

With respect to the evolution of insulin resistance, one working theory posits that impaired insulin action at the level of skeletal muscle results from diacylglycerol-mediated (via novel PKC isoform) interference with insulin signalling at the level of the myocyte. This then reduces glucose uptake and removes the ability of muscle to act as a major sink for glucose disposal and glycogen synthesis. Ingested carbohydrate, as a result, is diverted and ultimately undergoes lipogenic pathways in the liver.

Sophisticated mechanistic studies described in detail in Chapter 2 have unravelled the relationships between skeletal muscle insulin resistance and the development of the NAFLD and the metabolic syndrome. Fat accumulation in the liver has been linked to impaired mitochondrial function, endoplasmic reticulum stress, generation of reactive oxygen species (ROS) and ultimately a pro-inflammatory, pro-fibrogenic milieu. To this end, subtle restoration of mitochondrial antioxidant balance has been proposed as a potentially effective therapeutic avenue for NAFLD [168].

Although we cannot differentiate simple NAFL from NASH in our cohort, we can demonstrate that overall in early, non-fibrotic NAFLD, flux through the ATP synthase pathway is significantly diminished. Taken together, the implication from this data is that boosting mitochondrial lipid β -oxidation and/or increasing skeletal muscle lipid turnover, may confer early therapeutic benefit in a NAFLD population.

This study employed gold-standard metabolic methods in combination cutting edge imaging technology to explore a NAFLD phenotype. Limitations include not adjusting for BMI; the collinearity between BMI, IHTG and systemic insulin resistance means that BMI may have been a confounding variable, with metabolic disturbances as much due to the central adiposity as to ectopic fat deposition, However, a multitude of studies have explored such parameters while controlling for BMI, and demonstrating that presence of liver fat alone is an independent contributor to metabolic syndrome. In our study, a stepwise linear regression model showed that IHTG was the strongest predictor of insulin resistance, even when controlling for BMI. The relatively small sample size in this study means that findings may be less extrapolatable on a population level; in particular, including males only is potentially a limiting factor in the generalisability of these findings and indices of cardiometabolic risk may be different in the adult female population. The rationale for male recruitment was based on necessity of conducting a deep metabolic phenotype and evaluating body composition and metabolic biomarkers, with evidence of menstrual cycle-related variability in both parameters, which may affect interpretability of results [169, 170].

In conclusion, we have demonstrated profound tissue-specific and whole-body insulin resistance in young, non-diabetic men with NAFLD. These findings are associated with metabolic inflexibility and reduced hepatic ATP turnover, supporting the concept of mitochondrial maladaptation in the setting of chronic energy surplus, and strongly implicating skeletal muscle lipid fractions in the development and progression of NAFLD. We have further interrogated the longitudinal effects of mechanism-based therapy targeting skeletal muscle lipids and mitochondrial lipid β -oxidation on tissue fat fractions, metabolic flexibility, whole-body and hepatic insulin sensitivity and hepatic energy kinetics. Results from this randomised, placebo-controlled trial are presented in **Chapter 5**.

Chapter 4

L-carnitine Supplementation in Non-alcoholic Fatty Liver Disease: A systematic review and meta-analysis

4.1 Introduction

L-Carnitine is a naturally occurring water-soluble quaternary amine which acts as a crucial mediator of fatty acid metabolism *in vivo*. The role of carnitine as a key regulator of intracellular bioenergetics has gained traction in the search for broadly applicable treatments for metabolic disorders, including obesity and type 2 diabetes. The ability of L-carnitine to regulate muscle mitochondrial fuel selection, through promoting both lipid oxidation and non-oxidative glucose disposal, renders it an attractive target for therapeutic intervention in the context of insulin resistance [95]. Cumulative evidence in both animal and human models suggests that intrahepatic and skeletal muscle fatty acid transport and oxidation is impaired in NAFLD and insulin resistance, such that excessive lipid accretion is not matched by efficient utilisation [85, 86]. Thus, the effect of carnitine supplementation in the context of NAFLD specifically has been the focus of recent interest. This review aims to critically and systematically evaluate all human randomised trials investigating the effect of carnitine on liver fat and/or metabolic parameters in NAFLD.

4.2 Materials and Methods

Search strategies, eligibility criteria and analytic methods were specified *a priori* in the study protocol, which was registered with the PROSPERO database (CRD42018107063).

4.2.1 Search Strategy

We performed a systematic literature search for randomised trials reporting the effects of dietary L-carnitine supplementation on liver biochemistry and liver fat in adult individuals with NAFLD and NASH.

The databases searched were PubMed, OVID Embase, Ovid MEDLINE, Web of Science Core Collection and the Cochrane Library. The full search strategy used in Ovid MEDLINE is provided in [Appendix 1](#). Databases were searched from their inception until April 2019. No language restrictions were used. For each database, a comprehensive list of alternative terms for non-alcoholic fatty liver disease were

combined with alternative terms for L-carnitine, using the Boolean operator AND. Reference lists of studies ultimately selected for inclusion were searched to identify any other relevant research.

Diagnostic criteria for NAFLD varied significantly between studies, but eligible studies included adult individuals diagnosed with NAFLD on the basis of validated histological, imaging or biochemical tests, including the following, and where other causes of hepatic steatosis had been excluded:

- 1) Liver histology
- 2) Magnetic Resonance Imaging with proton density fat fraction (MRI-PDFF) or proton magnetic resonance spectroscopy (^1H -MRS)
- 3) Computed Tomography (CT)
- 4) Ultrasound
- 5) Serum concentrations of alanine aminotransferase (ALT) and aspartate aminotransferase (AST) in conjunction with impaired glucose tolerance and in the absence of documented alcohol excess.

Primary outcome measures included change in serum concentrations of ALT, AST and liver fat (as assessed either by liver biopsy, cross-sectional imaging or ultrasound). Secondary outcome measures included changes in insulin sensitivity parameters (as assessed by the HOMA-IR) and, where available, markers of inflammation and oxidative stress.

Study selection was performed independently by two separate reviewers (PT and JC) with any disagreements resolved by a third researcher (GPA). Titles and abstracts of returned searches were evaluated against eligibility criteria. Those meeting eligibility criteria based on title and abstract were subsequently read in full. Wherever journal articles were found to contain insufficient information for critical analysis, attempts were made to contact the authors directly for clarification of missing details.

4.2.2 Eligibility criteria

Eligible published studies included human randomised trials evaluating the effect of L-carnitine supplementation on liver fat, liver enzymes, plasma glucose and markers of inflammation or oxidative stress in adult individuals with NAFLD. Only full reports were considered as eligible for inclusion on the basis that they provided sufficient data to permit critical analysis.

Studies were considered eligible for inclusion if they:

1. Were randomised in design
2. Evaluated L-carnitine versus placebo, L-carnitine plus another intervention versus that intervention alone, or L-carnitine versus no intervention.
3. Included a patient population diagnosed with NAFLD and/or NASH based on validated histological, radiological or biochemical parameters as listed above.
4. Included only subjects aged 18 years or above

Studies were excluded if they:

1. Were non-randomised in design e.g. case reports, reviews or observational studies
2. Included patients with another cause of hepatic steatosis e.g. alcohol, genetic or viral liver disease
3. Were animal studies
4. Did not evaluate outcomes of interest as detailed above.

There were no restrictions based on dosage, formulation or frequency of administration. Interventions in the control group included active placebo supplementation, hypocaloric diet and metformin therapy. Trials evaluating L-carnitine supplementation together with other interventions, in the absence of a control group consisting of the other interventions alone, were excluded. No specific treatment duration was specified for inclusion in this review.

4.2.3 Data Extraction and Quality Assessment

Data extracted from individual studies included (1) participant demographics, (2) intervention type and dose, (3) method of NAFLD diagnosis, (4) outcome measurements of liver fat, liver enzymes, glycometabolic profile and markers of inflammation and oxidative stress, (5) documentation as to whether informed consent was gained, (6) methods of randomisation, (7) allocation concealment, (8) participant and staff blinding, (9) blinding of outcome assessment, (10) presence of incomplete outcome data and (11) evidence of any selective reporting. The Cochrane Risk of Bias tool [171] was then used to systematically appraise each included study in terms of methodological quality and validity according to the criteria of the Cochrane guidelines.

4.2.4 Statistical Analysis

A random effects meta-analysis was performed for ALT, AST and HOMA-IR measures separately. Weighted mean difference with 95% confidence intervals were calculated. Between-study heterogeneity was measured using I^2 statistics, with $I^2 > 50\%$ indicating significant heterogeneity. The analysis was performed using Stata software and the results were summarised using Forest plots.

4.3 Results

4.3.1 Search Results

Figure 1 depicts the PRISMA flowchart process of identification and selection of eligible studies for inclusion in the qualitative and quantitative syntheses. Primary database searches yielded 883 citations. After de-duplication, 692 remaining citations were screened for eligibility by reading titles and abstracts. Of these remaining studies, 675 were excluded. Of the remaining 17 citations, full text articles retrieved were read in full to determine eligibility. Twelve studies were subsequently excluded.

Table 1 summarises study characteristics for the five randomised trials ultimately included in the qualitative and quantitative synthesis [172,173, 174, 175, 176]. In total, these trials comprised 338 patients

(234 men, 104 women). In 3 trials, non-diabetic patients with NAFLD were recruited and the other 2 trials recruited individuals with type 2 diabetes mellitus and NAFLD.

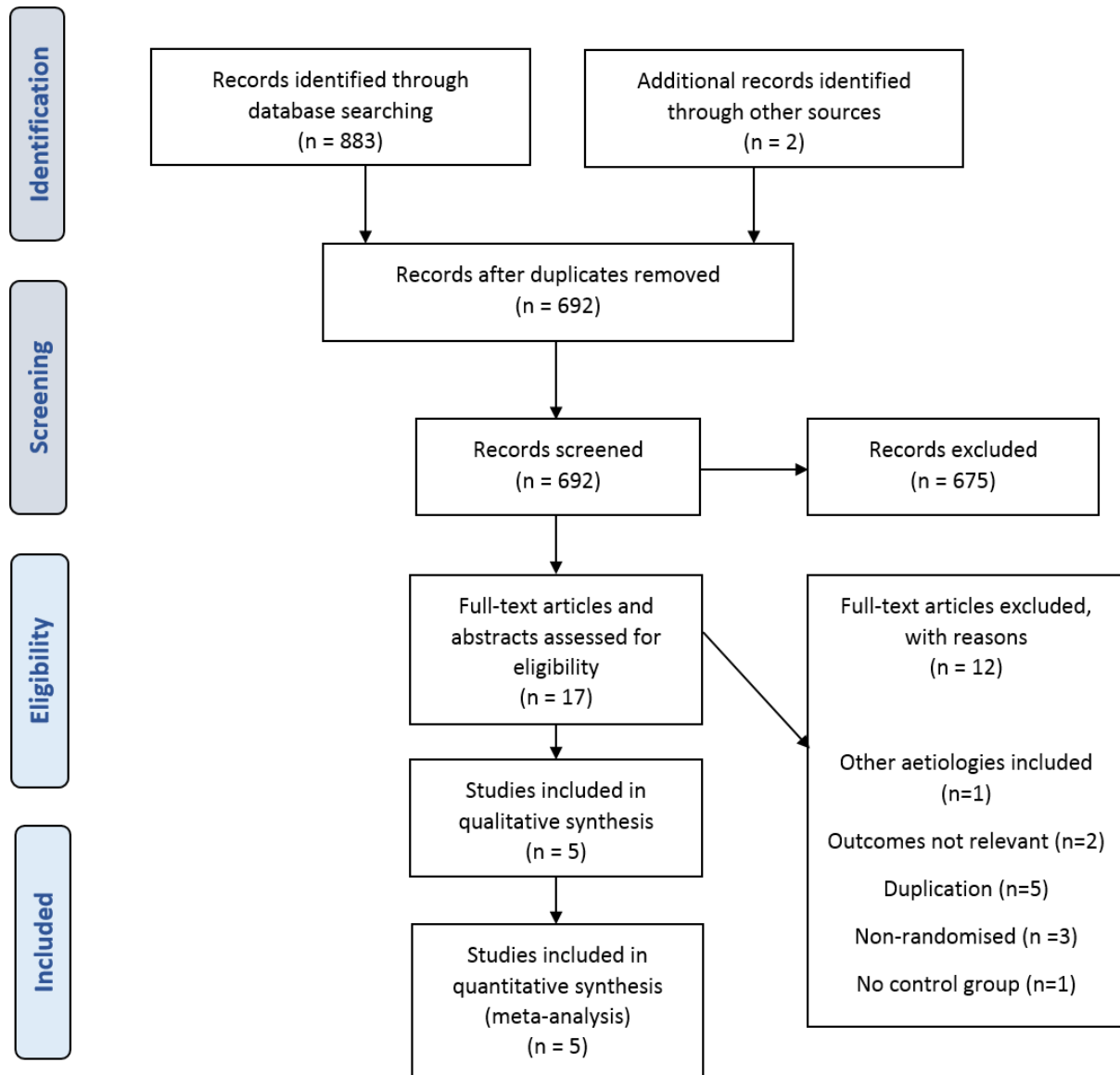


Figure 1. PRISMA flow diagram

Author (year); Country	Study population (diagnosis); comorbidities	Sample size (M/F) Control/Carnitine	Age (yrs)	BMI	Duration (wks)	Intervention (dose)	Outcome Measures	Control	Results
Malaguarnera (2010); Italy	Biopsy-proven NASH without diabetes	74 (40/34) 38 (CTRL) 36 (CAR)	47.8 ± 5.8 (CTRL) 47.9 ± 5.4 (CAR)	26.5 ± 3.8 (CTRL) 26.6 ± 3.7 (CAR)	24	L-carnitine (1000 mg BD) plus hypocaloric (1600 cal) diet	<i>Primary:</i> Improvement in histological features of NASH <i>Other:</i> ALT, AST, lipid profile, GLC, HOMA-IR, CRP, TNFα	Placebo plus Hypocaloric (1600 cal) diet	Primary Outcome: ↓ NASH activity score* (9.42-3.19), ↓ALT* ↓AST*, ↓GGT* ↓TC*, ↓LDL*, ↑HDL*, ↓GLC*, ↓HOMA-IR*, ↓CRP*, ↓TNFα*
Bae (2015); Korea	NAFLD with type 2 diabetes	78 (54/24) 39 (CTRL) 39 (CAR)	52 ± 9.4 (CTRL) 50.6 ± 9.3 (CAR)	26.7 ± 3.7 (CTRL) 28.2 ± 2.6 (CAR)	12	Carnitine orotate complex (824 mg TDS)	Primary: Change in ALT Other: liver attenuation index (CT)	Placebo	Primary outcome: ↓ALT (89.7% vs. 17.9%)* Other: ↓ Liver attenuation index* (0.74 ± 8.05 vs. 6.21 ± 8.96)*, ↓ HbA1c, ↓GLC, ↓HOMA-IR †
Alavinejad (2016); Iran	NAFLD (ultrasound+ raised ALT) with T2DM	54 (38/16) 26 (CTRL) 28 (CAR)	59 ± 9 (CTRL) 60 ± 5 (CAR)	29.5 ± 3.6 (CTRL) 28.6 ± 4.6 (CAR)	12	L-carnitine (750 mg TDS)	Primary: AST, ALT Other: TG, GLC, HbA1c	Placebo	Primary outcome: ↓ALT*, ↓AST* Other: ↓TG†, ↓GLC†, ↓HbA1c†
Hong (2014); Korea	NAFLD (plasma ALT 40-250) and impaired glucose tolerance (HbA1C >=6.0%)	52 (36/16) 26 (CTRL) 26 (CAR)	52.0 ± 9.6 (CTRL)	27.0 ± 3.1 (CTRL)	12	Carnitine-orotate complex (300)	Primary: change from baseline ALT Other: GLC, HbA1c, mt DNA copy	Metformin alone	Primary outcome: ↓ ALT* Other: ↓HbA1c†, ↑ plasma mtDNA copy

			51.5 ± 9.4 (CAR)	27.2 ± 2.6 (CAR)		mg TDS) + metformin	number, urine 8- OHdG		number*, ↓GLC†, ↓urine 8-OHdG
Somi (2014); Iran	NAFLD (ultrasound + plasma ALT >=40)	80 (66/14)	40.7 ± 8	29.4 ± 3.9	24	L-carnitine (250 mg BD)	Primary: ALT, AST Other: sonographic change in liver fat, BMI	No treatment	Primary outcome: ↓ ALT*, ↓AST* Other: ↓ liver fat on USS†

Table 1 Published studies to date evaluating the effect of L-carnitine supplementation on liver fat and/or biochemistry in Non-alcoholic Fatty Liver Disease (NAFLD)

Abbreviations: NASH = nonalcoholic steatohepatitis, ALT = alanine aminotransferase, AST = aspartate aminotransferase, GLC = glucose, HOMA-IR = homeostasis model of insulin resistance, CRP = C-reactive protein, TNFα = Tumour Necrosis Factor alpha, HbA1C = Haemoglobin A1C, T2DM =type 2 diabetes mellitus, TG = triglyceride, mt DNA = mitochondrial DNA, oHdg = 8-hydroxydeoxyguanosine * Denotes statistically significant results † Denotes non-statistically significant results

4.3.2 Quality of Included Studies

Methodological quality was assessed using criteria set out in the Cochrane Handbook for Systematic Reviews (**Figure 2**). All trials described randomising participants to L-carnitine and control arms. However, only two of the five trials [172,173] reported the methods used to generate random allocation sequence (i.e. computer generated tool) to a standard sufficient enough to be judged as having a low risk of bias. In the other 3 trials, no information was provided regarding methods of blinding and insufficient information was provided to enable informed decision-making regarding adequacy of randomisation. One trial reported randomising participants by using random numbers allocated to consecutive patients; this was considered to confer a high risk of selection bias [174].

Regarding allocation concealment, only two studies [172,173] reported efforts to conceal allocation sequences from personnel as well patients. In two of the studies, genuine blinding was considered impossible due to lack of a placebo arm [175, 176]. In the remaining two trials, insufficient information was given to determine whether a robust allocation concealment process was undertaken. Three of the five studies accounted for incomplete outcome data and clearly explained any loss to follow up and exclusions [172,173,175]. The other two studies lacked explanations for trial exclusion.

Selective reporting was considered to be present in two out of the five included studies. Alavinejad *et al.* (2016) with sonographic grade of liver fat as an outcome measure in their study, noted *that 'follow up ultrasonography did not show any significant change in comparison with baseline reports'* [174]. However no baseline or post-intervention values were reported. Somi *et al.* (2014) reported changes from baseline in sonographically-determined grade of NAFLD in patients in the L-carnitine arm of the study, with nine of the L-carnitine treated patients having no evidence of NAFLD on post-intervention ultrasound. However it was unclear how many patients had progressed or regressed in steatosis grade [176].

In three out of the five trials, funding sources and conflicts of interests were explicitly stated, whereas in the other two trials no mention was made of either [174,176]. Efficacy, safety and compliance

measures were reported in 3 studies but no description of methods to evaluate compliance was made in the other two studies and Somi *et al.* (2014) did not report any safety visits for subjects during 24 weeks of supplementation [174,176]. Statistical analyses were reported in all five trials.

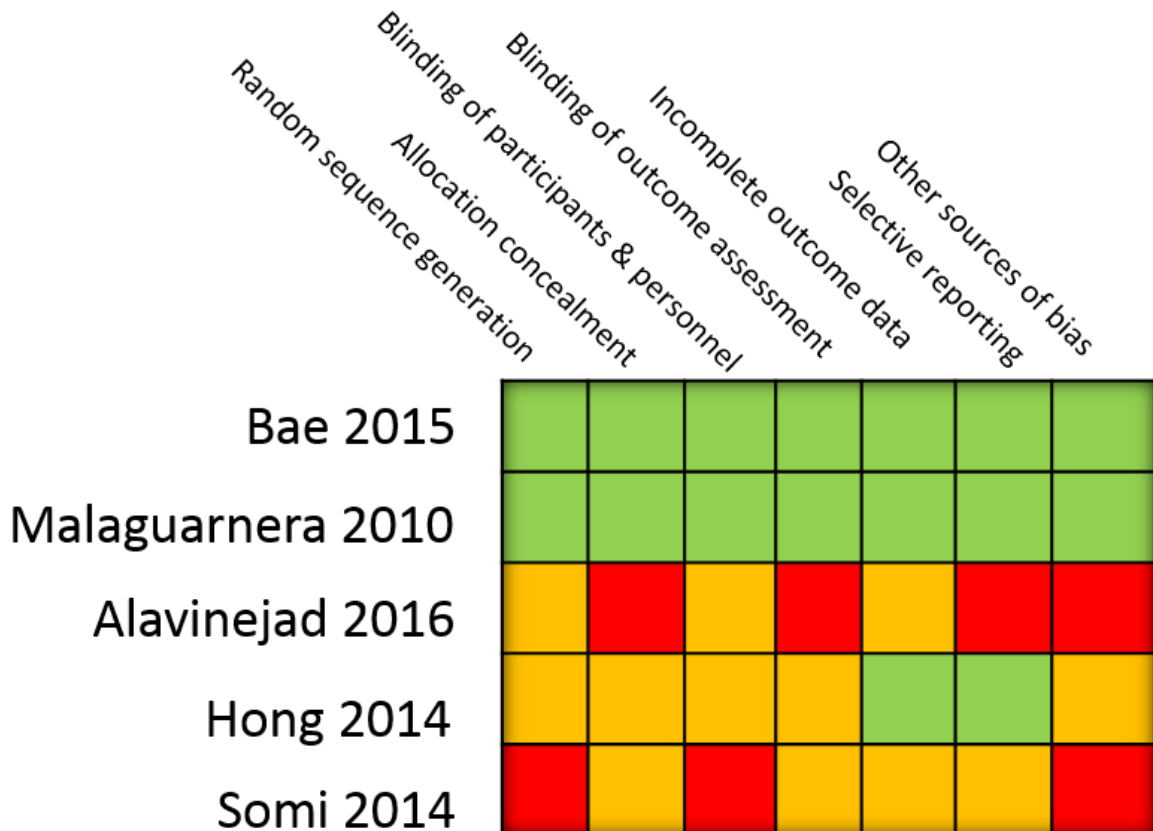


Figure 2: Methodological Quality Assessment according to the Cochrane Risk of Bias Tool

4.3.3 Outcomes

Estimates were made on the effect of L-carnitine on outcomes including liver transaminases, the homeostatic model assessment of insulin resistance (HOMA-IR) and liver fat (where measured).

4.3.3.1 ALT

All of the five included trials were included for meta-analysis of ALT measures after intervention (**Figure 3**). The weighted mean difference for ALT between the L-carnitine groups and the control

groups after intervention was -25.34 IU/L (95%CI $-41.74, -8.94$) ($p=0.002$) (Figure 3). The I^2 was 95.8%, indicating statistically significant heterogeneity between the studies.

4.3.3.2 AST

All five trials were included for meta-analysis of AST measures after intervention. The weighted mean difference for AST between the L-carnitine group and the control group after intervention was -13.68 IU/L (95%CI $-28.26, 0.89$) ($p=0.066$) (Figure 4). The I^2 was 93.4%, indicating high statistical heterogeneity between the studies.

4.3.3.3 Liver fat

Four of the included studies evaluated hepatic steatosis at baseline and post-intervention. Outcome measures differed between the studies, precluding the possibility of a quantitative synthesis of results. In two studies, ultrasonography was used to grade liver fat at baseline and post-intervention [^{174, 176}]. In another study, CT imaging was used [¹⁷³] and in the fourth study, liver fat was evaluated histologically [¹⁶²].

Malaguarnera *et al.* (2010) assessed liver fat using paired biopsies; the group reported a significant reduction in steatosis in the group randomised to L-carnitine compared to placebo (1.68 ± 0.76 versus 0.94 ± 0.88 , $P < 0.001$) [¹⁷²]. However, within-group analysis also demonstrated that steatosis reduction was significant in the placebo group (hypocaloric diet + placebo) compared to baseline values ($P < 0.001$). In the same study, other histological features of NASH were shown to be significantly attenuated following 24 weeks of L-carnitine therapy compared to placebo, including parenchymal inflammation ($P < 0.001$), hepatocellular injury ($P < 0.05$) and fibrosis ($P < 0.05$). However, it is again worth noting that within-group comparisons with baseline values also determined a significant reduction in these parameters following placebo supplementation.

Another study used hepatic CT with liver attenuation index (LAI) to evaluate steatosis before and after the study [¹⁷³]. Authors reported that the patient group receiving L-carnitine complex supplementation had a mean increase in LAI values of 6.21 ± 8.96 Hounsfield Units (HU) ($p < 0.001$), indicating significant

reduction in liver fat, whereas the placebo group showed no significant change (LAI increased by 0.74 ± 8.05 HU, $p = 0.582$). The changes in LAI were found to correlate inversely with changes in ALT.

Alavinejad *et al.* (2016) reported no significant difference between baseline and post-intervention sonographic liver fat in either the L-carnitine or placebo groups in their study [174]. However, absolute values were not provided in the published article. Finally, Somi *et al.* (2014) reported a significant reduction in patients with sonographic grade 2 liver fat in the placebo but not the L-carnitine groups [176]. In the L-carnitine group, 9 patients with sonographic evidence of fatty liver at baseline had resolution of fatty liver disease on post-intervention ultrasonography, suggesting a beneficial effect of L-carnitine on liver fat; however, this was reported to be non-significant.

Thus, two high quality RCTs utilising histology and cross-sectional imaging for quantifying liver fat reported significant outcomes following L-carnitine supplementation, whereas the two trials utilising ultrasonography reported no significant difference in liver fat with L-carnitine.

4.3.3.4 HOMA-IR and glycometabolic profile

Three papers were included for meta-analysis of HOMA-IR measures after intervention. The weighted mean difference for HOMA-IR between the L-carnitine and control groups after intervention was -0.74 units (95%CI $-1.02, -0.46$) ($p < 0.001$) (**Figure 5**). The I^2 was 0%, indicating statistical homogeneity between the studies.

Figure 3. Meta-analysis of ALT measures after intervention

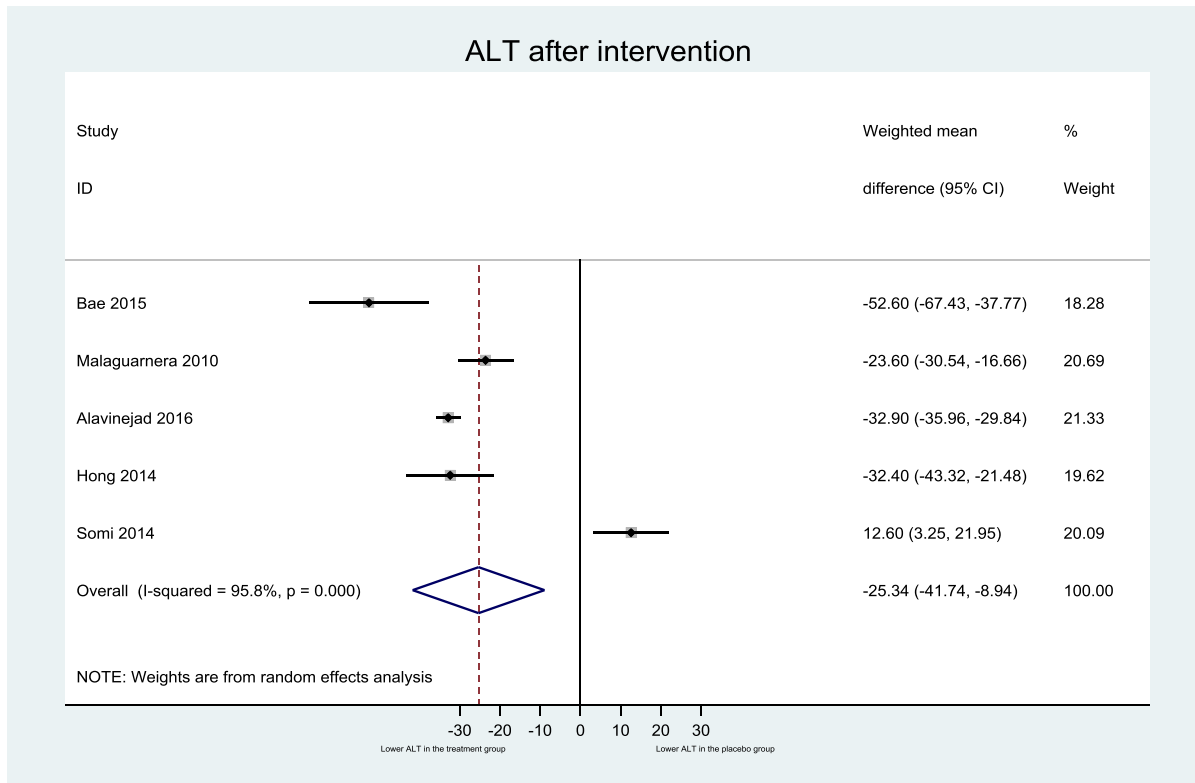


Figure 4 Meta-analysis of AST after intervention

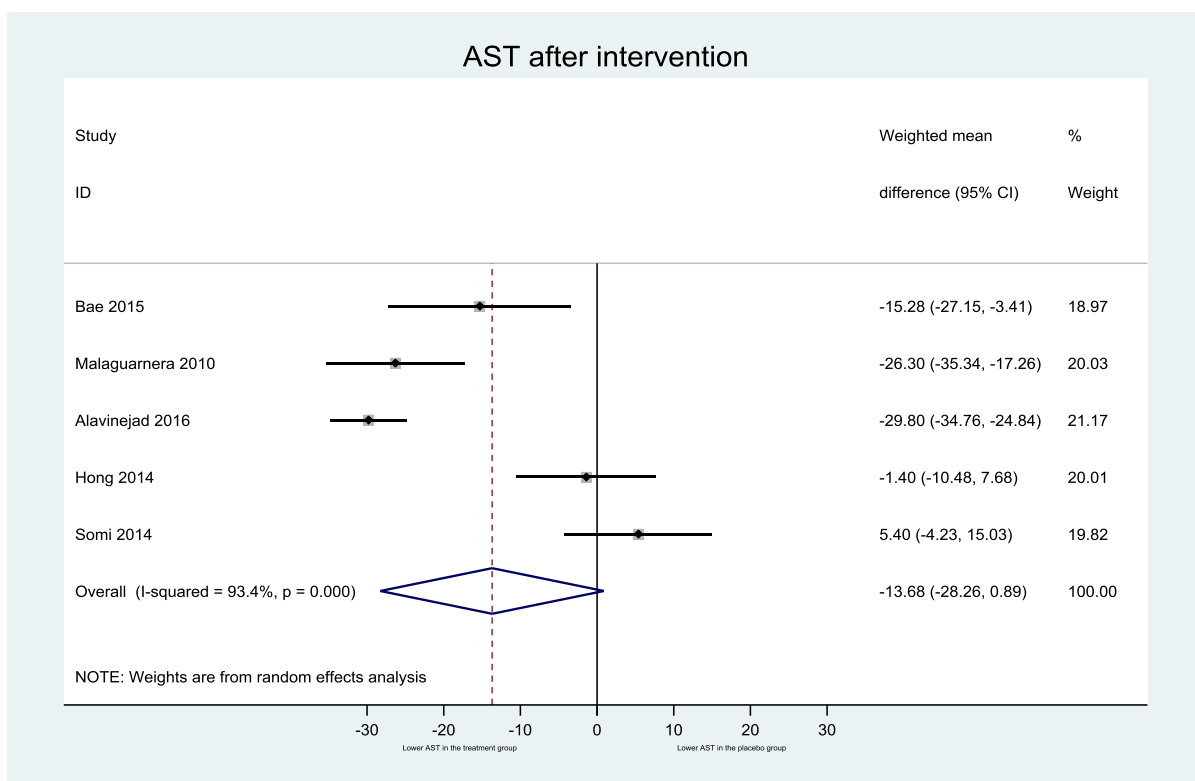
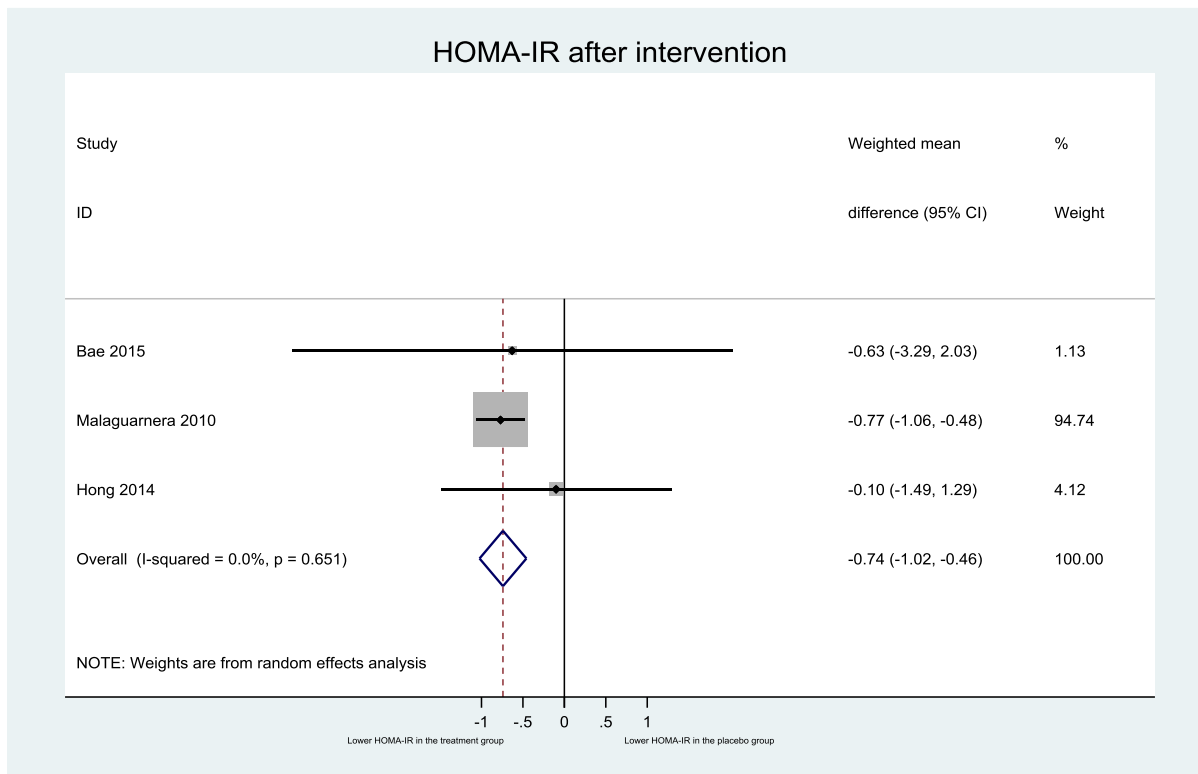


Figure 5 Meta-analysis of HOMA-IR measures after intervention



4.3.4 Adverse Events

Adverse events (AE) were reported in 3 studies included in this review, including mild headache, musculoskeletal pain and gastrointestinal disturbance. [172,173,175]. All AE rates were lower in the intervention versus placebo groups and no serious adverse events were reported.

4.3.5 Inflammation and Oxidative Stress

Malaguarnera *et al.* (2010) reported a significant reduction in hepatocellular injury ($P < 0.05$), parenchymal inflammation ($P < 0.001$), plasma C-reactive protein (CRP) and tumour necrosis factor alpha (TNF α) ($P < 0.001$) in L-carnitine treated patients compared to placebo [172]. Hong *et al.* (2014) evaluated inflammation and oxidative stress at baseline and post-intervention in using high-sensitivity CRP (hs-CRP) and urine 8-hydroxy-2'-deoxyguanosine (8OHdG), respectively [175] and report significant reduction in 8OHdG in the group treated with L-carnitine ($p = 0.034$).

4.4 Discussion

4.4.1 Summary of Evidence

To our knowledge, this is the first reported systematic review to evaluate the effect of dietary L-carnitine supplementation on liver fat, markers of liver injury and insulin resistance profiles in NAFLD populations. Pooled results from five randomised trials suggest that L-carnitine supplementation is associated with significant attenuation of liver fat, and reduction in serum ALT levels, the most commonly used surrogate biomarker of hepatocellular injury. A reduction in AST following L-carnitine therapy was also seen, though this did not reach statistical significance. Our results further suggest that L-carnitine can improve insulin sensitivity in NAFLD cohorts, as measured indirectly using the HOMA-IR index. These outcomes are potentially important to clinical practice, as they confirm a beneficial effect of a broadly available nutrient.

4.4.2 Strengths and Limitations

This review comprised a robust and comprehensive database search with no language restrictions. The search strategy was implemented by two reviewers separately, and both authors agreed on papers selected for inclusion as well as reasons for exclusion. Included studies were read and assessed for bias independently by each reviewer; any disagreements in the risk of bias tool were referred to a third reviewer for final arbitration. No publication bias was found to be present for selected outcomes entered into the meta-analysis.

There were several limitations associated with this review. Firstly, despite an extensive literature search, only five randomised studies were available evaluating L-carnitine on liver markers in NAFLD. Of these, only four evaluated change in liver fat as an outcome measure. Despite another trial being published, we were unable to obtain the full text after attempts to contact the authors of the paper.

Secondly, poor methodological quality was inherent in three of the included studies. For example, while all studies claimed randomisation, only Malaguarnera et al. (2010) and Bae et al. (2015) described robust methods of random sequence generation [172,173]. Lack of placebo control use in the studies conducted by Somi et al. (2014) and Hong et al. (2014) further reduced methodological quality and reliability of reported results [175,176]. Double-blind trial design is an important tool in minimising bias and maximising reliability of research outcomes. In two of the included studies, there was insufficient evidence to judge that robust blinding of participants and personnel occurred. In the study conducted by Somi et al. (2014) no mention of blinding was made [176]. This led us to judge these studies as having a high risk of bias and thus further reduced reliability of reported results.

There was heterogeneity of the trials with respect to duration, type of active comparator drug and background therapy, as well as L-carnitine formulation and dose. Two studies used L-carnitine in a complex with orotic acid (carnitine-orotate); thus establishing a true effect of L-carnitine alone on outcomes measures was not possible. Doses varied widely, from 500 mg daily to 2.25 grams daily, resulting in differential exposure to active L-carnitine among patients in each individual study. The NAFLD patient populations studied were also heterogenous, including patients both with and without diabetes, patients with different stages of NAFLD and geographical differences in populations. However, all 5 studies reported reductions in ALT, suggesting a consistent beneficial effect of L-carnitine on hepatocellular injury across populations.

As a marker of treatment response, ALT appears to be reliable, and has been closely correlated to objectively measured reductions in liver fat using histological and imaging methods in NAFLD post-intervention [177,178]. In phase 2 RCTs, ALT continues to be used as a surrogate marker of disease activity in addition to estimation of fat [179]. The overall significant reduction in ALT following intervention in the included studies suggests a global reduction in hepatocellular injury in patients treated with L-carnitine. Indeed, Malaguarnera et al. (2010) demonstrated an improvement in all histological parameters in their biopsied NAFLD cohort following L-carnitine therapy, including

steatosis, inflammatory activity and fibrosis [172]. Steatosis reduction was confirmed using CT with liver attenuation index by Bae et al. (2015) [173].

With respect to translation into clinical practice, none of the five trials evaluated plasma levels of Trimethylamine-N-Oxide (TMAO), a metabolite of L-carnitine associated with increased risk of atherosclerosis. In a population already at high risk for cardiovascular outcomes, the safety profile of L-carnitine supplementation would require rigorous assessment in this context. However, the evidence base for a direct adverse link between L-carnitine supplementation and cardiovascular events is to our knowledge limited. On the contrary, a meta-analysis of 13 placebo-controlled trials including 3629 patients evaluated the clinical impact of L-carnitine supplementation administration in patients with ischaemic heart disease and concluded that carnitine administration was associated with clinical benefit, including reduced mortality and reduction in onset of cardiac arrhythmias and angina [180]. A recently published study further [180] concluded that although 24-weeks of L-carnitine supplementation increased plasma TMAO concentrations, no changes in lipid profile or other serum biomarkers of atherosclerosis were seen [181].

4.4.3 Conclusion

The evidence collated from studies included in this review forms a compelling argument for further robust, randomised trial data evaluating mechanisms of action of L-carnitine on liver and muscle tissue in a NAFLD phenotype, as well as its effect on validated outcome measures such as liver histology, magnetic resonance imaging and spectroscopy. Further, effects of L-carnitine supplementation on metabolic outcomes in NAFLD require further attention, for example through utilising gold-standard measures of liver-specific and whole-body insulin sensitivity such as the euglycaemic hyperinsulinaemic clamp technique. As a naturally occurring, broadly applicable, safe and cost-effective agent, L-carnitine could overcome traditional barriers to translation to become routinely available for patients in clinical practice as an adjunctive treatment for NAFLD.

Chapter 5:

Effect of Dietary L-carnitine supplementation on liver fat, insulin sensitivity and hepatic energy kinetics.

This study aimed to investigate the impact of chronic L-carnitine supplementation on liver fat, indices of metabolic health and hepatic mitochondrial energy kinetics.

5.1 Introduction

L-carnitine is an essential metabolic cofactor in long-chain fatty acid metabolism, and acts as a crucial regulator of intracellular fuel selection. While the relative contribution of carbohydrate and lipid to the generation of mitochondrial ATP varies considerably according to physiological circumstance, metabolic inflexibility (i.e. a blunted ability to switch from lipid-predominant oxidation in the fasted state to carbohydrate oxidation in the fed – hyperinsulinaemic –state) is a hallmark feature of the metabolic syndrome.

In Chapter 3, we demonstrated that NAFLD is also characterised by metabolic inflexibility, even in the absence of established type 2 diabetes. The unique action of L-carnitine at the nexus of cellular carbohydrate and lipid kinetics, and thereby in the modulation of metabolic flexibility, has spawned intense research focus on its potentially therapeutic role in the metabolic syndrome. A recent meta-analysis of randomised controlled trials (n=37) reported that L-carnitine supplementation was associated with significant overall reductions in key biomarkers of glucose metabolism, including fasting blood glucose, fasting insulin, HOMA-IR and HbA1c levels [182]. Other studies have demonstrated a benefit of chronic carnitine supplementation on hallmark features of the metabolic syndrome, including NAFLD as discussed in chapter 4 [183]. However, the precise mechanisms through which L-carnitine exerts these favourable effects remain unclear.

With respect to the paradigm of lipid-induced insulin resistance and NAFLD, one plausible hypothesis for a benefit from L-carnitine supplementation is the facilitation of muscle lipid β -oxidation, particularly given skeletal muscle accounts for ~95% of the body carnitine pool. Reduced burden of bioactive lipid species (e.g. diacylglycerol) in myocytes would, through mechanisms previously discussed, attenuate PKC θ -mediated interference in cellular insulin signalling, thereby enhancing the

ability of skeletal muscle to act as a pool for glucose uptake and glycogen synthesis. The consequent reduction in diversion of carbohydrate substrate to the liver limits *de novo* lipogenesis (DNL) and reduces DNL-derived fat accumulation in the liver.

Lambert and colleagues (2014) used stable isotope tracer methodology to demonstrate that DNL is a key feature underpinning NAFLD and the development of selective hepatic insulin resistance, and that absolute *de novo* lipogenic flux (i.e. rate of *de novo* fatty acid synthesis) is increased by more than 3 fold in NAFLD patients compared to individuals without elevated liver fat [¹⁸⁴]. More recently, Smith et al (2019) used deuterated water labelling to demonstrate an incremental contribution from DNL towards hepatic steatosis in lean individuals, obese non-NAFLD and obese-NAFLD phenotypes. In the latter, DNL was shown to contribute to 38% of intrahepatic triglyceride load [¹⁸⁵]. This is thought to occur through insulin-mediated upregulation of the sterol regulatory element binding protein-1 (SREBP-1). This raises the interesting paradox of pathway-specific insulin resistance in the liver, with differential downstream effects of insulin depending on specific metabolic processes. For example, the hallmark of hepatic insulin resistance is failure of insulin to adequately suppress endogenous glucose production. Despite this 'resistance', pre-clinical and clinical studies support the hypothesis that the SREBP-1 pathway retains sensitivity to the upregulating effects of insulin. This mechanism implies differential effects of insulin action on specific metabolic functions in the liver, manifested by insulin resistance with respect to the suppression of hepatic glucose production, but preserved insulin sensitivity with respect to the SREBP-1c pathway that stimulates fatty acid synthesis.

Through mobilising intracellular fat stores, carnitine rescues metabolic flexibility in insulin resistant tissue, promoting non-oxidative glucose disposal in muscle. This then logically limits substrate delivery towards the liver to enter lipogenic pathways and contribute to hepatic steatosis, thereby indirectly improving NAFLD burden.

Another potential mechanism of action is a direct effect of L-carnitine on liver tissue. Plasma and urine carnitine pools have been investigated in individuals with chronic liver disease from a variety of

aetiologies, and have demonstrated no significant difference in cirrhotic versus control subjects [106]. However, analysis of plasma carnitine concentrations as an indicator of whole-body carnitine status is at best inaccurate, as discussed in Chapter 1, section 4. In several studies, no correlation has been shown between plasma and tissue carnitine concentrations [186,187].

Tissue carnitine content at the level of the liver has not been extensively studied in humans. Limited data suggest that absolute liver carnitine concentrations may in fact be increased in obese individuals undergoing bariatric surgery but this reflects an increase in whole-body carnitine pools and may in fact mask a relative carnitine deficiency in these populations [188]. Indeed, L-carnitine supplementation in animal models has been shown to augment hepatic carnitine concentrations and induce favourable metabolic effects both locally and peripherally. For example, Savic and colleagues recently demonstrated increased liver choline content in rats treated with L-carnitine, suggesting increased tissue-specific uptake at the level of the liver. The authors argue that L-carnitine supplementation could be beneficial in NASH through modulating hepatic choline content, with metabolic benefits including reduced body weight, improved serum triglyceride levels and reducing AST:ALT ratio [96]. In this instance, it would be logical to expect that L-carnitine action directly on hepatocyte metabolism may reduce accumulation of bioactive lipid species derived from other sources (e.g. FFA flux) rather than simply exerting an indirect effect by modulating influx of DNL substrate through increasing muscle metabolism.

In other animal models, including the Japanese medaka (*Oryzias Latipes*) fish, two weeks of L-carnitine supplementation increased liver carnitine content by 4.4 fold. This was associated with a reduction in liver fat following high fat diet (HFD) overfeeding, an increase in tissue-specific expression of superoxide dismutase (SOD), a potent antioxidant enzyme, increased liver ATP production and upregulation of several metabolic pathways governing lipid β -oxidation. Taken together, this data suggests that L-carnitine may act directly at the level of the liver (as well as muscle), to exert tissue

specific metabolic benefit [189], accepting the caveat that this work in animal models may translate imprecisely to human physiology.

Another plausible mechanism for benefit of L-carnitine supplementation in a metabolically challenged phenotype is modulation of the intracellular Acyl-CoA/CoA ratio through binding acyl-CoA into acylcarnitines via the enzyme carnitine acetyltransferase. This buffering action replenishes the free CoA pool, upregulating key enzymes involved in mitochondrial biogenesis and function. Acetyl CoA is a critical intermediate cellular metabolite, serving as the both the final common product of glucose and lipid metabolism and the universal substrate for oxidative phosphorylation. Subcellular concentrations of Acetyl CoA have myriad downstream effects on enzyme activity, fuel selection and bioenergetics, due to either allosteric modulation of enzymes or through alteration of substrate availability. The subcellular Acetyl CoA: Free CoA ratio is a sensitive marker of cellular metabolic status and exerts pleiotropic effects on gene transcription, mitosis and cell death. An increased ratio of Acetyl CoA/CoA promotes oxidative stress and cell death through removing inhibition of the apoptotic enzyme caspase 2, and a reduction in this ratio favours cell survival [190].

Here, we sought to more precisely establish mechanisms of L-carnitine action in the context of NAFLD. Through leveraging precision imaging techniques in combination with deep metabolic phenotyping, we were able to determine the nature and magnitude of carnitine-mediated metabolic effects in a NAFLD population.

5.2 Methods

5.2.1 Ethical Approval

This study was approved by the Nottingham 2 Research Ethics Committee (approval number: 17/EM/0441), by the Research & Innovation department at Nottingham University Hospitals NHS Trust (Study 17GA048) and by the Health Research Authority (**Appendix 2**) in February 2018. All

research was conducted in accordance with the Declaration of Helsinki [¹⁹¹] and participants provided written, informed consent prior to enrolment.

5.2.2 Recruitment

Recruitment commenced in March 2018 and ended in October 2019. Patients with NAFLD and without evidence of advanced fibrosis were recruited based on controlled attenuation parameter readings on vibration controlled transient elastography or liver biopsy. Inclusion criteria included: male patients \geq 18 years of age, BMI \leq 40 at the time of screening, evidence of NAFLD as assessed by transient elastography (CAP $>$ 288 Db/m), or liver biopsy, and self-reported alcohol intake less than 21 units (168 grams) per week. Exclusion criteria included presence of advanced fibrosis as determined by transient elastography (liver stiffness $>$ 8 kilopascals) or liver biopsy (Kleiner fibrosis score \geq 2), blood parameters indicating liver synthetic impairment (thrombocytopenia, hypoalbuminaemia, elevated prothrombin time or jaundice), presence of type 1 or type 2 diabetes mellitus, smoking history, chronic inflammatory disease including cardiovascular, respiratory or rheumatological disease, inflammatory bowel disease, coagulopathy, and patients taking regular medication including steroids, lipid lowering therapy, anti-metabolite treatment, biologic therapy or antihistamine agents were excluded. Other exclusions included known claustrophobia, presence of internal metallic implants incompatible with the Phillips MR scanner systems, history of any psychiatric disorders.

Recruitment pools predominantly comprised Hepatology outpatient clinics in Nottingham University Hospitals NHS trust, including patients attending for a Daycase Fibroscan via the locally commissioned Scarred Liver Project pathway [¹⁹²]. Other sources of recruitment were locally sited flyers, advertisements in local newspapers and the Call for Participants website (<https://www.callforparticipants.com/study/poster/J572X>). Flow through the study is summarised in

Figure 1. The recruitment process is summarised in **Figure 2.**

5.2.3 Screening visit

All subjects underwent a screening visit in the NIHR Nottingham Biomedical Research Centre. After an overnight fast, fasting blood samples were taken for determination of plasma glucose, lipid profile, full blood count, urea and electrolytes, liver function tests, serum insulin and free carnitine. Research bloods were taken simultaneously and stored in -20°C freezers with a view to analysis of plasma trimethylamine-N-oxide and hepatokines (FGF21 and LECT2). A non-invasive liver screen (including Hepatitis B and C serology, autoimmune liver panel and serum iron studies) was performed to exclude alternative causes of chronic liver disease.

After medical history taking and physical examination, a resting 12-lead ECG was performed and anthropometric measures including height, weight, waist and hip circumference were determined. Subjects who passed the screening visit subsequently returned for baseline study visits.

5.2.4 Randomisation

Subjects were randomised in a 1:1 ratio to receive either L-carnitine (2 grams twice daily) or maltodextrin placebo (2 grams twice daily), together with a Slimfast milkshake (325 ml twice daily). L-carnitine and placebo preparations were identical in appearance, supplied as sachets of white powder. Both the investigators and participants were blinded to treatment allocation until the end of the study. Subjects were block randomised via computer generated allocation sequence (www.randomization.com) to one of two treatment arms: A or B. Randomisation was in a 1:1 ratio using balanced block sizes by an independent party not affiliated with the study, within the Nottingham Digestive Diseases Biomedical Research Centre.

Compliance was assessed through counting returned empty sachets and measuring plasma carnitine levels. Compliance was considered effective if subjects returned >80% empty vials each month. Subjects returned to the NIHR Nottingham Biomedical Research Centre every 4 weeks for safety blood

tests, supplementation, compliance check and anthropometric assessments. Subjects were instructed not to commence any new diets or medication.

5.2.4 Metabolic Imaging

Metabolic and imaging assessments were identical for pre and post-intervention studies. After an overnight fast, subjects arrived at 08:00 to the Sir Peter Mansfield Imaging Centre (SPMIC), University of Nottingham. Each subject underwent three separate MR spectroscopy scans, with methods as described in Chapter 3:

- 1) ^1H -MRS for evaluation of liver fat (calculated as proton density fat fraction)
- 2) ^{31}P -MRS with saturation transfer for evaluation of liver ATP flux
- 3) ^1H -MRS for evaluation of muscle fat fractions (intra and extramyocellular lipid)

MR measurements were performed on a 3T (liver scans) or 7T (muscle scans) Phillips scanning system (Phillips, Best, The Netherlands).

T1-weighted axial and coronal scout imaging was initially used to guide voxel placement, avoiding major vascular or biliary structures, as well as diaphragmatic edges and subcutaneous fat. Liver fat was determined using STEAM-localised MRS sequences derived from a 20 x 20 x 20 mm voxel positioned in the right lower lobe of the liver, with and without water suppression. A Philips XL 16 channel torso coil was used for transmission and reception. Non-water suppressed spectra were acquired during a single breath hold (TR = 2000 ms, TE = 20, 40, 60, 80 ms, 2 averages per spectra) and were subsequently repeated with water suppression. Data was post-processed using jMRUI software (version 5.2) with manual phase correction, frequency alignment and line-broadening. Fitting was undertaken using AMARES peak fitting with prior knowledge. Amplitudes were fitted to a monoexponential decay curve for water and fat (T2). Fat fraction was expressed as the ratio of the fat peak ('area under the curve') over the cumulative water and fat peak areas (1.3 ppm/(1.3 ppm + 4.70 ppm)) as previously described [193]. Calculated peak areas of water and fat were corrected for T2 relaxation.

Slice localized ^{31}P MRS were acquired from the liver using a Philips ^{31}P single loop surface coil. Apparent T_1 ($T_{1\text{app}}$) was measured using progressive saturation ^{31}P MRS (five spectra fitted using jMRUI) as described previously [148]. ATP rate constant (k) was then calculated from two ^{31}P MRS spectra, one fully saturating γ -ATP (-2.5ppm) and the second mirrored about the Pi peak (14ppm). Total scan time for participants was approximately 1 hour and 15 minutes.

On a separate occasion (within 7 days of scanning), after an overnight fast, a two-stage euglycaemic hyperinsulinaemic clamp study was undertaken to determine hepatic and peripheral insulin sensitivity (Chapter 2, Figure 3). A continuous, primed infusion of dideuterated [6,6- D_2] glucose tracer was commenced 120 minutes prior to the first stage of the clamp and continued throughout both low (stage 1, 15mU/m²/min) and high (stage 2, 60 mU/m²/min) dose insulin infusions for quantification of endogenous glucose production. Blood glucose was maintained ('clamped') at the euglycaemic target of 4.50 mmol/l and peripheral insulin sensitivity was calculated as the glucose infusion rate required to maintain euglycaemia (glucose infusion rate assumed to equal whole-body glucose uptake) at steady state during the high dose clamp. Hepatic insulin sensitivity was calculated as % suppression of endogenous glucose production under insulin stimulated conditions during low dose (stage 1) insulin infusion. The method for calculation is described in **Chapter 2**.

Indirect calorimetry was performed at baseline, during low dose insulin infusion (stage 1) and again during high dose insulin infusion (stage 2) to evaluate resting energy expenditure (REE), and rates of oxygen (VO_2) and carbon dioxide (VCO_2) consumption. Body composition was determined by dual X-ray energy absorptiometry (DEXA) at baseline and post-intervention. Muscle biopsies were taken from the *vastus lateralis* using the modified Bergstrom technique. Biopsies were performed prior to initiation of the clamp, and again from the contralateral leg immediately following the stage 2 clamp. A maximum of two passes with the Bergstrom needle were made and muscle tissue was immediately frozen in liquid isopentane cooled over liquid nitrogen to -160°C as described previously. Samples were subsequently sectioned and stored in -80°C freezers until analysis. Specimens were analysed for

glycogen content using an amyloglucosidase-based spectrophotometric assay [¹⁹⁴]. Fresh samples were mounted for subsequent analysis of IMCL lipid droplet size using Bodipy-493/503 staining, as previously described [¹⁹⁵].

5.2.5 Statistical Analysis

Differences in baseline characteristics between groups were assessed using the independent samples *t*-test for continuous, normally distributed data. When parametric assumptions were not met, the non-parametric Mann Whitney U Test was used to compare baseline characteristics. Relationships between participant characteristics were assessed using bivariate Pearson's and Spearman's correlation coefficients as appropriate. Three-way, mixed-design analysis of variance (ANOVA) was used to assess repeated measures and significance of interactions both between and within subjects. A student's T test with Bonferroni correction was used to locate differences in instances of significant interactions. Homogeneity of variance between group data at each visit was assessed using Mauchley's test of sphericity. A Greenhouse-Geisser or Huynh-Feldt correction was applied, as needed, where assumptions of sphericity were violated.

Analysis of covariance (ANCOVA) using baseline values as covariates was used to evaluate change in continuous variables from baseline between groups. Overall within-subject changes before and after intervention were analysed using a two-sided paired samples Student's T-test for normally distributed variables or using a Related-Samples Wilcoxon Signed Rank test for pairwise comparisons in non-normally distributed variables.

Changes from baseline to post-intervention are presented as absolute and relative percentage change, with 95% confidence interval [CI]. Data was analysed using SPSS software version 24 (SPSS Inc., Chicago, Illinois, USA).

Sample size was calculated assuming an absolute reduction in IHTG of $2.4 \pm 1.5\%$ in the treatment group (with no change in the placebo group) after 24 weeks' intervention. A sample size of 16 patients

(8 per group) would provide statistical power of 80% ($1-\beta = 0.80$) with a two-sided α significance level of 0.05 and an effect size of 1.60. A final sample size of 10 participants per group was selected to account for 20% attrition. This would also power the study adequately for determination of the main secondary endpoint (liver insulin sensitivity).

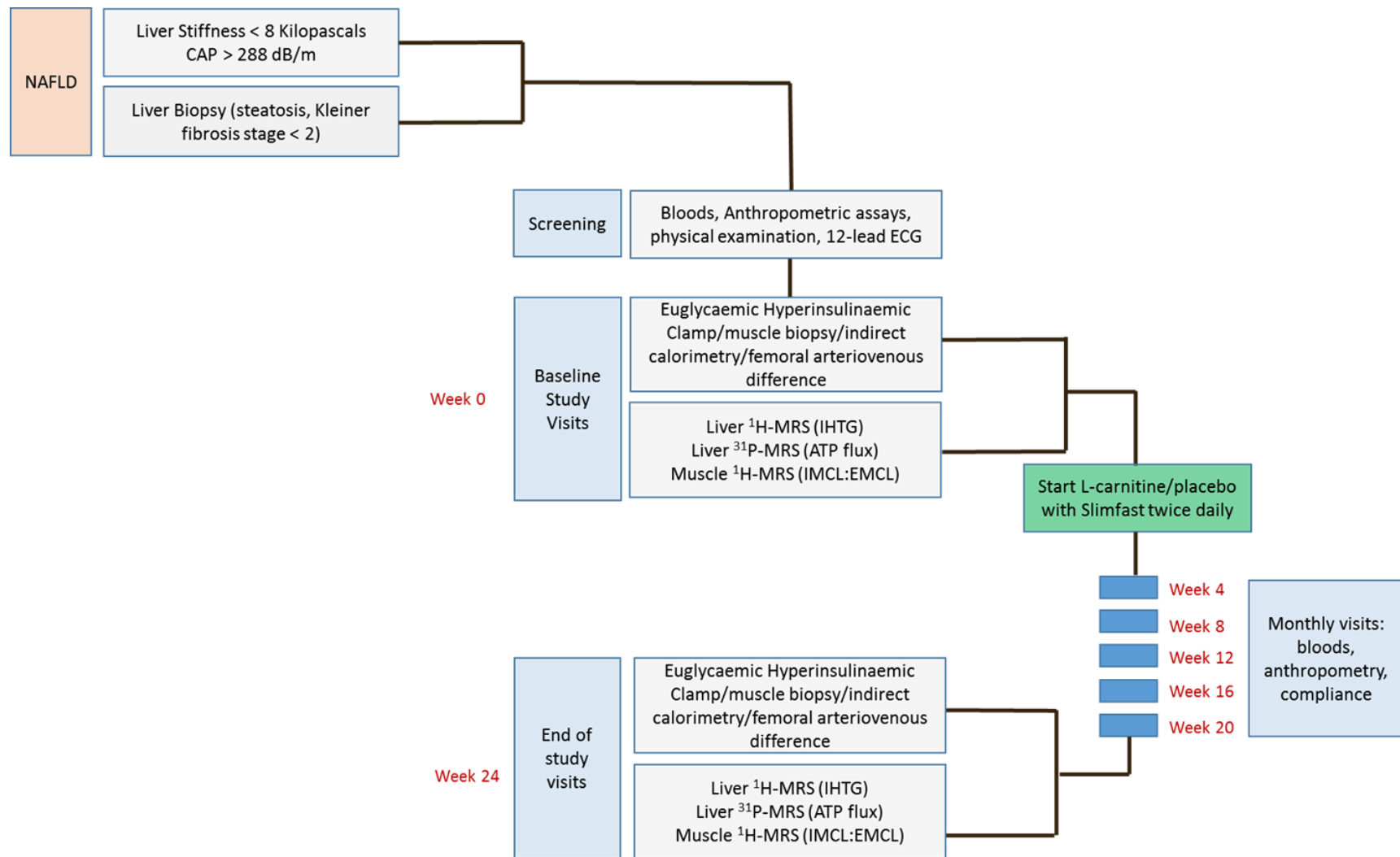


Figure 1. Schematic detailing flow through the ECLIPSE study. NAFLD was diagnosed on the basis of elevated controlled attenuation parameter (CAP) with liver stiffness measurement < 8 KpA (to exclude advanced fibrosis) on transient elastography or by presence of steatosis in the absence of advanced fibrosis on liver biopsy. Exclusion criteria included alcohol intake > 21 units per week or detection of an alternative aetiology of liver disease on the basis of a non-invasive liver screen performed during the screening visit. Following a screening visit, subjects attended for two separate baseline study visits. Following this, all subjects commenced twice daily supplementation of L-carnitine/placebo together with a 325 ml Slimfast® supplement twice daily. Subjects then returned at 4 weekly intervals to the Digestive Diseases Centre for safety bloods and anthropometric tests. At week 24, subjects underwent post-intervention study visits consisting of metabolic physiology and metabolic imaging assessments as per baseline.

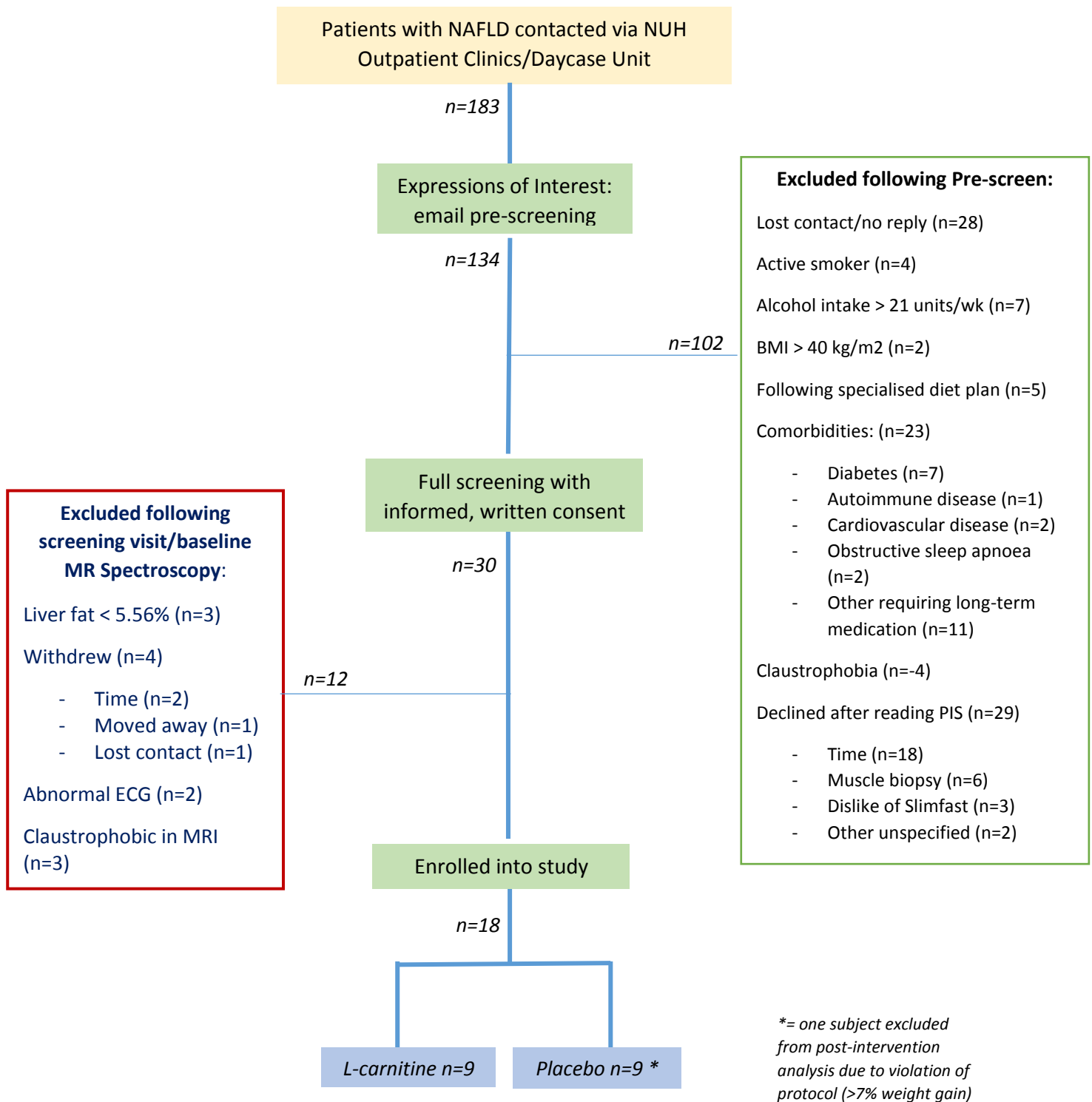


Figure 2. Outline of Study Recruitment

5.3 Results

Differences in baseline characteristics, including demographics, anthropometric measures and circulating metabolic biomarkers, are shown in **Table 1**. No significant differences in salient baseline metabolic characteristics were found. In particular, baseline intrahepatic triglyceride was similar between groups ($25.3 \pm 15.0\%$ versus $26.9 \pm 9.0\%$, $p=0.80$) albeit with lower variance in the placebo-treated group (**Figure 3**). Of the 30 subjects screened, 18 were ultimately included in the study. Nine men were randomised to receive L-carnitine and 9 to placebo. One subject in the placebo group was excluded due to $>7\%$ weight gain during the 24 weeks of the study protocol. Data is therefore presented for the 9 subjects randomised to receive L-carnitine and 8 subjects randomised to placebo.

	Reference Range	L-carnitine (n=9)	Placebo (n=8)	P value
Age (years)		36.8 ± 10	37.3 ± 6.0	0.90
Body Weight (kg)		102.2 ± 17	107.9 ± 14	0.47
ALT (IU/L)	0-45	73.5 ± 33	68.6 ± 28	0.97
AST (IU/L)	0-35	59.6 ± 39.7	35.1 ± 9.61	0.10
BMI (kg/m²)		31.3 ± 5.1	34.1 ± 1.7	0.19
IHTG content (%)		25.3 ± 15.0	26.9 ± 9.0	0.80
Fasting plasma glucose (mmol/l)	<5.50	4.96 ± 0.36	5.03 ± 0.75	0.98
Fasting insulin (U/L)		22.53 ± 11.7	18.2 ± 7.2	0.40
Waist circumference (cm)		108.1 ± 9.7	107.9 ± 9.5	
Hip circumference (cm)		111 ± 9.2	113.3 ± 10.2	0.64
Waist: Hip ratio		0.98 ± 0.04	0.96 ± 0.03	0.15
HOMA-IR		4.8 ± 2.9	4.2 ± 2.1	0.63
ADIPO-IR		8.49 ± 4.7	9.14 ± 5.2	0.79
Total Cholesterol (mmol/l)	≤ 5.0	5.2 ± 1.03	4.68 ± 0.95	0.27
Triglycerides (mmol/l)	0.4-1.8	1.91 ± 0.88	1.70 ± 0.86	0.62
HDL cholesterol (mmol/l)	≤ 1.0	1.12 ± 0.19	1.15 ± 0.20	0.77
LDL cholesterol (mmol/l)	≤ 3.0	3.30 ± 0.98	2.76 ± 0.72	0.23
Plasma Free Carnitine	15 -53	36.9 ± 12.3	37.5 ± 7.5	0.28
IMCL:EMCL Ratio		0.92 ± 0.61	1.53 ± 0.99	0.15
% EGP Suppression		17.7 ± 14.3	15.1 ± 18.6	0.75
Glucose Disposal Rate (mg/kg/min)		3.37 ± 1.62	3.48 ± 1.76	0.90
Leg Glucose Uptake ($\mu\text{mol/ml/kg leg}$)		10.6 ± 3.5	10.8 ± 4.1	0.94
FATP (Mm/S)		0.35 ± 0.23	0.36 ± 0.17	0.80

Table 1. Baseline Anthropometric and Metabolic Characteristics in L-carnitine and Placebo Groups. Normally distributed data expressed as mean (SD). Non-normally distributed data expressed as median (IQR). FATP = Forward rates of ATP synthesis; IMCL: EMCL = intramyocellular: extramyocellular lipid ratio.

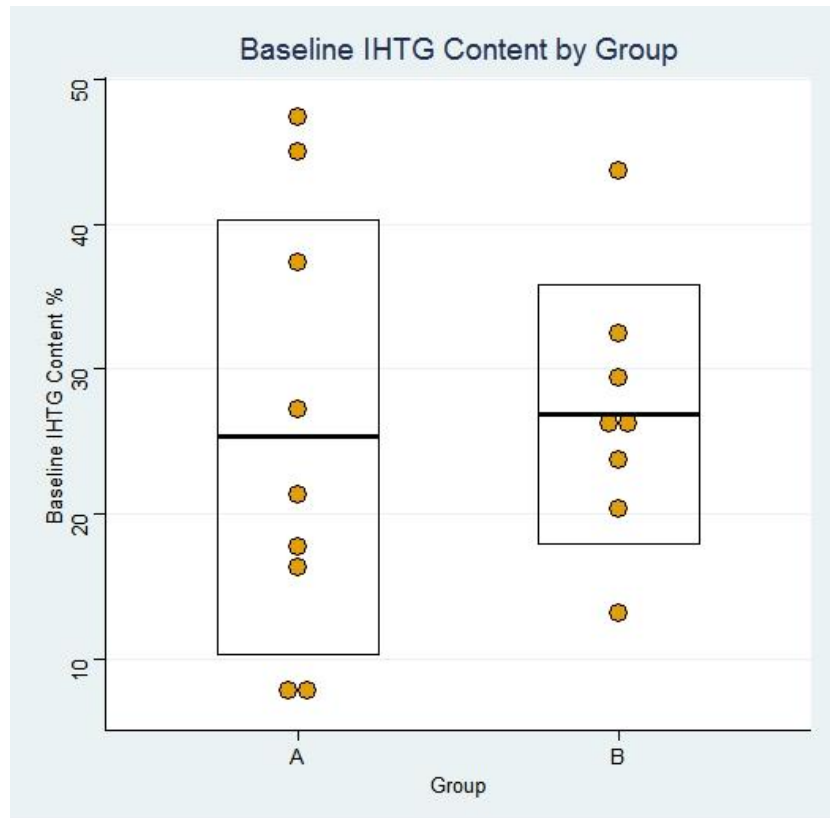


Figure 3. Mean IHTG (%) and individual data points in L-carnitine (Group A) and placebo (Group B) treated groups.

5.3.1 Effect of 24 weeks' L-carnitine supplementation on IHTG

IHTG data were normally distributed, as assessed by the Shapiro-Wilk's test ($p > 0.05$ for both groups). There was a linear relationship between pre and post-intervention IHTG (%) for each group, as assessed by visual inspection of a scatterplot. There was homogeneity of variances, as assessed by visual inspection of a scatterplot and Levene's test of homogeneity of variance ($p = 0.16$).

Despite no significant change in body weight between or within groups, L-carnitine treatment was associated with an absolute reduction in IHTG of 3.5 % (-5.7; -1.5%, $p = 0.01$) corresponding to a relative reduction of 20% [-39; -7.5%], compared with an absolute increase of 6% [1.9; 10.6 %] in the placebo group, corresponding to a relative increase of $19.7 \pm 17.9\%$ [7.03; 22.8] (**Figures 4 and 5**). Adjustment for baseline IHTG (%) content was undertaken using the analysis of covariance (ANCOVA)

statistical test with baseline values as covariates. This confirmed a significant change from baseline across groups, $F(1, 13) = 15.1$, partial $\eta^2 = 0.54$ ($p=0.002$). Within group comparisons using the Student's paired T test confirmed a significant reduction in liver fat from baseline in the L-carnitine group ($p=0.01$) and borderline significant increase in the placebo group (0.05).

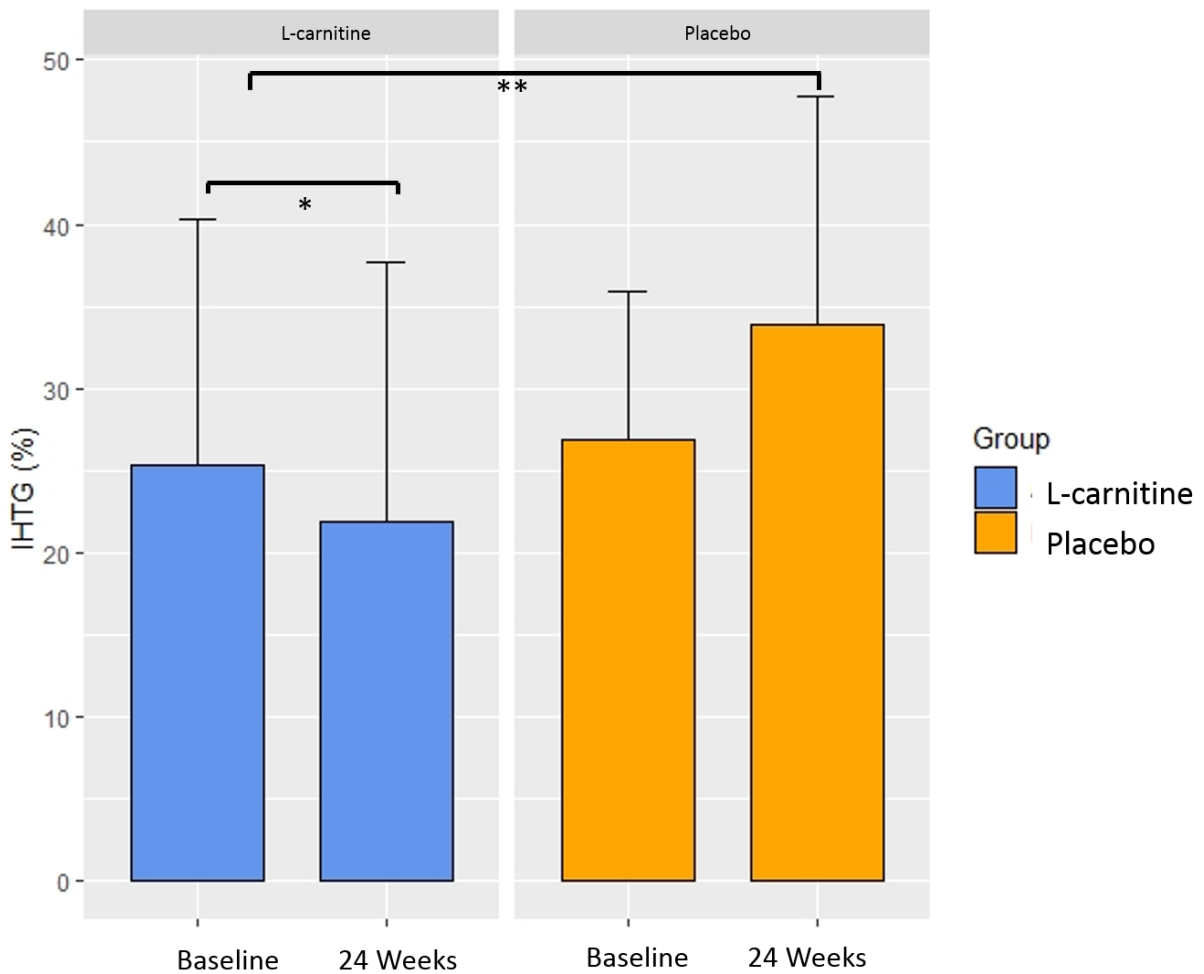


Figure 4. Absolute difference in IHTG (%) in L-carnitine and placebo- treated groups after 24 weeks. * $p<0.05$, ** $p \leq 0.01$, *** $p<0.005$

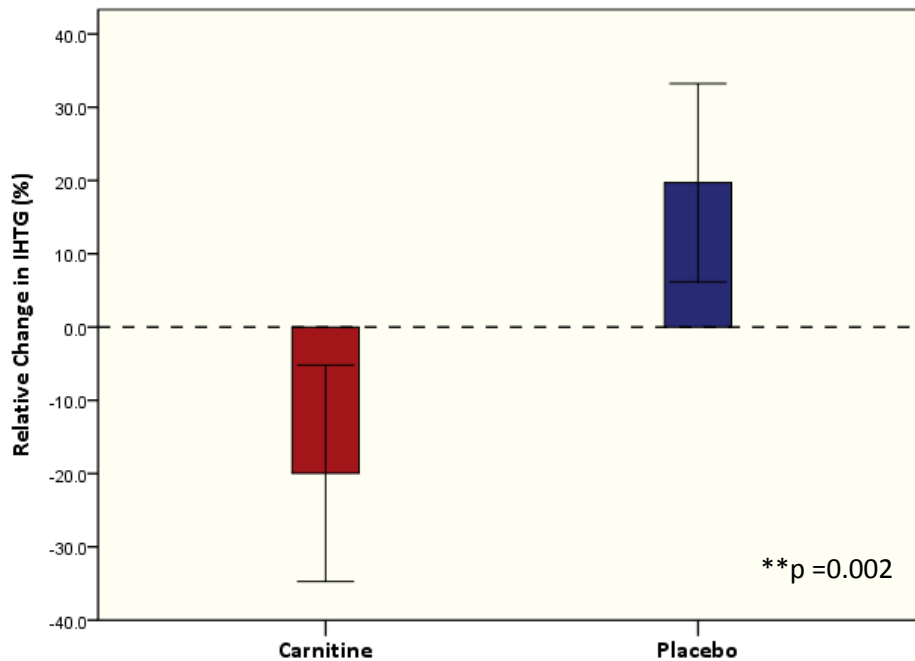


Figure 5. Relative change in IHTG (%) from baseline in L-carnitine (red bar) and placebo (blue bar) treated groups. Results expressed as mean \pm SEM, $p = 0.002$

5.3.2 Effect of L-carnitine supplementation on Glucose Metabolism

Data for whole-body glucose uptake were normally distributed in both groups, both at baseline and post-intervention, as assessed by the Shapiro-Wilks test ($p > 0.05$). There were no significant differences from baseline between groups in whole body glucose uptake (i.e. peripheral insulin sensitivity) during high dose insulin infusion, $F(1, 13) = 0.48$, $p = 0.829$. Paired t tests were used to compare within-group data from baseline, again demonstrating no significant change from baseline in either L-carnitine or placebo groups ($p = 0.33$ and 0.63 , respectively). This data is shown in **Figure 6**.

With respect to hepatic insulin sensitivity (calculated as % suppression of Endogenous glucose production during low dose hyperinsulinaemia), differences were seen between groups from baseline, with an increase in hepatic insulin sensitivity noted in the L-carnitine group (14.7 ± 12 to $23.1 \pm 16.1\%$) and a reduction in the placebo group (13.6 ± 21.6 to $7.08 \pm 6.29\%$). This is shown in **Figure 7**. Between group differences were borderline significant ($P_{ANCOVA} = 0.05$) although within group differences did

not meet statistical significance (Student's paired *t* test, $p = 0.25$ in the L-carnitine group from baseline and $p = 0.53$ in the placebo group from baseline).

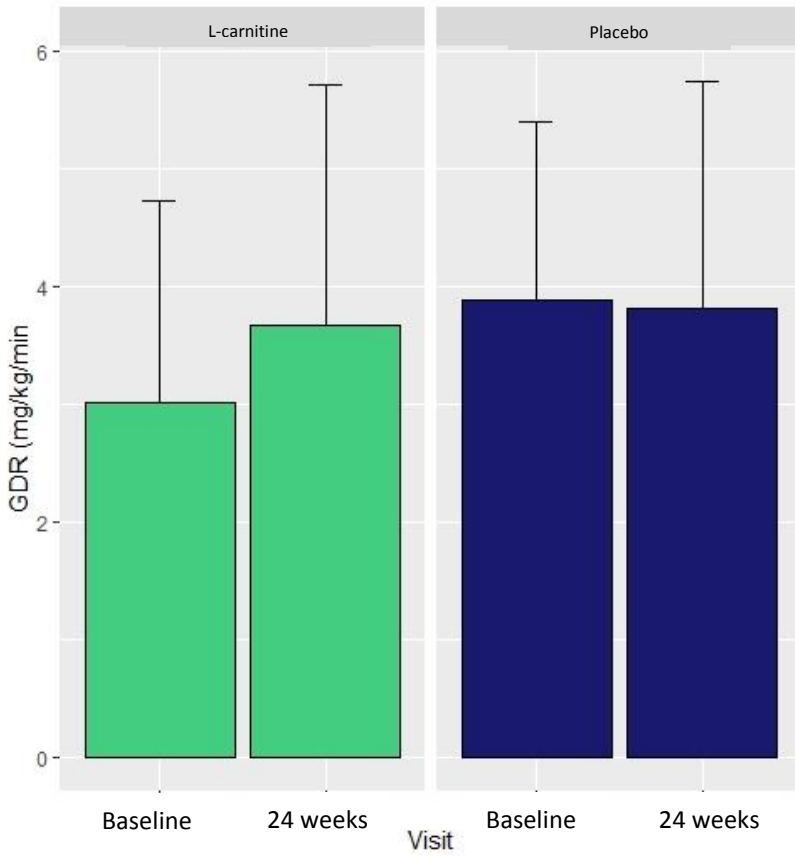


Figure 6 Peripheral insulin sensitivity (glucose disposal rate during steady state in stage 2 of the clamp, mg/kg/min) at baseline and post-intervention in L-carnitine (green bars) and placebo-treated (blue bars) groups. Ns= non-significant

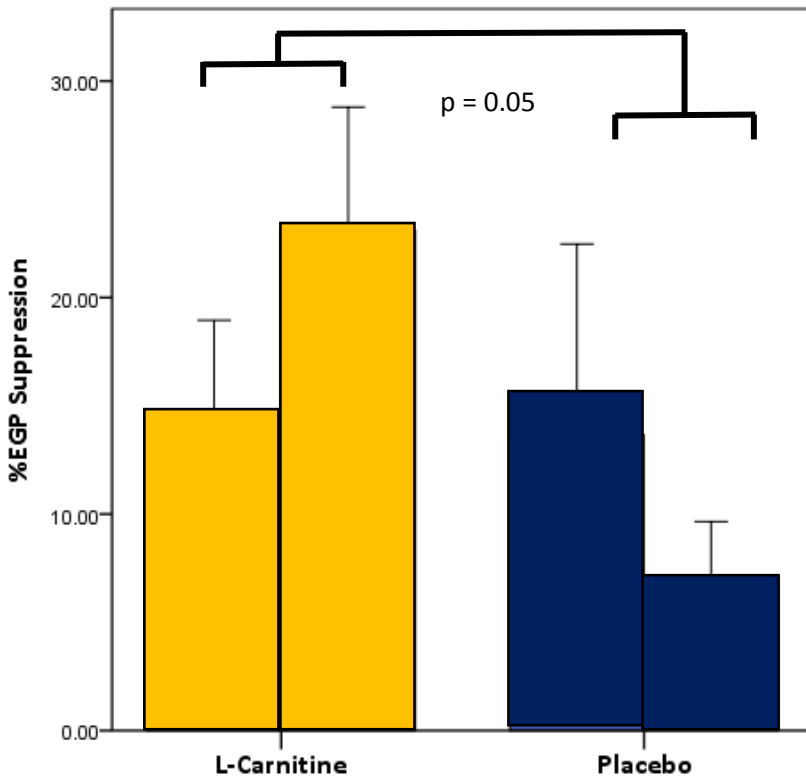


Figure 7 Change from baseline in Hepatic Insulin Sensitivity (%EGP suppression) in L-carnitine and placebo groups. $P_{ANCOVA} = 0.05$

Fasting plasma insulin concentration was lower post-intervention compared to baseline in the L-carnitine treated group (18.8 ± 10.1 versus 22.5 ± 11.7 mIU/L) although this was not statistically significant ($p=0.43$). In the placebo-treated group, a marginal increase in fasting plasma insulin post-intervention compared to baseline was observed (21.5 ± 18.0 versus 18.5 ± 6.7 mIU/L, $p=0.71$). **Figure 8** shows plasma insulin during each stage of the clamp at baseline (grey line) and post-intervention (green line) in the L-carnitine (Panel A) and Placebo (Panel B) treated groups. During the low-dose clamp, plasma insulin was lower in both groups post-intervention compared to baseline (41.0 ± 8.8 versus 53.0 ± 35.4 mIU/L in the L-carnitine group and 38.8 ± 8.9 versus 42.8 ± 7.2 mIU/L) although again these differences were not statistically significant ($p= 0.35$ and 0.26 , respectively). Plasma insulin during the high dose clamp was lower in the L-carnitine group compared to baseline (134.2 ± 35.3 versus 120.3 ± 11.5 mIU/L) whereas it was increased compared to baseline values in the placebo group (112.7 ± 19.8 versus 117.1 ± 17.3 mIU/L), although this did not reach statistical significance in either group ($p=0.24$ and 0.56 , respectively). Taken together, the data suggest slightly increased insulin clearance following L-carnitine supplementation, although this did not reach statistical significance (between groups comparison controlling for baseline covariates, $F(1, 10) = 0.21$, $p = 0.66$).

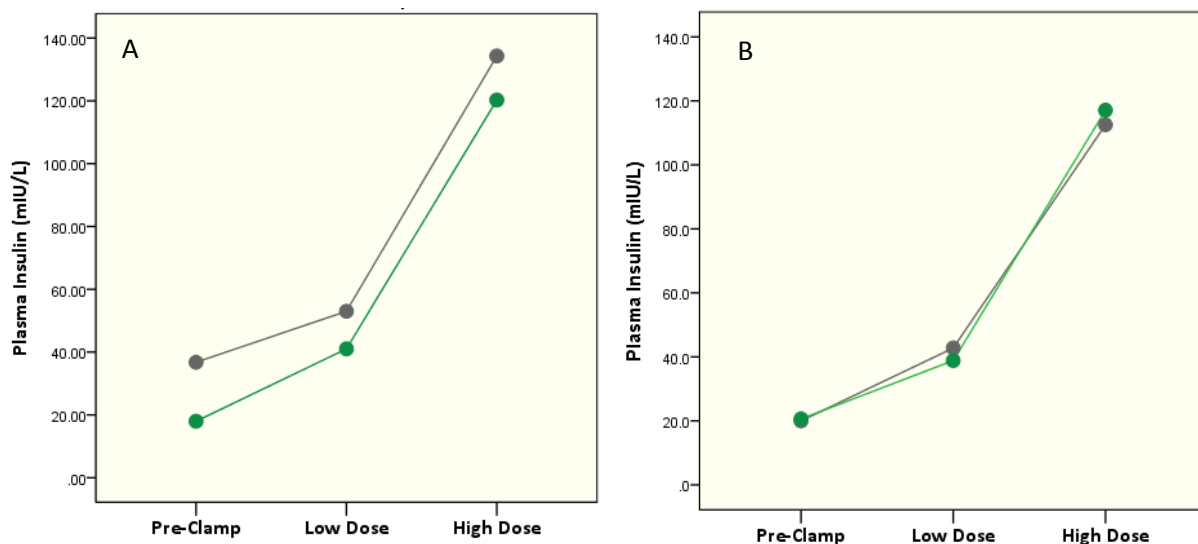


Figure 8 Serial plasma insulin during fasting, low-dose and high-dose hyperinsulinaemia in the euglycaemic hyperinsulinaemic clamp. **Panel A** – L-carnitine treated group at baseline (grey line) and post-intervention (green line). **Panel B** – Placebo-treated group at baseline (grey line) and post-intervention (green line).

5.3.3 Anthropometry

Waist: hip ratio increased significantly in the placebo treated group (0.96 ± 0.03 to 1.02 ± 0.04 $p=0.01$) potentially linking unfavourable metabolic phenotype post-intervention in this group to the development of central adiposity rather than whole-body weight gain *per se*. In the carnitine-treated group, there was no significant change in waist: hip ratio from baseline to post-intervention (0.98 ± 0.04 to 0.99 ± 0.04 , $p=0.46$). Grouped statistics using baseline values as covariates confirmed a non-statistically significant change in Waist: Hip ratio between groups, $F(1, 14) = 3.67$, $p=0.08$.

No statistically significant differences in body fat percentage were observed following intervention in either the L-carnitine treated ($35.5 \pm 4.3\%$ to $34.8 \pm 4.2\%$, $p=0.23$) or placebo treated groups ($34.2 \pm 7.6\%$ to $34.24 \pm 8.2\%$, $p=0.91$). Other regional fat depots as assessed by DEXA did not differ significantly within or between groups compared to baseline (**Table 2**). A slight increase in trunk fat (%) was observed in the placebo group (36.6 ± 9.3 to $39.1 \pm 8.5\%$) but this was not statistically significant.

	L-carnitine		P value	Placebo		P value	Overall significance (ANCOVA)
	Baseline	24 weeks		Baseline	24 weeks		
Body fat (%)	35.5 ± 4.3	34.8 ± 4.2	0.23	34.20 ± 7.6	34.24 ± 8.2	0.91	0.34
Arm fat (%)	31.6 ± 7.6	31.2 ± 7.8	0.65	30.5 ± 10.2	31.0 ± 10.1	0.54	0.49
Trunk fat (%)	41.0 ± 4.0	40.2 ± 4.1	0.24	36.6 ± 9.3	39.1 ± 8.5	0.34	0.27
Leg fat (%)	30.8 ± 4.0	30.2 ± 3.8	0.18	30.9 ± 7.1	30.6 ± 8.1	0.60	0.69
Arm lean mass (kg)	3.8 ± 0.48	3.7 ± 0.60	0.38	4.21 ± 0.72	4.25 ± 0.73	0.47	0.44
Leg lean mass (kg)	10.6 ± 1.7	10.8 ± 1.9	0.17	11.1 ± 1.6	11.4 ± 1.6	0.26	0.82
Trunk lean mass (kg)	13.8 ± 2.7	13.9 ± 2.3	0.65	15.3 ± 1.8	15.1 ± 1.6	0.19	0.87

Table 2 Anthropometric differences from baseline in L-carnitine and placebo treated groups.

5.3.4 Effect on Lipid Metabolism

No significant differences were seen between groups in Adipo IR, from baseline to post-intervention.

L-carnitine induced a minor reduction (2%) in Adipo IR, while Adipo IR was increased by 8.9% in the placebo group, $F(1, 12) = 0.139$, partial $\eta^2 = 0.11$, $p = 0.716$.

L-carnitine treatment was not associated with significant changes in HDL concentration from baseline (1.11 ± 0.16 versus 1.12 ± 0.19 mmol/l, $p = 0.84$), slight but non-significant reductions in LDL cholesterol concentration (3.01 ± 0.86 versus 3.3 ± 0.98 mmol/l, $p = 0.08$), circulating triglyceride concentration (1.72 ± 0.39 versus 1.91 ± 0.88 mmol/l, $p = 0.49$) and total cholesterol concentration (5.0 ± 1.02 versus 5.21 ± 0.96 units, $p = 0.23$). In the placebo-treated group there was likewise no significant difference in lipid profile parameters. Grouped statistics with baseline values as covariates showed no significant between-group differences compared with baseline (**Table 3**).

5.3.5 Effect of L-carnitine on muscle lipid fractions

L-carnitine induced a significant reduction in intramyocellular: extramyocellular lipid (IMCL: EMCL) ratio compared to placebo (0.92 ± 0.61 to 0.42 ± 0.29 versus 1.53 ± 0.99 to 1.48 ± 0.36 , $p < 0.001$). Within groups comparison confirmed non-significant reductions in both groups ($p = 0.09$ and 0.52 , respectively). Mean IMCL:EMCL ratio at baseline and post-intervention in L-carnitine and placebo groups is shown in **Figure 9**.

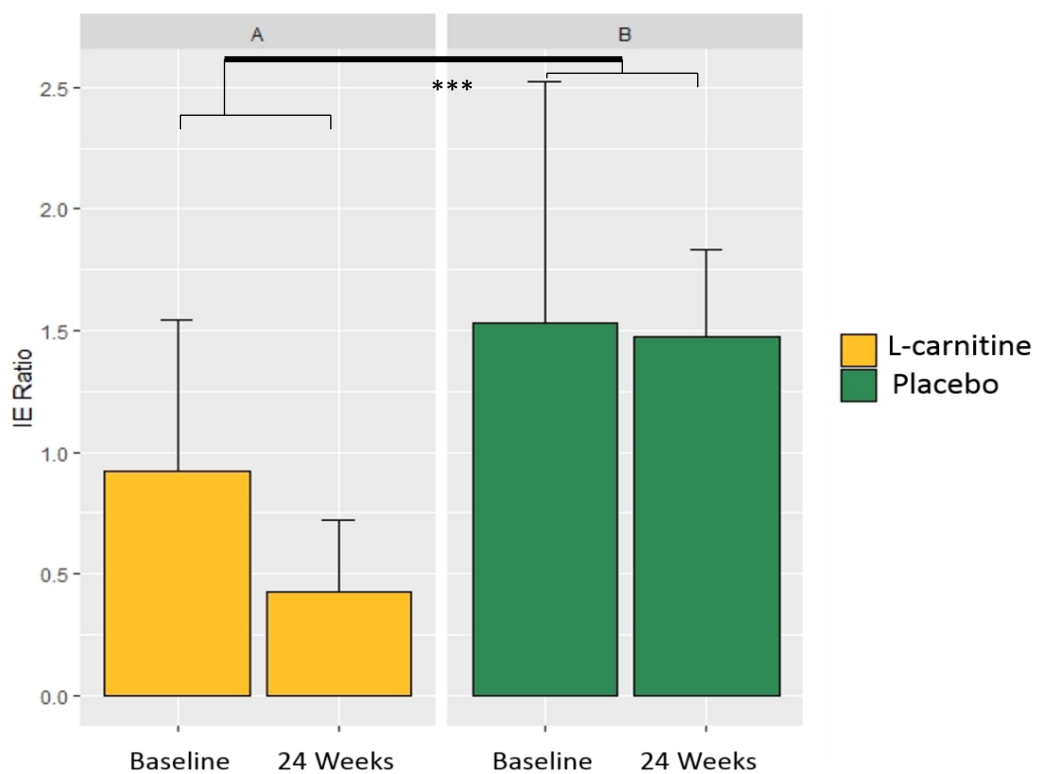


Figure 9 Intra-to-extramyocellular lipid (IMCL: EMCL) ratio in L-carnitine (golden bars) and placebo (green bars) groups at baseline and post-intervention. ****P<0.001**

5.3.6 Effect on hepatocellular enzymes

L-carnitine treatment was associated with a reduction in serum ALT concentration compared to baseline (48.1 ± 19.9 versus 73.6 ± 33.6 IU/L, $p=0.01$), with no significant change from baseline in the placebo group (67.3 ± 46.7 versus 64.4 ± 28.9). Between group differences demonstrated a significant change from baseline ($p= 0.04$). While AST also declined in the carnitine group (63.0 ± 40.4 to 46.6 ± 27.8) compared to the placebo group, variance was high and this did not reach statistical significance ($p=0.148$). In the placebo group, no change in AST was seen from baseline to post-intervention (35.1 ± 9.6 to 36.6 ± 13.8 IU/L, $p=0.67$). Mean serum ALT over time in the L-carnitine and placebo groups is shown in **Figure 10** with further data provided in **Table 4**.

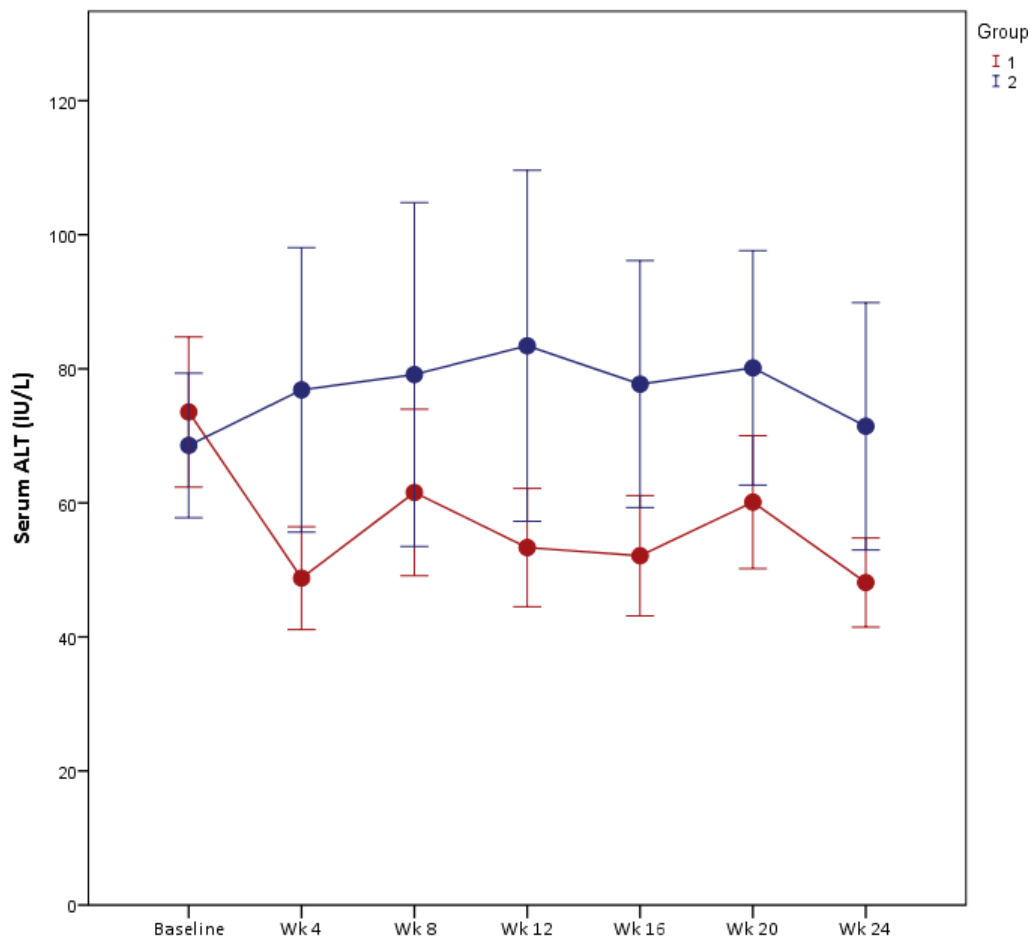


Figure 10 Mean serum alanine aminotransferase (ALT) over time, from baseline to week 24 in L-carnitine-treated (red line) and placebo (blue line) groups.

	Group A (L-carnitine), n = 9			Group B (Placebo), n = 8			Significance (ANCOVA)
	Before Treatment	After 24 weeks	Significance (paired T test)	Before Treatment	After 24 weeks	Significance (paired T test)	
Body Weight (kg)	102.2 ± 17.2	101.9 ± 17.7	0.725	107.9 ± 14.0	108.6 ± 14.6	0.283	0.44
ALT (IU/L)	73.6 ± 34	48.1 ± 19.9	0.01	64.4 ± 29	67.3 ± 46.7	0.78	0.04
AST (IU/L)	63.0 ± 40.4	46.6 ± 27.8	0.15	36.1 ± 9.9	38.0 ± 14.3	0.64	0.60
BMI (kg/m²)	31.2 ± 5.1	31.2 ± 5.2	0.98	32.9 ± 2.9	33.4 ± 3.0	0.02	
IHTG content (%)	25.3 ± 15	21.8 ± 15.8	0.01	26.9 ± 9	33.8 ± 14.0	0.05	0.002
EGP Suppression (%)	14.7 ± 12.0	23.1 ± 16.1	0.22	13.6 ± 21.6	7.08 ± 6.29	0.53	0.05
Waist circumference (cm)	107.1 ± 10.9	107.4 ± 11.9	0.814	107.9 ± 9.5	111.8 ± 8.7	0.01	0.12
Hip circumference (cm)	109.3 ± 10.3	108.2 ± 9.8	0.458	113.2 ± 10.2	111 ± 7.6	0.203	0.89
Fasting Glucose (mmol/l)	4.67 ± 0.46	4.42 ± 0.32	0.085	5.01 ± 0.78	4.78 ± 0.94	0.418	0.26
IMCL: EMCL Ratio	0.92 ± 0.61	0.42 ± 0.29	0.09	1.53 ± 0.99	1.48 ± 0.36	0.52	0.001
Plasma carnitine (mmol/l)	34.8 ± 12.3	46.5 ± 3.97	0.003	37.5 ± 7.5	37.0 ± 4.9	0.83	0.001
Fasting insulin (U/L)	22.5 ± 11.7	18.8 ± 10.1	0.429	18.5 ± 6.7	21.5 ± 18.0	0.71	0.746
HOMA-IR	4.8 ± 2.9	3.8 ± 2.2	0.339	4.2 ± 2.1	4.4 ± 3.3	0.88	0.603
ADIPO-IR	8.52 ± 5.0	8.31 ± 5.7	0.93	9.79 ± 5.3	9.95 ± 4.8	0.81	0.716
Total Cholesterol (mmol/l)	5.21 ± 0.96	5.0 ± 1.0	0.23	4.68 ± 0.95	4.32 ± 0.99	0.13	0.498
Triglycerides (mmol/l)	1.91 ± 0.88	1.72 ± 0.86	0.49	1.70 ± 0.86	1.88 ± 1.24	0.61	0.503
LDL cholesterol (mmol/l)	3.30 ± 0.98	3.01 ± 0.86	0.08	2.76 ± 0.72	2.46 ± 0.78	0.04	0.822
HDL cholesterol (mmol/l)	1.12 ± 0.19	1.11 ± 0.16	0.84	1.15 ± 0.20	1.14 ± 0.20	0.45	0.90
FATP (mM/s)	0.35 ± 0.23	0.84 ± 0.45	0.02	0.36 ± 0.17	0.27 ± 0.20	0.58	0.025

Serum ALT Over Time					
	Group	N	Mean	Std. Deviation	Std. Error Mean
Baseline	Carnitine	9	73.56	33.597	11.199
	Placebo	8	64.38	28.948	10.2
Week 4	Carnitine	9	48.78	23.021	7.674
	Placebo	8	70.63	54.884	19.404
Week 8	Carnitine	9	61.56	37.260	12.420
	Placebo	8	76.38	63.311	22.384
Week 12	Carnitine	9	53.33	26.486	8.829
	Placebo	7	83.43	69.267	26.181
Week 16	Carnitine	9	52.11	26.937	8.979
	Placebo	8	71.38	48.562	17.169
Week 20	Carnitine	9	60.11	29.730	9.910
	Placebo	8	74.50	45.729	16.168
Week 24	Carnitine	9	48.11	19.946	6.649
	Placebo	8	67.25	46.708	16.514

Table 4 ALT by week in L-carnitine versus placebo groups

5.3.7 Substrate Oxidation

Fat Oxidation

No significant differences were observed between L-carnitine and placebo treated groups in whole-body fat oxidation rates (FOX), at each clamp stage, either at baseline or post intervention (**Table 5**).

During the high dose insulin infusion, fat oxidation rates increased by 20.8% in the placebo group, versus 3.2% in the L-carnitine group. A three-way mixed ANOVA was calculated to determine the effects of Group (Carnitine vs Placebo), Visit (baseline vs post-intervention) and clamp stage on FOX.

The three way interaction was not statistically significant, $F(1, 28) = 2.41$, $p = 0.13$, partial $\eta^2 = 0.08$.

All other two way interactions were similarly not significant ($p > 0.05$), indicating that overall no significant change in whole-body FOX was notable over time in either L-carnitine or placebo treated groups compared to baseline values (**Figure 11/1**).

Substrate oxidation data for one participant in the L-carnitine group was excluded from the post-intervention analysis due to grossly outlying values where were not within physiological range.

Fat Oxidation (mg/kg/min)	Group	Pre-Clamp	Low Dose	High Dose
Baseline	L-carnitine	0.94 ± 0.28	0.93 ± 0.16	0.76 ± 0.32
	Placebo	1.20 ± 0.22	1.10 ± 0.20	0.74 ± 0.33
<i>Between Groups Significance (ANOVA)</i>		$p = 0.05$	$p = 0.07$	$p = 0.92$
Post-Intervention	L-carnitine	1.03 ± 0.20	0.998 ± 0.29	0.78 ± 0.44
	Placebo	1.16 ± 0.24	1.19 ± 0.30	0.89 ± 0.32
<i>Between Groups Significance (ANOVA)</i>		$p = 0.28$	$p = 0.221$	$p = 0.59$

Table 5 Whole body fat oxidation rates during three stages of the euglycaemic hyperinsulinaemic clamp (baseline, low dose and high dose infusions) at baseline and post-intervention between L-carnitine and placebo treated groups.

Carbohydrate Oxidation

No significant differences were observed between L-carnitine and placebo treated groups in whole-body carbohydrate oxidation (CHO Ox) at each clamp stage, either at baseline or post intervention. However, while carbohydrate fuel selection was maintained in the L-carnitine group under hyperinsulinaemic conditions, a 19.4% reduction in carbohydrate oxidation was seen in the placebo group during hyperinsulinaemia, implying blunting of insulin mediated glucose uptake and oxidative disposal (**Figure 11/2**). A three way interaction between carbohydrate oxidation, visit and group was assessed using a mixed ANOVA test with application of a Greenhouse Geisser correction (Mauchley's test of sphericity violated, $\chi^2 = 11.4$, $p=0.003$). The three way interaction was not statistically significant, $F(1, 10) = 0.24$, $p = 0.63$, partial $\eta^2 = 0.02$. Within-group comparisons were likewise not significant between baseline and post-intervention (**Table 6**).

CHO Oxidation (mg/kg/min)	Group	Pre-Clamp	Low Dose	High Dose
Baseline	L-carnitine	1.44 ± 0.85	1.38 ± 0.65	1.97 ± 0.76
	Placebo	0.87 ± 0.69	0.96 ± 0.55	2.01 ± 0.97
<i>Between Groups Significance (ANOVA)</i>		$p = 0.15$	$p = 0.17$	$p = 0.91$
Post-Intervention	L-carnitine	1.17 ± 0.37	1.13 ± 0.38	1.97 ± 0.63
	Placebo	0.87 ± 0.64	0.88 ± 0.73	1.60 ± 0.92
<i>Between Groups Significance (ANOVA)</i>		$p = 0.28$	$p = 0.40$	$p = 0.57$

Table 6 Whole body Carbohydrate oxidation rates during three stages of the euglycaemic hyperinsulinaemic clamp (baseline, low dose and high dose infusions) at baseline and post-intervention between L-carnitine and placebo treated groups.

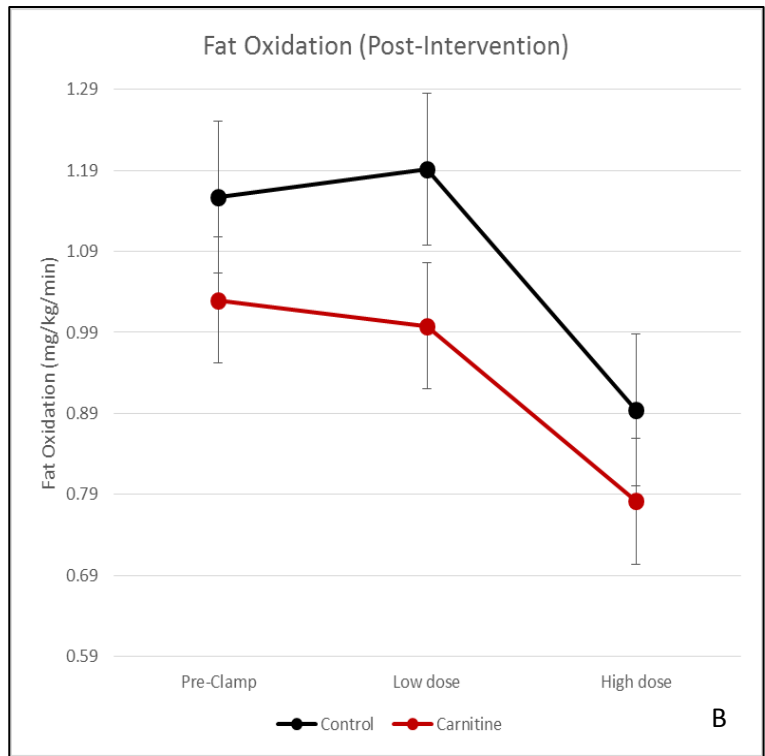
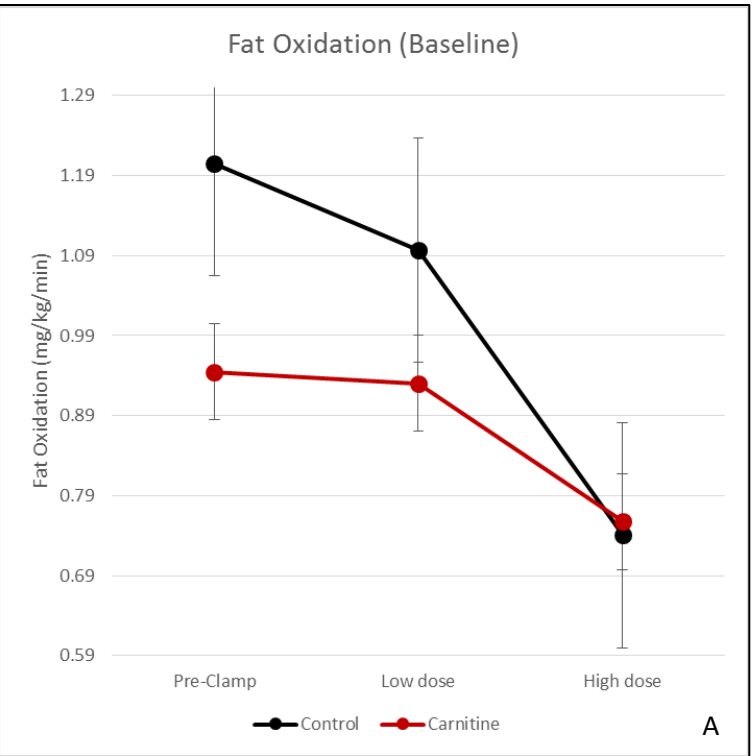


Figure 11/1 Whole body fat oxidation rates in L-carnitine (red line) and placebo (blue line) groups, at baseline (A) and post-intervention (B).

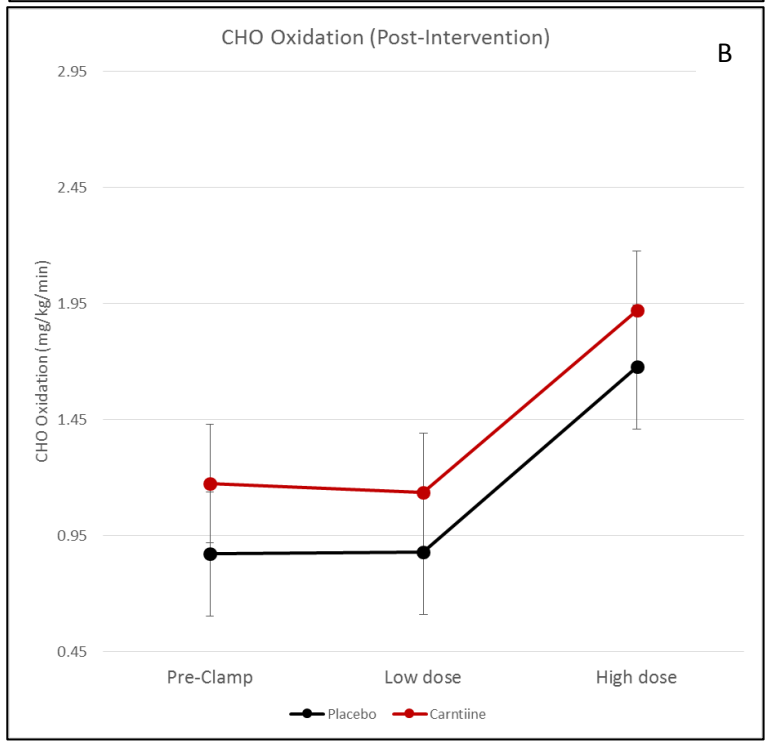
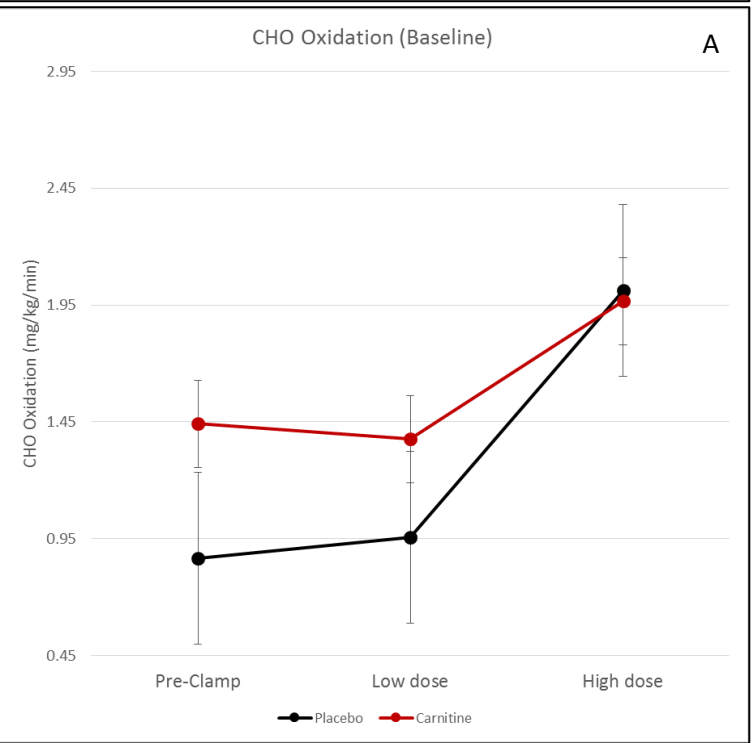


Figure 11/2 Whole body CHO oxidation rates in L-carnitine (red line) and placebo (blue line) groups, at baseline (A) and post-intervention (B).

Respiratory Quotient

There were no significant between-group differences in respiratory quotient when compared to baseline values (**Table 7**). However, a reduction in RQ during high dose hyperinsulinaemia was observed in the placebo group post-intervention, whereas it was maintained in L-carnitine treated participants. This reflects the trends seen in carbohydrate oxidation, with preserved metabolic flexibility in L-carnitine treated patients and reduced metabolic flexibility in placebo-treated patients.

Respiratory Quotient	Group	Pre-Clamp	Low Dose	High Dose
Baseline	Carnitine	0.81 ± 0.06	0.80 ± 0.04	0.85 ± 0.05
	Placebo	0.76 ± 0.05	0.77 ± 0.04	0.85 ± 0.06
<i>Between Groups Significance (ANOVA)</i>		<i>p = 0.09</i>	<i>p = 0.16</i>	<i>p = 0.98</i>
Post-Intervention	Carnitine	0.79 ± 0.03	0.79 ± 0.03	0.85 ± 0.07
	Placebo	0.77 ± 0.05	0.76 ± 0.05	0.82 ± 0.06
<i>Between Groups Significance (ANOVA)</i>		<i>p = 0.31</i>	<i>p = 0.13</i>	<i>p = 0.47</i>
<i>Overall significance (ANCOVA)</i>		<i>P= 0.77</i>	<i>P=0.24</i>	<i>P=0.45</i>

Table 7 Respiratory Quotient during three stages of the euglycaemic hyperinsulinaemic clamp (baseline, low dose and high dose infusions) at baseline and post-intervention between L-carnitine and placebo treated groups.

5.3.8 Hepatic Mitochondrial energetics

Progressive saturation of the γ ATP peak in the phosphorus spectrum was mirrored in the inorganic phosphate peak and the difference between suppressed and unsuppressed values was calculated ('area under the curve' analysis using an in-house Matlab script). Baseline forward rates of ATP synthesis were similar between groups (0.35 ± 0.23 versus 0.36 ± 0.17 mM/s). Both baseline and post-intervention data were normally distributed in each group, as assessed by the Shapiro Wilks' test ($p > 0.05$). ANCOVA was undertaken to establish between-group changes with baseline values as covariates. A significant increase in mean forward rates of ATP synthesis (F_{ATP} , mM/s) was noted in the L-carnitine treated group (0.35 ± 0.23 to 0.85 ± 0.45 Mm/s) versus a reduction in the placebo groups (0.36 ± 0.17 to 0.27 ± 0.32 mM/s), $p = 0.025$ (ANCOVA), **Figure 12**.

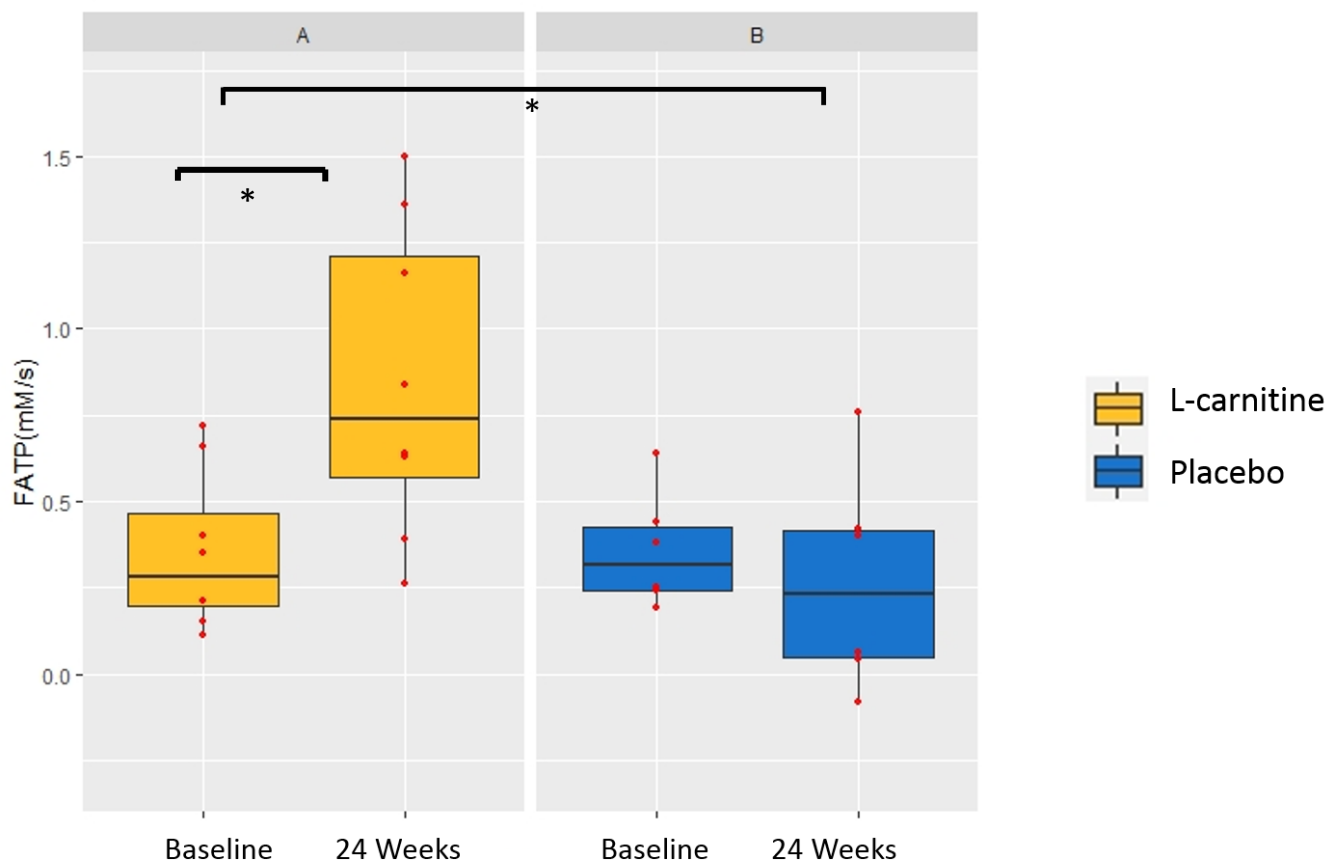


Figure 12 Change in hepatic ATP turnover from baseline in L-carnitine and placebo groups. Individual data points = red dots. Data presented as Median \pm IQR * $P < 0.05$

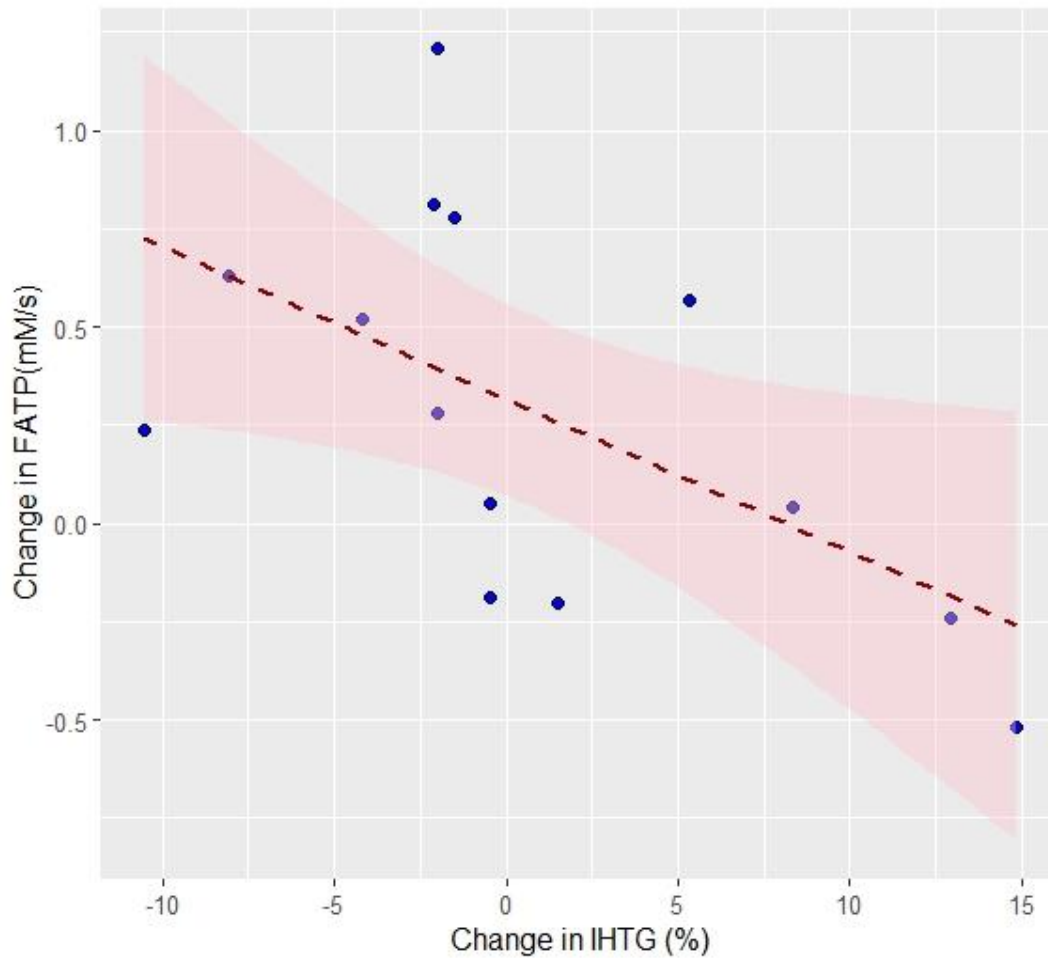


Figure 13 Relationship between change in IHTG (%) and change in forward rates of ATP synthesis (FATP, mM/s). Pearson’s correlation coefficient $r = -0.59$, $p=0.03$.

Differences in IHTG correlated negatively with changes in forward rates of ATP synthesis ($r = -0.59$, $p=0.03$), suggesting that reductions in IHTG are associated with improvements in mitochondrial oxidative phosphorylation (**Figure 13**).

5.3.9 Effect on circulating markers of inflammation

Baseline plasma C-reactive protein (CRP) concentrations were not significantly different between L-carnitine and placebo groups at baseline (3.52 ± 4.91 versus 1.45 ± 1.19 , $p=0.27$). There was likewise no significant impact on CRP post-intervention observed in either L-carnitine (3.52 ± 4.91 to 2.71 ± 3.53 , $p=0.26$), or placebo treated groups (1.45 ± 1.19 to 2.98 ± 2.60 , $p=0.23$) compared to baseline values.

Leg Glucose Uptake

Femoral arteriovenous differences were combined with US Doppler assessments of leg blood flow to calculate leg glucose uptake. At baseline, there were no significant differences in LGU (adjusted per kg leg weight) between L-carnitine and placebo groups either pre-clamp, or during low and high-dose hyperinsulinaemia (**Table 8**). Post-intervention, insulin-mediated LGU increased in both L-carnitine and placebo groups. A paired t-test in the L-carnitine group demonstrated significant improvement in leg glucose uptake/kg compared to baseline values during the high dose clamp ($p=0.02$). Results are shown in **Figure 14**. While insulin-mediated LGU also increased during the high dose clamp in the placebo group, the paired t-test indicated that this increase was not significantly different from baseline LGU ($p=0.22$). Basal LGU in the absence of hyperinsulinaemia ('pre-clamp') improved by over 3.5 fold in the L-carnitine-treated group compared to pre-intervention values ($p=0.04$).

LEG GLUCOSE UPTAKE		Pre-Clamp	Low Dose	High Dose
Baseline	Carnitine	1.21 ± 2.09	1.15 ± 1.32	11.9 ± 10.6
	Placebo	1.85 ± 1.20	3.41 ± 5.1	12.4 ± 10.8
<i>Between Groups Significance (ANOVA)</i>		0.55	0.381	0.937
Post-Intervention	Carnitine	4.35 ± 3.55	3.87 ± 3.67	21.32 ± 15.8
	Placebo	2.65 ± 3.45	3.73 ± 6.61	27.36 ± 17.3
<i>Within-Groups significance) – Carnitine</i>		0.04	0.24	0.02
<i>Within-Groups significance – Placebo</i>		0.52	0.99	0.22
<i>Between Groups Significance (ANOVA)</i>		0.84	0.29	0.11

Table 8. Leg Glucose Uptake in L-carnitine versus Placebo groups at baseline and post-intervention

5.3.10 Adverse events

Three subjects in the L-carnitine group reported mild gastrointestinal side effects, including abdominal bloating, altered bowel habit (diarrhoea) and occasional flatulence. None of these side effects were considered severe enough to unblind or discontinue treatment. Two subjects in the placebo group reported similar side effects (nausea, bloating, flatulence) but none reported altered bowel habit. The side effects noted are well established symptoms associated with high-dose carnitine supplementation.

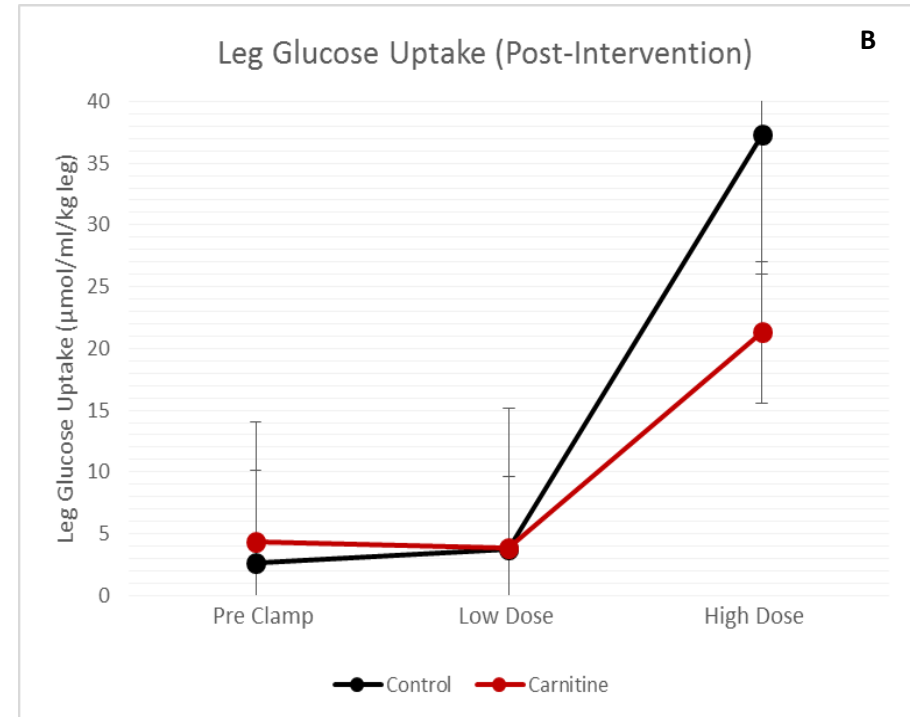
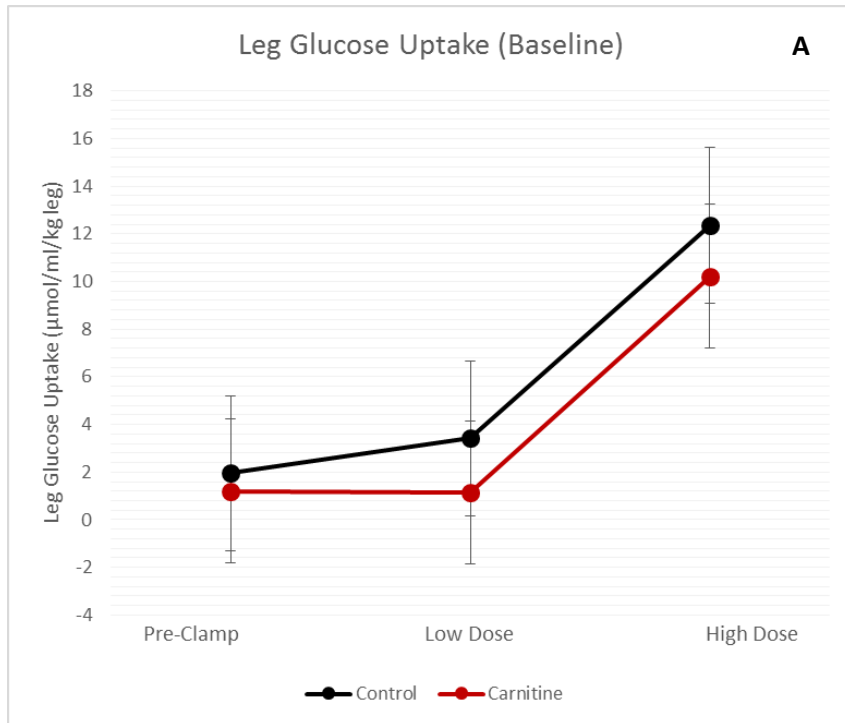


Figure 14. Leg glucose uptake at baseline (panel A) and post-intervention (panel B). L-carnitine group is shown in red lines and the placebo treated group is shown in black lines. Data presented as Mean \pm SEM

5.4 Discussion

5.4.1 Summary of major findings

In this placebo-controlled randomised trial, we found that chronic dietary L-carnitine supplementation was associated with a significant reduction in liver fat and muscle fat fractions, together with increased leg glucose uptake, improved hepatic insulin sensitivity and increased mitochondrial oxidative metabolism in the liver. These effects occurred in the absence of weight loss during an isocaloric diet plan with Slimfast[®] supplementation.

Previous work in this unit has demonstrated that L-carnitine uptake into muscle tissue is an insulin-dependent process [82]. Facilitating L-carnitine entry into muscle therefore requires an insulinogenic stimulus. Slimfast[®] was selected for this study in order to limit carbohydrate load in comparison to other supplements such as Vitargo (Swecarb AB, Stockholm, Sweden) which has previously been used to stimulate carnitine entry into muscle and involves an 80g carbohydrate load twice daily. The macronutrient composition of Slimfast is as follows (per 100g): 15 g Fat, 69 g carbohydrate (38 g sugars), and 8g protein.

While overall weight did not change, we observed a significant increase in liver fat in the placebo-treated group. Regional adiposity, manifested by an increase in truncal fat and waist: hip ratio, was also observed in this group. We hypothesise that this may have influenced an increase in liver fat through enhanced lipolytic flux from increased regional adipose tissue deposition, perhaps due to the carbohydrate load from Slimfast. This glycaemic load in a metabolically challenged population (despite isocaloric dietary restrictions) may also have upregulated *de novo* lipogenesis and exacerbated hepatic steatosis in this population. Indeed, this is supported by the observation that Adipo IR increased in the placebo group by 8% post-intervention.

L-carnitine is a well-characterised regulator of mitochondrial fuel selection. While it is tempting to speculate that a preservation of metabolic flexibility occurred following chronic L-carnitine loading

(with a reduction seen in the placebo group, manifested by reduced suppression of fat oxidation during hyperinsulinaemia and blunted carbohydrate oxidation during hyperinsulinaemic conditions), variance was high and the study was underpowered to detect significant differences in these parameters. Whether the data presented herein reflect the contribution of excess calories in Slimfast® supplementation, with L-carnitine acting to preserve/rescue metabolic flexibility, thereby negating the Slimfast-induced reduction, would require a larger sample size to determine decisively. Positive overall energy balance and regional fat mass accumulation are probably responsible for the deleterious metabolic effects observed in the placebo group in this study, with carnitine able to 'buffer' these effects. A similar phenomenon was observed by Stephens *et al* (2013) when 80g carbohydrate supplementation twice daily resulted in a control group which was 'overfed' carbohydrate with an increase in regional adiposity consequent to a long-term increase in daily energy intake, while in the L-carnitine group these effects were not seen [93]. Taken together, these findings suggest that chronic carnitine loading is capable of offsetting the increased adiposity and deleterious metabolic effects observed with protracted supplementation of a high carbohydrate milkshake by maintaining metabolic flexibility.

The rationale for using Slimfast® in this study was to provide an insulinogenic stimulus with which to increase muscle carnitine uptake. Entry of L-carnitine into muscle tissue is a sodium-dependent process via the novel organic cation transporter-2 (OCTN-2) which has both a low substrate affinity (K_m) and a low maximum rate of reaction (V_{max}) such that increasing circulating carnitine concentrations is insufficient to augment carnitine transport across this receptor. As discussed in **Chapter 1** (section 4), the bioavailability of orally ingested L-carnitine is also low (<20%), which, together with OCTN-2 kinetics being limiting to carnitine transport, may explain why chronic carnitine loading *per se* does not equate to increased muscle carnitine uptake [75].

Increasing sarcolemmal Na^+/K^+ ATPase activity would, in principle, lower intracellular sodium concentration, thereby enhancing the electrochemical gradient to favour Na^+ /carnitine transport into

myocytes. This can be achieved through insulin administration, which, when co-administered with intravenous or oral carnitine, has been shown to augment muscle carnitine content [75, 82]. An insulinogenic stimulus was necessary in this study to determine sites and mechanisms of L-carnitine action in muscle. However, many studies to date have shown that L-carnitine, even in the absence of an insulinogenic beverage, exerts beneficial actions on multiple indices of glucose and lipid metabolism in individuals with the metabolic syndrome and NAFLD patients, as well as reducing liver fat itself [172-176, 196]. We acknowledge the long-term risks of excess carbohydrate administration to an already overweight, insulin-resistant population. Therefore, translating our findings to a broader NAFLD population might require foregoing an exogenous insulinogenic stimulus, maintaining strict calorie intake or incorporating low-intensity exercise to stimulate muscle Na⁺/K⁺ flux in tandem with carnitine supplementation. Whether the hyperinsulinaemia associated with insulin resistance is sufficient in itself to augment carnitine transport via OCTN2, remains unknown.

We did not demonstrate significant alterations in key non-invasive markers of glucose or lipid homeostasis. In particular, no significant differences in fasting plasma glucose, HOMA-IR, NEFA, LDL cholesterol or circulating triglycerides were observed in L-carnitine treated groups. However, a broad trend towards reduction in these parameters was noted in L-carnitine treated participants, with either no change or increases in placebo-treated individuals. Reasons for failure to detect significant L-carnitine induced changes in circulating glucose and lipid indices may be considered to be twofold. First, sample size in this study was underpowered to detect significant differences in these parameters, although substantial reductions have been noticed with L-carnitine treatment in other research trials with larger sample populations [172, 173]. It is also tempting to speculate that the relative 'overfeeding' of carbohydrate in this study masked—at least to some extent—the beneficial properties of L-carnitine in modifying these parameters. This may be evidenced by our observations of actively deleterious effect of the placebo supplementation protocol in such parameters e.g. an increase in circulating insulin and NEFA in placebo-treated patients. Carnitine supplementation is likely to have

'offset' the effect of excess carbohydrate. If given without carbohydrate supplementation, changes in circulating glucose and lipid parameters with L-carnitine treatment *may* have been more pronounced.

In our cross-sectional study, we demonstrated that NAFLD is associated with a significant reduction in basal hepatic mitochondrial oxidative metabolism. Similar findings have been reported in skeletal muscle of individuals with the metabolic syndrome and in the offspring of individuals with T2DM [197]. Decreased lipid oxidation at the level of both liver and muscle results in accumulation of lipotoxic intermediaries, including diacylglycerol. As discussed in **Chapter 1**, these bioactive lipid species interfere directly with insulin signalling, attenuating insulin sensitivity in both organs. Increased hepatic mitochondrial ATP production occurred together with a reduction in liver fat in this study, suggesting that mitochondrial oxidative metabolic rate is directly linked to tissue fat depots, and potentially validates oxidative metabolism as a therapeutic target. A recent study by Fellingner and colleagues (2020) observed a similar association in acromegalic patients versus healthy control volunteers, demonstrating that lower hepatic lipid content in patients with acromegaly was associated with a 50% increase in hepatic mitochondrial ATP synthesis [198].

This link between perturbed hepatic mitochondrial energetics and increased liver fat is explained physiologically by reduced oxidative capacity in the lipotoxic, pro-inflammatory state. The scope for reversal of this trend has, to our knowledge, only been demonstrated in a small pilot study of individuals with NASH (n=3). In this group, a 12-month dietary intervention was associated with reduced hepatic lipid together with augmented hepatic ATP flux in 2 individuals. In the third individual, liver fat was increased, and this was associated with further reductions in hepatic ATP flux [49]. To our knowledge, this is the first study to demonstrate improvement in mitochondrial energy kinetics following intervention in a randomised controlled trial.

Our data demonstrate a significant reduction in intramyocellular: extramyocellular lipid (IMCL: EMCL) ratio, together with increased leg glucose uptake in L-carnitine treated patients. This suggests that L-carnitine exerts its actions at the level of the muscle, increasing local glucose disposal and probably

thereby limiting IHTG accumulation through attenuating DNL. It was beyond the scope of this study to quantitatively evaluate DNL using isotope tracer techniques.

Whether L-carnitine also exerts a local effect at the level of the liver remains unknown. We have demonstrated a significant correlation between reduction in liver fat and improved hepatic mitochondrial energetics (**Figure 13**). This may suggest a direct local effect of L-carnitine on hepatic mitochondrial performance, as has been shown in animal models. Conversely, it may simply reflect reduced hepatic lipid burden, with resultant reduction in free radical formation and improved fluency of mitochondrial oxidative metabolism - it is plausible, for example, that reduced lipid burden would abrogate the need for lipid oxidation to occur through incomplete/inappropriate pathways such as ω -oxidation [199]. With decreased lipid delivery to the liver via reduced FFA flux and/or reduced lipogenic flux from DNL, it is logical that rates of hepatic mitochondrial β -oxidation would be sufficient to secure an oxidative fate for incoming free fatty acids, rather than esterification (i.e. diversion towards storage as triglyceride), to avoid net retention of fat in the liver.

Whether ectopic lipid load drives mitochondrial stress or whether a primary reduction in mitochondrial performance facilitates lipid accumulation and local insulin resistance, remains a controversial 'chicken and egg' question. Mounting evidence (discussed in detail in Chapter 1) points to ectopic lipid deposition as a primary wound in the evolution of systemic insulin resistance. The relationship may well be bidirectional, with ectopic lipid deposition compromising fluency of mitochondrial oxidative metabolism, resulting in oxidative stress via production of free radicals, which then further impinges on mitochondrial structure and/or function, facilitating further lipid accumulation. Thus, the increase in mitochondrial bioenergetic capacity observed in L-carnitine treated patients may occur directly as a result of reduced lipid load.

A growing body of data suggests that L-carnitine, in addition to its primary role in augmenting long-chain fatty acid oxidation, also exerts local antioxidant effects, through scavenging of free radicals such as H_2O_2 [200]. Data in human patients with coronary artery disease suggests that 12 weeks' L-

carnitine supplementation upregulates activity of key antioxidant enzymes such as glutathione peroxidase (GPX), superoxide dismutase (SOD) and catalase (CAT), while downregulating malondialdehyde, a marker of oxidative stress [201]. Whether this has any bearing on mitochondrial oxidative capacity is unknown. If L-carnitine does accumulate locally in liver tissue, it would seem plausible for its local antioxidant effects to contribute to an improvement in mitochondrial performance. Certainly evidence from *in vitro* models with human hepatocyte cell lines points to a scavenging effect of L-carnitine on oxygen free radicals, with attenuated H₂O₂-induced inhibition of GPX and CAT in L-carnitine treated hepatocytes. This occurred in conjunction with an upregulation in peroxisome proliferator receptor alpha (PPAR α) activity [202]. This is important in the context of NASH, a condition typified by oxidative stress.

Koliaki and colleagues (2015) demonstrated an initial adaptive response of hepatic mitochondria to insulin resistance in its early stages (i.e. obesity in the absence of NASH) with augmented mitochondrial respiratory capacity [40]. However, these adaptive mechanisms appeared to become overwhelmed in NASH, with decoupling and loss of antioxidant defences. This data supports pre-clinical *in vivo* and *in vitro* models demonstrating a protective effect of L-carnitine supplementation on conditions typified by oxidative stress (e.g. hepatic encephalopathy) and a carnitine-mediated attenuation in free radical formation in cell lines and enhances antioxidant enzyme production. In a rat model, Hamza et al (2019) recently demonstrated that L-carnitine administration reversed aspartame-induced free radical damage to hepatocytes, and that these effects occurred through a carnitine mediated upregulation in expression of antioxidant enzymes such as CAT and an increase in hepatocyte glutathione [203]. Together, these findings suggest a pleiotropic effect of L-carnitine in modulating the intracellular redox environment, attenuating oxidative stress and promoting antioxidant defence mechanisms.

Based on available evidence to date, we can speculate that the eventual accumulation of IHTG may lead to a mitochondrial 'decompensation' in a lipotoxic, pro-inflammatory milieu driven by oxidative

stress. In facilitating the metabolism of local lipids/reducing delivery of lipid load from muscle, L-carnitine could plausibly attenuate the burden of excess lipid on mitochondrial function, as well as exerting local antioxidant effects through scavenging oxygen free radicals and promoting activity of key antioxidant enzymes.

Further directions for research will include exploiting ultra-high field MRI to map hepatic carnitine non-invasively (to sufficiently resolve trimethylamine resonance on ^1H -MRS) in conjunction with dynamic ^{13}C and ^{31}P MRS to quantitatively evaluate oxidative stress (glutathione activity) and ATP flux in a biopsy-proven NAFLD/NASH cohort. If multinuclear precision imaging techniques can be coupled with labelled tracer/magnetisation transfer experiments, mapping metabolic health in real time becomes a genuine possibility with tangible clinical applications. This could be validated against paired biopsy specimens to establish the impact of interventions on NAFLD/NASH and to map the natural history of the condition, with a view to developing clinically meaningful endpoints non-invasively.

From a mechanistic point of view, mapping hepatic carnitine non-invasively through 7T ^1H MRS, together with deuterated water experiments to track *de novo* lipogenesis, would more precisely enable adjudication of the sites and mechanisms of L-carnitine's beneficial actions in NAFLD and would help to answer the question as to whether this is a purely indirect effect consequent to muscle accretion of L-carnitine, or whether L-carnitine exerts a direct effect on liver metabolism.

While this research has shed mechanistic insight into the liver-muscle axis in NAFLD, further high-quality research is required to localise its site of action and probe multidimensional aspects of L-carnitine action on intracellular fuel metabolism, redox status and energy homeostasis.

5.4.2 Limitations

Much of the data on anthropometric measures and metabolic flexibility, while clearly demonstrating a favourable trend with L-carnitine supplementation, did not reach statistical significance. The study was underpowered to detect significant differences in these parameters and with a greater sample

size leading to reduced variance, it is possible that these changes might have been more readily defined.

While no overall weight change occurred, the deleterious metabolic effects of 'overfeeding' with an insulinogenic beverage were clearly demonstrated in the placebo group. If L-carnitine has potential to become a viable treatment for NAFLD and the metabolic syndrome, further carbohydrate intake would be undesirable for obvious reasons. Whether the hyperinsulinaemia resulting from insulin resistance would be sufficient to facilitate carnitine entry into muscle tissue is unknown and merits further investigation.

The Covid-19 pandemic has limited the scope of this section in terms of analysis and discussion of muscle L-carnitine moieties, muscle glycogen and gene expression arrays. All of these analyses were significantly delayed due to closures in the Medical School and restrictions on laboratory work. Therefore, they could not be included in this thesis.

5.4.3 Controversies

While L-carnitine has become a focus of research interest, its potential clinical applicability has been blighted by controversy due to concerns regarding production of trimethylamine-N-oxide (TMAO), a pro-atherogenic downstream metabolite of choline and carnitine degradation. Potential acceleration of atherosclerosis in an already at-risk population is of clear concern and requires clarity.

Non-absorbed carnitine is metabolised by intestinal microbiota to γ -butyrobetaine and to trimethylamine, which is systemically absorbed and oxidised via the enzyme Flavin mono-oxygenase in the liver to trimethylamine-N-oxide (TMAO), a pro-atherogenic metabolite. Elevated plasma TMAO levels have been linked to incident cardiovascular risk in clinical cohort studies of populations with established cardiovascular and chronic renal disease [204, 205, 206]. In a sophisticated study employing murine models and stable isotope tracer methodology *in vivo*, Koeth and colleagues demonstrated that chronic L-carnitine supplementation in mice induces TMAO production and accelerates

atherosclerosis in a gut-microbiota dependent fashion [207]. In omnivorous humans (n=5), the group demonstrated that labelled d_3 L-carnitine supplementation is associated with increased caecal production of TMAO through inducing specific gut microbiota. Suppression of gut microbial flora with poorly absorbed antibiotics for one week almost completely suppressed this production, strongly supporting the notion that carnitine-mediated TMAO production is an inducible process which is gut-microbiota dependent. Interestingly, L-carnitine supplementation in vegetarians and vegans was not associated with increased TMAO production, suggesting that microbiota induced by specific long-term dietary patterns are likely to be responsible for this conversion. The authors argue that this finding might provide a plausible explanation for the well-established link between red meat ingestion and adverse cardiovascular outcomes.

The central argument i.e. that dietary L-carnitine may contribute to incident cardiovascular risk through elevated TMAO production – has proved contentious, and the magnitude of its importance in the prospective evolution of cardiovascular disease has been questioned. For example, DiNicolantonio et al (2013) published a meta-analysis of 13 placebo-controlled trials involving > 3000 patients with established cardiovascular disease, demonstrating survival benefit and reduced incidence of arrhythmias and angina in carnitine-supplemented populations [180]. Equally, at the time of writing, there exist no published prospective studies evaluating the associations between L-carnitine ingestion, TMAO production and ‘hard’ cardiovascular outcomes in humans. This is important because extrapolating findings from murine models to human physiology is fraught with potential for error. One observation made in a response article [208] was that the plasma TMAO level reached in L-carnitine fed mice was several times higher (150 mM) than plasma TMAO in the top quartile of patients in epidemiological studies (6.18 mM). This is likely to be reflective of the fact that mice in this study were fed water containing 1.3% carnitine - the equivalent ingestion for humans would be 26 g of L-carnitine/day (an order of magnitude above daily recommended doses of 2-4g/day). Finally, decades of robust epidemiological data have demonstrated that regular consumption of fish – which contain large quantities of TMAO [209] - confers cardiovascular protection [210, 211].

Taken together, existing literature paints a picture of uncertainty regarding the risks versus benefits of dietary L-carnitine supplementation on cardiovascular health. While no robust evidence yet links L-carnitine supplementation to poor cardiovascular outcomes in healthy humans, it is necessary to recognise that individuals with NAFLD represent a higher risk population in terms of cardiovascular outcomes, and may be more vulnerable to adverse effects of TMAO production.

In this study, we quantified plasma TMAO following 6 months of L-carnitine supplementation. Plasma samples were isolated from whole blood for analysis of TMAO concentrations at baseline and post-intervention in our NAFLD cohort. This analysis (to be conducted at the University of Edinburgh) has been significantly delayed due to Covid-19 restrictions, precluding its inclusion in this thesis.

5.5 Conclusion

Carnitine is capable of manipulating whole-body fuel selection and abrogating specific aspects of metabolic 'remodelling' key to the propagation of insulin resistance and its associations. We have demonstrated that L-carnitine supplementation protects against some of the deleterious metabolic consequences of chronic energy surplus. L-carnitine loading is associated with reduced liver fat and improved hepatic mitochondrial energy kinetics, possibly mediated indirectly through its properties in muscle, reducing carbohydrate load to the liver and thereby limiting DNL. Whether L-carnitine exerts directly beneficial properties on liver fuel metabolism itself is unclear and merits probing in future studies by leveraging precision imaging, liver biopsy and detailed metabolic experiments, possibly evaluating hepatic fuel selection *in vivo* by sampling hepatic arterial, portal venous and hepatic venous blood for O₂ and CO₂ under postabsorptive conditions as well as under various experimental conditions involving carbohydrate or fat loading [212]. Measurement of O₂ consumption and CO₂ production via indirect calorimetry is not feasible when evaluating splanchnic net fuel consumption, as indirect calorimetric equations assume either complete oxidation or storage of macronutrients. Splanchnic metabolism does not conform to these simplistic assumptions, as partial

conversion of lipids to ketone bodies, glucose to lipids, glycerol to glucose etc are common features of this unique metabolic circuit.

This could feasibly be achieved through exploiting multinuclear MR Spectroscopy at ultra-high field strengths (e.g. 7T) to adequately resolve the trimethylamine resonance in the ^1H spectrum and thereby quantitatively evaluate hepatic free carnitine content, together with ATP flux data with ^{31}P MRS and incorporation of ^{13}C MRS techniques to map glucose homeostasis (e.g. glycogenolysis and gluconeogenesis) as well as oxidative stress through ^{13}C enrichment of substrates to quantitatively evaluate glutathione metabolism in the liver. In conjunction with endoscopic ultrasound (EUS)-guided sampling of hepatic venous and portal venous blood with subsequent blood gas analysis, these techniques would provide unprecedented insight into liver fuel selection, metabolism and the contribution of L-carnitine (if any) directly to this balance.

Chapter 6

Applications of non-proton MR Spectroscopy in NAFLD and Quantitative Assessment of Hepatic Energy Kinetics

6.1 Introduction

“The whole history of science has been the gradual realisation that events do not happen in an arbitrary manner, but that they reflect a certain underlying order, which may or may not be divinely inspired.”

– Stephen Hawking, *A Brief History of Time* (1988)

Metabolic imaging utilising MRI and MR spectroscopy provides a robust, accurate, non-invasive tool with which to probe human physiology *in vivo* [213]. While MRI provides anatomical and spatial information about the distribution of protons in water and lipid within a tissue of interest, MR spectroscopy enables quantification of tissue metabolite concentrations by mapping nuclei within an MR-visible spectrum. The advent of multinuclear technology, together with ultra-high field strength magnets, has enhanced the versatility and clinical applicability of MRS, offering a unique window for the study of phosphorus (^{31}P) and carbon (^{13}C) metabolites in addition to ‘traditional’ proton (^1H) based molecules [214]. As well as quantification of static metabolite concentrations for tissue characterisation in different disease states, functional MR spectroscopy has evolved in recent decades to incorporate techniques which allow quantitative assessment of dynamic metabolic fluxes. This ability to directly measure dynamic activity *in vivo* at the metabolic level has numerous applications in the liver [215].

Of particular relevance in NAFLD is the need for mechanistic insight into cellular pathological milestones such as oxidative stress and mitochondrial dysfunction. MRS is well suited to this endeavour, as ^{31}P and ^{13}C metabolites, as well as their fluxes, can be directly measured in the liver at rest. Not only does this enable resting characterisation of key biochemical pathways, but it may also be tracked in response to interventions such as exercise, bespoke diets or pharmacotherapy. To map metabolic fluxes, labelled tracers are used or specific magnetisation transfer (MT) techniques are added to the basal spectral acquisition. Fluxes of interest in NAFLD include tricarboxylic acid (TCA) cycle kinetics, hepatic ATP turnover (i.e. Flux through the ATP synthesis/hydrolysis cycle), which

provides a measure of mitochondrial oxidative capacity), and flux across the glutathione synthase pathway, involving ^{13}C MRS with labelled tracers to map oxidative stress.

6.1.1 Principles of MR Spectroscopy

The basic physical principles underpinning MRI and MRS technologies are identical and have been discussed in Chapter 2. Differences in output and scope are highlighted in **Table 1**.

Different biochemical signatures in healthy versus diseased tissue can help to identify and localise disease at an early stage in its natural history. This has been used to good effect in, for example, brain tumours, which display markedly lower concentrations of N-acetyl aspartate and higher concentrations of choline compared to healthy brain tissue [216]. While MRI is primarily concerned with building images from bulk signals of hydrogen nuclei (protons) in water and fat, MRS often focuses on the chemical composition of other metabolites, and employs techniques to suppress abundant water and fat signals to quantify these other metabolites, present in millimolar concentrations.

	MRI	MRS
Principle Output	Anatomic	Metabolic
Radiofrequency Signal	Spatial position of nuclei	Chemical composition of tissue
Voxels	Thousands	One (Single voxel spectroscopy) or multiple (chemical shift imaging)
Nuclei of interest	^1H signals from fat and water	^1H , ^{13}C , ^{31}P , ^{23}Na , ^{19}F
Data Acquisition	Images	Line Spectra

Table 1. Differences between MRI and MRS

6.1.2 Applications of MRS in Metabolic Liver Disease

Table 2 summarises the metabolic processes which constitute key milestones in NAFLD progression. Multinuclear MR spectroscopy offers an exciting and novel window into the metabolism of hydrogen, carbon and phosphorus-based compounds. This enables researchers to probe multiple dimensions of metabolic liver disease contemporaneously, including lipotoxicity, oxidative stress, β -oxidation, cell membrane integrity and bioenergetics. **Figure 1** summarises the metabolites and cellular processes potentially quantifiable by MRS.

Pathogenic Pathway	Biological Process	Precision Imaging Endpoints	Other Endpoints
Metabolic Inflexibility	Insulin Resistance	¹³ C MRS (↓ Glycogen synthesis)	Dual Step Euglycaemic Hyperinsulinaemic Clamp Oral glucose tolerance test Wet biomarkers: Adiponectin, HbA1c, HOMA-IR
	Liver fat Quantity (%)	MRI-PDFF, ¹ H MRS	TE with CAP, USS
	Liver fat Quality	¹ H MRS	
Inflammation	Oxidative Stress	¹³ C MRS (glutathione flux)	
	Impaired Energy Kinetics	³¹ P MRS (ATP flux) ¹³ C MRS (TCA cycle flux and beta-oxidation)	
	Steatohepatitis		Risk Prediction Tools: OxNASH, NASH resolution score Wet biomarkers: ALT
Collagen deposition	Fibrosis burden	Magnetic Resonance Elastography (MRE)	Wet biomarkers: ELF, ProC3
		³¹ P MRS (PME/PDE ratios)	Risk prediction tools: FIB-4, NAFLD Fibrosis Score

Table 2 Pathological milestones in the natural history of NAFLD together with potential invasive and non-invasive endpoints for their quantification

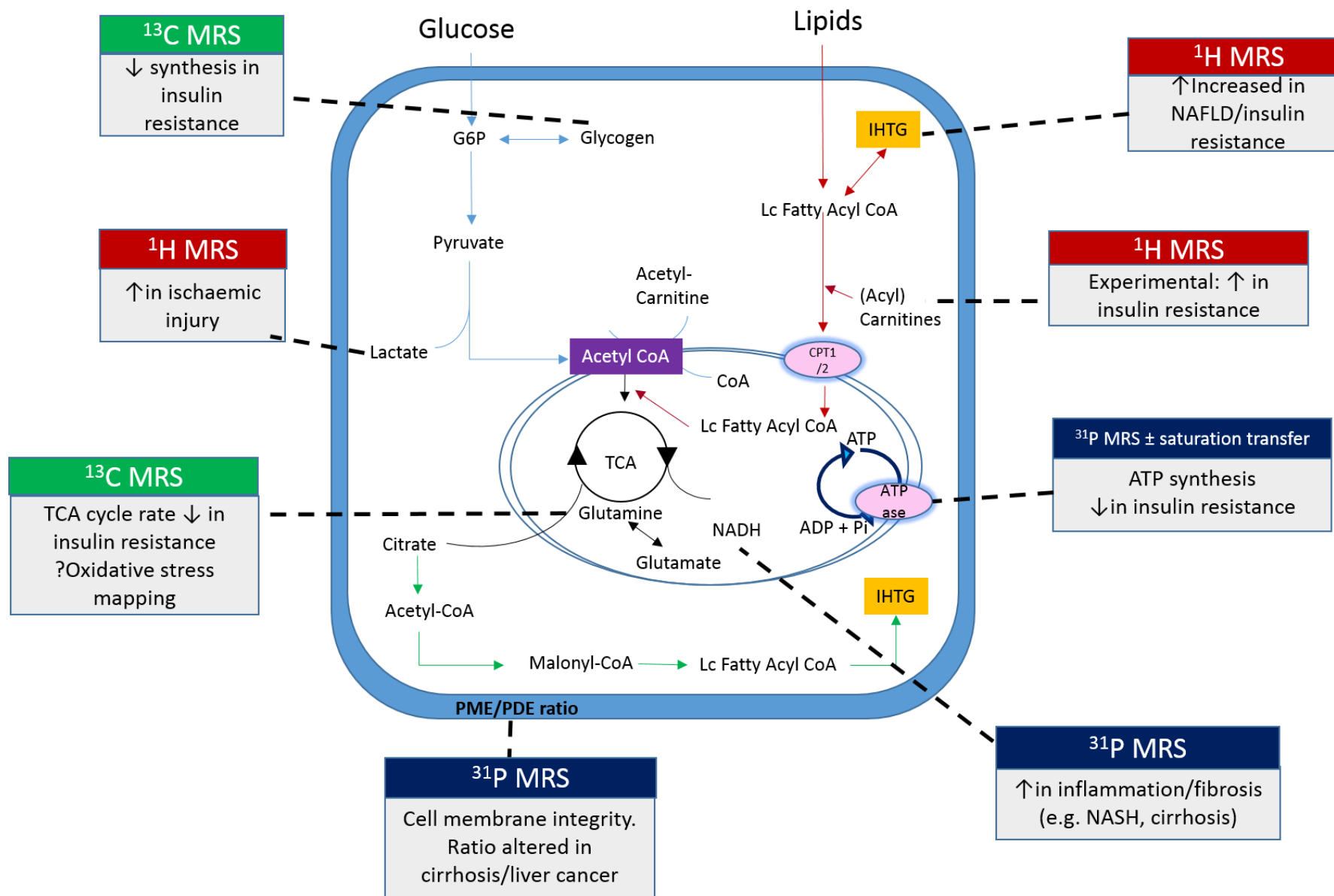


Figure 1 Range of metabolites and reaction kinetics potentially quantifiable using multinuclear MR Spectroscopy. Adapted from Valkovic et al (2018) Multinuclear MRS in skeletal muscle.

TCA = tricarboxylic acid, IHTG = intrahepatic triglyceride, CPT = carnitine palmitoyl transferase, Lc = Long chain, G6P = glucose 6 phosphate, ADP = adenosine diphosphate, ATP = adenosine triphosphate, Pi = inorganic phosphate, NADH = nicotinamide adenine dinucleotide + hydrogen, ATPase = ATP synthase enzyme.

6.1.3 ^{13}C MR Spectroscopy

The liver acts as an intermediary hub for both lipid and glucose metabolism. ^{13}C MR Spectroscopy adds enormous value in the interrogation of metabolic liver disease, enabling net glycogen synthesis, glycogenolysis and gluconeogenesis to be quantified, both at baseline and in response to various stimuli such as dietary and exercise interventions [217].

Spectral resolution of carbon nuclei in the liver is hindered by low natural abundance of the ^{13}C isotope, which alone is MR visible (1.1% of total carbon, the rest being ^{12}C which is not MR visible) [218]. In addition, the gyromagnetic ratio of ^{13}C is approximately $\frac{1}{4}$ that of ^1H , which reduces its signal to noise ratio compared to the latter. Methods commonly employed to address this low signal include long acquisition times for multiple averages and large regions of interest. The advantage of lower sensitivity is that ^{13}C labelled tracers (e.g. acetate or glycine) can be exploited as a powerful tool to determine various facets of metabolism, from tricarboxylic acid (TCA) cycle activity to cellular redox kinetics. These are usually administered via infusion in studies involving brain or musculoskeletal metabolism, whereas tracer ingestion provides a powerful non-invasive method to probe hepatic metabolism due to its rapid first pass absorption into the liver.

This technique relies on the principle that increases in ^{13}C signals following administration of enriched substrate reflect incorporation of that substrate into the metabolic pathway of interest [219]. An example schematic of isotopic enrichment of ^{13}C nuclei with incorporation of labelled [1, ^{13}C] acetate substrate into intermediates in the TCA cycle is shown in **Figure 2**. The rate of signal increase on ^{13}C MRS then reflects rate of TCA cycle flux, which can be mathematically modelled in both healthy and metabolically challenged phenotypes.

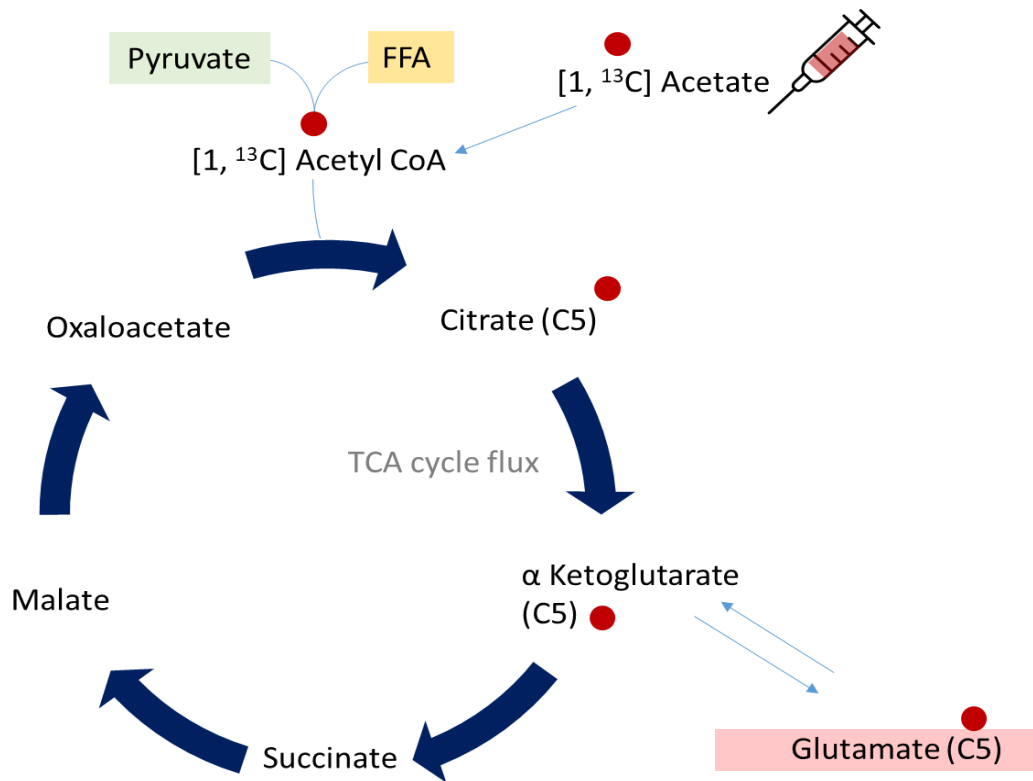


Figure 2 Schematic diagram demonstrating the fate of infused ^{13}C labelled acetate upon incorporation into hepatic metabolism. Following degradation to ^{13}C Acetyl CoA, fractional enrichment of hepatic ^{13}C glutamate (with the ^{13}C nucleus at the C_5 position) is measurable on the MR visible spectrum, enabling calculation of TCA cycle flux. Note other sources of mitochondrial acetyl CoA include pyruvate (from glycolysis) and free fatty acids.

6.1.4 Mitochondrial Oxidative Metabolism

Dysregulated hepatic oxidative metabolism lies is an important component of NAFLD pathogenesis. Disturbed mitochondrial structure, function, or both leads to impaired energy production, oxidative stress and release of reactive oxygen species (ROS), inflicting a pro-inflammatory milieu at the level of the liver. Although MRI and mass spectrometry techniques are well established, these provide limited information regarding mitochondrial metabolism in NAFLD as they measure static metabolite

concentrations. Metabolite kinetics, measurable by capturing flux rates through key enzymatic pathways, yield deeper mechanistic insight into NAFLD pathogenesis. MRS is ideally suited to this endeavour, as repeated perturbations in metabolite kinetics following intervention can be quantitated at serial time points. Using this framework, strategies have been developed to directly determine rates of hepatic mitochondrial oxidation as well as oxidative stress reactions noninvasively.

Befroy and colleagues recently developed a novel MRS-based protocol to quantify hepatic mitochondrial oxidative metabolism utilising localised in vivo ^{13}C -MRS. In this strategy, intravenous ^{13}C -labelled acetate (a stable isotope tracer) was administered to healthy volunteers to become incorporated, via its intermediate ^{13}C -acetyl-CoA, into the TCA cycle in the liver. The rate of ^{13}C enrichment of hepatic glutamate (its principal metabolite) can then be tracked as glutamate is MR-visible in ^{13}C -spectra at the C1 and C5 positions in the liver [220]. Modelling flux through the TCA cycle is valuable, as it forms the final common pathway for both carbohydrate and lipid metabolism.

A subsequent study incorporating this method in patients with NAFLD concluded, surprisingly, that rates of pyruvate cycling and mitochondrial oxidative metabolism were not diminished in subjects with NAFL (as defined by IHTG >4%) compared with control populations [39]. In this study, Petersen and colleagues utilised rate of ^{13}C enrichment of hepatic glutamate to measure mitochondrial oxidation flux and ^{13}C enrichment of hepatic alanine as an index of pyruvate cycling. However, the study specifically selected individuals without insulin resistance, who had simple steatosis on MRS but no evidence of NASH or fibrosis. Further studies in NASH populations are needed to determine whether mitochondrial pyruvate cycling and TCA activity are compromised in NASH, and thus to determine whether measuring hepatic oxidative metabolism could serve as an accurate imaging biomarker to discriminate NAFL from NASH.

6.1.5 Oxidative Stress

Oxidative stress – occurring mainly in the context of dysregulated mitochondrial metabolism - is another dynamic metabolic process which may be probed non-invasively using ^{13}C MRS labelling strategies. The ability of hepatocytes to maintain a reduced intracellular environment protects against oxidative stress and the associated onslaught of necroinflammation and fibrogenesis which underpin NAFLD progression. The prevailing endogenous hepatic antioxidant is glutathione, a tripeptide synthesised from glycine, glutamate and cysteine. Decreased glutathione synthesis is associated with impaired hepatocellular redox defences, leaving liver tissue vulnerable to free radical-induced damage. Glutathione turnover has thus been the focus of recent attention as a potentially useful biomarker for monitoring hepatic oxidative stress in NAFLD. By extension, the ability to track glutathione flux *in vivo* could yield a clinically useful quantitative biomarker for distinguishing the transition between simple steatosis (NAFL) and non-alcoholic steatohepatitis (NASH).

Skamarauskas et al (2014) developed a dynamic ^{13}C -MRS labelling strategy to measure flux through glutathione (GSH) synthesis pathways *in vivo* [221]. This approach was demonstrated in human volunteers in addition to rodent models of acute and chronic of oxidative stress. Briefly, ^{13}C -labelled glycine was administered via infusion in Sprague Dawley rats to measure hepatic glutathione flux in response to acute (CCl_4 induced injury) and chronic (high fat, high carbohydrate diet for 8 weeks) oxidative insults. Associated perturbations in glutathione metabolism were measured in a 7T MR scanner. In acute CCl_4 -induced oxidative stress, preclinical studies demonstrated a 54% elevation of GSH content and a 31% increase in GSH synthesis (as measured by ^{13}C label incorporation of hepatic glutathione), after 12 hours, indicating adaptive upregulation of glutathione utilisation in response to acute oxidative stress.

Conversely, the chronic model of oxidative stress revealed glutathione depletion in an early NASH phenotype after 8 weeks of a high-fat high carbohydrate feeding. This novel experimental approach

was successfully translated in human volunteers, with oral ingestion of ^{13}C labelled glycine detectable on ^{13}C MRS at 2, 4, 6 and 8 hours post-ingestion. Exciting clinical applications include a non-invasive approach for direct quantification of hepatic glutathione fluxes in response to intervention and use of such measures as a biomarker for NAFLD staging. Indeed, pharmacological therapies which increase glutathione synthesis in NAFLD may provide a therapeutic target with which to attenuate development of steatohepatitis.

6.1.6 ^{31}P MRS and ATP Kinetics

While capturing hepatic mitochondrial metabolism non-invasively is possible using labelled ^{13}C -MRS strategies, the utility of localised ^{31}P MRS in quantitating hepatic ATP production has gained traction in recent years as the phosphorus isotope is present in high natural abundance. ^{31}P MRS enables quantification of inorganic phosphorus compounds within the liver in a specified hepatic volume of interest (**Figure 3**). Hepatic ATP and inorganic phosphate (Pi) levels are also detectable and their absolute and relative quantification can provide insight into hepatic energy metabolism. This is of particular relevance in NAFLD, as progressive depletion in hepatic ATP stores are observed in individuals with features of the metabolic syndrome, including obesity and type 2 diabetes, reflecting impaired energy homeostasis associated with insulin resistance [222]. Thus, non-invasive monitoring of hepatic ATP stores could serve as a quantitative imaging biomarker for NAFLD and NASH.

Differential rates of activity across the hepatic ATP synthase pathway have recently been demonstrated in NAFLD versus NASH [49], potentially paving the way for a non-invasive tool with which to differentiate patients at risk of progressive disease from those with simple steatosis (NAFL). While hepatic oxidative metabolism has been reported to adaptively increase during IHTG accumulation, robust evidence points to a 'tipping point' at which these adaptive mechanisms become ultimately 'maladaptive' and lead to a decline in mitochondrial oxidative metabolism [40].

Leveraging both ^{13}C and ^{31}P techniques in combination to map glutathione turnover and ATP flux may offer exciting mechanistic insights into NASH progression as well as the yielding novel, metabolically relevant endpoints in NASH trials.

6.1.7 Magnetisation transfer

Precision imaging confers several advantages over liver biopsy, one of which is the ability to capture and quantitate dynamic metabolic fluxes within tissues. With the saturation transfer technique, real-time ATP kinetics can be mathematically modelled utilising a pseudo-first order differential equation together with a rate constant, to calculate forward rates of ATP synthesis catalysed by the enzyme ATP synthase through the following reaction:



For musculoskeletal ATP flux calculation, exchange with Phosphocreatine (PCr) is also factored in. The principle behind magnetisation transfer involves selective irradiation of one of the metabolites participating in the chemical exchange reaction, to alter its magnetisation from the equilibrium state (M_0) to steady state (M_z) and observing the fractional reduction effect on its exchange partner. In the context of hepatic energy kinetics, the γATP resonance ($\sim 2.5\text{ppm}$) is selectively saturated to perturb its magnetisation from equilibrium, and the corresponding reduction in the Pi peak (due to flux through the synthesis/hydrolysis cycle) is quantitatively determined. This fractional reduction in the Pi peak from M_0 to steady state (M_z) equals the forward rate constant (k) adjusted for the apparent longitudinal relaxation time ($T_{1\text{app}}$) of Pi as follows:

$$k = \left(1 - \frac{M_z}{M_0}\right) / T_1^{\text{app}}$$

First, T_1^{app} is calculated using either an inversion recovery technique [223] or progressive saturation [148] where $\gamma\text{-ATP}$ saturation pulses of varying length (t_{ir}) are applied and the reduction in Pi signal is related to apparent T1 (T_1^{app}) as follows:

$$M(t_{ir})/M_0 = 1 - kT_1^{app} \cdot \exp(-t_{ir}/T_1^{app})$$

The change in Pi signal with increasing saturation time can be fitted using least-squares fitting to determine T_{1app} .

Once obtained, two further spectra with increased SNR (more signal averaging and longer acquisition times) are used to accurately determine the forward rate constant, k . Firstly, M_z is measured by fully saturating the γ ATP resonance and measuring the subsequent Pi signal. Due to difficulties in specifically targeting γ ATP saturation, it is possible that other signals close to its resonance also experience a small degree of saturation. As such, M_0 is next obtained by applying a saturation pulse that mirrors the γ ATP about the Pi resonance and again measuring the Pi signal.

In an ideal setting the γ ATP signal is fully saturated, but in experimental application it is often the case that some residual γ ATP signal remains, introducing a potential for error in the final value. This is especially important when experiments are conducted at lower field strengths (3T) where spectral resolution is compromised. To correct for this, Valkovic et al (2017) proposed the following equation, in which M_{0ATP} is magnetisation of the γ ATP resonance during the control experiment and M_{zATP} is its magnetisation at steady state saturation [223].

$$k = \left(1 - \frac{M_z}{M_0}\right) [M_{0ATP}/(M_{0ATP} - M_{zATP})] / T_1^{app}$$

From this equation, k is derived. Finally, the forward rate of metabolic flux is the product of k and the concentration of Pi, such that:

$$F = k \times Pi$$

The saturation transfer experiment is cumbersome and lengthy, requiring a scanning time of up to 2 hours in a 3T scanner. This is due to the requirement for extensive signal averaging to achieve the required signal to noise ratio (SNR). Under 7T conditions, saturation transfer experiments for

derivation of hepatic ATP flux have been reported *in vivo*, with a scanning time of close to 20 minutes (due to superior SNR), which is more clinically applicable [226].

$$M_{Pi}(t_{sat}) = M_{Pi}^0 \left[\left(\frac{k_2}{R_{Pi}^{app}} \right) \exp(-R_{Pi}^{app} t_{sat}) + 1/(R_{Pi}^{app} T_{1,Pi}^{int}) \right]$$

We applied the saturation transfer technique with ^{31}P MRS to study differences in ATP turnover between NAFLD subjects and healthy volunteers. We further conducted longitudinal analyses of ATP flux in our NAFLD cohort following 24 weeks' L-carnitine supplementation to determine whether this exploratory endpoint carries relevance in the clinical domain.

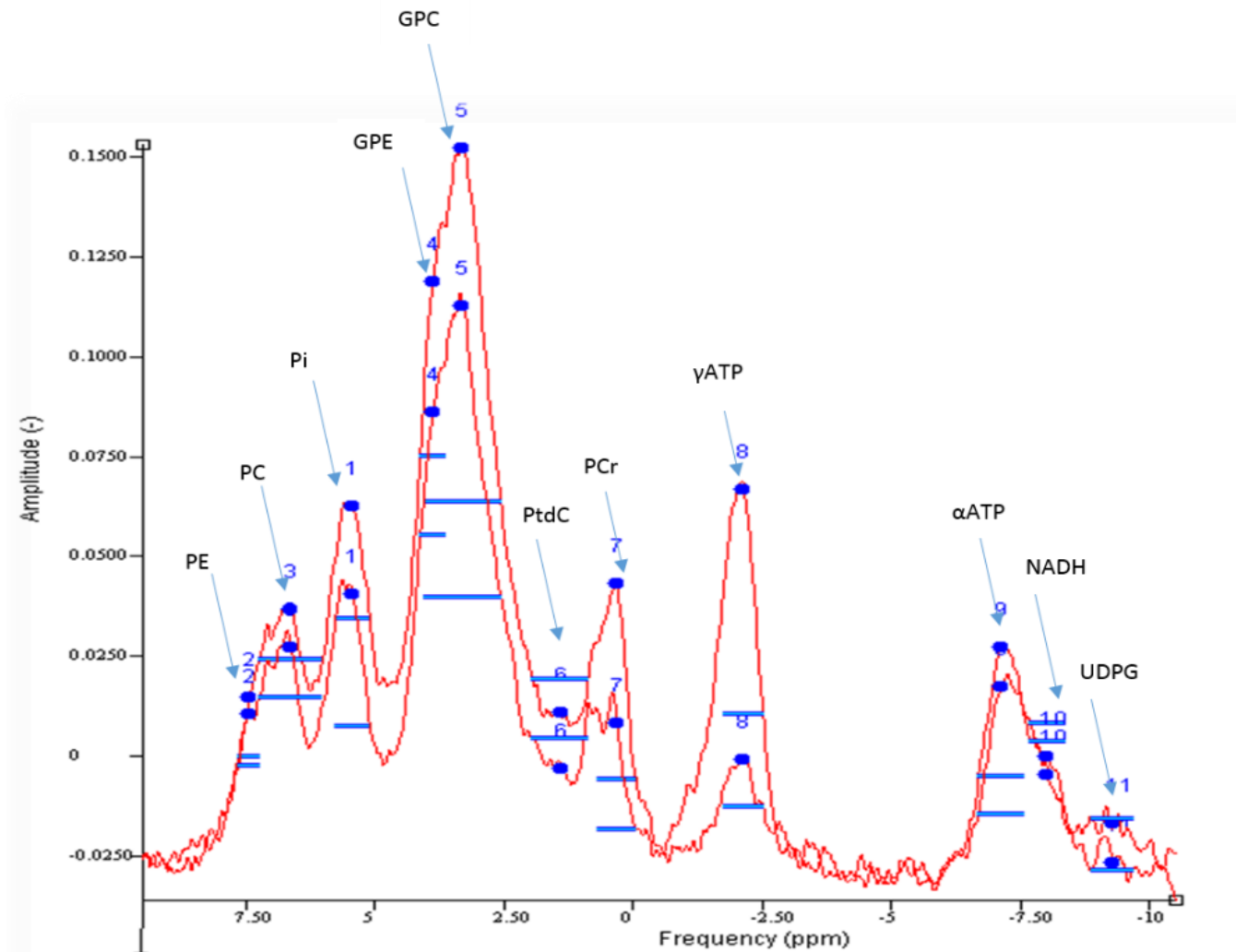


Figure 3 Example ^{31}P MR Spectrum acquired from the liver at 3T. Good spectral resolution enables quantification of phosphorus metabolites including adenosine triphosphate (ATP), phosphomonoesters (phosphocholine, PC and phosphoethanolamine, PE), phosphodiester (glycerophosphocholine, GPC and glycerophosphoethanolamine, GPE), nicotinamide adenine dinucleotide (NADH), uridine diphosphate glucose (UDPG) and phosphatidylcholine (PtdC).

6.2 Methods

Subjects were studied using a 3T Phillips Achieva system, with a dedicated single loop ^{31}P surface coil positioned for signal transmission and reception. Participants were scanned supine, with the surface coil positioned over the right lobe of the liver. Prior to each experiment, a ^1H image localizer was acquired and the ^{31}P surface coil was tuned before spectral acquisition. Higher order pencil beam shimming was applied to increase field homogeneity.

A 60 mm localisation slab was selected and positioned parallel to the surface coil in order to minimise contamination signals from subcutaneous tissue and in particular muscle tissue. Slab-selective localisation (i.e. 1-dimensional image-selected in vivo spectroscopy, 1D-ISIS) is suited to spectral acquisition from liver tissue, as 3D ISIS localisation techniques are vulnerable to signal artefact from respiratory triggered motion. Further, the 1D technique is ideally suited to the homogeneity of liver tissue and diffuse nature of diseases such as NAFLD. The slab is localised in one dimension by the applied pulse sequence, and sensitive volume of the coil is used for localisation in the other two dimensions. The resultant volume of tissue examined was 65 x 65 x 60 mm (**Figure 4**).

We performed a saturation transfer experiment using a 450 μs block pulse localised in one dimension for excitation. Spectra were then acquired with application of a continuous, low power, frequency selective saturation pulse to the γATP resonance in the phosphorus spectrum (position -2.5 ppm) and another mirrored around the Pi peak (+14 ppm). Five hundred averages were performed with a repetition time of 3 seconds. Spectral acquisition took place in the equilibrium state (M_0) –that is, with no saturation at γATP peak - and a further 4 spectra were acquired with progressive saturation of the ATP resonance, with the final spectra acquired at full saturation (M_z). The apparent longitudinal relaxation time ($T_{1\text{app}}$) was calculated using a progressive saturation sequence (rather than inversion recovery) during continuous saturation of the ATP peak. The Pi signal at full saturation (M_z) of the γATP peak was compared with the Pi signal in the equilibrium state (M_0), in which the saturation

frequency is mirrored around the Pi resonance. From this, the forward exchange rate constant (k) was calculated as follows:

$$k = 1/T1app(1 - M_z/M_0)$$

The forward rate of ATP synthesis was then determined by multiplying k by the concentration of Pi.

For each experiment (M_0 and M_z) approximately 2000 spectra were acquired and averaged.

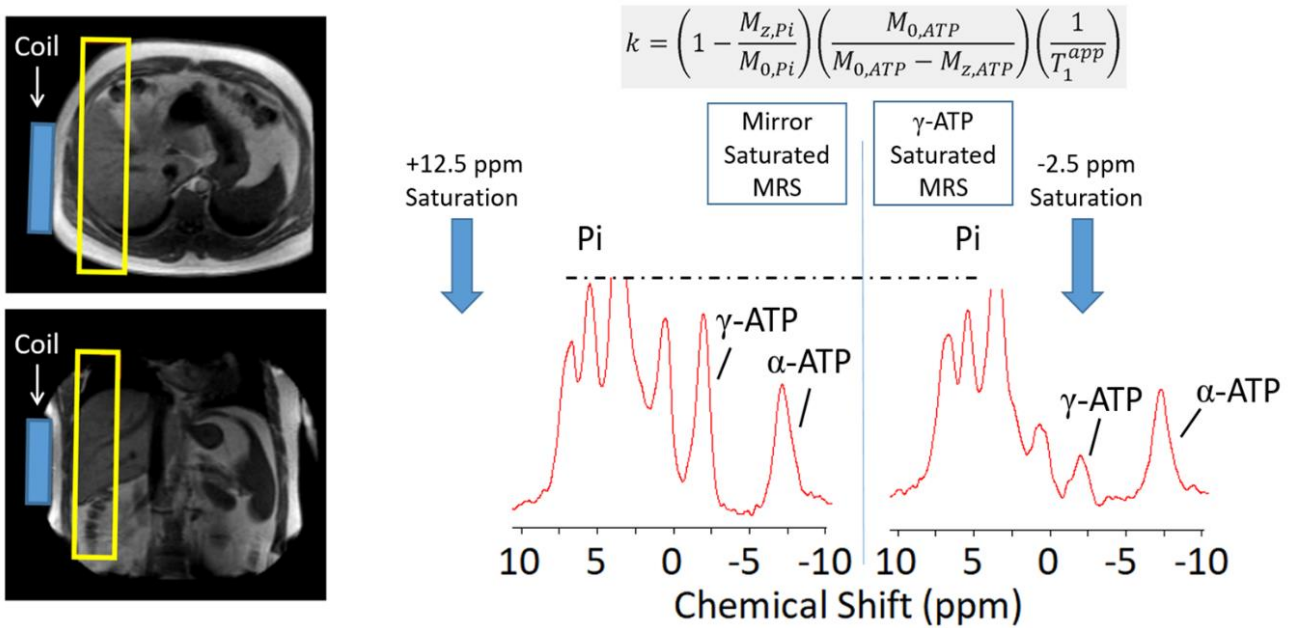


Figure 4 Axial and coronal scout imaging with slab-selective localisation for ^{31}P MRS with saturation transfer experiment. Progressive saturation of the γATP resonance was applied with corresponding saturation of the inorganic phosphate (Pi) peak

6.2.1 Post Processing

Spectra were processed using an in-house Matlab package (**Figure 5**). After Lorentzian line broadening (10 Hz) and phase correction, the baseline was fitted using regions of no signal and subtracted from the final spectra (to account for macromolecular effects). The γATP and Pi peaks were then fitted to a Gaussian peak model using Matlab's least square fitting algorithm.

AMARES (advanced method for accurate, robust and efficient spectral fitting of MRS data with use of prior knowledge) time domain fit algorithms were also used to quantify other metabolite signals. The basis set consisted of a simplified composition – the three ATP resonances, one NADPH, Pi, uridine diphosphoglucose (UDPG) and two phosphomonoester (PME) and phosphodiester (PDE) resonances. Prior knowledge was applied as: Gaussian shape; fixed relative phases in the negative and positive spectral region, respectively; soft constraints on the expected resonance frequency; equal linewidths of both PDE and PME signals; NADPH and UDPG, which again were constrained additively to the linewidth of α ATP.

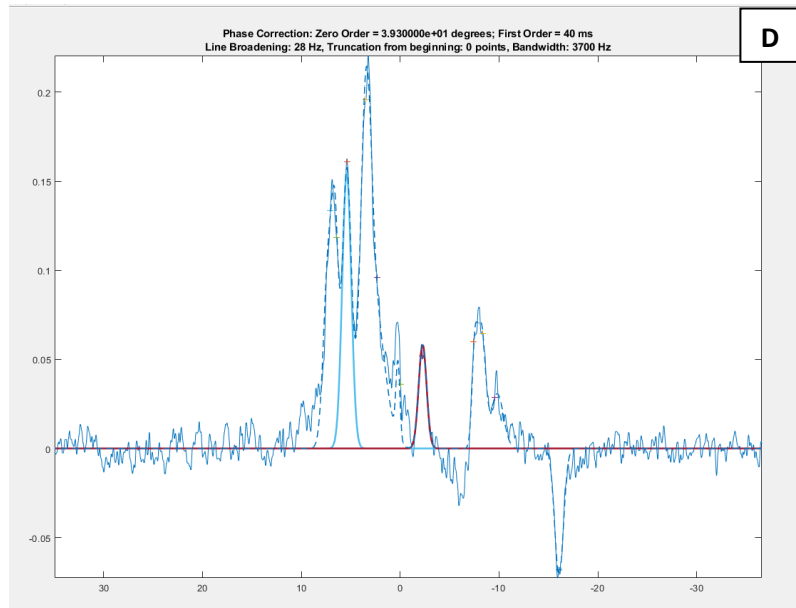
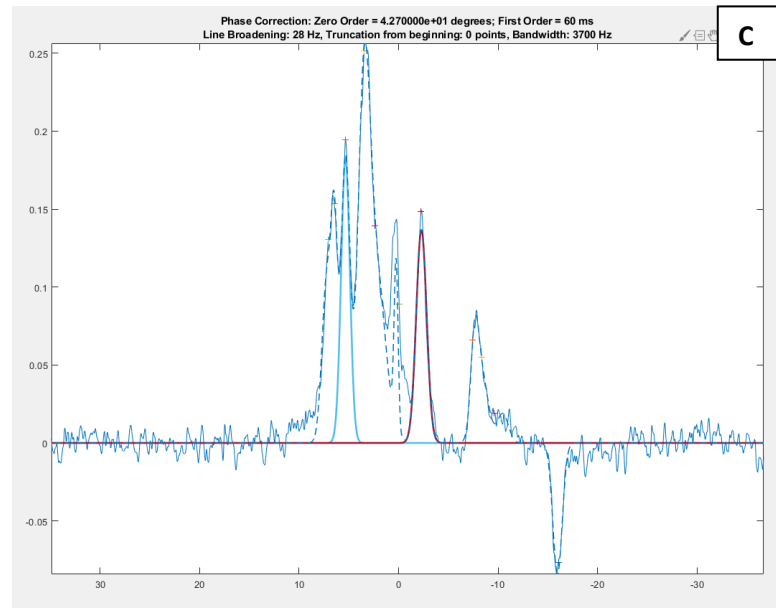
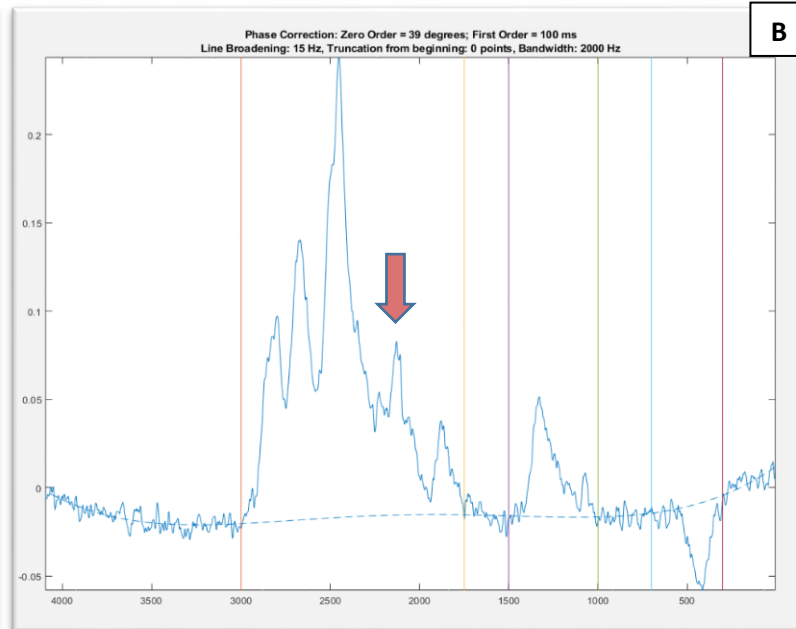
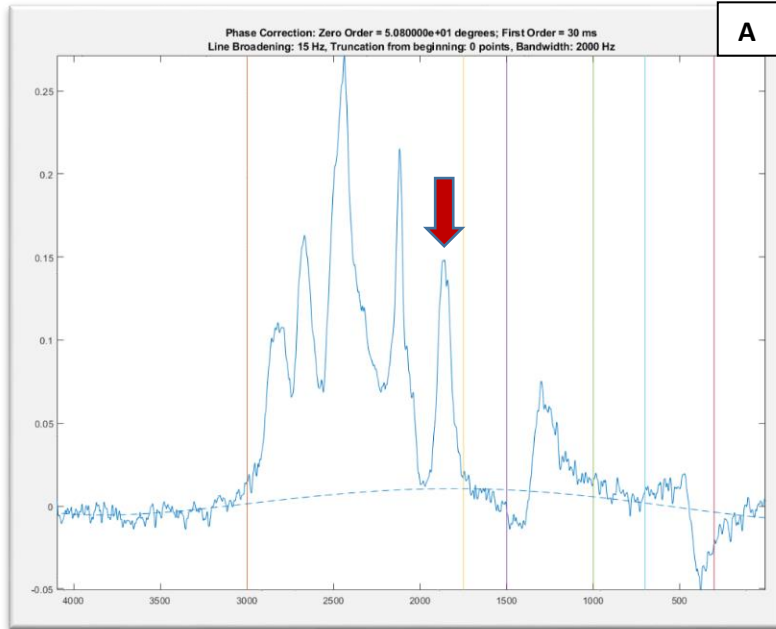


Figure 5. ^{31}P MR spectral output in Matlab, depicting:

Panel A: -2.5 ppm Non-saturated Spectrum. Red Arrow depicts non-saturated γ ATP peak.

Panel B: +14 ppm fully saturated spectrum. Red Arrow depicts saturated γ ATP peak.

Panel C: In-house Matlab fitting for non-saturated spectrum

Panel D: In-house Matlab fitting for fully saturated spectrum

'Area Under the curve' calculations of metabolite quantity are derived from the fitted peaks in panels C and D.

6.3 Results

Two researchers (PT and SB) analysed all spectra separately. Results were compared to assess inter-observer variability using a linear line of best fit approach. This revealed an r^2 of 0.81, suggesting good correlation with a large positive linear association.

At baseline, forward rates of hepatic ATP synthesis were lower in NAFLD compared to control (F_{ATP} (mM/s) = 0.98 ± 0.99 vs 0.25 ± 0.34 , $p < 0.001$), depicted in **Figure 6**. In the NAFLD cohort ($n=17$), forward rates of ATP synthesis were calculated before and after a placebo-controlled trial in which participants were randomised to receive L-carnitine or placebo for 24 weeks. This demonstrated a significant recovery in mitochondrial energy kinetics in L-carnitine supplemented patients, compared with a reduction in the placebo treated group (0.34 to 0.84 mM/s in the L-carnitine group vs 0.35 to 0.29 in the placebo group, $p = 0.025$, **Figure 7A**) with change in IHTG (%) correlating with change in ATP kinetics (**Figure 7B**).

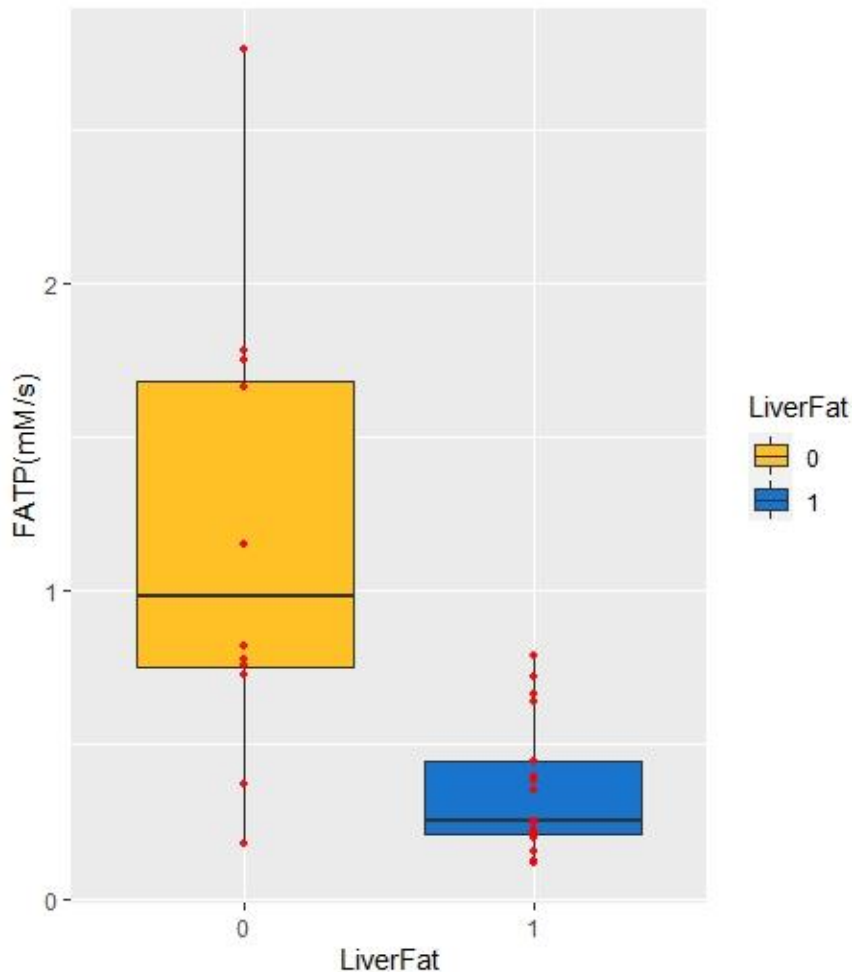


Figure 6. Median forward exchange flux through the ATP synthesis/hydrolysis cycle was significantly lower in NAFLD compared to healthy volunteers (F_{ATP} (mM/s) = 0.98 ± 0.99 vs 0.25 ± 0.34 , $p < 0.001$), indicative of impaired hepatic mitochondrial fat oxidation in NAFLD.

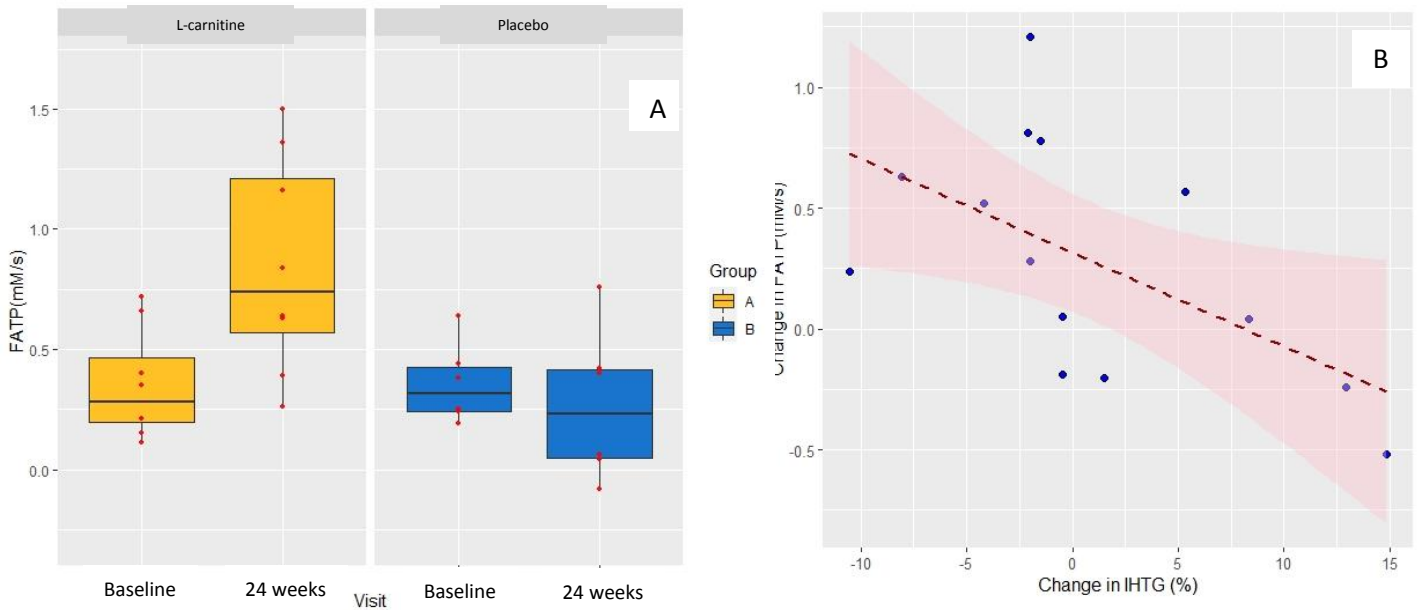


Figure 7 (A) Hepatic ATP flux in NAFLD at baseline and after 24 weeks of L-carnitine (gold) or placebo (blue) supplementation. **(B)** Correlation between change in IHTG (%) and change in forward rates of ATP synthesis.

6.4 Discussion

We have demonstrated that mitochondrial ATP synthesis at the level of the liver corresponds to intrahepatic triglyceride content, and that dynamic changes in mitochondrial metabolism reflect changes in IHTG ($r = -0.58$, $p = 0.03$). Similar observations have been made by other groups; Fellinger et al (2020) recently examined the relationship between IHTG and hepatic ATP flux in individuals with acromegaly ($n=15$) versus age and body-composition matched healthy control volunteers ($n=15$). The group demonstrated that IHTG was lower in acromegaly, coupled with a 50% increase in forward rates of ATP synthesis in this group, leading authors to conclude that lower IHTG in acromegaly is likely to be a consequence of enhanced mitochondrial β -oxidation [198].

In a preliminary analysis, Traussnigg and colleagues demonstrated recovery of Pi-to-ATP exchange rate constants in NAFLD individuals following a 12-month dietary intervention together with reduced IHTG ($n=2$). In contrast, where liver fat increased ($n=1$), there was a corresponding further reduction in forward rates of ATP synthesis. While very small numbers limit the conclusions that can be drawn from

this analysis, it illustrates a speculative clinical application of dynamic ^{31}P magnetisation transfer in mapping mitochondrial metabolism in real time in response to intervention [49]. We have expanded on this proof-of-principle study to demonstrate that changes in mitochondrial energy kinetics are observable following dietary supplementation with L-carnitine and that they correlate closely with changes in IHTG.

Future directions include incorporation of chemical exchange saturation transfer (CEST) to overcome inherent limitations of standard MRS, including the ability to quantify low concentration molecular compounds whose resonances lie close to that of water, e.g. amines, guanidine, hydroxyl groups. In addition, CEST offers high specificity for quantitative detection of protein, glucose, glycogen and glutamate in healthy tissue and disease states. Saturation of a molecule is a temporary state in which its net magnetisation is zero. This can be utilised to amplify chemical signal at particular resonances by transferring magnetisation from a molecule of interest to water. In ^1H MRS, this requires that the molecule of interest contains a proton (^1H) that it can readily exchange with water. A radiofrequency pulse is then applied to the molecule of interest at a particular resonance frequency, with a view to obtaining full saturation. Through chemical exchange of excited protons with zero magnetisation, the saturation effect is then transferred to the water molecule.

Incorporation of CEST imaging to liver MR protocols provides fertile ground for numerous clinical applications pertaining to metabolic liver disease. For example, amide proton transfer weighted imaging (APT_w) signal and GlycoCEST (rates of gluconeogenesis and hepatic glycogen stores) have been developed as novel contrast mechanisms, and demonstrated successfully *in vivo* at 3T and 7T field strengths [224]. Localised endogenous glycogen CEST (GlycoCEST) *in vivo* offers the exciting opportunity to simultaneously quantify both glucose and lipid metabolism in the liver. This is of relevance as the liver is a key intermediary hub for both glucose and lipid metabolism. Bawden *et al* developed a protocol for optimising GlycoCEST ^1H MRS to measure hepatic glycogen by suppressing the water peak and saturating the resonances of both glycogen and lipids, in real time [225]. The peak

is selectively saturated at the hydroxyl group of glycogen with subsequent transfer of that saturation to the water resonance.

In summary, quantifying metabolic fluxes *in vivo* provides unprecedented insight into the molecular pathology of NAFLD. Natural history studies as well as response to novel therapeutic interventions, may be developed using these protocols, providing a window into key biochemical pathways involved in NAFLD progression and the effect of pathway manipulation on energy kinetics, oxidative stress and substrate handling. In due course, validation of these non-invasive techniques against established methods (such as mass spectrometry using liver biopsy specimens) may yield novel endpoints with which to accelerate clinical trial design, recruitment, implementation and development of meaningful disease-modifying interventions to arrest progression/achieve regression in NAFLD pathogenesis.

Chapter 7: Role of Hepatokines as biomarkers in NAFLD

7.1 Introduction

Accumulation of intrahepatic triglyceride results from disequilibrium in several pathways governing lipid and carbohydrate metabolism. Adipose tissue dysfunction in the context of systemic inflammation/local insulin resistance leads to upregulated lipolysis and increased free fatty acid (FFA) flux, accounting for up to 60% of liver fat. A further contributor is dietary fat (20%), for which the liver is well placed to act as a sink, being the primary recipient of portal venous inflow. Finally, enhanced *de novo* lipogenesis due to impaired oxidative and non-oxidative glucose disposal at the level of the muscle, is thought to account for a further 20% (**Figure 1**). While very low-density lipoprotein (VLDL) secretion is enhanced in NAFLD, this is inadequate to account for impaired mitochondrial fat oxidation and increased FFA influx from dietary and lipolytic sources. Our previous data, discussed in **Chapters 3 and 5**, demonstrate an intricate link between lipid deposition in non-adipose tissues (i.e. liver and muscle) and development of a series of metabolic derangements underpinned by insulin resistance.

This metabolic ‘remodelling’ in the context of lipid surplus is characterised by altered gene expression, activation and circulation of key proteins governing pathways of lipid storage and oxidation, as well as glucose handling at the level of the liver and muscle [226]. Patterns of liver protein secretion are thus altered in a NAFLD phenotype, with growing evidence to suggest that steatosis in the liver results in the upregulated synthesis and release of specific proteins (termed ‘hepatokines’) which are secreted into the systemic circulation and influence insulin action both locally and at distant sites [227]. This ‘missing link’ supports the lipotoxicity paradigm in which hepatic steatosis is an early feature of, and is probably implicated in, whole-body insulin resistance and the development of systemic alterations in substrate trafficking which typify a metabolically challenged phenotype.

Hepatokines may be loosely considered akin to hormones, in that they are secreted by liver tissue but regulate metabolism at distant sites, including skeletal muscle and adipose tissue, via endocrine and paracrine effects, through mediating gene expression of multiple enzymes affecting pathways involving glucose and lipid handling. This ability to orchestrate inter-tissue ‘cross-talk’ has been

extensively studied in recent years as insight into the metabolic (mal)adaptations to chronically positive energy balance. Although a wide gamut of hepatokines have been identified (some of which are summarised in **Table 1**), we have focused on two specific hepatokines in this body of work:

- 1) **FGF 21** – a positive regulator of whole-body glucose and lipid metabolism. Circulating levels correlate closely with circulating insulin and triglyceride, but FGF21 exerts beneficial metabolic actions through promoting glucose disposal and insulin sensitivity.
- 2) **LECT2** – this hepatokine mediates glucose handling across the liver-muscle axis and is a negative regulator of insulin sensitivity. Levels are increased in NAFLD and LECT-2 induces insulin resistance.

Evaluating the mediators of dysregulated metabolic pathways may provide mechanistic insight into NAFLD pathogenesis, as well as adding to a body of evidence for use of FGF21 and LECT2 as early and sensitive metabolic biomarkers of insulin resistance.

	Metabolic Role	Change in NAFLD
FGF-21	Improves insulin sensitivity and energy expenditure	↑
LECT-2	Mediator of skeletal muscle insulin resistance. Impairs insulin signalling in muscle.	↑
Fetuin A	Mediator of insulin resistance. Mediates release of pro-inflammatory cytokines from ATMs	↑
Fetuin B	Perturbs glucose homeostasis. Impairs insulin action in hepatocytes and myocytes.	↑

Table 1 Important Hepatokines governing glucose and lipid homeostasis, together with circulating levels compared to baseline in a NAFLD phenotype.

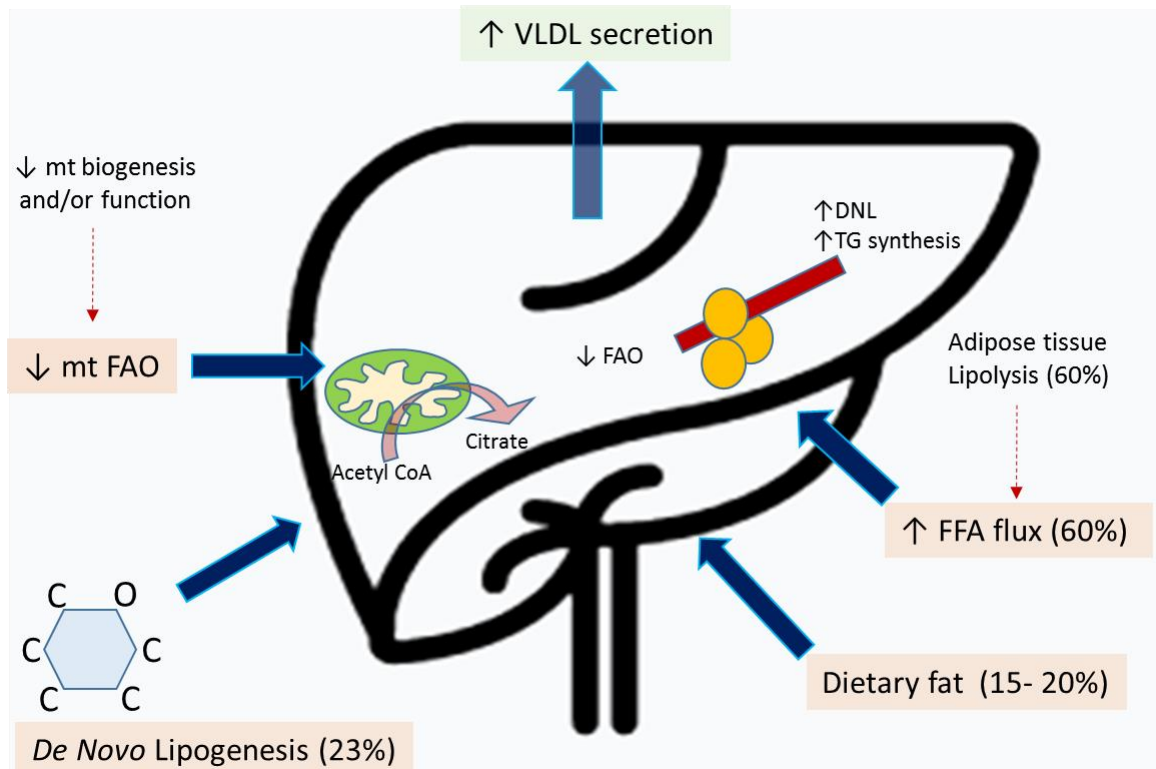


Figure 1. Schematic depicting pathways for lipid storage and disposal in the liver, and the contributors to hepatic steatosis. MT = mitochondrial; FAO = fatty acid oxidation; FFA = free fatty acids.

7.1.1 Fibroblast Growth Factor 21 (FGF-21)

Fibroblast Growth Factor 21 (FGF21) is a liver-derived protein which acts as a key metabolic regulator of glucose and lipid metabolism with pleiotropic beneficial effects. FGF21 receptors are highly expressed in metabolically active organs, including the liver, adipose tissue and skeletal muscle. In the liver, FGF21 attenuates intrahepatic lipid accumulation through insulin-independent mechanisms, including upregulation of fatty acid β -oxidation via PPAR α transcriptional axes as well as attenuating SREBP-1 activity [228]. The majority of its systemic effects are mediated at the level of adipose tissue, where FGF21 increases energy expenditure, suppresses lipolysis and upregulates GLUT-4 expression to enhance glucose transport. Finally, FGF21 downstream signalling in skeletal muscle enhances insulin-mediated glucose uptake [229]. The administration of recombinant FGF21 in murine models of obesity has been associated with improved insulin sensitivity, pancreatic islet β -cell function and

enhanced glucose transport [230], giving rise to the notion that FGF21 could act as a potential therapy in NAFLD, exerting a host of beneficial metabolic actions both locally and systemically [231].

Circulating levels of FGF21 are increased under conditions of chronic metabolic stress, including obesity, dyslipidaemia, type 2 diabetes and NAFLD [232]. This logically occurs as an adaptive mechanism to ameliorate glucose and lipid homeostasis in the context of chronic energy surplus. However, the pathogenic dichotomy of elevated circulating FGF21 in a metabolically challenged phenotype, together with the positive actions of FGF21 on metabolic profile appear to suggest that obesity and its associations reflect a state of FGF21 'resistance'. This hypothesis is supported in animal models wherein exogenous doses of FGF21 in mice are not associated with upregulation in its metabolic pathways [233]. In a large population-based study of >9000 individuals with type 2 diabetes, higher baseline circulating levels of FGF21 were independently predictive of adverse cardiovascular outcomes over a 5 year follow up period [234], with higher tertiles of serum FGF21 associated with higher cumulative event rate. Indeed, the authors found incremental value in adding FGF21 to risk prediction models. FGF21 has, to this end, been proposed as an early predictive biomarker for the metabolic syndrome, as serum concentrations have been shown to be elevated prior to the onset of frank insulin resistance [235].

Pharmacological administration of high-dose (> 4-fold circulating levels) FGF21 appears to overcome the problem of 'resistance' to exert favourable metabolic actions. For example, Camporez et al (2013) administered exogenous FGF21 through chronic infusion in a murine population, demonstrating that seven days of chronic FGF21 infusion in mice with diet induced obesity (high-fat feeding) reduced hepatic DAG-mediated activation of the novel protein kinase C isoform (PKC ϵ) and reduced myocellular DAG and PKC θ , thus attenuating the stimulus for impaired insulin action at a cellular level [236]. These findings suggest that at sufficiently high doses, FGF21 may be a potential therapeutic agent for NAFLD and insulin resistance.

7.1.2 Leukocyte-Derived Chemotaxin 2 (LECT-2)

Leukocyte derived Chemotaxin 2 (LECT2) is a liver-secreted cytokine which negatively impacts upon insulin signalling both at the level of the liver and muscle. LECT2 is considered to be a pro-inflammatory hepatokine, with its main downstream signalling target being skeletal muscle. Lan *et al* (2014) confirmed that circulating LECT2 levels correlated with severity of obesity and insulin resistance in human subjects [237]. Indeed, LECT2 deficient mice were found to have increased insulin-mediated glucose disposal at the level of the muscle, but adipose tissue and liver metabolism were unaltered. Expression of genes governing mitochondrial function was also found to be upregulated in LECT2 deficient mice, suggesting that overproduction of LECT2 detrimentally affects muscle insulin sensitivity and mitochondrial function.

In a recent study in humans with NAFLD (n=160) and age and gender-matched controls (n=160), Yoo *et al* (2017) demonstrated that circulating LECT2 was significantly elevated in NAFLD, and that this correlated well with anthropometric and biochemical measures consistent with the metabolic syndrome, such as waist circumference, aminotransferase levels, circulating lipid profile and inflammatory markers [238].

Specific therapeutic interventions downregulating LECT2 activity could, by logical extension, produce pleiotropic benefits on multiple signalling pathways governing insulin resistance. We sought to study circulating LECT2 levels in healthy volunteers versus a NAFLD cohort, to mechanistically investigate the liver-muscle axis in terms of insulin sensitivity. One major hypothesis underpinning our work so far has been the concept of muscle insulin resistance contributing to NAFLD and hepatic insulin resistance, through promoting diversion of carbohydrate substrate towards lipogenic pathways in the liver. Whether liver-derived proteins can also contribute to muscle insulin resistance (i.e. bidirectional lipotoxicity) in this context is unknown. Through analysing LECT2 concentrations in NAFLD and healthy volunteers, as well as analysing LECT2 levels before and after L-carnitine supplementation (which

preferentially affects muscle metabolism), we aimed to gain insight into mechanisms of liver-muscle axis lipotoxicity.

7.1.3 Aim

In this study, we sought to determine circulating FGF21 and LECT2 concentrations in non-diabetic individuals with NAFLD and healthy volunteers in a cross-sectional analysis. We further evaluated longitudinal responses in FGF21 and LECT2 concentrations following L-carnitine or placebo supplementation in NAFLD patients (n=17) to evaluate whether these hepatokines are implicated in the beneficial metabolic effects associated with L-carnitine therapy.

7.2 Methods

We examined serum FGF21 and LECT2 levels in healthy volunteers (n=13) and in age-matched non-diabetic individuals with NAFLD (n=19), and examined the associations between serum FGF21 concentrations and intrahepatic triglyceride, myocellular lipid fractions, anthropometric parameters and circulating biomarkers of glucose and lipid homeostasis. We also examined FGF21 and LECT2 concentrations in NAFLD patients (n=17) at baseline and post-intervention with L-carnitine or placebo.

Plasma was isolated from whole blood at baseline and post-intervention in NAFLD patients, as well as during the screening visits for healthy volunteers in the cross-sectional study. Briefly, whole blood was collected in serum tubes, which were spun in a centrifuge at 4°C for 10 minutes at 2000 × g. Isolated plasma supernatant was subsequently removed and stored in aliquots at -80°C for subsequent batch analysis.

Commercially available enzyme-linked immunosorbent assay (ELISA) kits were used to measure plasma concentrations of FGF21 (Quantikine®, R & D systems, Oxford, UK) and LECT2 (MBL International, Massachusetts, USA). All assays were performed according to instructions in the manufacturer booklets. Dilutions and washes were performed manually according to manufacturer instructions with a multi-channel pipette. Measurement of optical density was performed on an

automatic plate reader (Thermo Scientific Multiskan FC, USA) and subsequent log curve fitting was performed manually.

7.2.1 Detailed procedure:

Plasma was thawed for one hour, and reagents were prepared for both FGF21 and LECT2 kits, including wash buffer, substrate solution, calibrator diluent, Human FGF21 standard, master LECT2 standard, dilution buffers and biotin antibody diluent (for LECT2 assay procedure). Following addition of reagents as per manufacturer instructions, standards, controls and samples were added to the wells in duplicate or triplicate. The ELISA plates were subsequently incubated at room temperature for 1 hour (LECT2) or 2 hours (FGF21). Aspiration and washing were subsequently performed according to manufacturer instructions using 350 μ l (LECT2) or 400 μ l (FGF21) of wash buffer. Conjugate was added to each well using manual pipettes, and the incubation/wash/aspiration cycle was repeated. Substrate solution was then added, with the observed colour change from blue to yellow confirming adequacy of reaction and reagent mixing. The optical density was then determined using a microplate reader as described above.

A standard curve was generated for FGF21 concentration from plotting mean standard concentration against the optical density. A best fit line was subsequently derived using linear regression (**Figure 2A**). For LECT2 samples, a standard curve was generated by plotting standards against absorbance, generating a polynomial (compound quadratic) curve as shown in **Figure 2B**.

7.2.2 Statistical Analysis

Between-group differences in baseline characteristics were analysed using the independent sample's T test for normally distributed data or the Mann Whitney U test for non-parametric data. Relationships between variables were assessed using the bivariate Pearson's and Spearman's correlation coefficients as appropriate. Data was tested for normality using visual inspection of histograms and the Shapiro-Wilks test. Analysis of covariance (ANCOVA) using baseline values as covariates was used to evaluate change in continuous variables from baseline between groups. Overall within-subject changes before and after intervention were analysed using a two-sided paired samples Student's T-test for normally distributed variables or using a Related-Samples Wilcoxon Signed Rank test for pairwise comparisons in non-normally distributed variables. Data was analysed using Microsoft Excel (2013) for generation of standard curves, SPSS version 24.0 (IBM, Armonk, NY, USA) for statistical comparison tests and graphs were generated with the ggplot 2 package using 'R' software (version 3.3.2).

7.3 Results

A standard curve was produced from mean values of control samples in each row of wells. A linear standard curve was produced for FGF21 calculations and quadratic curves were produced for LECT2 calculations, as shown in **Figure 2** (A and B) with associated equations enabling derivation of hepatokine concentrations from mean values in duplicate or triplicate readings.

Inter and intraplate variability were assessed and the coefficient of variation between plates was <10% for both FGF21 and LECT2.

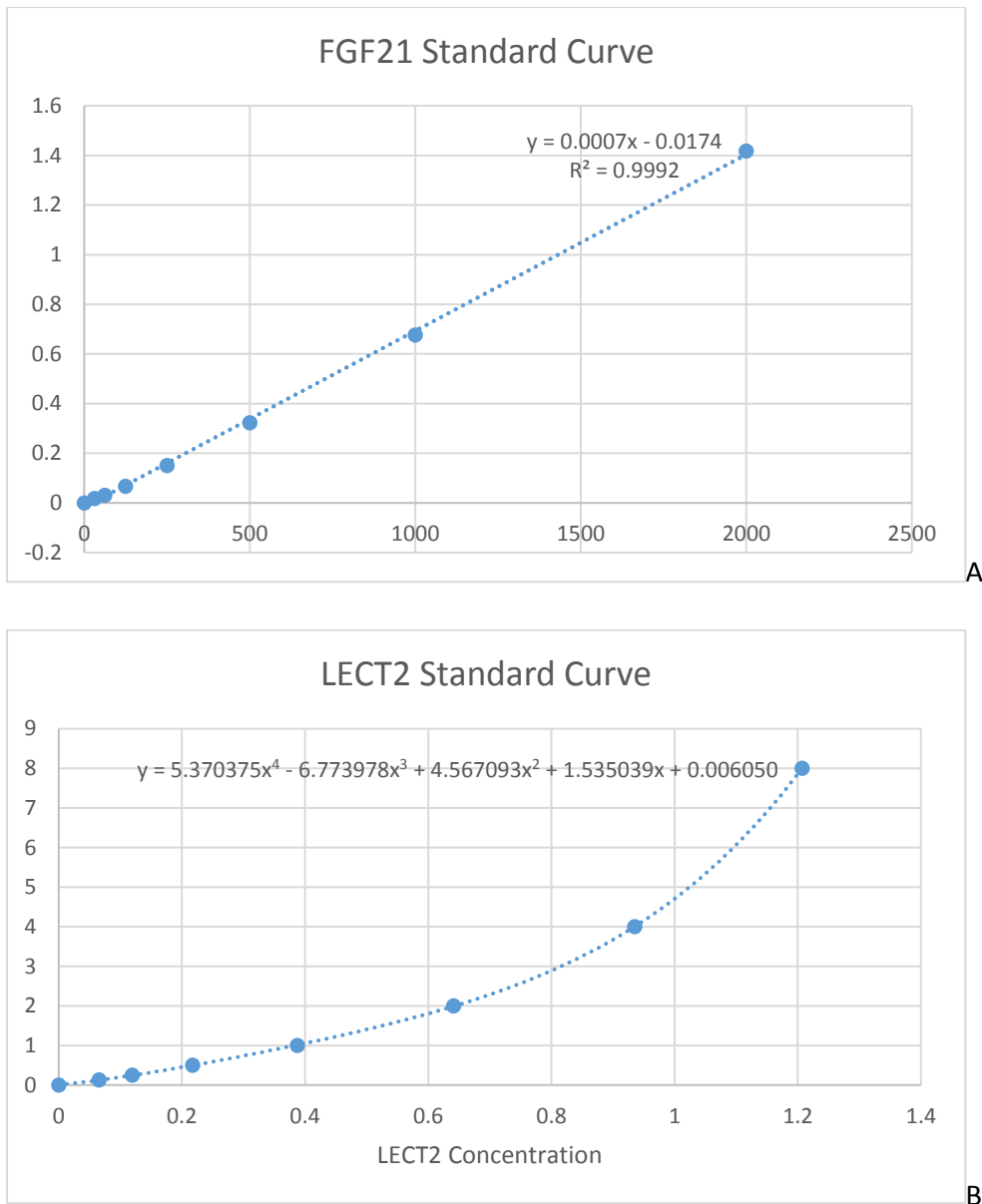


Figure 2 Standard curves generated for FGF21 (panel A) and LECT2 (panel B) from standards, with regression lines and equations for derivation of serum concentrations shown.

7.3.1 LECT2: cross sectional study

Serum concentrations of LECT2 were normally distributed among NAFLD and healthy volunteer groups (Shapiro Wilks statistic > 0.05 in both groups). Mean serum concentrations of LECT2 were significantly higher among NAFLD participants versus healthy volunteers (30.9 ± 6.3 versus 24.9 ± 2.9 ng/ml, $p=0.001$), **Figure 3**. Inter-plate coefficient of variation was 6%.

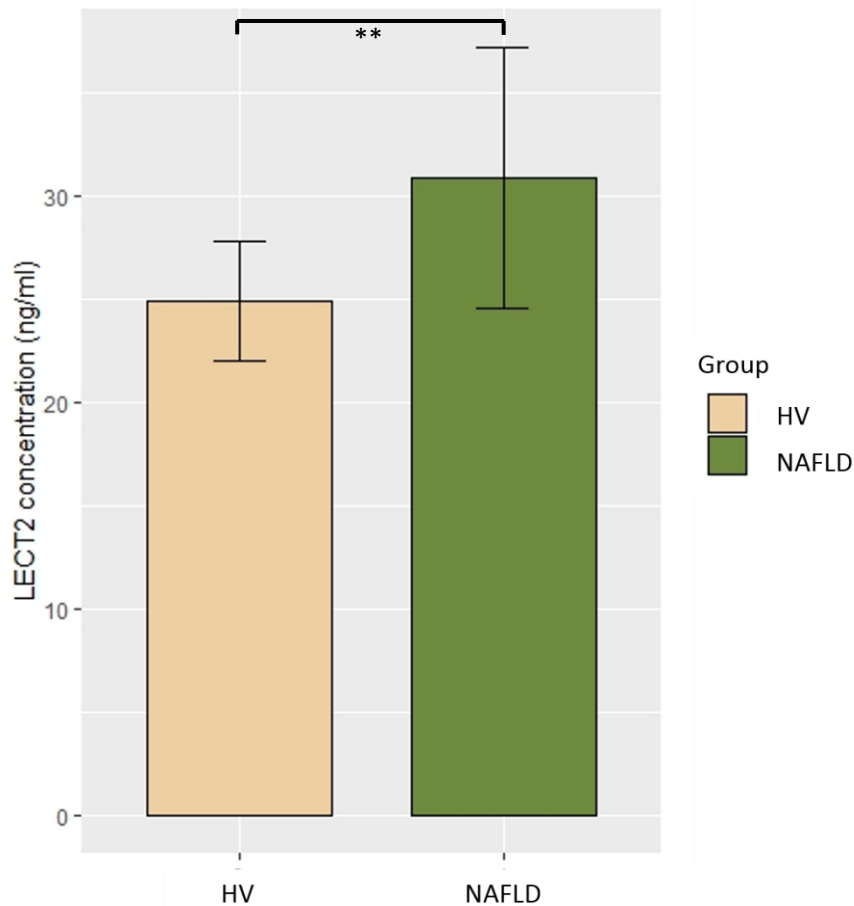


Figure 3 Mean circulating LECT2 concentrations in healthy volunteers (brown bar) and NAFLD patients (green bar).

Relationships between LECT2 concentrations and parameters of metabolic health were assessed using the Pearson's or Spearman's correlation coefficients, as appropriate. Results are shown in **Table 2**. There was a positive correlation between LECT2 and % IHTG, (Pearson's $r=0.561$, $p=0.001$, **Figure 4**). LECT2 concentration also correlated significantly with anthropometric measures including BMI ($p=0.009$), waist circumference ($p = 0.003$), total body fat mass (%) ($p = 0.025$) and leg fat mass ($p = 0.037$). With respect to glucose handling, LECT2 correlated with the HOMA-IR index ($p=0.037$) and whole-body glucose disposal as measured with the hyperinsulinaemic euglycaemic clamp ($p = 0.04$), as well as carbohydrate oxidation under hyperinsulinaemic conditions ($p=0.06$).

Non-significant correlations were shown between LECT2 and serum ALT ($p = 0.08$) and serum insulin ($p = 0.07$). However, LECT2 concentrations did not correlate with IMCL concentrations or with the ratio

of IMCL: EMCL ($p = 0.475$). In addition, serum LECT2 concentrations did not correlate with hepatic ATP flux ($p = 0.82$), serum CRP ($p = 0.178$), HDL or LDL cholesterol or serum triglyceride ($p = 0.395$ and 0.464 , respectively).

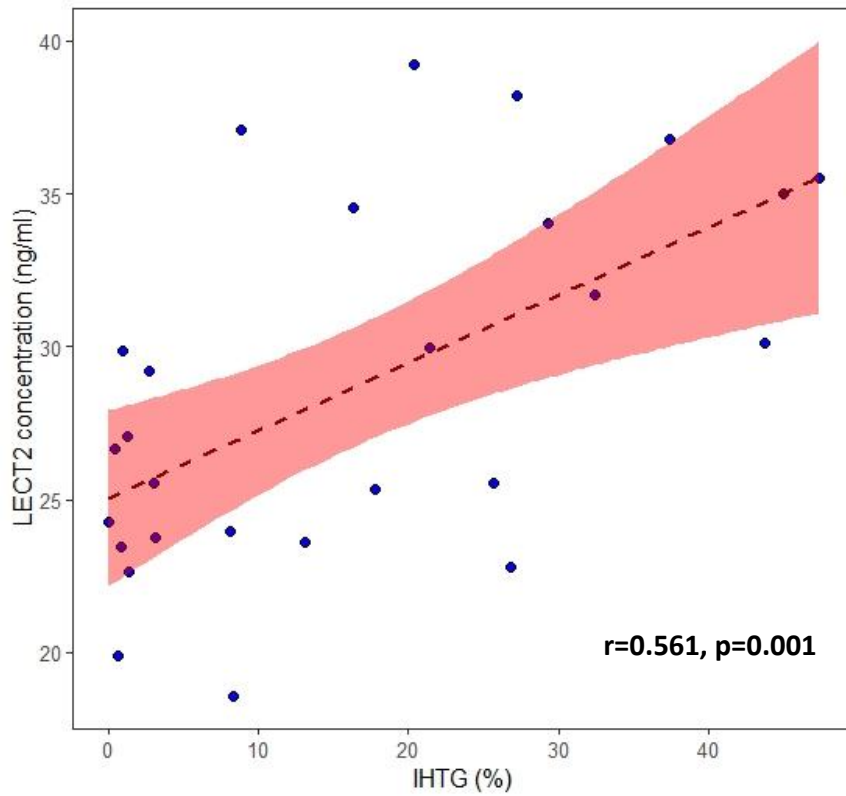


Figure 4 Relationship between circulating LECT2 concentrations and intrahepatic triglyceride (linear regression line with 95% confidence interval displayed).

Stepwise Linear Regression

A hierarchical multiple regression model was run to determine the impact of various metabolic parameters on serum LECT concentration. Stepwise regression analysis showed that only IHTG ($\beta = 0.567$, $t = 3.29$, $p = 0.003$) was an independent predictor of LECT2 levels (**Table 2**).

Variable	Pearson's/Spearman's correlation coefficient		Multiple Linear Regression	
	R/rho	P	β	P
BMI	0.466	0.009		
Waist circumference	0.547	0.003		
Waist: Hip Ratio	0.287	0.138		
Body fat (%)	0.438	0.025		
Leg fat mass (g)	0.411	0.037		
ALT	0.328	0.080		
AST	0.194	0.303		
IHTG (%)	0.561	0.001	0.567	0.003
Total cholesterol	0.202	0.285		
Triglyceride	0.031	0.872		
HDL cholesterol	-0.077	0.684		
LDL cholesterol	0.268	0.160		
NEFA	-0.139	0.488		
Adipo IR	0.201	0.316		
Fasting insulin	0.345	0.057		
Fasting glucose	0.169	0.371		
HOMA-IR	0.382	0.037		
Glucose Disposal Rate	-0.393	0.043		
Insulin-stimulated CHO oxidation	-0.365	0.061		

Table 2 Correlation between circulating LECT2 concentrations and indices of glucose and lipid metabolism and the metabolic syndrome.

7.3.2 LECT2: Longitudinal Assessment

Baseline LECT2 concentrations were not significantly different between L-carnitine and placebo group (32.9 ± 5.3 versus 29.4 ± 5.7 ng/ml, $p=0.174$). L-carnitine treated patients demonstrated a significant reduction in mean serum LECT2 concentrations (32.9 ± 5.2 to 27.8 ± 6.7 ng/ml, $p=0.01$) following intervention, compared with minimal reduction in the placebo group (29.4 ± 5.7 to 27.4 ± 7.25 , $p = 0.279$). Two-way ANOVA analysis using baseline values as covariates revealed no significant between

group difference ($p = 0.198$, **Figure 5**). A significant negative correlation was demonstrated between change in circulating LECT2 concentrations and change in intrahepatic triglyceride among study participants (Pearson's $r = 0.594$, $p = 0.015$).

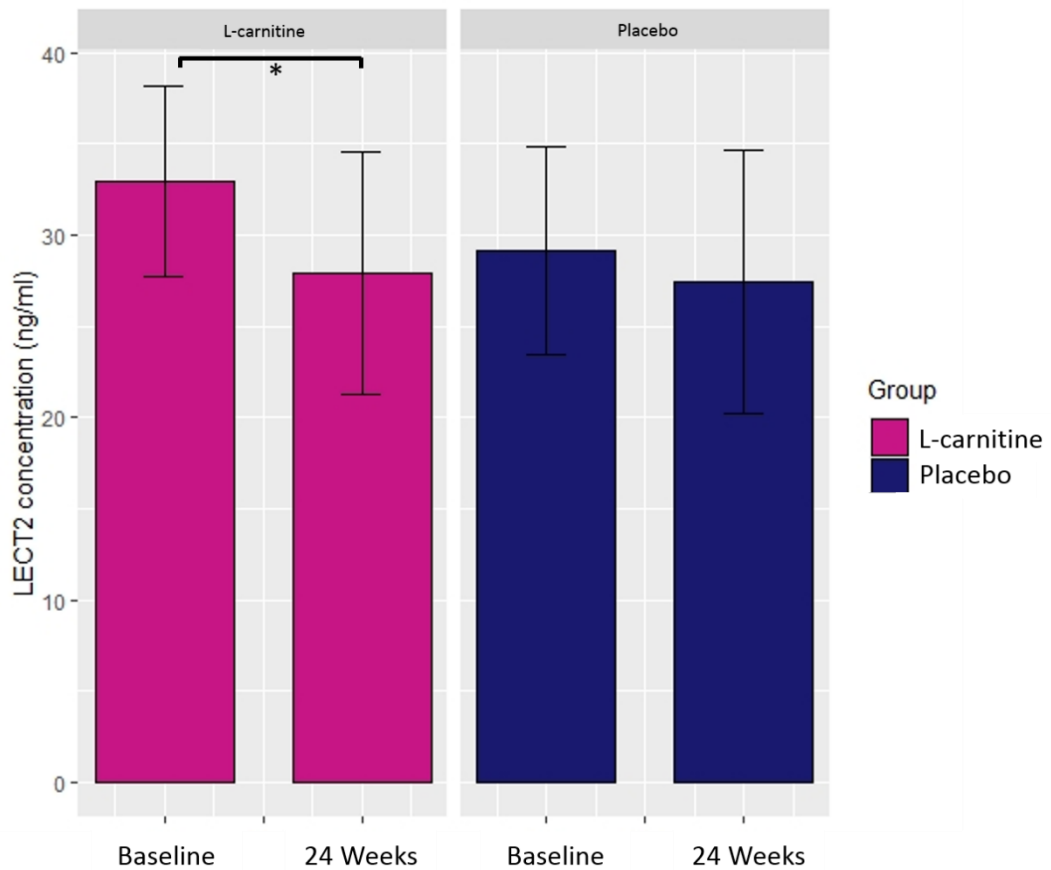


Figure 5 Change in circulating LECT2 concentrations from baseline in L-carnitine supplemented (pink bars) and placebo-supplemented (blue bars) groups.

7.3.3 FGF21: Cross-sectional study

Circulating concentrations of FGF21 were higher in NAFLD versus healthy volunteers (205.3 ± 172.1 versus 133.2 ± 155.1 pg/ml, $p = 0.059$), although this did not reach statistical significance (**Figure 6**). A loose positive correlation was demonstrated between circulating FGF21 concentrations and IHTG (%), ($r=0.381$, $P= 0.038$, **Figure 7**). Circulating FGF21 concentrations also correlated positively with lipid indices, including total cholesterol ($p = 0.01$), triglyceride ($p=0.08$) and LDL concentrations ($p=0.002$). No significant associations were found between circulating FGF21 concentrations and other metabolic biomarkers, insulin sensitivity indices, anthropometric measures, muscle lipid fractions or hepatic ATP flux (**Table 3**).

	FGF21	
	Spearman's rho	p-value
IHTG	0.38	0.038
I:E Ratio	0.08	0.704
Hepatic ATP Flux	0.121	0.535
BMI	0.18	0.33
Waist circumference	0.29	0.136
Total body fat (%)	-0.097	0.638
Leg fat (%)	-0.369	0.06
CHO oxidation	-0.28	0.163
Total cholesterol	0.45	0.012
Triglyceride	0.32	0.08
HDL	-0.12	0.53
LDL	0.54	0.002
Serum insulin	0.054	0.798
Glucose disposal (mg/min/kg)	-0.341	0.08
HOMA-IR	0.150	0.430

Table 3. Correlation between circulating FGF21 concentrations and indices of glucose and lipid metabolism and the metabolic syndrome.

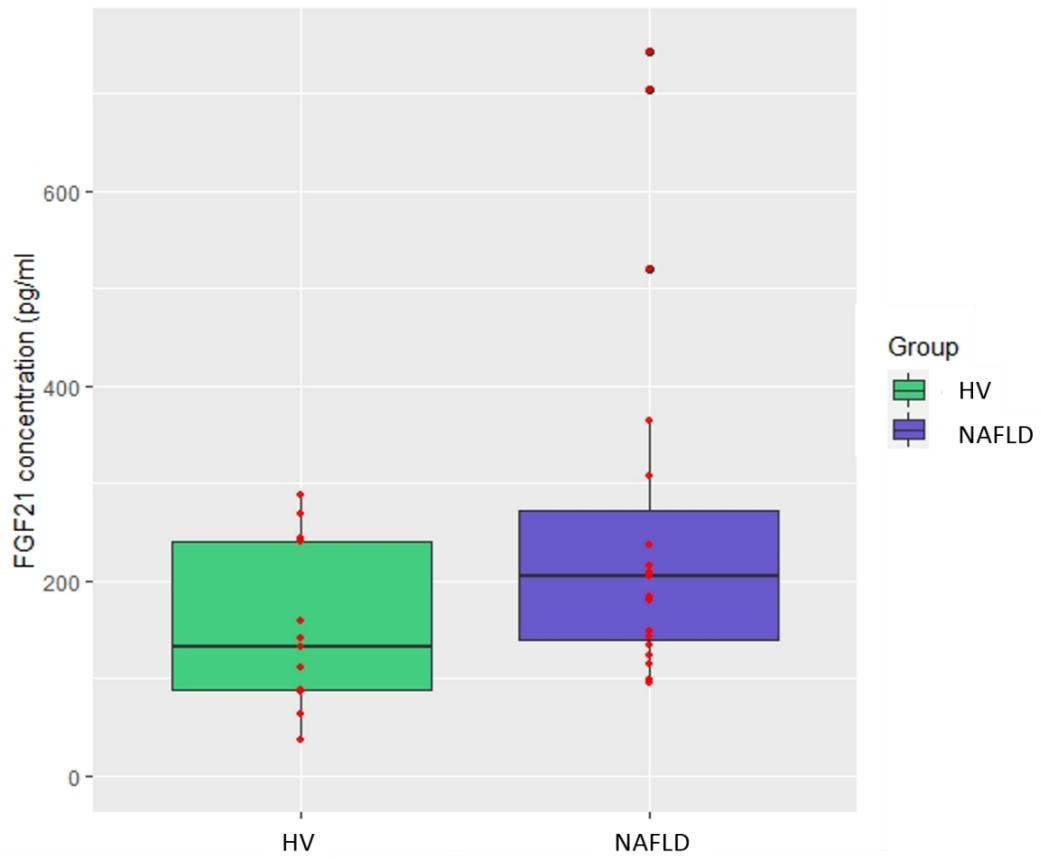


Figure 6 Median circulating FGF21 concentrations in HV (green) and NAFLD (purple) subjects)

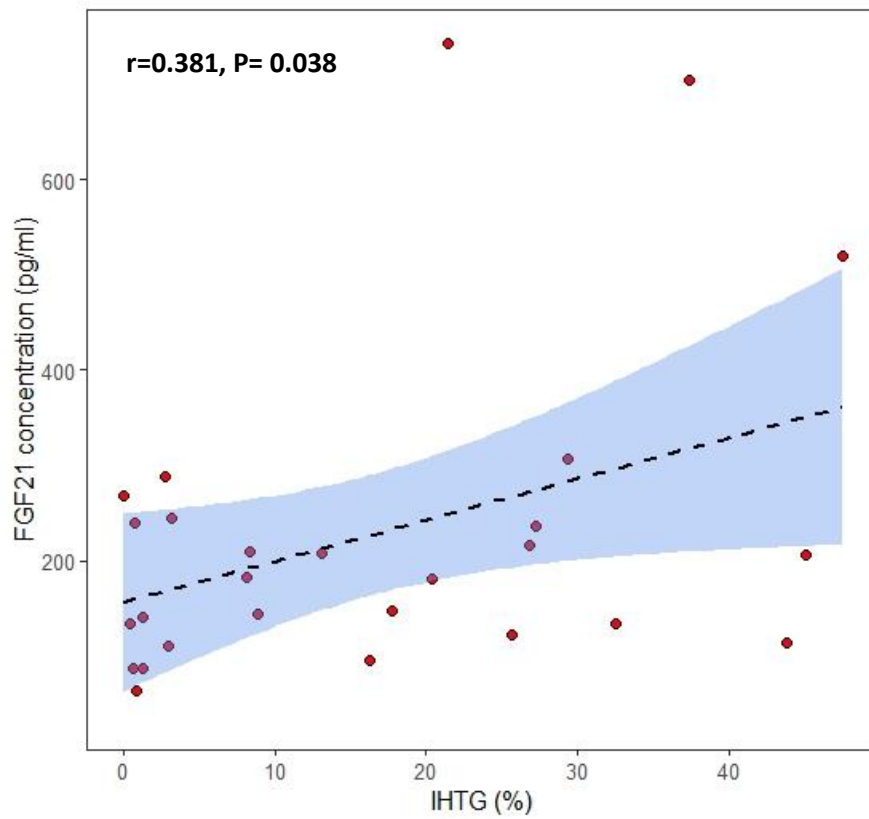


Figure 7 Relationship between circulating FGF21 concentrations and IHTG (%).

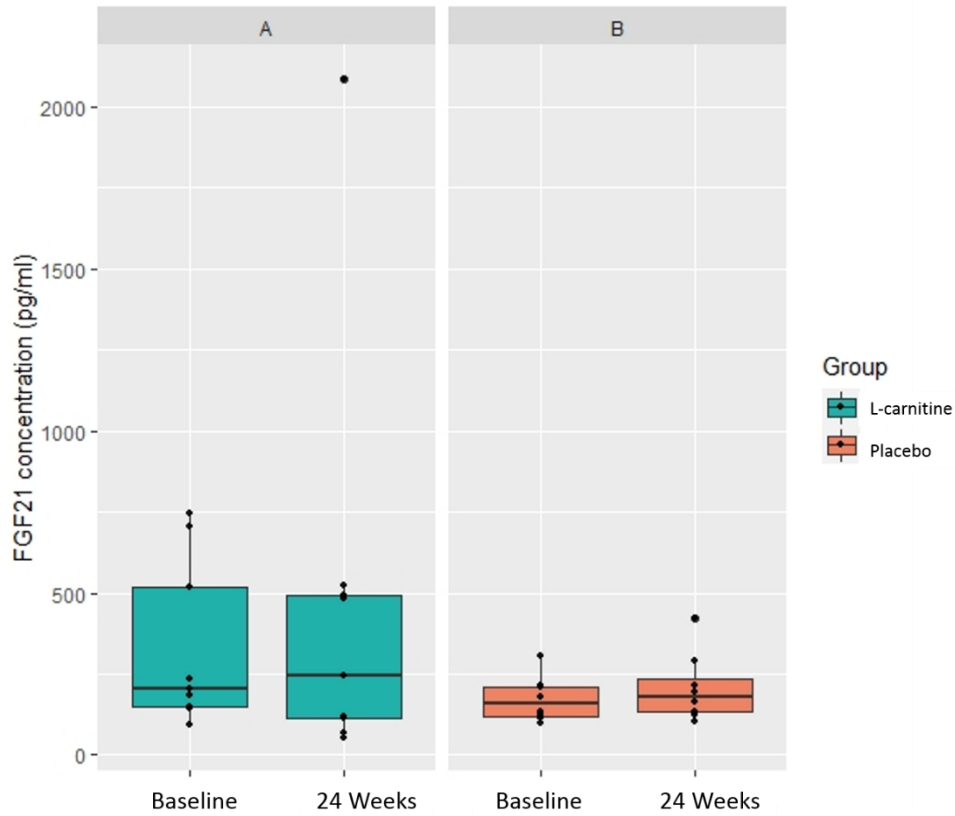


Figure 8 Change in median FGF21 concentrations in L-carnitine (teal bars) versus placebo (peach bars). Individual data points are shown as black dots.

7.3.4 FGF21 Longitudinal Assessment

Quade's test was used to evaluate between-group differences from baseline, as FGF21 values were not normally distributed. Median FGF21 concentration increased slightly in both L-carnitine and placebo groups, but although a bigger increase was seen in L-carnitine treated patients (205.3 to 243.7 versus 157.5 to 178.9 pg/ml) this was not statistically significant within or between groups (Quade's ANCOVA, $p=0.63$, **Figure 8**).

7.4 Discussion

The metabolic signatures of hepatokines, their importance in influencing an insulin resistant phenotype and the potential for intervention through manipulating their signal cascades presents a fertile ground for novel research in insulin resistance and the quest for effective therapies in NAFLD. It is well established that insulin resistance is present many years before the onset of frank T2DM, and early biomarkers permitting its identification in community settings may afford opportunities for disease modifying interventions to mitigate progression.

In this work, we have demonstrated that FGF21 and LECT2 are both biomarkers for the metabolic syndrome and are associated with NAFLD, demonstrating a positive correlation with intrahepatic triglyceride. Indeed, intrahepatic triglyceride was shown in multiple regression analysis to be the strongest independent predictor of circulating LECT2 levels. While existing literature is more extensively focused on FGF21, we did not observe a significant change in FGF21 levels upon L-carnitine supplementation. In contrast, LECT2 concentration reduced significantly following L-carnitine supplementation, suggesting that the actions of L-carnitine may impact upon LECT2-mediated networks of gene expression and protein activation.

Interestingly, dietary betaine was recently noted to upregulate FGF21 expression with associated improvements in glucose homeostasis and liver fat in mice with diet-induced obesity [239]. These beneficial effects on glucose tolerance and lipid metabolism were absent in FGF21 $-/-$ mice, suggesting that betaine exerts its metabolic effects via FGF21 mediated networks, including transcriptional effects on PPAR α . Carnitine is structurally and functionally related to betaine. Indeed, long-term betaine supplementation has been shown to induce carnitine metabolites in liver and muscle, with beneficial metabolic effects of betaine probably being effected through increased endogenous carnitine production [240]. By logical extension, it would therefore follow that L-carnitine exerts its own beneficial metabolic effects via PPAR α transcriptional axes, potentially mediated via FGF21. However,

in this study, although a modest FGF21 increase was seen with L-carnitine supplementation, no significant increase was seen compared with placebo. While FGF21 would be a logical candidate metabolic regulator to mediate adaptations to carnitine supplementation, our findings are consistent with those in animal models failing to demonstrate any increase in FGF21 mRNA expression following dietary L-carnitine supplementation [241]. This may be due to L-carnitine exerting its metabolic effects via pathways independent of FGF21 secretion. However, L-carnitine has been shown to exert some of its antioxidant effects via PPAR α related mechanisms [242]. Our small sample size results in high variability of findings, and thus a firm conclusion regarding the true effect of dietary L-carnitine on circulating FGF21 levels is difficult to establish.

In contrast, a clear effect of L-carnitine supplementation on LECT2 levels was observed, with reduced circulating LECT2 concentrations following L-carnitine supplementation. This suggests that L-carnitine supplementation may – either directly or through indirect mechanisms – exert inhibitory actions on LECT2 expression or downstream protein networks. As a novel hepatokine, there exist several unknowns regarding mechanisms of LECT2 action, but a clear correlation between circulating levels and the features of the metabolic syndrome (including NAFLD) have been established, suggesting that LECT2 may mediate several of the pleiotropic features of insulin resistance as a ‘master’ regulator. This has led to speculation that LECT2 could be incorporated into predictive algorithms in NAFLD, for example to evaluate risk of cardiovascular events and progression to cirrhosis [243]. LECT2 may also be considered a candidate for therapeutic targeting in the settings of obesity and insulin resistance. For example, LECT2 knockout (-/-) mice demonstrate improved skeletal muscle insulin sensitivity [237]. Given that the main site of L-carnitine action occurs in skeletal muscle, which also happens to be the main downstream target for liver-derived LECT2, it is tempting to speculate that L-carnitine mediates at least some of its actions via LECT2-regulated protein networks.

The role of hepatokines in regulating human physiology in the context of insulin resistance warrants further research. In particular, the scope for therapeutic targeting with multiple downstream effects

on inter-tissue cross-talk and the potential for simultaneous, multiplicative actions on glucose and lipid homeostasis through a single target protein is potentially enormous. The observation in this work that IHTG is independently associated with circulating LECT2 levels, and that L-carnitine supplementation is associated with decreased circulating LECT2 in tandem with reduced muscle and liver lipid fractions, affords an exciting window into the pleiotropic effects of this hormone in mediating the beneficial metabolic actions of L-carnitine supplementation.

Chapter 8: General Discussion

8.1 Aims

“A vaincre sans péril, on triomphe sans gloire” - Peirre Corneile, in *Le Cid (1636), II, 2, Le Comte*

The aims of this project were primarily fivefold:

1. To deeply phenotype a cohort of young, non-diabetic subjects with NAFLD and to map degree of metabolic disturbance to muscle fat fractions, substrate oxidation and hepatic energy kinetics.
2. To synthesise existing evidence base for the effect of L-carnitine on metabolic health in NAFLD
3. To evaluate the impact of chronic dietary L-carnitine loading on metabolic phenotype in NAFLD, including liver fat, hepatic and whole-body insulin resistance, fuel selection and hepatic bioenergetics, and to build mechanistic insights into L-carnitine action in liver and muscle.
4. To evaluate the role of circulating biomarkers including FGF21 and LECT2 in predicting metabolic phenotype and to determine responsiveness to long term dietary intervention
5. To develop clinically applicable techniques for the determination of hepatic ATP flux through exploiting ^{31}P MRS with novel saturation transfer techniques.

Major findings from this research include:

1. Detailed metabolic characterisation of young, non-diabetic males with NAFLD, including mechanistic insight into the contributions of IMCL in the development of an insulin-resistant phenotype.
2. Demonstration that hepatic mitochondrial energetics is altered at an early stage in NAFLD
3. Demonstration that chronic L-carnitine loading is capable of reducing liver fat and IMCL:EMCL ratio
4. Demonstration that chronic L-carnitine loading boosts hepatic mitochondrial oxidative metabolism as evidenced by an increase in liver ATP flux.

5. Confirmation that circulating LECT2 and FGF21 correlate with intrahepatic triglyceride, impaired glucose homeostasis and dyslipidaemia. Further, responsiveness of circulating LECT2 to L-carnitine supplementation which correlates well with improvement in other metabolic indices, including liver fat.

8.2 General Summary

In this body of work, we have metabolically characterised a young NAFLD cohort, demonstrating that elevated intrahepatic lipid in healthy, young, non-diabetic individuals occurs with a multitude of metabolic associations. These include hepatic and whole-body insulin resistance, elevated intramyocellular lipid, metabolic inflexibility, elevated circulating triglyceride, raised circulating levels of inflammatory markers and Hepatokines, reduced leg glucose uptake and diminished hepatic mitochondrial energetics. We further demonstrated that elevated IHTG is the strongest predictor of whole-body insulin resistance in a multivariate analysis. The close association between elevated intrahepatic fat and whole-body insulin resistance has been extensively demonstrated *in vivo*, and appears to persist when body weight is controlled for [244], indicating that IHTG is a more sensitive biomarker of metabolic dysregulation than generalised adiposity itself – indeed, low intrahepatic lipid is a marker of metabolically healthy obesity [245].

With respect to advancing the discussion on targeted therapeutics, pathogenic mechanisms and metabolic profile, we have highlighted four main points from this work:

1. The pathophysiology of NAFLD extends to skeletal muscle and in particular intramyocellular lipid fractions. This supports the growing body of evidence that lipid accumulation in non-adipose tissues impairs local insulin signalling. In the context of NAFLD, targeting muscle lipid could feasibly enhance muscle glucose uptake and attenuate carbohydrate diversion to the liver, thereby lowering the proportion of IHTG derived as a result of *de novo* lipogenesis.
2. IHTG is a more sensitive predictor than measures which may be readily available in primary care (e.g. triglyceride, body mass index) for the determination of insulin resistance in an

otherwise healthy phenotype. This is relevant, especially given the growing recognition of so-called 'lean' NAFLD and the metabolic risk conferred by altered fat *distribution*, rather than excess adiposity *per se*. Given that cardiovascular disease remains the major source of morbidity and mortality for individuals with NAFLD, the potential value of early intervention in the pre-diabetic phase merits consideration. We propose that further research is conducted in a primary care setting to evaluate the feasibility of (a) conducting assessments of liver fat in an unselected population e.g. with transient elastography using controlled attenuation parameter (b) bespoke interventions in a group of otherwise healthy individuals with elevated liver fat to determine longitudinally the benefit (if any) of such interventions in reducing long term metabolic risk.

3. Targeting hepatic mitochondrial metabolism may confer benefit in enhancing the fluency of β -oxidation, attenuating intrahepatic lipid accumulation and mitigating against the cascade of oxidative stress, lipotoxicity, necroinflammation and fibrogenesis spawned by mitochondrial gridlock.
4. The serum Hepatokines FGF21 and LECT2 are elevated early in the natural history of NAFLD and insulin resistance, prior to the onset of frank T2DM. Given that IHTG (%) was independently predictive of circulating LECT2 when controlling for associated metabolic disturbances (e.g. waist circumference, dyslipidaemia, HOMA-IR). LECT2 may be a particularly sensitive biomarker for NAFLD and may be useful to develop as a point-of-care test, alone or in conjunction with other predictive algorithms. There is a paucity of data in humans on association between LECT2 levels and NAFLD progression/fibrosis stage. However, this would be an interesting line of work with a view to developing and validating LECT2 as a novel predictive biomarker in NAFLD.

Our longitudinal data has expanded on some of this mechanistic insight, by manipulating the body carnitine pool through chronic dietary loading with L-carnitine L-tartrate. Our pilot placebo-controlled, randomised data has demonstrated that:

1. L-carnitine supplementation is capable of reducing liver fat as measured by ^1H -MRS, despite excess calories conferred by Slimfast[®] supplementation.
2. L-carnitine promotes hepatic mitochondrial energy kinetics, as evidenced by an increase in ATP turnover in the liver. Quantitative assessment of dynamic metabolic reactions in the liver is feasible in a human trial population and carries exciting prospects with development of targeted therapies and novel trial endpoints.
3. L-carnitine reduces liver transaminases and in particular serum ALT, suggesting attenuation of hepatocellular inflammation.

Development of specific laboratory skills and exploratory outcomes in this doctoral thesis have focused on novel circulating and imaging biomarkers of metabolic health and the liver-muscle axis, and have evolved to include:

1. Hepatokine analysis via enzyme linked immunosorbent assay (FGF21 and LECT2) in both a cross-sectional cohort and longitudinally following intervention in NAFLD subjects.
2. Development of a localised saturation transfer experiment protocol for hepatic ^{31}P MRS to determine resting ATP flux both cross-sectionally and in response to targeted intervention (Chapter 6).
3. Incorporation of sophisticated metabolic techniques to deeply phenotype cohorts cross-sectionally and longitudinally, including indirect calorimetry, two-step hyperinsulinaemic clamps, femoral arteriovenous difference studies and Bergstrom muscle biopsy techniques.

8.3 Limitations

There are several limitations regarding translatability and methodological quality of this work. Firstly, we did not match control volunteers for BMI with NAFLD patients. This potentially limits applicability of findings due to multicollinearity of several dependent variables, for example BMI and circulating triglycerides/Adipo-IR/muscle insulin resistance. However, in the multivariate analysis, we did adjust for BMI and found IHTG to be an independent predictor of adverse metabolic profile including whole-

body insulin resistance. This strongly support the notion that locality of fat deposition is a strong predictor of metabolic profile.

Secondly, our sample size in the RCT, although powered sufficiently to reach the primary endpoint of reduced liver fat, was insufficient to power a number of other outcome measures, in particular substrate oxidation data. While the data suggest a trend towards preserved metabolic flexibility in L-carnitine supplemented patients, we cannot confirm that L-carnitine significantly improves metabolic flexibility – rather, our data suggest it mitigated against carbohydrate-induced impairment in the context of Slimfast[®] supplementation. A larger sample size may have enabled observed trends in metabolic flexibility to stand out more clearly, with lower margins of error. Variance across almost all parameters was also high. A larger sample size would have reduced variability in data and increased confidence in results. The Smaller sample size in this study means that many non-primary and secondary outcome measures were insufficiently powered to determine significance of effect, with wide confidence intervals.

Subjects included in these studies were all male and had no underlying health conditions. This potentially limits applicability of our findings across a broader NAFLD population, in whom prevalence of frank type 2 diabetes, cardiovascular disease, hypertension and dyslipidaemia is high, and introduction of novel therapies in this context is fraught with obvious and valid challenges. However, our aim was to provide mechanistic insight into the early stages of NAFLD, to identify whether muscle involvement was present at an early stage in the disease process and to determine whether mechanism-based intervention would be effective both at the level of the muscle and liver with respect to fat accumulation, insulin sensitivity and metabolic flexibility. This necessitated implementation of methods to deeply phenotype our cohorts, including dual step euglycaemic hyperinsulinaemic clamp studies together with femoral catheterisation, indirect calorimetry and muscle biopsies. Combined with a scanning protocol of almost three hours, workforce/resource limited to a single site, this necessarily curtailed the possibility of a significant expansion in sample

size. Differences in regional fat deposition and temporal variation in relation to the menstrual cycle meant that applying similar techniques in a female population would have entailed a number of potentially confounding variables, reducing reliability of results.

Thirdly, although overall body weight (kg) did not significantly change within groups over the course of the study, data would suggest that twice daily Slimfast was not overall isocaloric and contributed towards increasing regional adiposity with consequent effects on metabolic flexibility. While carnitine entry into muscle is an OCTN2 dependent process, accelerated by carbohydrate supplementation, there is evidence from the Faroe Island population (highest worldwide prevalence of primary carnitine deficiency, 1:300) that exogenous carnitine supplementation increases carnitine content in skeletal muscle, even in the absence of an insulinogenic stimulus [246]. One option for facilitating chronic carnitine supplementation in a population with the metabolic syndrome might be to consider a protein-based insulinogenic stimulus, either alone or together with a low-intensity exercise protocol [247].

Finally, given emerging data demonstrating a link between dietary L-carnitine supplementation and caecal production of the pro-atherogenic metabolite TMAO, long-term safety of L-carnitine supplementation in a group already at high risk of incident cardiovascular events remains in question.

8.4 Mechanistic Approach to L-carnitine Treatment in NAFLD

Figure 1 provides an overview of the metabolic adaptations occurring in the context of chronic energy surplus, together with the pleiotropic benefits associated with L-carnitine supplementation, some of which have been demonstrated at a metabolic level in this thesis.

Chronic excess intake of carbohydrate and fat disrupt finely tuned metabolic pathways which evolved for efficient energy storage and utilisation, resulting in ectopic lipid accumulation, local insulin resistance and diversion of standard pathways for oxidative and non-oxidative carbohydrate metabolism. Mitochondrial gridlock and metabolic inflexibility result in production of reactive oxygen

species, spawning a cascade of oxidative stress, lipotoxicity and necroinflammation, propagating hepatocyte damage in NAFLD. An increased intracellular acetyl-CoA/CoA ratio derails reducing mechanisms and in the liver, increases gluconeogenesis via acetyl-CoA induced activation of pyruvate carboxylase. Carnitine can attenuate these metabolic (mal) adaptations as shown (**Figure 1**).

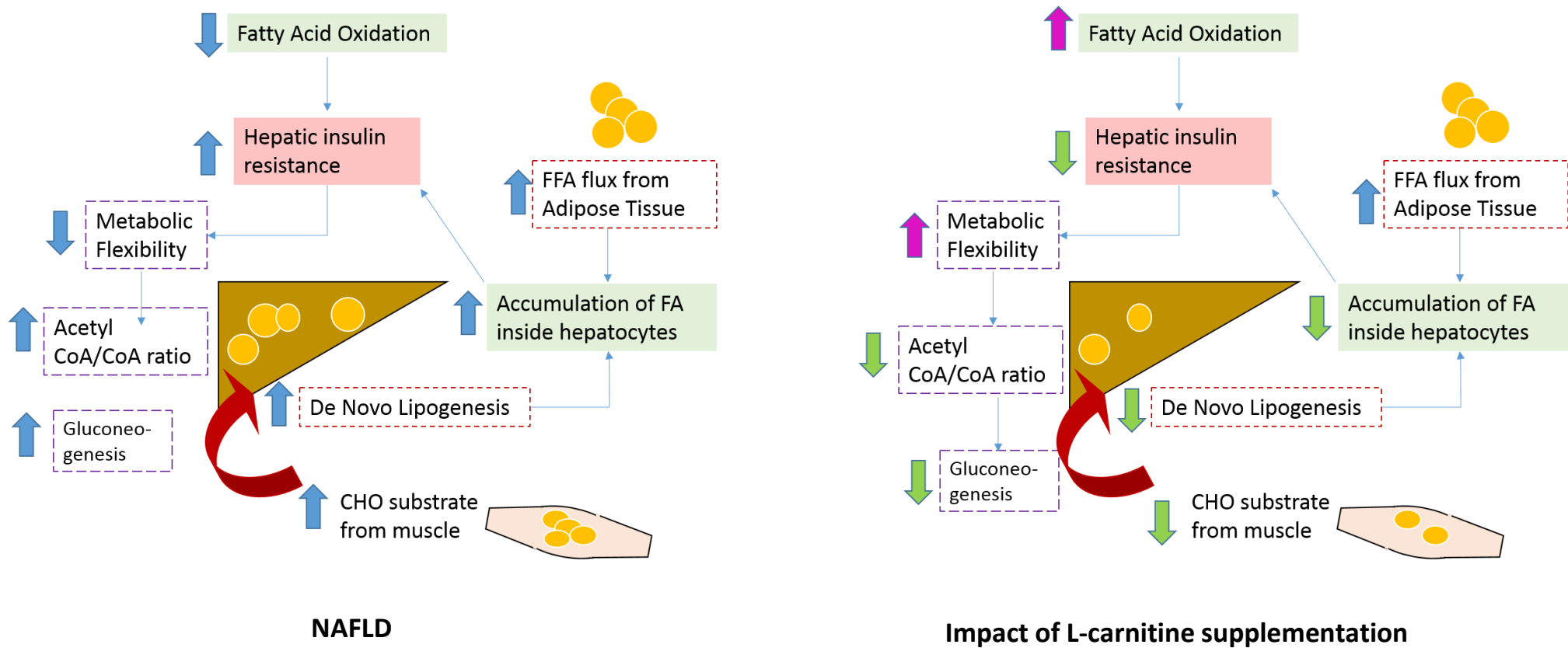


Figure 1. Panel A. Metabolic (mal) adaptations in NAFLD depicting both upstream contributors to, and downstream effects of, insulin resistance. Panel B – Mechanistic overview of impact of L-carnitine supplementation on metabolic derangements occurring in NAFLD.

8.5 Research Implications

The work presented in this thesis gives rise to numerous potential applications in both research and clinical spheres. Firstly, this body of works demonstrates that skeletal muscle has an important contributory role in the pathogenesis of NAFLD, has metabolic plasticity and merits targeted intervention in itself as part of a holistic approach to ameliorating the deleterious metabolic associations with NAFLD. Secondly, we demonstrate that hepatic ATP flux is significantly impaired in healthy, overweight individuals with elevated liver fat, implicating mitochondrial metabolism directly in the pathogenesis of NAFLD. These mechanistic insights corroborate calls for a multi-pronged approach when targeting the metabolic syndrome from a therapeutic angle.

Secondly, with respect to non-invasive quantitative imaging biomarkers, this is to our knowledge the first registered study to demonstrate applicability of longitudinal hepatic ATP flux mapping in response to intervention. This is a potentially exciting avenue which merits development and validation in future exploratory analyses, possibly combined with paired biopsy studies. MRS is likely to gain increasing traction as a metabolic imaging technique in NAFLD, capable of probing several different aspects of glucose and lipid metabolism, in different tissues (e.g. liver and muscle), simultaneously.

Thirdly, we have demonstrated that L-carnitine is an effective adjunctive therapy in NAFLD, conferring several metabolic benefits. These include reduced liver fat, improved hepatic ATP production and reduced deleterious muscle fat fractions, corresponding to an increase in leg glucose uptake. While overall insulin sensitivity was not significantly improved, hepatic insulin sensitivity increased with L-carnitine supplementation and surrogate markers (e.g. lower HOMA-IR) suggest slightly improved glucose tolerance following L-carnitine supplementation. It may well be the case that a longer period of supplementation is required before a significant effect on whole-body insulin sensitivity is seen.

Finally, we have shown that circulating biomarkers FGF21 and LECT2 are associated with NAFLD, and that intrahepatic triglyceride content is an independent predictor of serum LECT2 levels. This suggests that hepatokines can serve as important circulating biomarkers of insulin resistance and NAFLD, and

their levels are elevated early in the natural history of the metabolic syndrome. This discovery may enable incorporation of hepatokines into existing algorithms to enhance community detection of individuals at risk of NAFLD progression or adverse cardiovascular outcomes, especially given that elevated LECT2 levels have been linked to incident cardiovascular events. We have shown a reduction in LECT2 levels following L-carnitine supplementation, shedding mechanistic insight into modes of L-carnitine action and supporting established paradigms of liver-muscle cross-talk in the generation of insulin resistance, supporting a role for LECT2 as a marker of treatment response.

Quantifying rates of *de novo* lipogenesis was beyond the scope of this trial. However, evaluating DNL would add a useful dimension to this work, enabling localisation of L-carnitine mechanisms of action. We hypothesise that L-carnitine acts primarily to reduce muscle lipid fractions. In this paradigm, improved glucose uptake at the level of muscle (due to attenuation in lipid-induced impairment in insulin signalling) would plausibly reduce carbohydrate load to the liver, limiting substrate for DNL and subsequently reducing IHTG (%). It may be possible to retrospectively estimate DNL via qualitative fat evaluation and calculation of liver saturated fat index from ^1H MRS [248]. This is a potential line of future work which would enrich our existing analyses.

Finally, quantifying carnitine moieties in both liver and muscle simultaneously and non-invasively by leveraging ^1H MRS at 7T would enable localisation of the primary site of L-carnitine action in the metabolic syndrome and effects on the body carnitine pool of dietary and exercise interventions. Incorporation of multinuclear MR spectroscopy, including CEST, into these proposals, would enable construction of a comprehensive, multidimensional 'window' into NAFLD metabolism, offering unprecedented insight into both glucose and lipid metabolism, together with energy kinetics, qualitative fat fractions and effect of specific intervention on these metabolic indices in real time. The ability to extract data from multiple tissues simultaneously enables us to probe the role of the liver-muscle axis in NAFLD *in vivo*, in real time, and to measure its response to therapeutic intervention.

Combining MR spectroscopy with MR Elastography (to quantify hepatic fibrosis) and sophisticated MRI techniques (to quantify portal pressure and systemic haemodynamics, as well as gut permeability) could build a dynamic, entirely non-invasive protocol for risk stratification of individuals with chronic liver disease. The development of non-invasive endpoints which reflect cellular and molecular pathogenic processes, including effects of intervention on oxidative stress, energy metabolism and fibrogenesis, could accelerate trial design, recruitment and establishment of metabolically meaningful endpoints. At ultra-high field strengths (e.g. 7T) these techniques carry considerable scope for translation into the clinical domain, with serial quantitation of multiple metabolic endpoints becoming a powerful tool with which to probe the natural history of NAFLD, the heterogeneity and bidirectionality of its pathogenesis and the impact of intervention on multiple mechanistic pathways. Ultimately, the ability to leverage these sophisticated tools on a population level would represent a step-change in NAFLD research and a boon in the quest for disease-modifying intervention.



Conclusion

“An expert is one who knows more and more about less and less until he knows absolutely everything about nothing.” – Nicholas Butler

The complexity and multiplicity of signals governing insulin action, glucose handling and lipid metabolism are difficult to fathom. Decades of high quality research has spawned the emergence of several paradigms, of which the ectopic lipid deposition hypothesis is best supported by evidence. The roles of the liver-muscle axis, mitochondrial inflexibility and hepatokine signalling, and their combined importance in influencing an insulin resistant phenotype has been demonstrated in this thesis.

The beneficial effect of dietary L-carnitine supplementation, through attenuating muscle and liver lipid and boosting mitochondrial oxidative phosphorylation, has been demonstrated in a NAFLD population. The potential for intervention through manipulating hepatokine signal transduction, harnessing novel technologies to assess splanchnic substrate trafficking, and leveraging MR-based quantitative imaging techniques, all remain fertile ground for novel research in insulin resistance and would advance scope for the development and validation of effective therapies with which to combat the rising tide of NAFLD.

Appendix 1

List of search terms used in Ovid MEDLINE, for systematic review (Chapter 4)

- 1 (liver OR hepatic).mp.
- 2 (fatty OR steatosis OR steatoses OR steatotic OR steatohepatitis).mp.
- 3 (non-alcoholic OR nonalcoholic OR non alcoholic).mp.
- 4 1 and 2 and 3
- 5 NAFLD.mp.
- 6 NASH.mp.
- 7 exp Non-alcoholic Fatty Liver Disease/
- 8 4 or 5 or 6 or 7
- 9 carnitine.mp.
- 10 l-carnitine.mp.
- 11 lcarnitine.mp.
- 12 carnipure.mp.
- 13 exp Carnitine/
- 14 9 or 10 or 11 or 12 or 13
- 15 8 and 14



Appendix 2

REC, HRA and R&I approval letters for the ECLIPSE Study

Page 1 of 17



NON-COMMERCIAL RESEARCH AGREEMENT

This Agreement is made between

The University of Nottingham
(referred to as the 'Sponsor')

AND

Nottingham University Hospitals NHS Trust
(referred to as the 'Participating Party')

and are collectively referred to as the "Parties" or individually referred to as a "Participating Party" or "Party"

Agreement of the responsibilities, liabilities and relationship between the University of Nottingham and non-commercial parties undertaking University of Nottingham Sponsored research. The above Parties agree to the following obligations, terms and conditions when carrying out the clinical research study entitled:

ECLIPSE: Effect of Carnitine supplementation on Liver steatosis, Insulin sensitivity, Plasma glucose homeostasis, Skeletal muscle metabolism and Energetics: a pilot study.

Sponsor's Protocol Reference:	17086
IRAS Project ID:	228690
MHRA Reference:	N/A
EudraCT Number:	N/A



**Health Research
Authority**

East Midlands - Nottingham 2 Research Ethics Committee

The Old Chapel
Royal Standard Place
Nottingham
NG1 6FS

Please note: This is the favourable opinion of the REC only and does not allow the amendment to be implemented at NHS sites in England until the outcome of the HRA assessment has been confirmed.

26 February 2018

Dr Prarthana Thiagarajan
Nottingham Digestive Disease Centre Biomedical Research Centre
Nottingham University Hospitals NHS Trust
Derby Road
NG72UH

Dear Dr Thiagarajan

Study title:	ECLIPSE: Effect of Carnitine supplementation on Liver steatosis, Insulin sensitivity, Plasma glucose homeostasis, Skeletal muscle metabolism and Energetics: a pilot study.
REC reference:	17/EM/0441
Protocol number:	17086
Amendment number:	1.0
Amendment date:	15 February 2018
IRAS project ID:	228690

The above amendment was reviewed by the Sub-Committee in correspondence.

Ethical opinion

The members of the Committee taking part in the review gave a favourable ethical opinion of the amendment on the basis described in the notice of amendment form and supporting documentation.

Discussion

There were no ethical issues raised.

To: [Aithal Guru \(Gastrointestinal Services\); Prarthana Thiagarajan](#)
Cc: [Ryder Stephen \(Acute Medicine\); Koufali Maria \(Research & Innovation\)](#)
Subject: RE: IRAS 228690 Confirmation of Capacity and Capability at Nottingham University Hospitals NHS Trust
Date: 07 March 2018 08:39:30

Dear Guru Aithal,

RE: IRAS 228690 Confirmation of Capacity and Capability at Nottingham University Hospitals NHS Trust

R&I Ref: 17GA048

Full Study Title: ECLIPSE: Effect of Carnitine supplementation on Liver steatosis, Insulin sensitivity, Plasma glucose homeostasis, Skeletal muscle metabolism and Energetics, a pilot study

Sponsoring Organisation: **University of Nottingham**

This email confirms that **Nottingham University Hospitals NHS Trust** has the capacity and capability to deliver the above referenced study. Please find attached our signed agreement as confirmation.

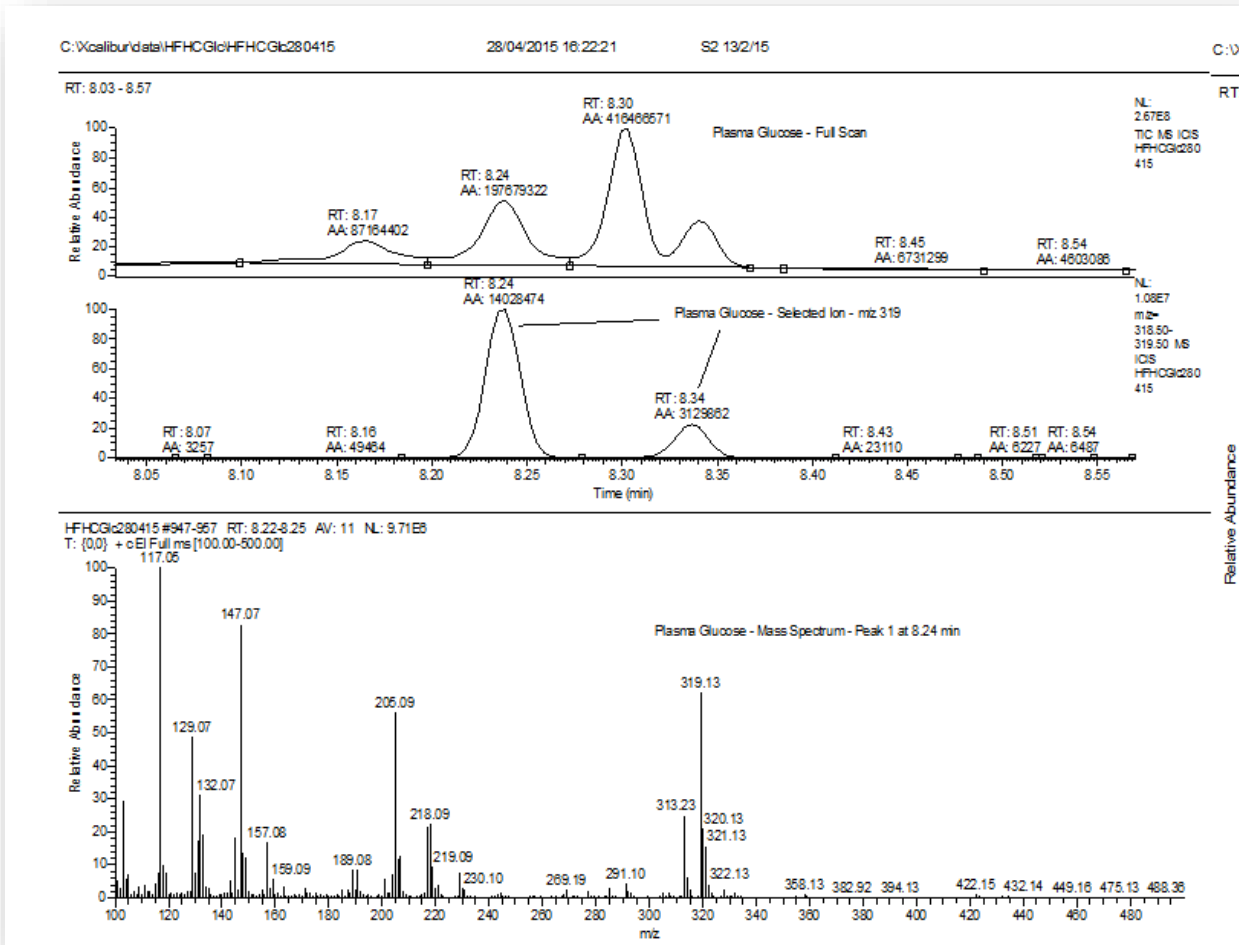
We agree to start this study on **07/03/2018**, as previously discussed.

Please be aware this confirmation of capacity is provided on the understanding and provision that you will follow the conditions set out in the attached document (NUH R&I of Confirmation of Capacity and Capability Conditions, v1).

The following documents were reviewed:

Document	Dated	Version
Copies of advertisement materials for research participants [ECLIPSE Poster]	14 September 2017	2.0
Costing template (commercial projects)	03 November 2017	
Evidence of Sponsor insurance or indemnity (non NHS Sponsors only)		
GP/consultant information sheets or letters [GP Information Sheet]		
HRA Schedule of Events [SoE Site]	05 January 2018	1
HRA Statement of Activities [SoA Site]	05 January 2018	1.0
IRAS Application Form [IRAS_Form_19122017]	19 December 2017	

Appendix 3 Measuring Endogenous Glucose Production



Atoms Percent Excess: GC/MS calculations of glucose isotopic enrichment

1. Basal EGP

EGP was calculated at baseline and during low dose insulin infusion. The difference between these calculations was measured as %EGP suppression during low dose hyperinsulinaemia.

The following equations were used to calculate basal EGP, at -20 and 0 min post-tracer equilibrium.

The mean of the two values was then calculated and reported as basal EGP.

$$APE = (TTR_{\text{measured}} - TTR_{\text{baseline}}) / [1 + (TTR_{\text{measured}} - TTR_{\text{baseline}})] \times 100$$

Where APE = atoms percent excess, TTR_{measured} = tracer: tracee ratio at timepoint of interest (-20 and 0 min samples) and TTR_{baseline} = tracer: tracee ratio at baseline (prior to tracer infusion).

$$\text{EGP } (\mu\text{mol/kg/min}) = \text{Ra} = \text{F} / \text{APE} \times 100$$

Where F = the continuous tracer infusion rate (0.222 $\mu\text{mol/kg/min}$).

2. EGP during low dose hyperinsulinaemia (stage 1 of the insulin clamp):

The following calculation was used to determine EGP during low dose hyperinsulinaemic conditions:

$$\text{Non-steady state Ra} = \{ \text{F} - \text{pV} \times [(\text{C1} + \text{C2}) / 2] \times [(\text{APE2} - \text{APE1}) / (\text{t2} - \text{t1})] \}$$

Where Ra continuous is the Ra contribution from the continuous tracer infusion ($\mu\text{mol/kg/min}$), pV is the fractional pool of distribution (a constant of 160mL/kg was used in this study), C1, C2, APE1, APE2, t1 and t2 are glucose concentrations (mmol/l), enrichment (APE) and time (min) at consecutive timepoints of interest (in this study, at 90, 105 and 120 minutes into the clamp).

Appendix 4 Protocol Summary for the ECLIPSE Study

	SCREENING	RANDOMISATION SCHEDULE						
		BASELINE						
STUDY ACTIVITIES	Screening visit	Baseline visit (2 days):	Monitoring visit 1	Monitoring visit 2	Monitoring visit 3	Monitoring visit 4	Monitoring visit 5	End of Study visit (2 days):
<i>Study visit</i>	1	2	3	4	5	6	7	8
<i>Time</i>	-28 days (week -4)	Day+ 1 and +2 (week 1)	+28 days (week 4)	+56 days (week 8)	+84 days (week 12)	+112 days (week 16)	+140 days (week 20)	Day +168 and +169 (week 24)
<i>Informed consent.</i>	✓							
<i>Medical History</i>	✓							
<i>Physical examination</i>	✓	✓ (Day 2)	✓	✓	✓	✓	✓	✓
<i>Fasting bloods incl. carnitine</i>	✓	✓ (Day 2)	✓	✓	✓	✓	✓	✓
<i>Screening ultrasound scan</i>	✓							
<i>Review dietary intake</i>		✓	✓	✓	✓	✓	✓	✓
<i>Calculate energy requirements</i>		✓	✓	✓	✓	✓	✓	
<i>Accelerometry</i>		✓	✓	✓	✓	✓	✓	
<i>Height, weight, waist/hip circumference</i>	✓		✓	✓	✓	✓	✓	
<i>12-lead ECG</i>	✓							
<i>MRI/MRS scan</i>		✓ (Day 1)						✓ (Day 1)
<i>DEXA scan</i>		✓ (Day 2)						✓ (Day 2)
<i>Dual-step insulin clamp</i>		✓ (Day 2)						✓ (Day 2)
<i>Indirect calorimetry</i>		✓ (Day 2)						✓ (Day 2)
<i>Muscle biopsies</i>		✓ (Day 2)						✓ (Day 2)
<i>Bioimpedance</i>			✓	✓	✓	✓	✓	
<i>Study supplements dispensed</i>		✓ (Day 2)	✓	✓	✓	✓	✓	

Appendix 5 Example Data Collection Sheet for Clamp Studies

ECLIPSE Study

Clamp Sheet

Subject ID :

Date :/...../.....

Visit No:1 2

Height: cm

Weight: kg

Surface area:m²

Calculations:

15mls of stock solution are provided by pharmacy @ 200mg/ml

Tracer Bolus;

Take 5ml of stock solution (1000mg glucose) and make up to 50ml with 0.9% saline in a 50ml syringe to give a 20mg/ml solution

4mg x _____ kg = _____ mg / 20 = _____ ml bolus delivered over 1min

Tracer Infusion;

Take 5ml of stock solution (1000mg) and make up to 50ml with 0.9% saline in a 50ml syringe

0.04mg x _____ kg x 60min = _____ / (20mg/ml) = _____ ml/hr
6 hour Infusion @

Glucose Infusion;

Take 5ml of stock solution (1000mg) and add to a 500ml bag of 20% glucose to give ~1% enrichment

_____ m ²	x	<u>15</u>	=	x 7.52 = mls/hr
0.5				40		x 3.28 = mls/hr
						x 2.99 = mls/hr
						x 2.82 = mls/hr
						x 2.57 = mls/hr
						x 2.40 = mls/hr

_____ m ²	x	<u>60</u>	=	x 7.52 = mls/hr
0.5				40		x 3.28 = mls/hr
						x 2.99 = mls/hr
						x 2.82 = mls/hr
						x 2.57 = mls/hr

x 2.40 = mls/hr

Glucose @ 2mg / kg / min @ 4 min

Glucose @ 2.5mg / kg / min @ 10 min

$\frac{2 \times \text{kg}}{200\text{mg}} \times 60 = \dots\dots\dots\text{ml/hr}$

$\frac{2.5 \times \text{kg}}{200\text{mg}} \times 60 = \dots\dots\dots\text{ml/hr}$

Infusion start time:

Time	Ins Inf ⁿ	Blood G	G Inf ⁿ	Ins / tracer sample	Calorimetry	Comments
-120				1		No AV diff
-20						
-10						
-5				2		
0						
2						
4						
5						
6						
8						
10						
15						
20						
25						
30						
35						
40						
45						
50						
55						
60						
65						
70						
75						
80						
85						
90				3		
95						
100						
105				4		
110						
115						
120				5		
122						
124						
125						
126						
128						

130						
135						
140						
145						
150						
Time	Ins Inf ⁿ	Blood G	G Inf ⁿ	Ins / tracer sample	Calorimetry	Comments
155						
160						
165						
170						
175						
180						
185						
190						
195						
200						
205						
210				6		
215						
220						
225				7		
230						
235						
240				8		
	Subject	fed and	insulin	discontinued		
250						
255						
260						
265						
270						
275						
280						
285						
290						
295						
300						
305						

Comments:

AV-V Difference measures PT Carnitine study

Participant ID:

Visit Number: 1 2

Date :

Time point	AV Glucose mmol/l	V Glucose mmol/l	Comments
Pre			
90			
105			
120			
210			
225			
240			

Time point	Sys 1 mm	Sys 2 mm	Sys 3 mm	Dia 1 mm	Dia 2 mm	Dia 3 mm	Velocity cm ²
Pre							
90							
105							
120							
210							
225							
240							

REFERENCES

- ¹ Byrne CD, Targher G. NAFLD: a multisystem disease. *J Hepatol.* 2015 Apr;62(1 Suppl):S47-64.
- ² Estes C, Razavi H, Loomba R, Younossi Z, Sanyal AJ. Modeling the epidemic of nonalcoholic fatty liver disease demonstrates an exponential increase in burden of disease. *Hepatology.* 2018 Jan;67(1):123-133
- ³ Younossi ZM, Koenig AB, Abdelatif D, Fazel Y, Henry L, Wymer M. Global epidemiology of nonalcoholic fatty liver disease-Meta-analytic assessment of prevalence, incidence, and outcomes. *Hepatology.* 2016 Jul;64(1):73-84.
- ⁴ Bellentani S, Scaglioni F, Marino M, Bedogni G. Epidemiology of non-alcoholic fatty liver disease. *Dig Dis.* 2010;28(1):155-61.
- ⁵ DeWeerd S. Disease progression: Divergent paths. *Nature.* 2017 Nov 23;551(7681).
- ⁶ Younossi ZM, Blissett D, Blissett R, Henry L, Stepanova M, Younossi Y, Racila A, Hunt S, Beckerman R. The economic and clinical burden of nonalcoholic fatty liver disease in the United States and Europe. *Hepatology.* 2016 Nov;64(5):1577-1586.
- ⁷ Drew L. Drug development: Sprint finish. *Nature.* 2017 Nov 23;551(7681).
- ⁸ Thiagarajan P, Aithal GP. Drug Development for Nonalcoholic Fatty Liver Disease: Landscape and Challenges. *J Clin Exp Hepatol.* 2019 Jul-Aug;9(4):515-521
- ⁹ Hagström H, Nasr P, Ekstedt M, Hammar U, Stal P, Hultcrantz R, et al. Fibrosis stage but not NASH predicts mortality and time to development of severe liver disease in biopsy-proven NAFLD. *Journal of Hepatology* 2017;67(6):1265-73.
- ¹⁰ Dulai PS, Singh S, Patel J, Soni M, Prokop LJ, Younossi Z, Sebastiani G, Ekstedt M, Hagström H, Nasr P, Stal P, Wong VW, Kechagias S, Hultcrantz R, Loomba R. Increased risk of mortality by fibrosis stage in nonalcoholic fatty liver disease: Systematic review and meta-analysis. *Hepatology.* 2017 May;65(5):1557-1565.
- ¹¹ Sanyal AJ, Brunt EM, Kleiner DE, et al. Endpoints and Clinical Trial Design for Nonalcoholic Steatohepatitis. *Hepatology.* 2011;54(1):344-353.
- ¹² Vilar-Gomez E, Chalasani N. Non-invasive assessment of non-alcoholic fatty liver disease: clinical prediction rules and blood-based biomarkers. *J Hepatol* 2018;68:305–315
- ¹³ Loomba R. Role of imaging-based biomarkers in NAFLD: Recent advances in clinical application and future research directions. *J Hepatol.* 2018 Feb;68(2):296-304.
- ¹⁴ Hannah WN, Torres DM, Harrison SA. Nonalcoholic Steatohepatitis and Endpoints in Clinical Trials. *Gastroenterology & Hepatology.* 2016;12(12):756-763.

-
- ¹⁵ Jornayvaz FR, Samuel VT, Shulman GI. The Role of Muscle Insulin Resistance in the Pathogenesis of Atherogenic Dyslipidemia and Nonalcoholic Fatty Liver Disease Associated with the Metabolic Syndrome. *Annual review of nutrition*. 2010;30:273-290. doi:10.1146/annurev.nutr.012809.104726.
- ¹⁶ Laurens C, Moro C. Intramyocellular fat storage in metabolic diseases. *Hormone molecular biology and clinical investigation*. 2016;26(1):43-52.
- ¹⁷ Shulman GI. Ectopic fat in insulin resistance, dyslipidemia, and cardiometabolic disease. *N Engl J Med*. 2014 Sep 18;371(12):1131-41.
- ¹⁸ Petersen KF, Dufour S, Savage DB, Bilz S, Solomon G, Yonemitsu S, Cline GW, Befroy D, Zeman L, Kahn BB, Papademetris X, Rothman DL, Shulman GI. The role of skeletal muscle insulin resistance in the pathogenesis of the metabolic syndrome. *Proc Natl Acad Sci U S A*. 2007 Jul 31;104(31):12587-94
- ¹⁹ Flannery C, Dufour S, Rabøl R, Shulman GI, Petersen KF. Skeletal muscle insulin resistance promotes increased hepatic de novo lipogenesis, hyperlipidemia, and hepatic steatosis in the elderly. *Diabetes*. 2012 Nov;61(11):2711-7.
- ²⁰ Rabøl R, Petersen KF, Dufour S, Flannery C, Shulman GI. Reversal of muscle insulin resistance with exercise reduces postprandial hepatic de novo lipogenesis in insulin resistant individuals. *Proc Natl Acad Sci U S A*. 2011 Aug 16;108(33):13705-9.
- ²¹ Bril F, Barb D, Portillo-Sanchez P, Biernacki D, Lomonaco R, Suman A, Weber MH, Budd JT, Lupi ME, Cusi K. Metabolic and histological implications of intrahepatic triglyceride content in nonalcoholic fatty liver disease. *Hepatology*. 2017 Apr;65(4):1132-1144.
- ²² Kuhlmann J, Neumann-Haefelin C, Belz U, Kalisch J, Juretschke HP, Stein M, et al. Intramyocellular lipid and insulin resistance: a longitudinal in vivo 1H-spectroscopic study in Zucker diabetic fatty rats. *Diabetes*. 2003;52(1):138-44.
- ²³ Weiss R, Taksali SE, Dufour S, Yeckel CW, Papademetris X, Cline G, et al. The "obese insulin-sensitive" adolescent: importance of adiponectin and lipid partitioning. *The Journal of clinical endocrinology and metabolism*. 2005;90(6):3731-7.
- ²⁴ Boden G, Lebed B, Schatz M, Homko C, Lemieux S. Effects of acute changes of plasma free fatty acids on intramyocellular fat content and insulin resistance in healthy subjects. *Diabetes*. 2001;50(7):1612-7.
- ²⁵ Krssak M, Falk Petersen K, Dresner A, et al. Intramyocellular lipid concentrations are correlated with insulin sensitivity in humans: a 1H NMR spectroscopy study. *Diabetologia* 1999; 42: 113–16
- ²⁶ Perseghin G, Scifo P, De Cobelli F, Pagliato E, Battezzati A, Arcelloni C, Vanzulli A, Testolin G, Pozza G, Del Maschio A, Luzi L. Intramyocellular triglyceride content is a determinant of in vivo insulin resistance in humans: a 1H-13C nuclear magnetic resonance spectroscopy assessment in offspring of type 2 diabetic parents. *Diabetes*. 1999 Aug;48(8):1600-6.
- ²⁷ Randle PJ, Garland PB, Hales CN, Newsholme EA. The glucose fatty-acid cycle: its role in insulin sensitivity and the metabolic disturbances of diabetes mellitus. *Lancet* 1963;1:785-9
- ²⁸ Constantin-Teodosiu D, Constantin D, Stephens F, Laithwaite D, Greenhaff PL. The role of FOXO and PPAR transcription factors in diet-mediated inhibition of PDC activation and carbohydrate

oxidation during exercise in humans and the role of pharmacological activation of PDC in overriding these changes. *Diabetes*. 2012 May; 61(5):1017-24.

²⁹ Roden M, Price TB, Perseghin G, et al. Mechanism of free fatty acid-induced insulin resistance in humans. *Journal of Clinical Investigation*. 1996;97(12):2859-2865.

³⁰ Samuel VT, Petersen KF, Shulman GI. Lipid-induced insulin resistance: unravelling the mechanism. *Lancet* 2010;375(9733):2267-77

³¹ Lebon V, Dufour S, Petersen KF, et al. Effect of triiodothyronine on mitochondrial energy coupling in human skeletal muscle. *J Clin Invest* 2001; **108**: 733–37.

³² Al-Serri A, Anstee QM, Valenti L, et al. The SOD2 C47T polymorphism influences NAFLD fibrosis severity: evidence from case-control and intra-familial allele association studies. *Journal of Hepatology*. 2012;56:448–54.

³³ Dongiovanni P, Anstee QM, Valenti L. Genetic Predisposition in NAFLD and NASH: Impact on Severity of Liver Disease and Response to Treatment. *Current Pharmaceutical Design*. 2013;19(29):5219-5238.

³⁴ Sunny NE, Parks EJ, Browning JD, Burgess SC. Excessive hepatic mitochondrial TCA cycle and gluconeogenesis in humans with nonalcoholic fatty liver disease. *Cell Metab*. 2011 Dec 7;14(6):804-10.

³⁵ Rector R.S., Morris E.M., Ridenhour S., Meers G.M., Hsu F.F., Turk J., Ibdah J.A. Selective hepatic insulin resistance in a murine model heterozygous for a mitochondrial trifunctional protein defect. *Hepatology*. 2013; 57:2213–2223

³⁶ Morino K, Petersen KF, Dufour S, Befroy D, Frattini J, Shatzkes N, et al. Reduced mitochondrial density and increased IRS-1 serine phosphorylation in muscle of insulin-resistant offspring of type 2 diabetic parents. *The Journal of clinical investigation*. 2005;115(12):3587-93.

³⁷ Bellafante E, Murzilli S, Salvatore L, Latorre D, Villani G, Moschetta A. Hepatic-specific activation of peroxisome proliferator-activated receptor γ coactivator-1 β protects against steatohepatitis. *Hepatology*. 2013 Apr;57(4):1343-56.

³⁸ Sunny, Nishanth E., et al. (2011). "Excessive Hepatic Mitochondrial TCA Cycle and Gluconeogenesis in Humans with Nonalcoholic Fatty Liver Disease." *Cell Metab* **14**(6): 804-810.

³⁹ Petersen KF, Befroy DE, Dufour S, Rothman DL, Shulman GI. Assessment of Hepatic Mitochondrial Oxidation and Pyruvate Cycling in NAFLD by (13)C Magnetic Resonance Spectroscopy. *Cell Metab*. 2016 Jul 12;24(1):167-71

⁴⁰ Koliaki, C., et al. (2015). "Adaptation of hepatic mitochondrial function in humans with non-alcoholic fatty liver is lost in steatohepatitis." *Cell Metab* **21**(5): 739-746.

⁴¹ Valkovič L, Klepochová R, Krššák M. Multinuclear Magnetic Resonance Spectroscopy of Human Skeletal Muscle Metabolism in Training and Disease, *Muscle Cell and Tissue – Current Status of Research Field*, Kunihiro Sakuma, IntechOpen, (October 10, 2018). DOI: 10.5772/intechopen.77107. Available from: <https://www.intechopen.com/books/muscle-cell-and-tissue-current-status-of->

[research-field/multinuclear-magnetic-resonance-spectroscopy-of-human-skeletal-muscle-metabolism-in-training-and-dis.](#) (accessed 1/5/2020)

⁴² Noren B, Dahlqvist O, Lundberg P, Almer S, Kechagias S, Ekstedt M, Franzén L, Wirell S, Smedby O. Separation of advanced from mild fibrosis in diffuse liver disease using 31P magnetic resonance spectroscopy. *Eur J Radiol.* 2008 May;66(2):313-20.

⁴³ Nair S, Chacko VP, Arnold C, Diehl AM. Hepatic ATP reserve and efficiency of replenishing: comparison between obese and nonobese normal individuals. *Am J Gastroenterology* 2003;98(2):466e70.

⁴⁴ Abdelmalek, M. F., et al. (2012). "Higher dietary fructose is associated with impaired hepatic adenosine triphosphate homeostasis in obese individuals with type 2 diabetes." *Hepatology* **56**(3): 952-960.

⁴⁵ Bawden, S. J., et al. (2016). "Investigating the effects of an oral fructose challenge on hepatic ATP reserves in healthy volunteers: A (31)P MRS study." *Clin Nutr* **35**(3): 645-649.

⁴⁶ Szendroedi, J., et al. (2009). "Abnormal hepatic energy homeostasis in type 2 diabetes." *Hepatology* **50**(4): 1079-1086.

⁴⁷ Schmid AI, Szendroedi J, Chmelik M, Krssák M, Moser E, Roden M. Liver ATP synthesis is lower and relates to insulin sensitivity in patients with type 2 diabetes. *Diabetes Care.* 2011 Feb;34(2):448-53.

⁴⁸ Valkovic, L., et al. (2014). "Application of localized 31P MRS saturation transfer at 7 T for measurement of ATP metabolism in the liver: reproducibility and initial clinical application in patients with non-alcoholic fatty liver disease." *Eur Radiol* 24(7): 1602-1609.

⁴⁹ Traussnigg S, Kienbacher C, Gajdošík M, et al. Ultra-high-field magnetic resonance spectroscopy in non-alcoholic fatty liver disease: Novel mechanistic and diagnostic insights of energy metabolism in non-alcoholic steatohepatitis and advanced fibrosis. *Liver Int.* 2017;37(10):1544-1553.

⁵⁰ Sevastianova K, Santos A, Kotronen A, et al. Effect of short-term carbohydrate overfeeding and long-term weight loss on liver fat in overweight humans. *Am J Clin Nutr* 2012; 96:727-34.

⁵¹ Browning JD, Baker JA, Rogers T, et al. Short-term weight loss and hepatic triglyceride reduction: evidence of a metabolic advantage with dietary carbohydrate restriction. *Am J Clin Nutr* 2011; 93:1048-52.

⁵² Haufe S, Engeli S, Kast P, et al. Randomised comparison of reduced fat and reduced carbohydrate hypocaloric diets on intrahepatic fat in overweight and obese human subjects. *Hepatology* 2011;53:1504-14.

⁵³ Rivellese AA, Giacco R, Annuzzi G, et al. Effects of monounsaturated vs. saturated fat on postprandial lipemia and adipose tissue lipases in type 2 diabetes. *Clin Nutr* 2008;27:133-41.

⁵⁴ Parry SA, Hodson L. Influence of dietary macronutrients on liver fat accumulation and metabolism. *J Investig Med.* 2017 Dec;65(8):1102-1115

⁵⁵ Martinez Steele E, Raubenheimer D, Simpson SJ, Baraldi LG, Monteiro CA. Ultra-processed foods, protein leverage and energy intake in the USA. *Public health nutrition.* 2018;21(1):114-24.

-
- ⁵⁶ Simpson SJ, Raubenheimer D, Cogger VC, Macia L, Solon-Biet SM, Le Couteur DG, George J. The nutritional geometry of liver disease including non-alcoholic fatty liver disease. *J Hepatol.* 2018 Feb;68(2):316-325
- ⁵⁷ Markova M, Pivovarova O, Hornemann S, Sucher S, Frahnw T, Wegner K, Machann J, Petzke KJ, Hierholzer J, Lichtinghagen R, et al (2016). Isocaloric diets high in animal or plant protein reduce liver fat and inflammation in individuals with type 2 diabetes. *Gastroenterology* 2017;152: 571–585
- ⁵⁸Freidoony L, Kong ID. Practical approaches to the nutritional management of nonalcoholic fatty liver disease. *Integr Med Res.* 2014 Dec;3(4):192-197
- ⁵⁹ Chen G, Ni Y, Nagata N, Xu L, Ota T (2016). Micronutrient antioxidants and nonalcoholic fatty liver disease. *Int J Mol Sci.* 17(9):137
- ⁶⁰ Rochlani Y, Pothineni NV, Kovelamudi S, Mehta JL. Metabolic syndrome: pathophysiology, management, and modulation by natural compounds. *Therapeutic advances in cardiovascular disease.* 2017;11(8):215-25.
- ⁶¹ Savic D, Hodson L, Neubauer S, Pavlides M. The Importance of the Fatty Acid Transporter L-Carnitine in Non-Alcoholic Fatty Liver Disease (NAFLD). *Nutrients.* 2020;12(8):E2178.
- ⁶² Uziel G, Garavaglia B, Di Donato S. Carnitine stimulation of pyruvate dehydrogenase complex (PDHC) in isolated human skeletal muscle mitochondria. *Muscle Nerve.* 1988 Jul;11(7):720-4
- ⁶³ Noland RC , Koves TR , Seiler SE , Lum H , Lust RM , Ilkayeva O , et al. Carnitine insufficiency caused by aging and overnutrition compromises mitochondrial performance and metabolic control. *J Biol Chem* 2009;284(34):22840–52 .
- ⁶⁴ Power RA , Hulver MW , Zhang JY , Dubois J , Marchand RM , Ilkayeva O , et al. Carnitine revisited: potential use as adjunctive treatment in diabetes. *Diabetologia* 2007;50(4):824–32 .
- ⁶⁵ Gulewitsch W, Krimberg R. Zur kenntnis der extractivstoffe der muskeln. *Physiol Chem* 1905;45:326–330.
- ⁶⁶ Kutscher, F. Über Liebig's Fleischextrakt. *Zeitschr. f. Untersuchung d. Nahr.-u. Genußmittel.* **10**, 528–537 (1905).
- ⁶⁷ Fraenkel G, Blewett M. The vitamin B-complex requirements of several insects. *Biochem J.* 1943;37:686–92.
- ⁶⁸ Fraenkel G, Blewett M. The importance of folic acid and unidentified members of the vitamin B complex in the nutrition of certain insects. *Biochem. J.* 1947; 41:469–475.
- ⁶⁹ MacFarlane JE. (1955) Carnitine and fat metabolism in *Tenebrio molitor* [dissertation]. Urbana (IL) University of Illinois; 1955.
- ⁷⁰ Fritz, I.B. Action of carnitine on long chain fatty acid oxidation by liver. *Am. J. Physiol.* **1959**, 197, 297–304

-
- ⁷¹ Bode, C and Klingenberg M. Carnitine and fatty acid oxidation in mitochondria of various organs. *Biochim Biophys Acta* 1964; 84 (1); 93-95
- ⁷² Childress CC, Sacktor B & Travnor D. Function of carnitine in the fatty acid-oxidase deficient insect flight muscle. *J Biol Chem* 1966; 242, 754–760.
- ⁷³ Wall BT, Stephens FB, van Loon LJC, Constantin-Teodosiu D, Macdonald IA, Greenhaff PL. Reduced fat oxidation during high intensity, submaximal exercise: is the availability of carnitine important? *European Journal of Sport Science*. 2013;13(2):191-9.
- ⁷⁴ Wall B, Porter C. *Carnitine Metabolism and Human Nutrition* (2014) ISBN 9781466554269
- ⁷⁵ Wall BT, Stephens FB, Constantin-Teodosiu D, Marimuthu K, Macdonald IA, Greenhaff PL. Chronic oral ingestion of L-carnitine and carbohydrate increases muscle carnitine content and alters muscle fuel metabolism during exercise in humans. *J Physiol*. 2011;589(Pt 4):963-973.
- ⁷⁶ Stephens FB, Constantin-Teodosiu D, Greenhaff PL. New insights concerning the role of carnitine in the regulation of fuel metabolism in skeletal muscle. *J Physiol*. 2007 Jun 1; 581(Pt 2):431-44.
- ⁷⁷ Rebouche CJ. Kinetics, pharmacokinetics, and regulation of L-carnitine and acetyl-L-carnitine metabolism. *Annals of the New York Academy of Sciences*. 2004; 1033:30-41.
- ⁷⁸ Rebouche CJ, Chenard CA. Metabolic fate of dietary carnitine in human adults: identification and quantification of urinary and fecal metabolites. *The Journal of nutrition*. 1991;121(4):539-46.
- ⁷⁹ Sahajwalla CG, Helton ED, Purich ED, Hoppel CL, Cabana BE. Multiple-dose pharmacokinetics and bioequivalence of L-carnitine 330-mg tablet versus 1-g chewable tablet versus enteral solution in healthy adult male volunteers. *J Pharm Sci*. 1995 May;84(5):627-33.
- ⁸⁰ Rebouche CJ. Quantitative estimation of absorption and degradation of a carnitine supplement by human adults. *Metabolism*. 1991 Dec;40(12):1305-10.
- ⁸¹ Arenas J, Ricoy JR, Encinas AR, Pola P, D'Iddio S, Zeviani M, Didonato S, Corsi M. Carnitine in muscle, serum, and urine of nonprofessional athletes: effects of physical exercise, training, and L-carnitine administration. *Muscle Nerve*. 1991 Jul;14(7):598-604.
- ⁸² Stephens FB, Constantin-Teodosiu D, Laithwaite D, Simpson EJ, Greenhaff PL. Insulin stimulates L-carnitine accumulation in human skeletal muscle. *FASEB journal : official publication of the Federation of American Societies for Experimental Biology*. 2006;20(2):377-9.
- ⁸³ Stephens FB, Evans CE, Constantin-Teodosiu D, Greenhaff PL. Carbohydrate ingestion augments L-carnitine retention in humans. *Journal of applied physiology (Bethesda, Md : 1985)*. 2007;102(3):1065-70.
- ⁸⁴ Angelini C, Vergani L, Martinuzzi A. Clinical and biochemical aspects of carnitine deficiency and insufficiency: transport defects and inborn errors of beta-oxidation. *Critical reviews in clinical laboratory sciences*. 1992;29(3-4):217-42.
- ⁸⁵ Evans AM, Fornasini G. Pharmacokinetics of L-carnitine. *Clinical pharmacokinetics*. 2003;42(11):941-67

-
- ⁸⁶ Porter C, Constantin-Teodosiu D, Constantin D, Leighton B, Poucher SM, Greenhaff PL. Muscle carnitine availability plays a central role in regulating fuel metabolism in the rodent. *J Physiol.* 2017;595(17):5765-80.
- ⁸⁷ Croci I *et al.* (2013). Whole-body substrate metabolism is associated with disease severity in patients with non-alcoholic fatty liver disease. *Gut* 62(11): 1625-33.
- ⁸⁸ Simoneau JA, Veerkamp JH, Turcotte LP, Kelley DE. Markers of capacity to utilize fatty acids in human skeletal muscle: relation to insulin resistance and obesity and effects of weight loss. *FASEB J.* 1999 Nov;13(14):2051-60.
- ⁸⁹ Luci S, Hirche F, Eder K. Fasting and caloric restriction increases mRNA concentrations of novel organic cation transporter-2 and carnitine concentrations in rat tissues. *Ann Nutr Metab.* 2008;52(1):58-67
- ⁹⁰ Ferrannini E, Buzzigoli G, Bevilacqua S, Boni C, Del Chiaro D, Oleggini M, Brandi L, Maccari F. Interaction of carnitine with insulin-stimulated glucose metabolism in humans. *Am J Physiol.* 1988 Dec;255(6 Pt 1):E946-52.
- ⁹¹ Mingrone G, Greco AV, Capristo E, Benedetti G, Giancaterini A, De Gaetano A, Gasbarrini G. L-carnitine improves glucose disposal in type 2 diabetic patients. *J Am Coll Nutr.* 1999 Feb;18(1):77-82.
- ⁹² Stephens FB, Constantin-Teodosiu D, Laithwaite D, Simpson EJ, Greenhaff PL. An acute increase in skeletal muscle carnitine content alters fuel metabolism in resting human skeletal muscle. *J Clin Endocrinol Metab.* 2006 Dec;91(12):5013-8.
- ⁹³ Stephens FB, Wall BT, Marimuthu K, Shannon CE, Constantin-Teodosiu D, Macdonald IA, Greenhaff PL. Skeletal muscle carnitine loading increases energy expenditure, modulates fuel metabolism gene networks and prevents body fat accumulation in humans. *J Physiol.* 2013 Sep 15;591(18):4655-66
- ⁹⁴ Muoio DM, Noland RC, Kovalik JP, Seiler SE, Davies MN, DeBalsi KL, Ilkayeva OR, Stevens RD, Kheterpal I, Zhang J, Covington JD, Bajpeyi S, Ravussin E, Kraus W, Koves TR, Mynatt RL. Muscle-specific deletion of carnitine acetyltransferase compromises glucose tolerance and metabolic flexibility. *Cell Metab.* 2012 May 2;15(5):764-77.
- ⁹⁵ Xu Y, Jiang W, Chen G, Zhu W, Ding W, Ge Z, Tan Y, Ma T, Cui G. L-carnitine treatment of insulin resistance: A systematic review and meta-analysis. *Adv Clin Exp Med.* 2017;26(2):333-338
- ⁹⁶ Savic D, Ball V, Pavlides M, Heather LC, Tyler DJ. THU-367-Linking diabetic cardiovascular disease with non-alcoholic fatty liver disease through L-carnitine: A hyperpolarized MRS study. *Journal of hepatology.* 2019;70(1, Supplement):e315-e6
- ⁹⁷ Corbin, Karen D.; Zeisel, Steven H. Choline metabolism provides novel insights into nonalcoholic fatty liver disease and its progression, *Current Opinion in Gastroenterology*: March 2012 - Volume 28 - Issue 2 - p 159-165
- ⁹⁸ Francque SM, van der Graaff D, Kwanten WJ. Non-alcoholic fatty liver disease and cardiovascular risk: Pathophysiological mechanisms and implications. *J Hepatol.* 2016 Aug;65(2):425-43
- ⁹⁹ Muoio DM. Metabolic inflexibility: when mitochondrial indecision leads to metabolic gridlock. *Cell.* 2014;159(6):1253-62.

-
- ¹⁰⁰ Smith RL, Soeters MR, Wust RCI, Houtkooper RH. Metabolic Flexibility as an Adaptation to Energy Resources and Requirements in Health and Disease. *Endocrine reviews*. 2018;39(4):489-517.
- ¹⁰¹ Goedeke L, Bates J, Vatner DF, Perry RJ, Wang T, Ramirez R, et al. Acetyl-CoA Carboxylase Inhibition Reverses NAFLD and Hepatic Insulin Resistance but Promotes Hypertriglyceridemia in Rodents. *Hepatology (Baltimore, Md)*. 2018;68(6):2197-211.
- ¹⁰² Perry RJ, Camporez JG, Kursawe R, Titchenell PM, Zhang D, Perry CJ, et al. Hepatic acetyl CoA links adipose tissue inflammation to hepatic insulin resistance and type 2 diabetes. *Cell*. 2015;160(4):745-58.
- ¹⁰³ Patterson R. E., Kalavalapalli S., Williams C. M., et al. Lipotoxicity in steatohepatitis occurs despite an increase in tricarboxylic acid cycle activity. *American Journal of Physiology Endocrinology and Metabolism*. 2016;310(7):E484–E494.
- ¹⁰⁴ Foster DW. Malonyl-CoA: the regulator of fatty acid synthesis and oxidation. *The Journal of clinical investigation*. 2012;122(6):1958-9.
- ¹⁰⁵ Bruls YM, de Ligt M, Lindeboom L, Phielix E, Havekes B, Schaart G, et al. Carnitine supplementation improves metabolic flexibility and skeletal muscle acetylcarnitine formation in volunteers with impaired glucose tolerance: A randomised controlled trial. *EBioMedicine*. 2019;49:318-30.
- ¹⁰⁶ Krahenbuhl S, Reichen J. Carnitine metabolism in patients with chronic liver disease. *Hepatology (Baltimore, Md)*. 1997;25(1):148-53.
- ¹⁰⁷ Schooneman MG, Vaz FM, Houten SM, Soeters MR. Acylcarnitines: reflecting or inflicting insulin resistance? *Diabetes*. 2013;62(1):1-8.
- ¹⁰⁸ Rudman D, Sewell CW, Ansley JD. Deficiency of carnitine in cachectic cirrhotic patients. *The Journal of clinical investigation*. 1977;60(3):716-23.
- ¹⁰⁹ Brady LJ, Brady PS, Albers L, Davis AT, Hoppel CL. Carnitine metabolism in lean and obese Zucker rats during starvation. *The Journal of nutrition*. 1986;116(4):668-74.
- ¹¹⁰ Harper P, Wadstrom C, Backman L, Cederblad G. Increased liver carnitine content in obese women. *The American journal of clinical nutrition*. 1995;61(1):18-25.
- ¹¹¹ DeFronzo RA, Tobin JD, Andres R. Glucose clamp technique: a method for quantifying insulin secretion and resistance. *The American journal of physiology*. 1979;237(3):E214-23.
- ¹¹² DeFronzo RA, Tripathy D. Skeletal muscle insulin resistance is the primary defect in type 2 diabetes. *Diabetes Care*. 2009;32 Suppl 2(Suppl 2):S157–S163.
- ¹¹³ Heise T, Zijlstra E, Nosek L, Heckermann S, Plum-Morschel L, Forst T. Euglycaemic glucose clamp: what it can and cannot do, and how to do it. *Diabetes, obesity & metabolism*. 2016;18(10):962-72.
- ¹¹⁴ Tam CS, Xie W, Johnson WD, Cefalu WT, Redman LM, Ravussin E. Defining insulin resistance from hyperinsulinemic-euglycemic clamps. *Diabetes Care*. 2012;35(7):1605–1610.

-
- ¹¹⁵ Brooks DC, Black PR, Arcangeli MA, Aoki TT, Wilmore DW. The heated dorsal hand vein: an alternative arterial sampling site. *JPEN J Parenter Enteral Nutr.* 1989 Jan-Feb;13(1):102-5
- ¹¹⁶ Sonnenberg GE, Keller U: Sampling of arterialized heated-hand venous blood as a noninvasive technique for the study of ketone body kinetics in man. *Metabolism* 1982; 31:1-5
- ¹¹⁷ McGuire EA, Helderman JH, Tobin JD, Andres R, Berman M. Effects of arterial versus venous sampling on analysis of glucose kinetics in man. *J Appl Physiol.* 1976;41(4):565-573
- ¹¹⁸ Liu D, Moberg E, Kollind M, Lins PE, Adamson U, Macdonald IA. Arterial, arterialized venous, venous and capillary blood glucose measurements in normal man during hyperinsulinaemic euglycaemia and hypoglycaemia. *Diabetologia.* 1992;35(3):287-290.
- ¹¹⁹ Nauck M, Liess H, Siegel E, et al. Critical evaluation of the 'heated-hand-technique' for obtaining 'arterialized' venous blood: incomplete arterialization and alterations in glucagon responses. *Clin Physiol* 1992; 12, 537–552.
- ¹²⁰ Kim I-Y, Suh S-H, Lee I-K, Wolfe RR. Applications of stable, nonradioactive isotope tracers in in vivo human metabolic research. *Experimental & molecular medicine.* 2016;48(1):e203-e.
- ¹²¹ Steele R. Influences of glucose loading and of injected insulin on hepatic glucose output. *Ann N Y Acad Sci* 1959; 82: 420-30.
- ¹²² Vella A, Rizza RA. Application of isotopic techniques using constant specific activity or enrichment to the study of carbohydrate metabolism. *Diabetes.* 2009;58(10):2168-2174.
- ¹²³ Choukem SP, Gautier JF. How to measure hepatic insulin resistance? *Diabetes & metabolism.* 2008;34(6 Pt 2):664-73.
- ¹²⁴ Gerich JE. Role of the kidney in normal glucose homeostasis and in the hyperglycaemia of diabetes mellitus: therapeutic implications. *Diabetic medicine : a journal of the British Diabetic Association.* 2010;27(2):136-4
- ¹²⁵ Neely RD, Rooney DP, Atkinson AB, Sheridan B, Ennis CN, Trimble ER, et al. Underestimation of glucose turnover determined using [6-3H]glucose tracer in non-steady state. The role of a tritiated tracer impurity. *Diabetologia.* 1990;33(11):681-7.
- ¹²⁶ Laakso M, Edelman SV, Olefsky JM, Brechtel G, Wallace P, Baron AD. Kinetics of in vivo muscle insulin-mediated glucose uptake in human obesity. *Diabetes.* 1990;39(8):965-74.
- ¹²⁷ Zierler KL: Theory and the use of arteriovenous concentration differences for measuring metabolism in steady and non-steady state. *J Clin Invest* 1961; 40:2111-25
- ¹²⁸ Wesche J. The time course and magnitude of blood flow changes in the human quadriceps muscles following isometric contraction. *J Physiol Lond* 1986;377: 445±62.

-
- ¹²⁹ Andersson P, Lind L, Berne C, Berglund L, Lithell HO. Insulin-mediated vasodilation and glucose uptake are independently related to fasting serum nonesterified fatty acids in elderly men. *Journal of internal medicine*. 1999;246(6):529-37.
- ¹³⁰ Gupta RD, Ramachandran R, Venkatesan P, Anoop S, Joseph M, Thomas N. Indirect Calorimetry: From Bench to Bedside. *Indian journal of endocrinology and metabolism*. 2017;21(4):594-9.
- ¹³¹ Ferrannini E. The theoretical bases of indirect calorimetry: a review. *Metabolism*. 1988;37(3):287-301.
- ¹³² McClave SA, Lowen CC, Kleber MJ, McConnell JW, Jung LY, Goldsmith LJ. Clinical use of the respiratory quotient obtained from indirect calorimetry. *JPEN Journal of parenteral and enteral nutrition*. 2003;27(1):21-6.
- ¹³³ Peronnet F, Massicotte D. Table of nonprotein respiratory quotient: an update. *Canadian journal of sport sciences = Journal canadien des sciences du sport*. 1991;16(1):23-9.
- ¹³⁴ Bergstrom, J. Percutaneous needle biopsy of skeletal muscle in physiological and clinical research. *Scand J Clin Lab Invest*. 1975; 35, 609-616
- ¹³⁵ Evans, W. J., Phinney, S. D., & Young, V. R. Suction applied to a muscle biopsy maximizes sample size. *Med Sci Sports Exerc*. 1982; 14, 101-102
- ¹³⁶ Shanely RA, Zwetsloot KA, Triplett NT, Meaney MP, Farris GE, Nieman DC. Human skeletal muscle biopsy procedures using the modified Bergstrom technique. *Journal of visualized experiments : JoVE*. 2014(91):51812.
- ¹³⁷ Prats C, Gomez-Cabello A, Nordby P, Andersen JL, Helge JW, et al. An Optimized Histochemical Method to Assess Skeletal Muscle Glycogen and Lipid Stores Reveals Two Metabolically Distinct Populations of Type I Muscle Fibers. *PLOS ONE* 2013; 8(10): e77774.
- ¹³⁸ Søndergaard E, Espinosa De Ycaza AE, Morgan-Bathke M, Jensen MD. How to Measure Adipose Tissue Insulin Sensitivity. *J Clin Endocrinol Metab*. 2017;102(4):1193-1199.
- ¹³⁹ Ter Horst KW, van Galen KA, Gilijamse PW, et al. Methods for quantifying adipose tissue insulin resistance in overweight/obese humans. *Int J Obes (Lond)*. 2017;41(8):1288-1294.
- ¹⁴⁰ Gastaldelli A, Harrison SA, Belfort-Aguilar R, et al. Importance of changes in adipose tissue insulin resistance to histological response during thiazolidinedione treatment of patients with nonalcoholic steatohepatitis. *Hepatology*. 2009;50(4):1087-1093.
- ¹⁴¹ Bell LN, Wang J, Muralidharan S, Chalasani S, Fullenkamp AM, Wilson LA, Sanyal AJ, Kowdley KV, Neuschwander-Tetri BA, Brunt EM, McCullough AJ, Bass NM, Diehl AM, Unalp-Arida A, Chalasani N; Nonalcoholic Steatohepatitis Clinical Research Network . Relationship between adipose tissue insulin resistance and liver histology in nonalcoholic steatohepatitis: a pioglitazone versus vitamin E versus placebo for the treatment of nondiabetic patients with nonalcoholic steatohepatitis trial follow-up study. *Hepatology*. 2012;56(4):1311–1318.

¹⁴² Szczepaniak LS, Babcock EE, Schick F, Dobbins RL, Garg A, Burns DK, et al. Measurement of

intracellular triglyceride stores by H spectroscopy: validation in vivo. *Am.J.Physiol* 1999;276:E977-E989

¹⁴³ Di Martino M, Pacifico L, Bezzi M, et al. Comparison of magnetic resonance spectroscopy, proton density fat fraction and histological analysis in the quantification of liver steatosis in children and adolescents. *World J Gastroenterol*. 2016;22(39):8812–8819.

¹⁴⁴ Bawden SJ, Scott RA, Aithal GP. Current and Future Magnetic Resonance Technologies for Assessing Liver Disease in Clinical and Experimental Medicine. *Dig Dis*. 2017;35(4):314–322. doi:10.1159/000456582

¹⁴⁵ Hamilton G, Middleton MS, Bydder M, et al. Effect of PRESS and STEAM sequences on magnetic resonance spectroscopic liver fat quantification. *J Magn Reson Imaging*. 2009;30(1):145-152.

¹⁴⁶ Mandal PK. In vivo proton magnetic resonance spectroscopic signal processing for the absolute quantitation of brain metabolites. *Eur J Radiol*. 2012;81(4):e653–e664.

¹⁴⁷ Hamilton, G., et al., In vivo characterization of the liver fat H-1 MR spectrum. *Nmr in Biomedicine*, 2011. 24(7): p. 784-790

¹⁴⁸ Chen, C., et al., P-31 magnetization transfer magnetic resonance spectroscopy: Assessing the activation induced change in cerebral ATP metabolic rates at 3 T. *Magnetic Resonance in Medicine*, 2018. 79(1): p. 22-30.

¹⁴⁹ Petersen, K.F., Dufour, S., Befroy, D. *et al*. Impaired mitochondrial activity in the insulin-resistant offspring of patients with type 2 diabetes. *N Engl J Med*, 2004;350(7):664–71

¹⁵⁰ Lara-Castro C, Newcomer BR, Rowell J, et al. Effects of short-term very low-calorie diet on intramyocellular lipid and insulin sensitivity in nondiabetic and type 2 diabetic subjects. *Metabolism*. 2008;57(1):1-8.

¹⁵¹ Jacob S, Machann J, Rett K, et al. Association of increased intramyocellular lipid content with insulin resistance in lean nondiabetic offspring of type 2 diabetic subjects. *Diabetes*. 1999;48(5):1113-1119.

¹⁵² Krssak M, Falk Petersen K, Dresner A, et al. Intramyocellular lipid concentrations are correlated with insulin sensitivity in humans: a ¹H NMR spectroscopy study [published correction appears in *Diabetologia* 1999 Mar;42(3):386] [published correction appears in *Diabetologia* 1999 Oct;42(10):1269]. *Diabetologia*. 1999;42(1):113-116.

¹⁵³ Petersen, M.C., Samuel, V.T., Petersen, K.F. and Shulman, G.I. (2020). Non-alcoholic Fatty Liver Disease and Insulin Resistance. *In The Liver: Biology and Pathobiology, 6th Edition* (eds I.M. Arias, H.J. Alter, J.L. Boyer, D.E. Cohen, D.A. Shafritz, S.S. Thorgeirsson and A.W. Wolkoff). doi:10.1002/9781119436812.ch37

¹⁵⁴ Caussy C, Alquiraish MH, Nguyen P, et al. Optimal threshold of controlled attenuation parameter with MRI-PDFF as the gold standard for the detection of hepatic steatosis. *Hepatology*. 2018;67(4):1348-1359. doi:10.1002/hep.29639

¹⁵⁵ Cederblad G, Carlin JI, Constantin-Teodosiu D, Harper P, Hultman E. Radioisotopic assays of CoASH

and carnitine and their acetylated forms in human skeletal muscle. *Anal Biochem.* 1990;185(2):274-278. doi:10.1016/0003-2697(90)90292-h

¹⁵⁶ Saukkonen T, Heikkinen S, Hakkarainen A, et al. Association of intramyocellular, intraperitoneal and liver fat with glucose tolerance in severely obese adolescents. *Eur J Endocrinol.* 2010;163(3):413-419.

¹⁵⁷ Morino K, Petersen KF, Dufour S, et al. Reduced mitochondrial density and increased IRS-1 serine phosphorylation in muscle of insulin-resistant offspring of type 2 diabetic parents. *J Clin Invest.* 2005;115(12):3587-3593.

¹⁵⁸ Rotman Y, Neuschwander-Tetri BA. Liver fat accumulation as a barometer of insulin responsiveness again points to adipose tissue as the culprit. *Hepatology.* 2017 Apr;65(4):1088-1090.

¹⁵⁹ Guha IN, Harris R, Berhane S, et al. Validation of a Model for Identification of Patients With Compensated Cirrhosis at High Risk of Decompensation. *Clin Gastroenterol Hepatol.* 2019;17(11):2330-2338.e1. doi:10.1016/j.cgh.2019.01.042

¹⁶⁰ Chalmers J, Wilkes E, Harris R, Kent L, Kinra S, Aithal G, et al. Development and implementation of a commissioned pathway for the identification and stratification of liver disease in the community. *Frontline Gastroenterology.* 2020;11(2):86.

¹⁶¹ Thiagarajan P, Chalmers J, Guha IN, James MW. Detecting chronic liver disease: are liver function tests the solution?. *Br J Hosp Med (Lond).* 2020;81(2):1-8.

¹⁶² European Association for the Study of the Liver (EASL); European Association for the Study of Diabetes (EASD); European Association for the Study of Obesity (EASO). EASL-EASD-EASO Clinical Practice Guidelines for the management of non-alcoholic fatty liver disease. *J Hepatol.* 2016 Jun;64(6):1388-402.

¹⁶³ Allen AM, Therneau TM, Larson JJ, Coward A, Somers VK, Kamath PS. Nonalcoholic fatty liver disease incidence and impact on metabolic burden and death: A 20 year-community study. *Hepatology.* 2018;67(5):1726-1736.

¹⁶⁴ Ekstedt M, Franzén LE, Mathiesen UL, et al. Long-term follow-up of patients with NAFLD and elevated liver enzymes. *Hepatology.* 2006;44(4):865-873. doi:10.1002/hep.21327

¹⁶⁵ Dam-Larsen S, Franzmann M, Andersen IB, et al. Long term prognosis of fatty liver: risk of chronic liver disease and death. *Gut.* 2004;53(5):750-755.

¹⁶⁶ Targher G, Day CP, Bonora E. Risk of cardiovascular disease in patients with nonalcoholic fatty liver disease. *N Engl J Med* 2010;363:1341–1350

¹⁶⁷ Wu S, Wu F, Ding Y, Hou J, Bi J, Zhang Z. Association of non- alcoholic fatty liver disease with major adverse cardiovascular events: A systematic review and meta-analysis. *Sci Rep* 2016;6:33386

¹⁶⁸ García-Ruiz C, Fernández-Checa JC. Mitochondrial Oxidative Stress and Antioxidants Balance in Fatty Liver Disease. *Hepatol Commun.* 2018;2(12):1425-1439.

-
- ¹⁶⁹ Schisterman EF, Mumford SL, Sjaarda LA. Failure to consider the menstrual cycle phase may cause misinterpretation of clinical and research findings of cardiometabolic biomarkers in premenopausal women. *Epidemiol Rev.* 2014;36(1):71-82.
- ¹⁷⁰ Stachoń AJ. Menstrual Changes in Body Composition of Female Athletes. *Coll Antropol.* 2016;40(2):111-122.
- ¹⁷¹ Higgins JP, Altman DG, Gøtzsche PC, Jüni P, Moher D, Oxman AD, Savovic J, Schulz KF, Weeks L, Sterne JA; Cochrane Bias Methods Group; Cochrane Statistical Methods Group. The CochraneCollaboration's tool for assessing risk of bias in randomised trials. *BMJ* 2011; **343**: d5928
- ¹⁷² Malaguarnera M, Gargante MP, Russo C, Antic T, Vacante M, Malaguarnera M, Avitabile T, Li Volti G, Galvano F. L-carnitine supplementation to diet: a new tool in treatment of nonalcoholic steatohepatitis--a randomized and controlled clinical trial. *Am J Gastroenterol.* 2010 Jun;105(6):1338-45. doi: 10.1038/ajg.2009.719
- ¹⁷³ Bae JC, Lee WY, Yoon KH, Park JY, Son HS, Han KA, Lee KW, Woo JT, Ju YC, Lee WJ, Cho YY, Lee MK. Improvement of Nonalcoholic Fatty Liver Disease With Carnitine-Orotate Complex in Type 2 Diabetes (CORONA): A Randomized Controlled Trial. *Diabetes Care* 2015; **38**: 1245-1252
- ¹⁷⁴ Alavinejad P, Zakerkish M, Hajiani E, Hashemi SJ, Chobineh M, Moghaddam E. Evaluation of LCarnitine Efficacy in the Treatment of Non-Alcoholic Fatty Liver Disease among Diabetic Patients: A Randomized Double Blind Pilot Study (2016). *J Gastroenterol Hepatol Res* 2016; 5; 2191-2195
- ¹⁷⁵ Hong ES, Kim EK, Kang SM, Khang AR, Choi SH, Park KS, Jang HC, Lim S. Effect of carnitine-ornotate complex on glucose metabolism and fatty liver: a double-blind, placebo-controlled study. *J Gastroenterol Hepatol* 2014; **29**: 1449-1457
- ¹⁷⁶ Somi MH, Fatahi E, Panahi J, Havasian MR, Judaki A. Data from a randomized and controlled trial of L-Carnitine prescription for the treatment for Non- Alcoholic Fatty Liver Disease. *Bioinformation* 2014; **10**:575-579
- ¹⁷⁷ Hoofnagle JH, Van Natta ML, Kleiner DE, Clark JM, Kowdley KV, Loomba R, Neuschwander-Tetri BA, Sanyal AJ, Tonascia J; Non-alcoholic Steatohepatitis Clinical Research Network (NASH CRN). Vitamin E and changes in serum alanine aminotransferase levels in patients with non-alcoholic steatohepatitis. *Aliment Pharmacol Ther* 2013; **38**: 134-143
- ¹⁷⁸ **Aithal GP**, Thomas JA, Kaye PV, Lawson A, Ryder SD, Spendlove I, Austin AS, Freeman JG, Morgan L, Webber J. Randomized, placebo-controlled trial of pioglitazone in nondiabetic subjects with nonalcoholic steatohepatitis. *Gastroenterology* 2008; **135**: 1176-1184
- ¹⁷⁹ Harrison SA, Rinella ME, Abdelmalek MF, Trotter JF, Paredes AH, Arnold HL, Kugelmas M, Bashir MR, Jaros MJ, Ling L, Rossi SJ, DePaoli AM, Loomba R. NGM282 for treatment of non-alcoholic steatohepatitis: a multicentre, randomised, double-blind, placebo-controlled, phase 2 trial. *Lancet* 2018; 391: 1174-1185
- ¹⁸⁰ DiNicolantonio JJ, Lavie CJ, Fares H, Menezes AR, O'Keefe JH. L-carnitine in the secondary prevention of cardiovascular disease: systematic review and meta-analysis. *Mayo Clin Proc* 2013; **88**: 544-551

-
- ¹⁸¹ Samulak JJ, Sawicka AK, Hartmane D, Grinberga S, Pugovics O, Lysiak-Szydłowska W, Olek RA. L-Carnitine Supplementation Increases Trimethylamine-N-Oxide but not Markers of Atherosclerosis in Healthy Aged Women. *Ann Nutr Metab.* 2019;74(1):11-17
- ¹⁸² Fathizadeh H, Milajerdi A, Reiner Ž, Kolahehdooz F, Asemi Z. The effects of L-carnitine supplementation on glycemic control: a systematic review and meta-analysis of randomized controlled trials. *EXCLI J.* 2019;18:631-643.
- ¹⁸³ Thiagarajan, P.; Chalmers, J.; Ban, L.; Grindlay, D.; Aithal, G.P. L-carnitine supplementation in non-alcoholic fatty liver disease: A systematic review and meta-analysis. *WJMA* 2020, 8, 4–14.
- ¹⁸⁴ Lambert, J.E., Ramos-Roman, M.A., Browning, J.D. et al. Increased de novo lipogenesis is a distinct characteristic of individuals with nonalcoholic fatty liver disease. *Gastroenterology*, 2014;146 (3):726–35.
- ¹⁸⁵ Smith GI, Shankaran M, Yoshino M, et al. Insulin resistance drives hepatic de novo lipogenesis in nonalcoholic fatty liver disease. *J Clin Invest.* 2020;130(3):1453-1460. doi:10.1172/JCI134165
- ¹⁸⁶ Harper P, Wadström C, Cederblad G. Carnitine measurement in liver, muscle tissue, and blood in normal subjects. *Clin Chem* 1993;39: 592-9
- ¹⁸⁷ Cederblad G, Lindstedt S, Lundholm K. Concentration of carnitine in human muscle tissue. *Clin Chim Acta.* 1974;53(3):311-321. doi:10.1016/0009-8981(74)90270-8
- ¹⁸⁸ Harper P, Wadström C, Backman L, Cederblad G. Increased liver carnitine content in obese women. *Am J Clin Nutr.* 1995;61(1):18-25.
- ¹⁸⁹ Fujisawa K, Takami T, Matsuzaki A, et al. Evaluation of the effects of L-carnitine on medaka (*Oryzias latipes*) fatty liver. *Sci Rep.* 2017;7(1):2749.
- ¹⁹⁰ Pietrocola F, Galluzzi L, Bravo-San Pedro JM, Madeo F, Kroemer G. Acetyl coenzyme A: a central metabolite and second messenger. *Cell Metab.* 2015;21(6):805-821.
- ¹⁹¹ World Medical Association. World Medical Association Declaration of Helsinki: ethical principles for medical research involving human subjects. *JAMA.* 2013;310(20):2191-2194.
- ¹⁹² Chalmers J, Wilkes E, Harris R, Kent L, Kinra S, Aithal G, et al. Development and implementation of a commissioned pathway for the identification and stratification of liver disease in the community. *Frontline Gastroenterology.* 2020;11(2):86.
- ¹⁹³ Versteeg RI, Ackermans MT, Nederveen AJ, Fliers E, Serlie MJ, la Fleur SE. Meal timing effects on insulin sensitivity and intrahepatic triglycerides during weight loss. *Int J Obes (Lond).* 2018;42(2):156-162.
- ¹⁹⁴ Harris RC, Hultman E, Nordesjö LO. Glycogen, glycolytic intermediates and high-energy phosphates determined in biopsy samples of musculus quadriceps femoris of man at rest. Methods and variance of values. *Scand J Clin Lab Invest.* 1974 Apr;33(2):109-20.

-
- ¹⁹⁵ Prats C, Gomez-Cabello A, Nordby P, et al. An optimized histochemical method to assess skeletal muscle glycogen and lipid stores reveals two metabolically distinct populations of type I muscle fibers. *PLoS One*. 2013;8(10):e77774.
- ¹⁹⁶ Samimi M, Jamilian M, Ebrahimi FA, Rahimi M, Tajbakhsh B, Asemi Z. Oral carnitine supplementation reduces body weight and insulin resistance in women with polycystic ovary syndrome: a randomized, double-blind, placebo-controlled trial. *Clin Endocrinol (Oxf)*. 2016;84(6):851-857.
- ¹⁹⁷ Petersen KF, Dufour S, Shulman GI. Decreased insulin-stimulated ATP synthesis and phosphate transport in muscle of insulin-resistant offspring of type 2 diabetic parents. *PLoS Med*. 2005;2(9):e233
- ¹⁹⁸ Fellingner P, Wolf P, Pflieger L, et al. Increased ATP synthesis might counteract hepatic lipid accumulation in acromegaly. *JCI Insight*. 2020;5(5):e134638.
- ¹⁹⁹ Moreno Sánchez D. Patogenia de la hepatopatía grasa no alcohólica primaria [Pathogenesis of primary nonalcoholic fatty liver disease]. *Med Clin (Barc)*. 2005;124(17):668-677.
- ²⁰⁰ Gülçin I: Antioxidant and antiradical activities of L-carnitine. *Life Sci* 2006, 78:803–811.
- ²⁰¹ Lee BJ, Lin JS, Lin YC, Lin PT. Effects of L-carnitine supplementation on oxidative stress and antioxidant enzymes activities in patients with coronary artery disease: a randomized, placebo-controlled trial. *Nutr J*. 2014;13:79. Published 2014 Aug 4. doi:10.1186/1475-2891-13-79
- ²⁰² Li JL, Wang QY, Luan HY, Kang ZC, Wang CB. Effects of L-carnitine against oxidative stress in human hepatocytes: involvement of peroxisome proliferator-activated receptor alpha. *J Biomed Sci*. 2012;19(1):32.
- ²⁰³ Hamza RZ, Al-Eisa RA, Mehana AE, El-Shenawy NS. Effect of l-carnitine on aspartame-induced oxidative stress, histopathological changes, and genotoxicity in liver of male rats. *J Basic Clin Physiol Pharmacol*. 2019;30(2):219-232.
- ²⁰⁴ Li XS, et al. Gut microbiota-dependent trimethylamine N-oxide in acute coronary syndromes: a prognostic marker for incident cardiovascular events beyond traditional risk factors. *Eur Heart J*. 2017;38(11):814–824
- ²⁰⁵ Senthong V, et al. Intestinal microbiota-generated metabolite trimethylamine-N-oxide and 5-year mortality risk in stable coronary artery disease: the contributory role of intestinal microbiota in a COURAGE-like patient cohort. *J Am Heart Assoc*. 2016;5(6):e002816.
- ²⁰⁶ Trøseid M, Ueland T, Hov JR, et al. Microbiota-dependent metabolite trimethylamine-N-oxide is associated with disease severity and survival of patients with chronic heart failure. *J Intern Med*. 2015;277(6):717-726.
- ²⁰⁷ Koeth RA, Wang Z, Levison BS, et al. Intestinal microbiota metabolism of L-carnitine, a nutrient in red meat, promotes atherosclerosis. *Nat Med*. 2013;19(5):576-585.
- ²⁰⁸ McCarty MF. L-carnitine consumption, its metabolism by intestinal microbiota, and cardiovascular health. *Mayo Clin Proc*. 2013;88(8):786-789.

-
- ²⁰⁹ Samerotte AL, Drazen JC, Brand GL, Seibel BA, Yancey PH. Correlation of trimethylamine oxide and habitat depth within and among species of teleost fish: an analysis of causation. *Physiol Biochem Zool.* 2007;80(2):197-208.
- ²¹⁰ Lajous M, Willett WC, Robins J, et al. Changes in fish consumption in midlife and the risk of coronary heart disease in men and women. *Am J Epidemiol.* 2013;178(3):382-391.
- ²¹¹ Mozaffarian D, Lemaitre RN, Kuller LH, et al. Cardiac benefits of fish consumption may depend on the type of fish meal consumed: the Cardiovascular Health Study. *Circulation.* 2003;107(10):1372-1377.
- ²¹² Müller MJ. Hepatic fuel selection. *Proc Nutr Soc.* 1995;54(1):139-150.
- ²¹³ Qayyum A. MR spectroscopy of the liver: principles and clinical applications. Radiographics : a review publication of the Radiological Society of North America, Inc. 2009;29(6):1653-64.
- ²¹⁴ Verma A, Kumar I, Verma N, Aggarwal P, Ojha R. Magnetic resonance spectroscopy - Revisiting the biochemical and molecular milieu of brain tumors. *BBA Clin.* 2016; 5:170–178.
- ²¹⁵ Befroy DE, Shulman GI. Magnetic resonance spectroscopy studies of human metabolism. *Diabetes.* 2011;60(5):1361–1369.
- ²¹⁶ Horská A, Barker PB. Imaging of brain tumors: MR spectroscopy and metabolic imaging. *Neuroimaging Clin N Am.* 2010;20(3):293-310
- ²¹⁷ Krssak M, Brehm A, Bernroider E, Anderwald C, Nowotny P, Dalla MC, et al. Alterations in postprandial hepatic glycogen metabolism in type 2 diabetes. *Diabetes* 2004;53:3048-3056.
- ²¹⁸ Krššák M. Novel labeling approaches for the assessment of human hepatic metabolism by in vivo magnetic resonance spectroscopy. *Hepatology.* 2014;59(6):2077–2079.
- ²¹⁹ Tyson RL, Gallagher C, Sutherland GR. 13C-Labeled substrates and the cerebral metabolic compartmentalization of acetate and lactate. *Brain Res.* 2003;992(1):43-52.
- ²²⁰ Befroy DE, Perry RJ, Jain N, Dufour S, Cline GW, Trimmer JK, Brosnan J, Rothman DL, Petersen KF, Shulman GI. Direct assessment of hepatic mitochondrial oxidative and anaplerotic fluxes in humans using dynamic 13C magnetic resonance spectroscopy. *Nat Med.* 2014 Jan;20(1):98-102.
- ²²¹ Skamarauskas JT, Oakley F, Smith FE, et al. Noninvasive in vivo magnetic resonance measures of glutathione synthesis in human and rat liver as an oxidative stress biomarker. *Hepatology.* 2014;59(6):2321-2330.
- ²²² Nair S, Chacko VP, Arnold C, Diehl AM. Hepatic ATP reserve and efficiency of replenishing: comparison between obese and nonobese normal individuals. *Am J Gastroenterology* 2003;98(2):466e70.
- ²²³ Valkovič L, Chmelík M, Krššák M. In-vivo³¹P-MRS of skeletal muscle and liver: A way for non-invasive assessment of their metabolism. *Anal Biochem.* 2017;529:193-215.

-
- ²²⁴ Deng M, Chen SZ, Yuan J, Chan Q, Zhou J, Wáng YX. Chemical Exchange Saturation Transfer (CEST) MR Technique for Liver Imaging at 3.0 Tesla: an Evaluation of Different Offset Number and an After-Meal and Over-Night-Fast Comparison. *Mol Imaging Biol.* 2016;18(2):274-282.
- ²²⁵ Bawden SJ, Mougin O, Hunter K, et al. Simultaneously Measuring Glycogen and Lipid Levels Using Localized CEST Spectroscopy at 3T. *Proc Intl Soc Mag Reson Med.* 2014;22:3159
- ²²⁶ Meex RCR, Watt MJ. Hepatokines: linking nonalcoholic fatty liver disease and insulin resistance. *Nat Rev Endocrinol.* 2017 Sep;13(9):509-520.
- ²²⁷ Lebensztejn DM, Flisiak-Jackiewicz M, Białokoz-Kalinowska I, Bobrus-Chociej A, Kowalska I. Hepatokines and non-alcoholic fatty liver disease. *Acta Biochim Pol.* 2016;63(3):459-67
- ²²⁸ Liu J, Xu Y, Hu Y, Wang G. The role of fibroblast growth factor 21 in the pathogenesis of non-alcoholic fatty liver disease and implications for therapy. *Metabolism.* 2015;64(3):380-390.
- ²²⁹ Mashili FL, Austin RL, Deshmukh AS, et al. Direct effects of FGF21 on glucose uptake in human skeletal muscle: implications for type 2 diabetes and obesity. *Diabetes Metab Res Rev.* 2011;27(3):286-297.
- ²³⁰ Kharitononkov, A. *et al.* FGF-21 as a novel metabolic regulator. *J. Clin. Invest.* **115**, 1627–1635 (2005)
- ²³¹ Gaich, G. *et al.* The effects of LY2405319, an FGF21 analog, in obese human subjects with type 2 diabetes. *Cell Metab.* **18**, 333–340 (2013).
- ²³² Tucker B, Li H, Long X, Rye KA, Ong KL. Fibroblast growth factor 21 in non-alcoholic fatty liver disease. *Metabolism.* 2019 Dec;101:153994
- ²³³ Fisher FM, Chui PC, Antonellis PJ, et al. Obesity is a fibroblast growth factor 21 (FGF21)-resistant state. *Diabetes.* 2010;59(11):2781-2789.
- ²³⁴ Ong KL, Januszewski AS, O'Connell R, et al. The relationship of fibroblast growth factor 21 with cardiovascular outcome events in the Fenofibrate Intervention and Event Lowering in Diabetes study. *Diabetologia.* 2015;58(3):464-473.
- ²³⁵ Tanajak P, Pongkan W, Chattipakorn SC, Chattipakorn N. Increased plasma FGF21 level as an early biomarker for insulin resistance and metabolic disturbance in obese insulin-resistant rats. *Diab Vasc Dis Res.* 2018;15(3):263-269.
- ²³⁶ Camporez JP, Jornayvaz FR, Petersen MC, et al. Cellular mechanisms by which FGF21 improves insulin sensitivity in male mice. *Endocrinology.* 2013;154(9):3099-3109.
- ²³⁷ Lan F, Misu H, Chikamoto K, Takayama H, Kikuchi A, Mohri K, et al. LECT2 functions as a hepatokine that links obesity to skeletal muscle insulin resistance. *Diabetes.* 2014; 63: 1649–1664.
- ²³⁸ Yoo HJ, Hwang SY, Choi JH, et al. Association of leukocyte cell-derived chemotaxin 2 (LECT2) with NAFLD, metabolic syndrome, and atherosclerosis. *PLoS One.* 2017;12(4):e0174717.

-
- ²³⁹ Ejaz A, Martinez-Guino L, Goldfine AB, et al. Dietary Betaine Supplementation Increases Fgf21 Levels to Improve Glucose Homeostasis and Reduce Hepatic Lipid Accumulation in Mice. *Diabetes*. 2016;65(4):902-912.
- ²⁴⁰ Pekkinen J, Olli K, Huotari A, et al. Betaine supplementation causes increase in carnitine metabolites in the muscle and liver of mice fed a high-fat diet as studied by nontargeted LC-MS metabolomics approach. *Mol Nutr Food Res*. 2013;57(11):1959-1968.
- ²⁴¹ Akbar H, Batistel F, Drackley JK, Loor JJ. Alterations in Hepatic FGF21, Co-Regulated Genes, and Upstream Metabolic Genes in Response to Nutrition, Ketosis and Inflammation in Peripartal Holstein Cows. *PLoS One*. 2015;10(10):e0139963.
- ²⁴² Li J-L, Wang Q-Y, Luan H-Y, Kang Z-C, Wang C-B. Effects of L-carnitine against oxidative stress in human hepatocytes: involvement of peroxisome proliferator-activated receptor alpha. *Journal of Biomedical Science*. 2012;19(1):32.
- ²⁴³ Slowik V, Apte U. Leukocyte Cell-Derived Chemotaxin-2: It's Role in Pathophysiology and Future in Clinical Medicine. *Clin Transl Sci*. 2017;10(4):249-259.
- ²⁴⁴ Fabbrini E, Magkos F, Mohammed BS, et al. Intrahepatic fat, not visceral fat, is linked with metabolic complications of obesity. *Proc Natl Acad Sci U S A*. 2009;106(36):15430-15435.
- ²⁴⁵ Stefan, N. *et al.* Identification and characterization of metabolically benign obesity in humans. *Arch. Intern. Med*. 2008; **168**, 1609–1616
- ²⁴⁶ Rasmussen J, Lund AM, Risom L, Wibrand F, Gislason H, Nielsen OW, Køber L, Duno M. Residual OCTN2 transporter activity, carnitine levels and symptoms correlate in patients with primary carnitine deficiency. *Mol Genet Metab Rep*. 2014 May 22;1:241-248.
- ²⁴⁷ Stephens FB, Galloway SD. Carnitine and fat oxidation. *Nestle Nutr Inst Workshop Ser*. 2013;76:13-23.
- ²⁴⁸ Roumans KHM, Lindeboom L, Veeraiah P, Remie CME, Phielix E, Havekes B, Bruls YMH, Brouwers MCGJ, Ståhlman M, Alsema M, Peters HPF, de Mutsert R, Staels B, Taskinen MR, Borén J, Schrauwen P, Schrauwen-Hinderling VB. Hepatic saturated fatty acid fraction is associated with de novo lipogenesis and hepatic insulin resistance. *Nat Commun*. 2020 Apr 20;11(1):1891.